Synthesis, reactivity and catalytic application of ferrocenyl-functionalized 1,2,3-triazol-5-ylidene complexes

by

Danielle Aucamp

Submitted in partial fulfillment of the requirements for the degree

Magister Scientiae

In the Faculty of Natural and Agricultural Sciences

University of Pretoria

Pretoria

November 2016

Supervisor: Prof Daniela I. Bezuidenhout

Acknowledgements

Firstly, I express my deepest gratitude to my Heavenly Father for the good health and well-being necessary to complete this project.

My supervisor, Prof Daniela Bezuidenhout for being available always, ready to give advice, mentor, support and simply motivate when so often needed. For having a turnover frequency on a respond to emails, much higher than the best catalyst out there.

To Prof Gregory Smith, for the kind support on my research visit.

To my fellow lab mates, for the swift hand here and there, quick tips, advice, and inspiration.

To my parents and my family, for their care, understanding and encouragement throughout.

Lastly, to Johan, for all the listening, and listening and more listening, even when nothing made sense. For reinforcing my will and passion for chemistry and this project and the never-failing support.

Declaration

I, Danielle Aucamp, declare that the dissertation, which I hereby submit for the degree MSc. Chemistry at the University of Pretoria, is my own work and has not previously been submitted by me for a degree at this or any other institution.

The hydroformylation reactivity testing of the rhodium(I) complexes were done by me and Shepherd Siangwata at the University of Cape Town, under the supervision of Prof Gregory S. Smith.

Mr David Liles at the University of Pretoria solved the crystal structures presented in this dissertation.

The financial assistance from Sasol Technology R&D Pty. Ltd. South Africa and from the National Research Foundation (NRF) towards this research is hereby recognized and appreciated. Opinions expressed and conclusions arrived at, are those of the author and are not necessarily to be attributed to the NRF.

Results obtained from this study has been presented at the following conferences:

Die Suid-Afrikaanse Akademie vir Wetenskap en Kuns se Studentesimposium in die Natuurwetenskappe, Bloemfontein, 29–30 October, 2015.

The 42nd National Convention of the South African Chemical Institute, Durban, 29 November to 4 December 2015.

The 42nd International Conference on Coordination Chemistry, Brest, France, 3-8 July, 2016.

Signature: ……....

Date: …….

Abstract

Herein is presented the synthesis and characterization of ferrocenyl functionalized 1,2,3-triazolium salts, as precursors to stable mesoionic carbenes (MICs) or 1,2,3-triazol-5-ylidenes (trz). The synthesis of the N1, N3-diarylated ferrocenyl triazolium salt (**1**: [N1-dipp, N3-dipp, 4-Fc(trz-H)]PF_6) (dipp = 2,6-diisopropylphenyl) involved the cycloaddition of *N*-chlorotriazenes with ethynyl ferrocene. For comparative purposes, N1-aryl, N3-alkyl functionalized triazolium salts (**2**: [N1-dipp, N3-ethyl, 4-Fc (trz-H)]BF_4; **3**: [N1-dipp, N3-ethyl, 4-Ph (trz-H)]BF_4) were synthesized according to the one-pot copper catalyzed alkyne-azide cycloaddition (CuAAC) of 2,6-diisopropylaniline and the respective alkyne (**2**: ethynylferrocene; **3**: phenylacetylene), followed by alkylation on N3. It was reasoned that the ligand scaffold of the ferrocenyl triazolium salts (**1** and **2**) would enhance the donating ability of the corresponding carbene when coordinated, given that ferrocene is a strong electron donor. However, on closer scrutiny of the chemical shifts (in NMR spectroscopy) of the acidic triazolium protons of salts **1**–**3**, it was found that the arylated substituent on N3 has a more profound effect on the electronics of the precursor salt, than the substituent on C4 (ferrocene vs. phenyl).

Coordination of the triazolium salts to rhodium(I) cod chloride (cod = 1,5-cyclooctadiene) precursors followed either the free carbene route (synthesis of **4**) or base mediated C-H activation (synthesis of **5** and **6**) to synthesize the corresponding [Rh(trz)(cod)Cl] complexes (**4**–**6**). The electronic properties of the triazolylidenes were further investigated by means of measuring the stretching frequencies of the corresponding dicarbonyl complexes (**7**–**9**), whereby the calculated TEPs of all three complexes were found to be equal (2047 cm^{-1}). Slight differences in donating strengths were observed in the carbene resonances, whereby the trend were followed regarding the acidity of their triazolium precursor salts.

Furthermore, the Rh(I)-cod complexes, **4**–**6**, underwent reactivity testing for the hydroformylation of 1-octene. To the best of our knowledge, no examples of rhodium(I) triazolylidenes as precursors catalysts for hydroformylation exist, and thus the Rh(I)-cod complexes, **N** (Rh(cod)(trz-NBoc) and **O** ([Rh(cod)(trz-

NMe_2), were also evaluated alongside complexes **4**–**6** for comparative reasons. All complexes were active in the hydroformylation of 1-octene and reported TOFs of 151.6–78.4 hr^{-1}, and n/*iso* values of 2.43–1.16 were obtained. The addition of an oxidant to **4**, to generate **4ox** *in situ* resulted in increased activity at a cost to regioselectivity.

Lastly, the synthesis of the gold(I) chlorido complex **10** follows the hydrolysis of the gold(I) phenyl complex **12**. Gold(I) chlorido triazolylidene complexes have been applied to various catalytic conversions in organic syntheses in the presence of silver salts. Indeed, complex **10** is an active precursor catalyst in the synthesis of oxazolines, with an increase in conversion with the addition of silver salt.

Contents

List of Figures

List of Schemes

List of Tables

List of Novel Complexes

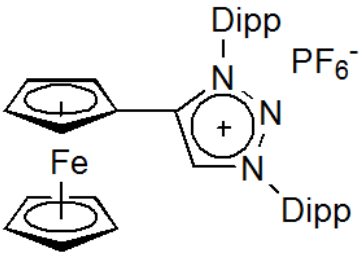

1

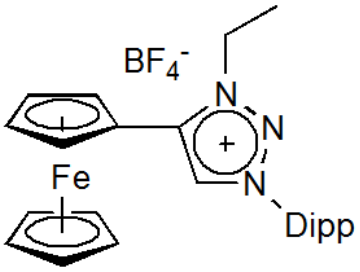

2

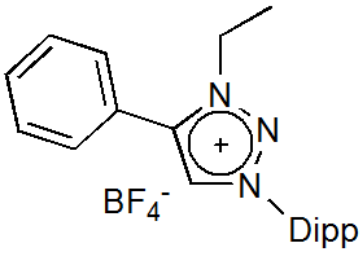

3

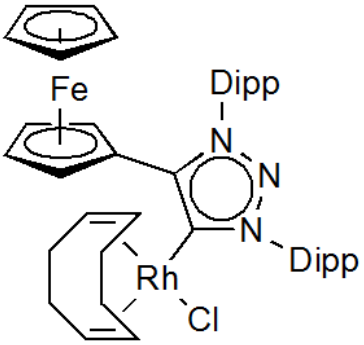

4

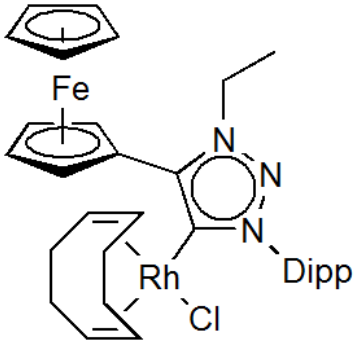

5

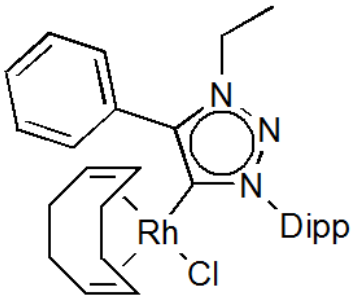

6

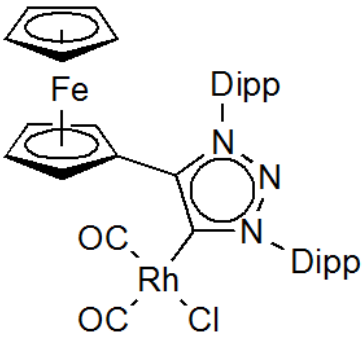

7

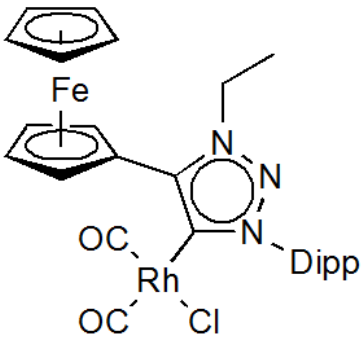

8

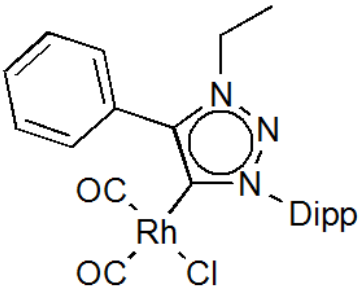

9

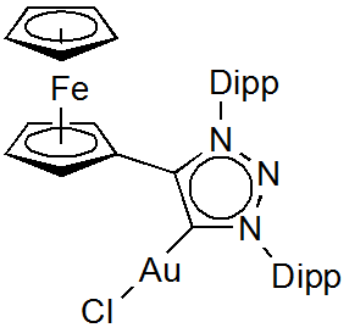
Fe
Dipp
N
N
N
Au
Cl
Dipp

10

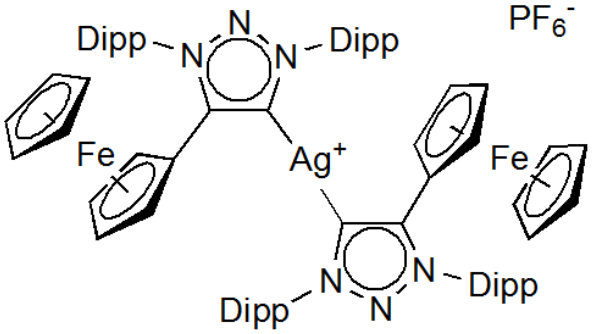
Dipp
N
N
Dipp
PF6-
Fe
Ag+
Fe
N
N
Dipp
Dipp
N

11

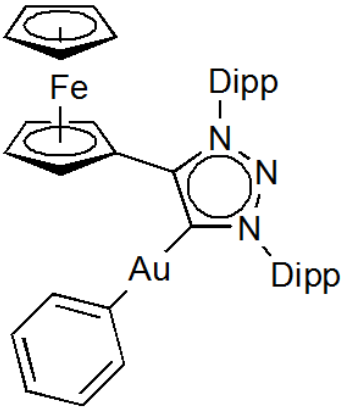
Fe
Dipp
N
N
N
Au
Dipp

12

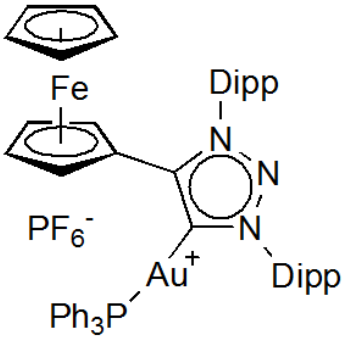
Fe
Dipp
N
N
N
PF6-
Au+
Ph3P
Dipp

13

Abbreviations

Anti-M	Anti-Markonikov
*a*NHC	abnormal *N*-heterocyclic carbene
Bn	Benzyl
Bu	Butyl
cod	1,5-cyclooctadiene
Cp	cyclopentadienyl
Cy	cyclohexyl
CuAAC	copper catalyzed alkyne-azide cycloaddition
CV	cyclic voltammetry/cyclic voltammogram
DCM	dichloromethane
dd	doublet of doublets
d	doublet
Dipp	2,6-diisopropylphenyl
Et	ethyl
Fc	ferrocenyl
FT-IT	Fourier Transform Infrared
HOMO	highest occupied molecular orbital
Hours	hrs
LUMO	lowest unoccupied molecular orbital
m	multiplet

M	Markonikov
MS	Mass spectrometry
Me	methyl
Mes	1, 3, 5-trimethylphenyl
MIC	Mesoionic carbene
NHC	N-Heterocyclic Carbene
NMR	Nuclear Magnetic Resonance
Ph	Phenyl
PGM	Platinum Group Metal
ppm	parts per million
rt	room temperature
s	singlet
TEP	Tolman electronic parameter
THF	tetrahydrafuran
TON	Turnover number
TOF	Turnover frequency
t	triplet
trz	1,2,3-triazol-5-ylidene
XRD	X-ray diffraction

Chapter 1

Introduction

Utilization of the PGMs (platinum group metals), such as rhodium, in the design of catalysts creates a potential economic growth since South Africa is the leading producer of rhodium in the world.[1] Rhodium is regarded, alongside platinum and palladium as the most economically significant PGM. Gold mining is the largest mining industry in terms of employment, investment and revenue generation in South Africa.

The development of catalysts for organic reactions, such as the hydroformylation and hydroamination reactions, allow for the synthesis of compounds used in the bulk chemical supply, pharmaceuticals and the agricultural industry. In fact, SASOL employs the hydroformylation of 1-hexene and 1-octene with suitable rhodium catalysts to produce surfactants, polymers etc.[2] Optimal energy distribution, with a positive economic impact is possible with the development of catalysts designed with natural resources.

1.1 Carbenes in catalysis

The first metal-carbon double bond complex, namely a Fischer carbene complex, was reported by Fischer and Maasböl in 1964 (**A**, Figure 1.1).[3] The first application of these types of Fischer carbenes appeared a few years later in organic synthesis with carbenoid addition to olefins. [4–7]

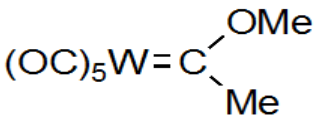

A

Figure 1.1. The first heteroatom stabilized metal-carbon double bond complex reported by Fischer in 1964.[1]

Also in 1964, Banks and Bailey reported on the disproportionation of carbon chains, referring overall to olefin metathesis and isomerization.[4,8,9] The mechanism of olefin metathesis was proposed by Chauvin[10] in 1971; whereby a metallacyclobutane intermediate decomposes to a new metal-alkylidene and a new olefin. This proposal indirectly prompted the isolation of the first alkylidene complex of a transition metal by Schrock in 1974. (**B**, Figure

1.2).[11] Schrock-type high oxidation-state molybdenum and tungsten catalysts have shown to be highly active towards olefin metathesis[12,13] and have ultimately lead to the development of the air-stable Grubbs catalysts of the type **C** and **D** (Figure 1.2).[14–16]

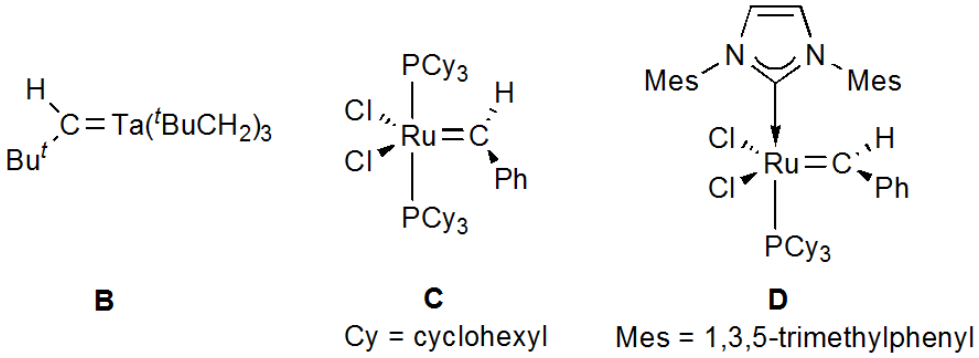

B **C** **D**

Cy = cyclohexyl Mes = 1,3,5-trimethylphenyl

Figure 1.2. The first transition metal carbene complex, not stabilized by a heteroatom (**B**),[11] 1st generation Grubbs catalyst (**C**) and 2nd generation Grubbs catalyst (**D**).[14–16]

Mechanistic studies on the first-generation Grubbs catalysts[17] (**C**, Figure 1.2) have revealed that the mono(phosphine) intermediate is the active catalytic species, and that catalyst decomposition were inversely proportional (2nd order) to the phosphine concentration. Thus, the 2nd generation Grubbs catalyst (**D**, Figure 1.2) had to have an ancillary ligand which is labile enough to activate the catalyst (PCy_3), and another ligand to provide sufficient stabilization of reaction intermediates (NHC). Compared to phosphines, NHCs (*N*-heterocyclic carbenes, *vide infra*) are stronger sigma donors and can therefore possibly influence the dissociation of the more labile *trans* phosphine ligand. Moreover, the steric bulk of the NHC can provide the stability required for the reaction intermediates. The activity of **D** did exceed that of **C**, but not due to the expected *trans* influence, especially since **D**'s initiation rate was twice as slow as for **C**. The increase in catalytic activity was rather attributed to the increased affinity of the ruthenium metal center to the π-acidic olefins, due to the strength of the σ-donating NHC rather than that provided by the phosphine.[8] The trend whereby phosphines have been replaced by NHCs to improve the activity and substrate functionality has been followed in palladium C-C coupling reactions as well.[18]

1.2. *N*-heterocyclic carbenes (NHCs)

The first NHC complexes were synthesized independently by Öfele[19] (**E**, Figure 1.3) and Wanzlick and Schönherr[20] (**F**, Figure 1.3) in 1968. The potential for NHCs as pre-catalysts, however, were only recognized by Herrmann et al.,[21] several years later in 1995 when complexes **G** (Figure 1.3) successfully catalyzed the Heck olefination of aryl halides. Herrmann[21] reported that the NHC-complex was "unexpectedly efficient" and possessed long-term stability. Here, phosphines and phosphites were replaced effectively due to their inevitable degradation over time (P-C bond cleavage) and the requirement to add an excess of ligand (in some cases 100 times more than the metal) to control the activation and duration of the reaction.

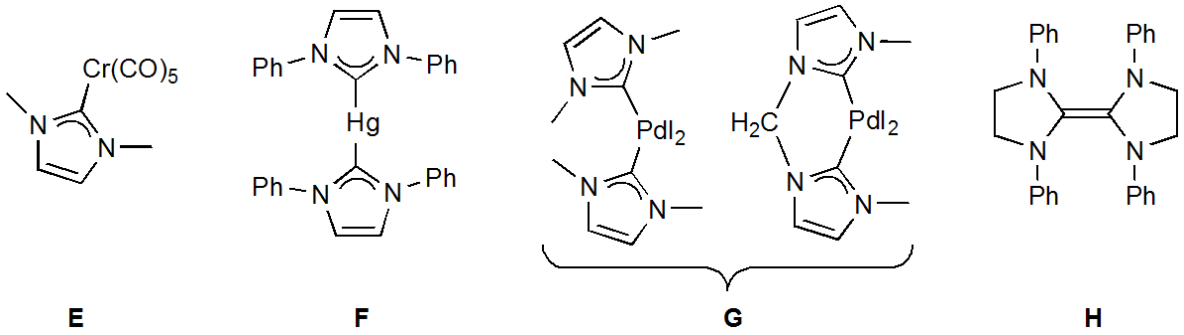

Figure 1.3. The first NHC-complexes synthesized, **E**[19] and **F**[20], the first NHC complexes, **G**,[21] applied in homogenous catalysis and the entetraamine reported by Herrmann after an attempt at isolating the free-NHC.[22]

Between the late 1960's and 1991, research on applications of NHCs were barren ground mainly due to the failed attempts of isolating the free NHC, and the formation of the olefinic entetraamines of the type **H** (Figure 1.3).[22,23] The successful isolation of the free NHC (**I**, Scheme 1.1) by Arduengo et al.,[24] in 1991, however revolutionized research in NHCs. The impact of this discovery was already seen only four years later, with Herrmann's report on complexes **G**'s (Figure 1.3) successful catalytic performance in organic transformations.

Arduengo's success story began with the need for imidazolin-2-thiones for the use in cross-linkers for water-soluble car coatings.[23] However, no synthesis for these compounds were available, especially on an industrial scale. He went on to deprotonate imidazolium salts, generating the free carbene *in situ*, followed

by the addition of elemental sulfur to generate the imidazoline-2-thiones. He then proceeded in studying the deprotonation of the imidazolium salt, by using 1,3-di-admantyl-imidazolium chloride, and deprotonating the salt with a catalytic amount of dimethyl sulfoxide in the presence of NaH - hereby isolating the first free stable cyclic singlet carbene, **I** (Scheme 1.1).[24] It was mentioned that having strong π-donors adjacent to the carbene, like nitrogen atoms, enhances the effective isolation of the NHC but are also aided by the fine-tuning of the electronic and steric properties of the imidazole.

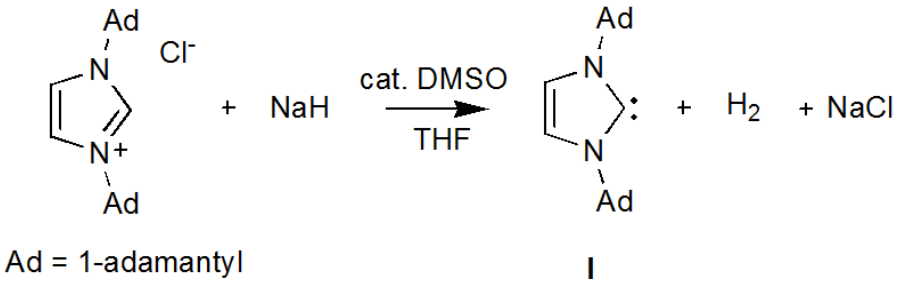

Scheme 1.1. The isolation of the first free stable NHC (**I**) by Arduengo et al.,[24] in 1991.

Singlet carbenes can be electronically stabilised by either a σ-withdrawing substituent (pull inductive) or a π-donating (push mesomeric) substituent.[25] The σ-withdrawing substituent stabilises the σ non-bonding orbital thereby increasing the s-character of the carbene while leaving the π-orbital unchanged. A π-donating substituent, increases the energy of the vacant π orbital of the carbene. The increase in s-character influences the p_x orbital, while the p_y orbital remains relatively unchanged, which results in a lack of degeneracy between the two orbitals, therefore creating a bent carbene, with sp^2 hybridisation. Nitrogens are good σ-withdrawing and π-donating substituents, and carbenes flanked by two nitrogens (like NHCs), have increased electron donation capability (due to the π-donation) but also experience increased stability by the inductive effect provided by the electron negative heteroatoms (Figure 1.4).

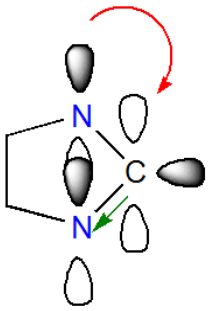

Figure 1.4. The electronic stabilization of diaminocarbenes

NHCs have the exact properties required to make them contenders in catalyst design; they are easily synthesized and exhibit flexibility in design in terms of the substituents on the neighbouring *N*-atoms - allowing for fine-tuning per the contemplated function. The free carbene is stable (for possible commercial availability and storage) and metal complexation is straight-forward.[26]

1.3 Abnormal *N*-heterocyclic carbenes (*a*NHCs)

When Crabtree[27] in 2001 (Scheme 1.2) opted for metalation of iridium to a pyridine-substituted imidazolium, coordination occurred instead at C5, rather than the expected C2. The chelated iridium metal complex, **J** holds the claim for the first abnormal NHC (*a*NHC) complex synthesized (Scheme 1.2), with no hurry to isomerize to the C2 isomer. This pioneering work led to the investigation by numerous research groups to comprehend the formation of the C5 (*a*NHC) isomer.

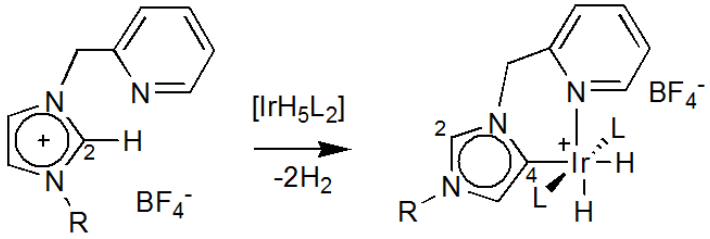

Scheme 1.2. The first abnormal NHC complex, **J**, reported by Crabtree and co-workers.[27]

The coordination of the metal to C5 was unforeseen, since DFT calculations done by Sini, Eisenstein and Crabtree[28] indicated that the more stable isomer, C2-carbene, lies 20 kcal.mol^{-1} lower than the abnormal C5 free carbene. The barrier for C5-metallation via C-H activation increases furthermore since the p*K*a is 24.9 and 33 for NHCs and *a*NHCs repectively.[29,30] However, metalation can be directed towards the C5, if the C2 position is blocked for coordination, but spontaneous metalation on C5 still occurs when a unprotected imidazolium salt is reacted with iridium hydrides and osmium hydrates, such as in Scheme 1.2. In that case, mixtures between C2 and C5 exists but the ratio is found to

depend on the *N*,*N'*-substituents and the nature of the counter-anion of the imidazolium salt.

With the intention to isolate the free *a*NHC, Bertrand et al.,[31] proposed deprotonation of the C5 with a strong, non-nucleophilic base. Seeing as the p*K*a for the C5 proton[30] is roughly 9 units higher than the C2 bounded proton, protection of the C2 proton was necessary. The effort proved successful and Bertrand's team managed to isolate the first free *a*NHC in 2009 (**K**, Scheme 1.3). Addition to the kinetic stability provided by the phenyl blocking group, aromatic wingtip (2,6-diisopropylphenyl) groups on each nitrogen atom and a phenyl group on C5 were also supplied.

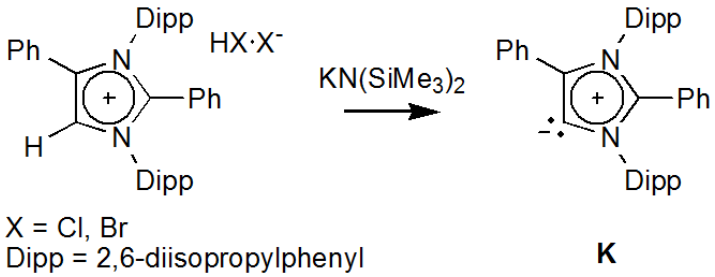

Scheme 1.3. The synthesis and isolation of the free *a*NHC (**K**), by Bertrand et al.,[31] in 2009.

This new class of ligands, the *a*NHCs, provide stronger metal-carbene bonds, due to the enhanced donor abilities compared to normal NHC, and are potentially capable of stabilizing metals in higher oxidation states, leading to rising interest in the NHCs' potential in oxidation catalysis, among others.[26] The increased donor ability can be justified firstly by the absence of one heteroatom adjacent to the carbene carbon, which in turns decreases the stability of the free carbene but the carbene also experience a decrease in the inductive effect, creating stronger σ-bonds with metals. Secondly, *a*NHCs are also mesoionic carbenes (MICs), where no resonance structure of the free ligand can be drawn without the presence of formal charges (Scheme 1.4 (b)). MICs, due to their zwitterionic nature, often have better charge separation than neutral carbenes (Scheme 1.4 (a)), which can emphasize the anionic nature on the carbene carbon, implying an increase in donor strength.[32]

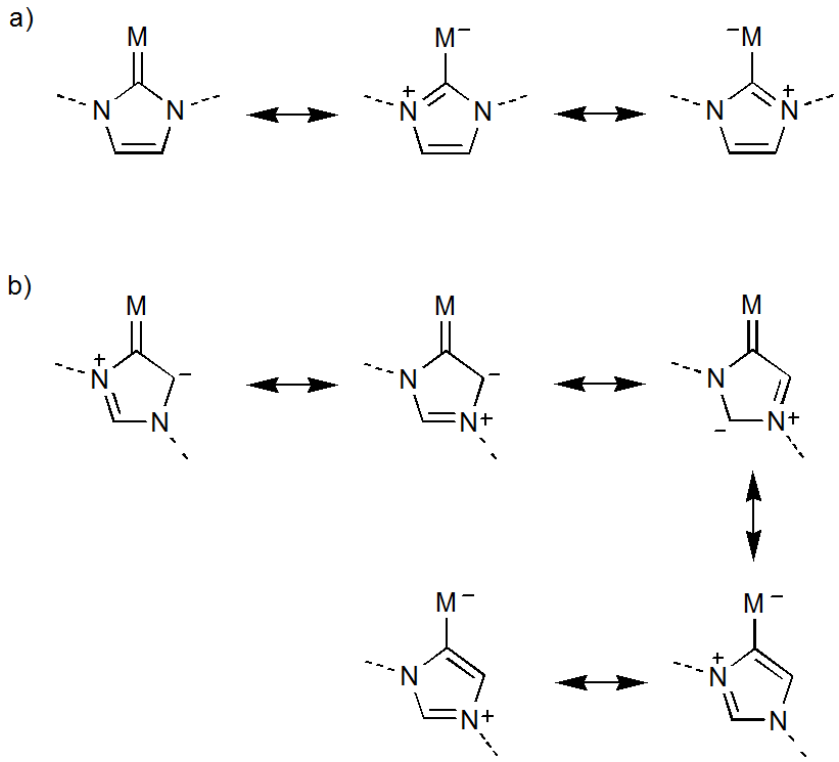

Scheme 1.4. The resonance structures for (a) C2-bound carbenes (NHCs) and (b) C5-bound carbenes (*a*NHCs).[29]

1.4 Triazolylidenes

Pioneering work led by Albrecht[33] resulted in the first triazolylidene complexes (**L**, Scheme 1.5 (a)) in 2008 (see later – Chapter 3). In this case, the C2 in the five-membered ring was replaced with an additional nitrogen atom – bypassing the requirement to block the C2 position to avoid unwanted deprotonation. The isolation of the free triazolylidene (**M**, Scheme1.5 (b)) followed soon by the group of Bertrand in 2010.

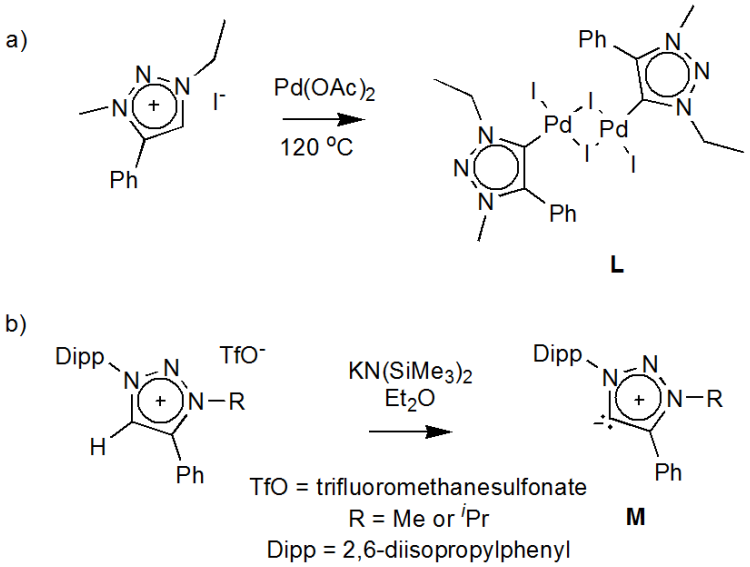

Scheme 1.5. The first triazolylidene metal complex synthesis, (a) **L** reported by Albrecht in 2008[33] and the isolation of the (b) free triazolylidene, **M**, reported by Bertrand in 2010.[34]

Triazolylidenes, due to the additional nitrogen atom present in the ring, are weaker donors than *a*NHCs, but since the carbene is flanked by only one heteroatom, remains more donating than the normal NHCs (Figure 1.5). Evaluation of donor properties by means of comparison of the carbonyl stretching frequencies of various iridium complexes, showed stretching frequencies between 2018 cm^{-1} and 2021 cm^{-1}. The stretching frequencies of the abnormal NHC analogue is 2003 cm^{-1}, and the normal NHC analogues between 2024-2021 cm^{-1}; which indicates that even though triazolylidenes are classified as *a*NHCs/MICs, their donating strengths relate closely to that of the normal NHC, rather than the *a*NHCs.[35] Therefore, triazolylidenes provide slightly stronger donor strength (than NHCs), but also offer increased versatility and stability (than *a*NHCs) as precursor catalysts, with ease of synthesis and modulation required for functionalization.

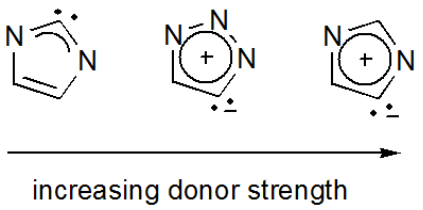

Figure 1.5. The donating ability trend of normal NHCs to *a*NHCs.

In 2010, Albrecht reported the remarkable catalytic activity of triazolylidene chelating iridium complexes in water oxidation.[36] Their activity surpassed that of the benchmark compound, $[Ir(ppy)_2(OH_2)_2]OTf$, where Hppy = 2-phenylpyridine; and the recorded TONs (turn-over numbers) were significantly higher than the known ruthenium catalysts, and hereby announcing triazolylidene metal complexes as contenders in homogenous catalysis.

1.5 Aim and outline

Triazolylidene metal complexes have proven themselves over the last few years as capable and competitive catalyst precursors in various catalytic applications.[35] The aim of this project is to evaluate triazolylidenes as potential redox-tunable catalysts; whereby the triazolylidene is substituted with the well-known redox-active and strongly donating ferrocenyl moiety.[37]

The synthesis and characterization of the ferrocenyl triazolium salts, as well as for comparative reasons, the phenyl substituted salt, are discussed in Chapter 2, followed by the metalation of the precursor ligand salts to rhodium(I) (Chapter 3). Rhodium(I) is a highly catalytic relevant metal in the hydroformylation of aromatic- and aliphatic alkenes.[38] To the best of our knowledge, ferrocenyl-triazolylidene rhodium(I) complexes have not been catalytically assessed in the hydroformylation of alkenes (Chapter 5). Furthermore, the effect of the (oxidized) ferrocenium-substituted triazolylidene on the catalytic activity on hydroformylation is also evaluated, as an expectation of either increased or no catalytic activity, to ultimately function as a redox-switchable pre-catalyst. The electrochemistry and chemical oxidation of the ferrocenyl rhodium triazolylidenes are discussed in Chapter 4. Moreover, the complexation to gold(I), the synthesis, electrochemistry and evaluation as pre-catalyst for the synthesis of oxazolines are conferred in Chapter 6.

1.6 References

1 G. Montmasson-Clair, *Mining, Energy and Low-Carbon Economy in South Africa: A Platinum Case Study*, 2016.

2 Sasol Ltd., *Sasol Facts contents*, 2013.

3 E. O. Fischer and A. Maasböl, *Angew. Chemie Int. Ed.* , 1964, **3**, 580–581.

4 D. Astruc, *Organometallic Chemistry and Catalysis*, Springer Berlin Heidelberg, Berlin, Heidelberg, 2007, vol. 31.

5 K. H. Dötz and J. Stendel, *Chem. Rev.*, 2009, **109**, 3227–3274.

6 E. O. Fischer and K. H.Dötz, *Chem. Ber.*, 1970, **103**, 1273–1278.

7 K. H. Dötz and E. O. Fischer, *Chem. Ber.*, 1972, **105**, 1356–1367.

8 G. C. Vougioukalakis and R. H. Grubbs, *Chem. Rev.*, 2010, **110**, 1746–1787.

9 R. L. Banks and G. C. Bailey, *Ind. Eng. Chem. Prod. Res. Dev.*, 1964, **3**, 170–173.

10 P. Jean-Louis Hérisson and Y. Chauvin, *Die Makromol. Chemie*, 1971, **141**, 161–176.

11 R. R. Schrock, *J. Am. Chem. Soc.*, 1974, **96**, 6796–6797.

12 R. R. Schrock, *Chem. Rev.*, 2009, **109**, 3211–3226.

13 R. R. Schrock, *Angew. Chemie. Int. Ed.*, 2006, **45**, 3748–3759.

14 M. Scholl, T. M. Trnka, J. P. Morgan and R. H. Grubbs, *Tetrahedron Lett.*, 1999, **40**, 2247–2250.

15 S. T. Nguyen, R. H. Grubbs and J. W. Ziller, *J. Am. Chem. Soc.*, 1993, **115**, 9858–9859.

16 S. T. Nguyen, L. K. Johnson, R. H. Grubbs and J. W. Ziller, *J. Am. Chem. Soc.*, 1992, **114**, 3974–3975.

17 T. M. Trnka and R. H. Grubbs, *Acc. Chem. Res.*, 2001, **34**, 18–29.

18 E. A. B. Kantchev, C. J. O'Brien and M. G. Organ, *Angew. Chemie Int. Ed.*, 2007, **46**, 2768–2813.

19 K. Öfele, *J. Organomet. Chem.*, 1968, **12**, P42–P43.

20 H.-W. Wanzlick and H.-J. Schönherr, *Angew. Chemie Int. Ed.* , 1968, **7**, 141–142.

21 W. A. Herrmann, M. Elison, J. Fischer, C. Köcher and G. R. J. Artus, *Angew. Chemie Int. Ed.* , 1995, **34**, 2371–2374.

22 H. W. Wanzlick, *Angew. Chemie Int. Ed.* , 1962, **1**, 75–80.

23 F. E. Hahn and M. C. Jahnke, *Angew. Chemie Int. Ed.*, 2008, **47**, 3122–3172.

24 A. J. Arduengo, R. L. Harlow and M. Kline, *J. Am. Chem. Soc.*, 1991, **113**, 361–363.

25 D. Bourissou, O. Guerret, F. P. Gabbaie and G. Bertrand, *Chem. Rev.* , 2000, **100**, 39–91.

26 M. Albrecht, in *Advances in Organometallic Chemistry*, Elsevier Inc., 1st edn., 2014, vol. 62, pp. 111–158.

27 S. Gründemann, A. Kovacevic, M. Albrecht, J. W. Faller and R. H. Crabtree, *Chem. Comm.*, 2001, **4**, 2274–2275.

28 G. Sini, O. Eisenstein and R. H. Crabtree, *Inorg. Chem.*, 2002, **41**, 602–604.

29 M. Albrecht, *Chem. Comm.*, 2008, 3601–3610.

30 A. M. Magill and B. F. Yates, *Aust. J. Chem.*, 2004, **57**, 1205–1210.

31 E. Aldeco-Perez, A. J. Rosenthal, B. Donnadieu, P. Parameswaran, G. Frenking and G. Bertrand, *Science*, 2009, **326**, 556–559.

32 M. Heckenroth, A. Neels, M. G. Garnier, P. Aebi, A. W. Ehlers and M. Albrecht, *Chem. Eur. J.*, 2009, **15**, 9375–9386.

33 P. Mathew, A. Neels and M. Albrecht, *J. Am. Chem. Soc.*, 2008, **130**,

13534–13535.

34 G. Guisado-Barrios, J. Bouffard, B. Donnadieu and G. Bertrand, *Angew. Chemie. Int. Ed.*, 2010, **49**, 4759–4762.

35 K. F. Donnelly, A. Petronilho and M. Albrecht, *Chem. Comm.*, 2013, **49**, 1145–59.

36 R. Lalrempuia, N. D. McDaniel, H. Müller-Bunz, S. Bernhard and M. Albrecht, *Angew. Chemie. Int. Ed.*, 2010, **49**, 9765–9768.

37 B. van der Westhuizen, P. J. Swarts, L. M. van Jaarsveld, D. C. Liles, U. Siegert, J. C. Swarts, I. Fernández and D. I. Bezuidenhout, *Inorg. Chem.*, 2013, **52**, 6674–6684.

38 W. Gil and A. M. Trzeciak, *Coord. Chem. Rev.*, 2011, **255**, 473–483.

Chapter 2

Ligand Precursor Synthesis

2.1 Background

As stated in the first chapter, the isolation of the first triazolylidene was reported by Bertrand's group in 2011 (**C**, Scheme 2.1).[1] The synthetic approach involved a one-pot copper catalyzed alkyne-azide cycloaddition (CuAAC) for the preparation of triazole **A**, reported by Moses et al.,[2] with a sterically hindering flanking aryl substituent (2,6-diisopropylphenyl) on N1, to ensure kinetic stabilization of the end-product free carbene. Alkylation of the triazole N3 afforded the corresponding triazolium salt **B** and subsequent deprotonation with $KN(SiMe_3)_2$ presented the consequent free carbene, **C.** However, upon heating to 50 °C, decomposition of the free carbene occurred, by N3-alkyl bond cleavage. Although, not kinetically stable,[3] these ligands exhibit enhanced donor properties when complexed to metals like Cu, Pd and Ru. In addition, these triazolylidene complexes have proven to be catalytically applicable in numerous organic transformations such as cycloadditions, C-C cross couplings and olefin metathesis reactions.

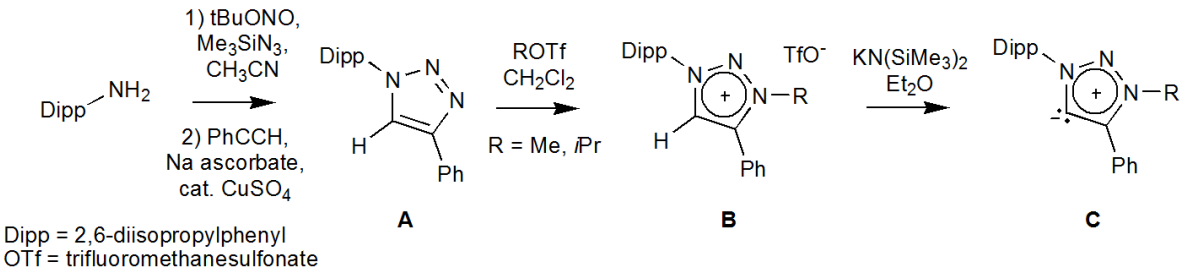

Scheme 2.1. One-pot cycloaddition followed by alkylation to afford the triazolium salt, **B**. Isolation of the free triazolylidene, **C** from the deprotonation of **B**.[1,2]

To circumvent the possibility of decomposition, Bertrand's solution was to synthesize triazolylidenes with diarylated wingtips.[4] For an additional aryl group on N3, the synthetic route employed for **C** did not suffice. The CuAAC synthetic route produces neutral triazole rings such as **A**, which are alkylated on N3 to produce charged triazolium rings, **B**. For N1, N3- diarylated triazolylidene precursors, the product of cycloaddition should be charged, (**F**, Scheme 2.2)

with no necessity to alkylate, hence a one-pot triazolium synthesis. An adapted version[5,6] of Huisgen's [3+2] cycloaddition, was employed by Bertrand et al., to synthesize the diarylated triazolium salt, **F.**

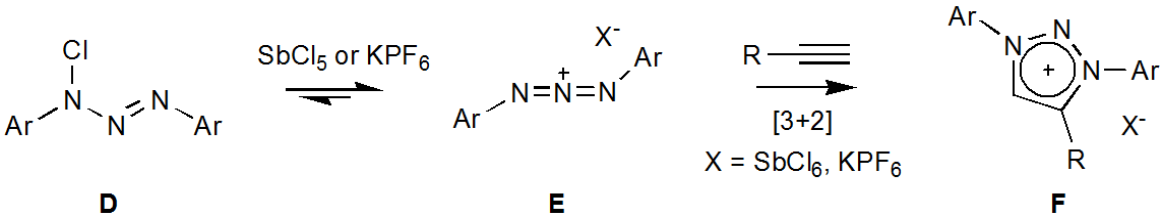

Scheme 2.2. Synthesis of the diarylated triazolium salt, **F** done by Bertrand et al.[4]

Cycloaddition reactions can be classified in two ways, either by the size of the ring formed or the number of new σ bonds formed.[7–9] In [3+2] cycloadditions, specific to 1,3-dipolar cycloadditions, two reactants form a cyclic entity by creating two new σ bonds while forsaking two π bonds. The formation of uncharged rings, requires the addition of a 3-membered 1,3-dipolar molecule with a multiple bond system (Figure 2.1).

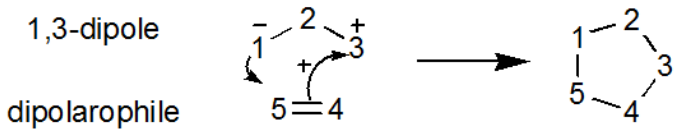

Figure 2.1. General [3+2] 1,3-dipolar cycloaddition.[7]

The uncharged heterocycle cannot be prepared, if an octet-stabilized reactant is used, but rather a 1,3-dipole, where both nucleophilic and electrophilic activity are displayed. Insertion of the unsaturated bond to the dipolarophile termini and cyclic electron displacement occurs with displacement of formal charges, forming an uncharged five-membered ring (Figure 2.1). The synthesis of triazoles are mainly done by employing azides and alkynes, acting as the 1,3-dipole and dipolarophile, correspondingly. Azides are stable 1,3-dipoles, since internal octet stabilization[7] is provided by the central nitrogen atom, increasing their convenience as substrates in organic reactions. Furthermore, azides are stable to water and oxygen and react readily with good dipolarophiles (activated alkenes, alkynes), void of side reactions. However, due to the thermal stability of both reactants, these cycloaddition reactions tend to react over long periods

of time at elevated temperatures. Which led to the optimization of the process by Sharpless[9] and Meldal,[10] with the independent discoveries of Cu(I)-catalyzed cycloaddition (also known as 'click'-chemistry), providing ambient reaction conditions with the formation of only one regio-isomer (Scheme 2.3).

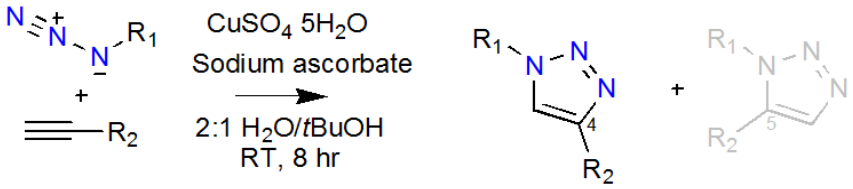

Scheme 2.3. Formation of 1,4-triazol (no formation of 1,5-isomer) from the Cu(I)-catalyzed [3+2] cycloaddition between an azide and an alkyne.[9]

Recently, clarification of the mechanism for CuAAC surfaced with the isolation of the bis(copper) reaction intermediates[11] initially proposed by Fokin et al. in 2013 (Scheme 2.4 (a)). The suggestion came after kinetic studies showed that the monomeric copper-acetylene species, which were previously thought to be the catalytically active species, are not active towards cycloaddition.[12] The proposed mechanism (Scheme 2.4 (b)) involves the bis(copper)-acetylene (one copper atom σ bound, another π-bonded) binding reversibly to the organic azide. The first C-N bond is then formed and the resultant metallocycle intermediate is thought to be stabilized by the additional Cu-atom. However, by being able to isolate the reactive intermediates, it was proved that the monomeric copper species can still catalyze the cycloaddition between an azide and an alkyne, but that the binuclear species displays enhanced catalytic performance and forms part of the kinetically favoured route (Scheme 2.4 (b)).

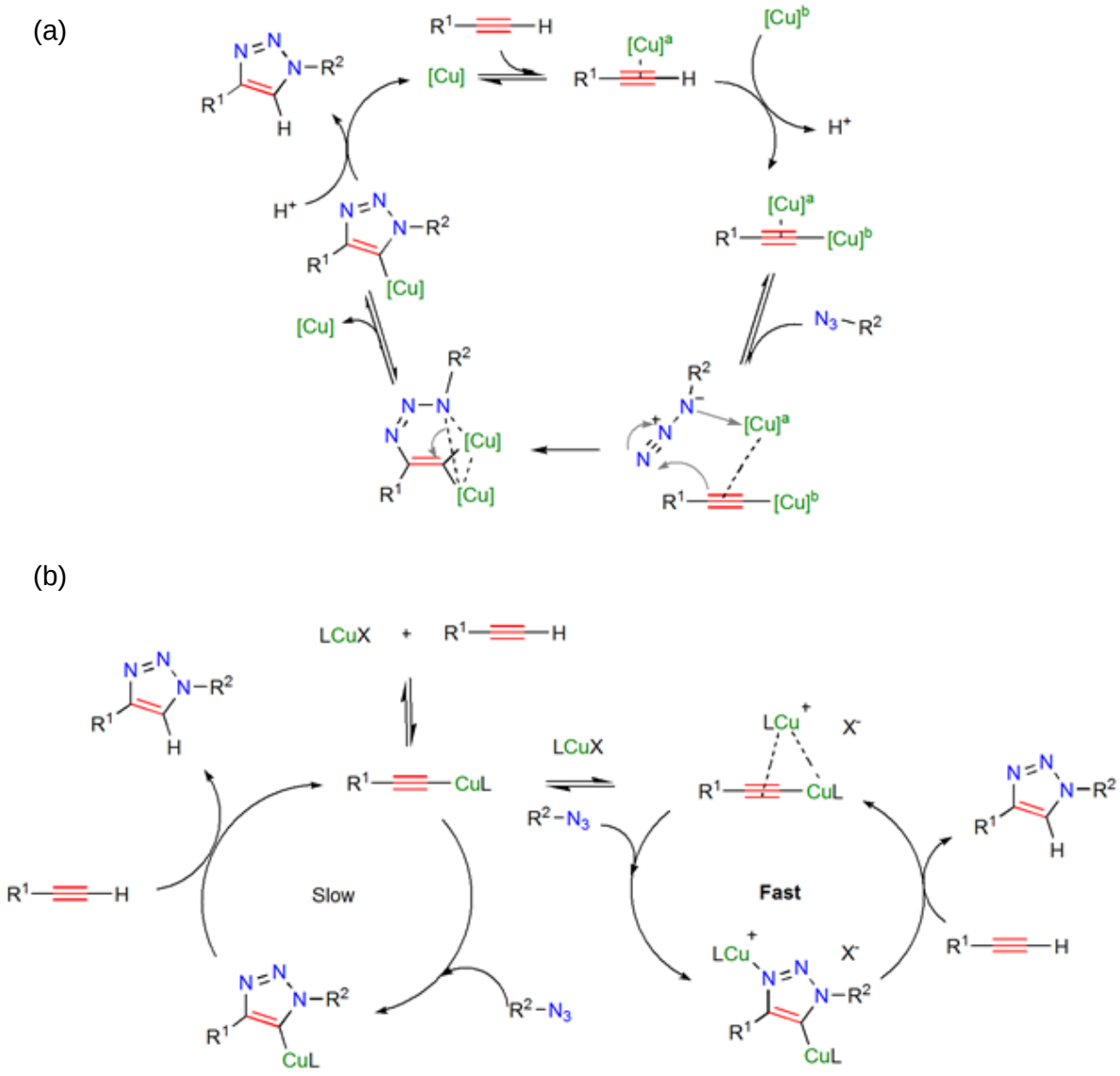

Scheme 2.4. The CuAAC mechanistic proposal done by (a) Fokin et al.,[9] and (b) Bertrand et al.[11]

To synthesize the N1, N3-diarylated triazolium salt, the product of cycloaddition must be charged, since alkylation of the triazole with an aryl group is not facile. Therefore, azides used as substrate for the synthesis of N1, N3-diarylated triazolium salts will be inefficient in obtaining the anticipated results. Instead, Jochims and Wirschun[5,6,13] incorporated 1,3-diaza-2-azoniaallene salts (**H**, Scheme 2.5) as the 1,3-dipolar nitrogen donor in cycloadditions to produce 1,2,3-diarylated triazolium salts (**I**, Scheme 2.5).

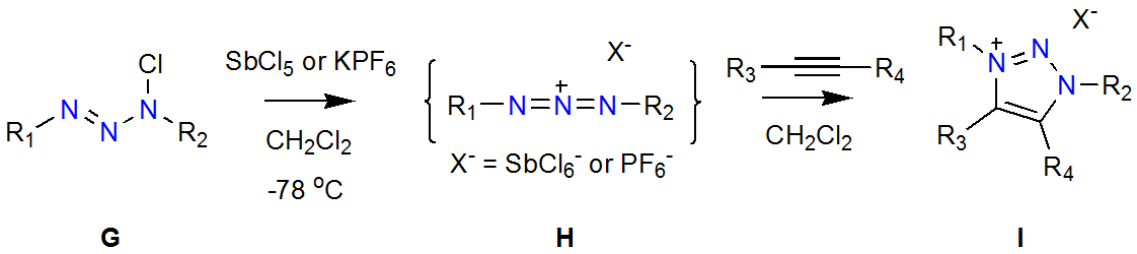

Scheme 2.5. Synthesis of diarylated-1,2,3-triazolium salts (**I**).[5]

N-chlorotriazenes (**G**, Scheme 2.5), obtained from the oxidation of 1,3-disubstituted triazene with *tert*-butyl hypochlorite, react eagerly with Lewis acids e.g. KPF_6 or $SBCl_5$, to form the corresponding 1,3-diaza-2-azoniaallene salts (**I**). These salts act as 1,3-dipoles and undergo 1,3-dipolar cycloadditions with a range of electron deficient and electron donating alkenes and alkynes to form the corresponding heterocycle.

2.2 Aim

Herein is presented the synthesis of a triarylated-1,2,3-triazolium salt substituted with a redox-active ferrocenyl moiety on C-4 (**1**, Figure 2.2). An adapted cycloaddition method reported by Jochims and Wirschun is employed,[6] resulting in diarylated wingtips on N-1 and N-3 of the triazolium. In addition, the synthesis of alkylated triazolium salts (**2**–**3**, Figure 2.2), whereby the N1 is alkylated, and variation of the aryl group on C4 (ferrocenyl (**2**) vs. phenyl (**3**)) is reported for comparative purposes. The Cu(I)-catalyzed azide-alkyne cycloaddition adapted from Huisgen's 'click'-chemistry is utilized for the synthesis of **2** and **3**. These salts will be employed as ligand precursors in subsequent chapters, for complexation to catalytically relevant metals, such as rhodium and gold.

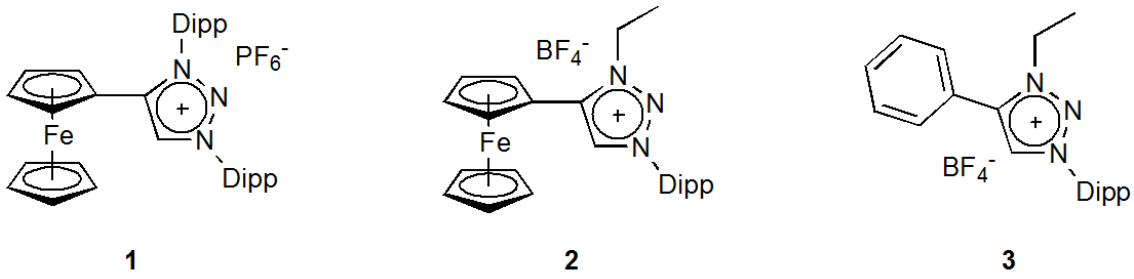

1 **2** **3**

Dipp = 2,6-diisopropylphenyl

Figure 2.2. The 1,2,3-triazolium salts as ligand precursors synthesized in this chapter.

2.3 Results and discussion

2.3.1 Synthesis and characterization of the N1, N3-diarylated ferrocenyl triazolium salt (**1**):

The synthesis of the 1,3-diarylated-ferrocenyl triazolium salt (**1**, Scheme 2.6) followed the adapted cycloaddition method, originally done by Jochims and Wurschin[6] in 1998, and modified by Bertrand and co-workers[4] in 2011 to synthesize diarylated triazolium salts. The synthesis requires the addition of 1,3-diarylated triazenes to substituted alkynes, in the presence of a Lewis acid and an oxidant to afford the respective heterocycle.

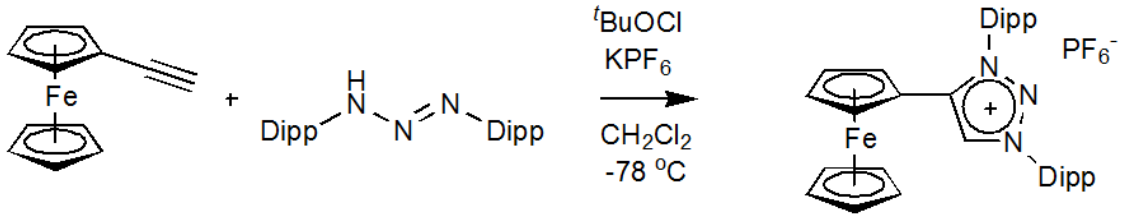

Dipp = 2,6-diisopropylphenyl

1 (85%)

Scheme 2.6. The synthesis of N1, N3-diarylated ferrocenyl triazolium salt (**1**).

The synthesis of **1**, involved the cycloaddition of ethynylferrocene and 1,3-bis(2,6-diisopropylphenyl)triazene. The diarylated triazene was oxidized to an unstable open-chain *N*-chloro-triazene by *tert*-butylhypochlorite, which in turn reacted readily with the Lewis acid, KPF_6. The *N*-chloro-triazenes have reported decomposition temperatures between -60 °C to 0 °C, thus the reaction temperature was set at -78 °C. For cycloaddition to be successful, the chlorination of the triazene should occur in the presence of both the Lewis acid

and the alkyne. Once the diarylated azoniallene salt was formed, the cycloaddition with ethynylferrocene took place in good yield. The reaction was quenched by filtration of excess potassium salts, and the filtrate was dried under reduced pressure. The dark brown solid was triturated with hexane, where a light brown solid precipitated out. Further purification of the light brown solid by washings with ether afforded the triazolium salt, **1** as an orange powder in 85% yield.

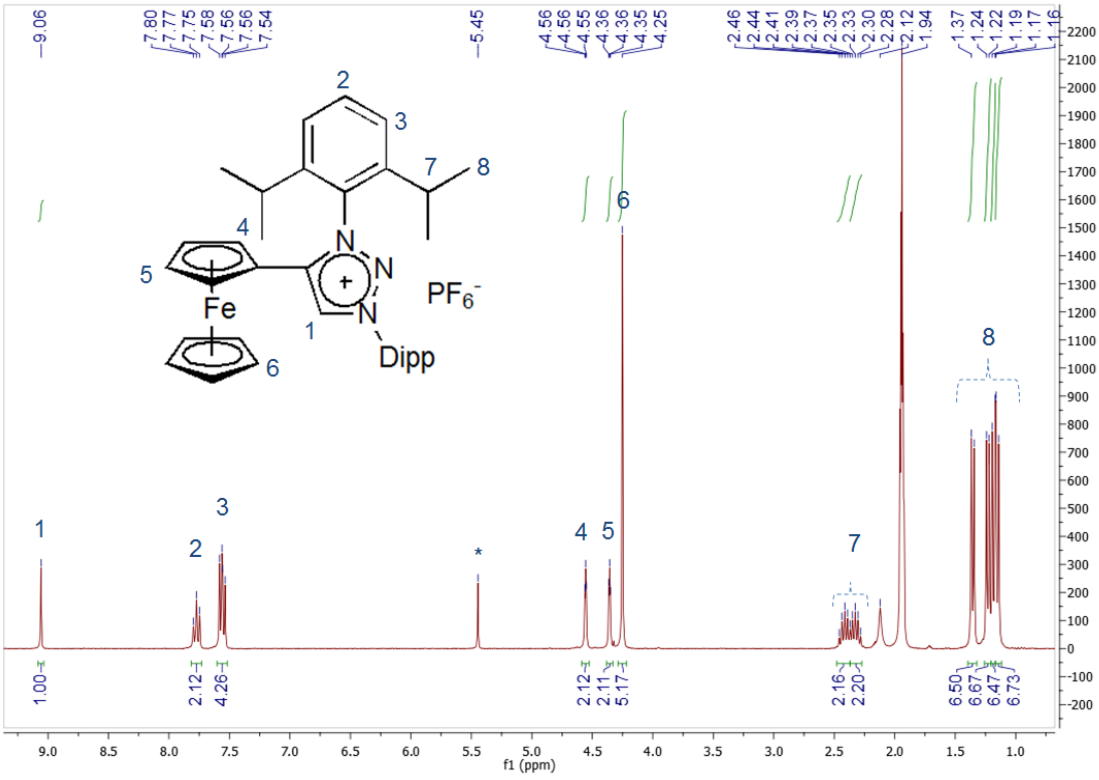

Figure 2.3. ^{1}H NMR spectrum of the N1, N3-diaryl-ferrocenyl triazolium salt (**1**) in solvent CD_3CN.

The chemical shift of the acidic triazolium ring proton of **1** was observed at 9.06 ppm in solvent CD_3CN (Figure 2.3), which corresponds to other diarylated triazolium rings, with an arylated substituent on C4. Bertrand[4] reported the acidic protons of the C4-phenyl, -mesityl and -dipp analogs, at 9.17, 9.11, 9.02 ppm in solvent CD_3CN, respectively. Single crystals suitable for X-ray diffraction was obtained by dissolving **1** (Figure 2.4) in minimum dichloromethane (DCM), followed by a layer of toluene. The wingtips (2,6-diisopropylphenyl) are orientated at approximately 120° with respect to each other, and the ferrocenyl

substituent lies 15° out of plane in terms of the triazole ring. Bond lengths of the triazole vary between 1.328–1.383 Å, alongside a C1-C2-N1 bond angle of 106(19)°, which corresponds well to other reported salts.[1,4] The bond angle is expected to decrease with deprotonation to form the corresponding carbene, which is indicative of increased s-character on σ-lone pair orbital of the carbene.[1]

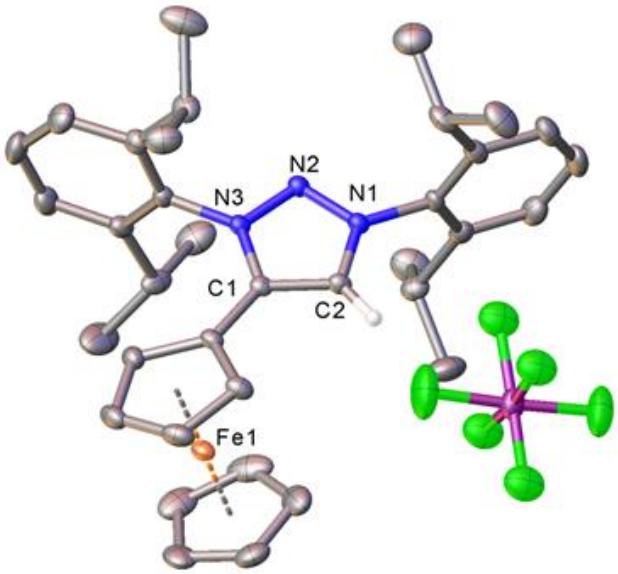

Figure 2.4. Molecular structure of triazolium salt, **1** showing 50% probability ellipsoids and partial atom-numbering scheme. Selected bond lengths (Å) and angles (°) for **1**: N1–N2 1.328(3); N1–C2 1.348(3); N2–N3 1.338(3); N3–C1 1.369(3); C1–C2 1.383(3); N1–C2–C1 106.00(19).

2.3.2 Synthesis and characterization of N1-aryl-, N3-alkylated triazolium salts (**2**,**3**)

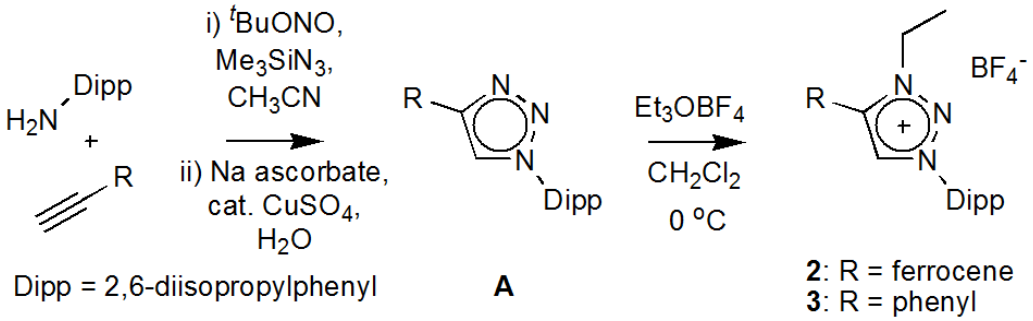

Scheme 2.7. The synthesis of 1-aryl, 3-alkylated triazolium salts, **2** and **3**.

The synthesis of the N3-alkylated salts, **2** and **3** required a two-step procedure whereby azide-alkyne cycloaddition was followed by alkylation with triethyloxonium tetrafluoroborate (Scheme 2.7). The cycloaddition reaction was originally reported by Moses et al.,[2] and allows for the azide-alkyne cycloaddition to take place in one-pot directly from the amine without the isolation of the respective azide. This reduces the handling of hazardous chemicals, such as NaN_3 and increases the ease of access to these triazolium salts; an important feature to consider when designing pre-catalysts.

The organic azide, in this case 2,6-diisopropylphenyl azide (dipp-N_3), was synthesized *in situ* from dipp-aniline (2,6-diisopropylphenylaniline), *tert*-butyl nitrite and azide trimethylsilane, as a non-hazardous alternative to the explosive NaN_3 and TfN_3 used in previously reported methods.[2] The reaction took place at 0 °C, for one hour –illustrating the efficiency of the reaction even at very mild conditions. After the addition of the alkyne along with the Cu(II) salt and the sodium ascorbate (which operates as the reducing agent to generate Cu(I)). The reduction of Cu(II) *in situ* was proved more effective and yielded purer products than using Cu(I) salts from the start.[14]

Even though high yields and excellent functional group compatibility were reported by Moses et al.[2] from the one-pot cycloaddition executed directly from the respective anilines, this cannot be translated for the synthesis carried out to afford the ferrocenyl -and phenyl triazole. The yield obtained were as low as 10-18%, in both cases. This was rectified however, by isolating the diisopropylphenyl-azide as a colourless oil by using the same method described by Moses et al.,[2] and then only adding the alkyne, with the Cu(I) salts, and sodium ascorbate to the azide to undergo azide-alkyne cycloaddition. The yields improved to 49% and 46% for the ferrocenyl- and phenyl triazole respectively as no flash chromatography was required.

After the synthesis of the triazole with CuAAC, alkylation with triethyloxonium salt afforded the respective triazolium salts, **2** and **3**. The reaction is exothermic in nature and required low temperatures of -20 °C to 0 °C to take place, after which the reaction mixture was left to warm up to room temperature overnight. The solvent was evaporated under reduced pressure and the solid was

dissolved in minimum ethyl acetate. The addition of diethyl ether aided the precipitation of the purified salts, both in quantitative yield.

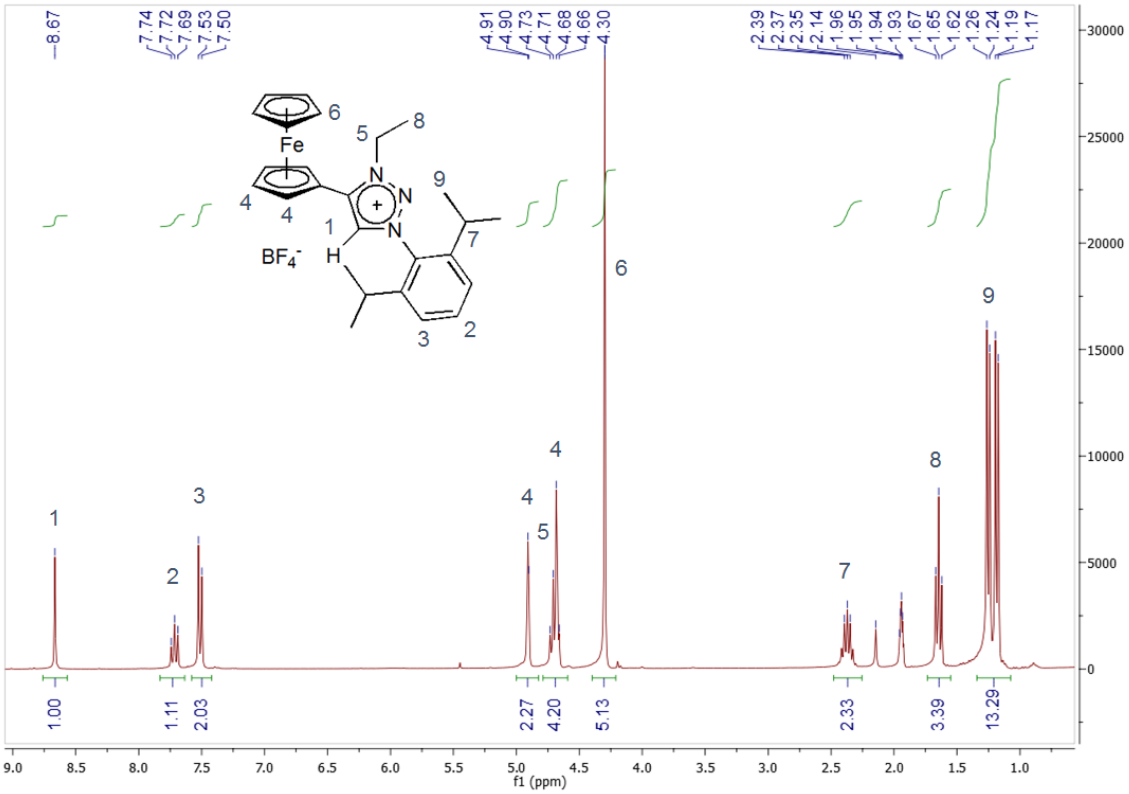

Figure 2.5. ^{1}H NMR spectrum of N1-aryl, N3-ethyl-ferrocenyl triazolium salt (**2**) in solvent CD_3CN.

The acidic triazolium ring proton of **2** and **3** resonated at very similar frequencies, namely 8.67 ppm (Figure 2.5) and 8.66 ppm (Figure 8.7, Chapter 8) in solvent CD_3CN, respectively. These values corresponded well with previously reported triazolium salt acidic protons; for example, the chemical shift of an analogous ferrocenyl-triazolium salt ring proton, with a methyl group instead of an ethyl on the N3-position, was reported by Sarkar[15] at 8.53 ppm in CD_2Cl_2. For other triazolium salts that contain a phenyl substituent on C4, such as **3**, alkylated on N3 with methyl -and isopropyl groups had ring protons reported at 8.62 and 8.81 ppm in CD_3Cl, respectively.[1]

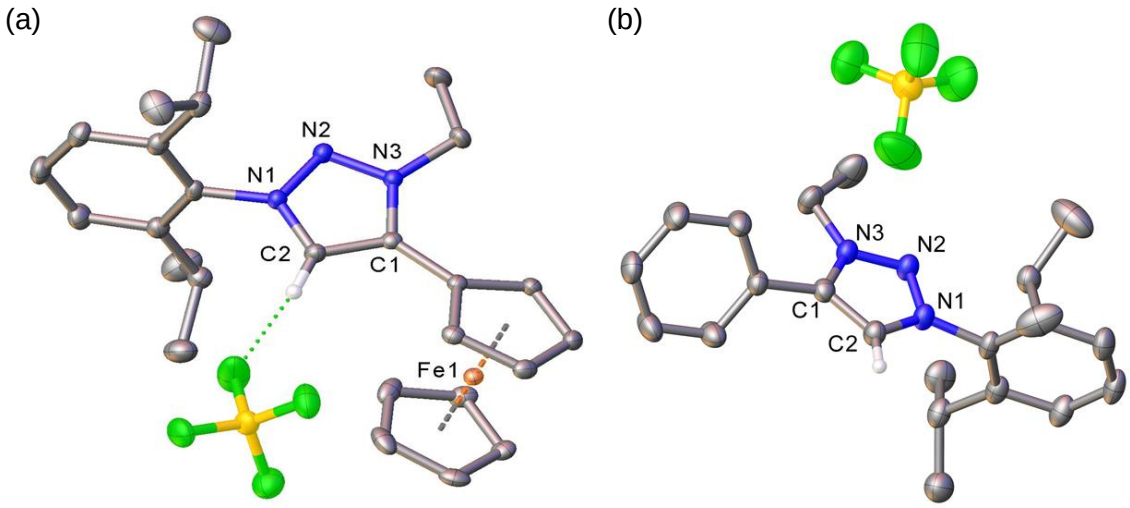

Figure 2.6. Molecular structure of triazolium salt, (a) **2** and (b) **3**, showing 50% probability ellipsoids and partial atom-numbering scheme. Selected bond lengths (Å) and bond angles (°) for **2**: N1–N2 1.326 (17); N1–C2 1.350 (17); N2–N3 1.329 (15); N3–C1 1.364 (17); C1–C2 1.376 (18); N1–C2–C1 105.70 (11). For **3**: N1–N2 1.325 (19); N1–C2 1.355 (2); N2–N3 1.316 (18); N3–C1 1.363 (2); C1–C2 1.368 (2); N1–C2–C1 105.45 (14).

Suitable single crystals for X-ray diffraction of **2** and **3** were obtained from a saturated DCM solution of the precursor salt, layered with toluene, and is shown in Figure 2.6. The triazolium ring bond lengths for **2** and **3** are between 1.326–1.376 Å and 1.316–1.368 Å respectively, and are within the reported ranges.[1] The triazolium bond lengths for **1**, were reported as 1.328–1.383 Å and an observable trend is seen, where the bond lengths decrease from **1** > **2** > **3**. The bond angle (N1–C2–C1) also decrease slightly following the similar trend, **1** (106.00°(19)) > **2** (105.70(11)°) > **3** (105.45(14)°).

From the experimental spectroscopic observation for **2** and **3**, and comparison with literature examples, the effect of the ferrocenyl C4-substituent, known to be a donating aryl substituent (both by π-resonance and inductive effects),[16] is negligible compared to the phenyl C4-substituent. However, it seems that the nature of the N3-substituent has a more pronounced effect on the triazole ring electronics: the N3-aryl triazolium salt, **1** with the triazolium ring proton resonance of 9.06 ppm, as well as the reported literature values for other Fc-functionalized triazolium, ranging from 9.02–9.17 ppm,[4] is more downfield compared to the alkyl-N3 triazolium salts, ranging from 8.53–8.81 ppm.[1,15]

2.4 Conclusion

The synthesis and characterization of precursor ligand salts, 1–3 were carried out successfully. For the synthesis of 1, the N1, N3-diarylated triazolium salt, the one-pot cycloaddition was used, whereas the popular CuAAC route were employed for the synthesis of the N3-alkylated salts, **2** and **3**. Minor alterations of the published methods were executed for optimal yield of the triazole precursors. Evidence obtained from NMR experiments, indicates that the substituent on N3 has a more significant effect on the electronics (aryl vs. alkyl) rather than the substituent of C4 (metal vs. non-metal-containing moiety).

2.5 References

1 G. Guisado-Barrios, J. Bouffard, B. Donnadieu and G. Bertrand, *Angew. Chem. Int. Ed.*, 2010, **49**, 4759–4762.

2 K. Barral, A. D. Moorhouse and J. E. Moses, *Org. Lett.*, 2007, **9**, 1809–1811.

3 K. F. Donnelly, A. Petronilho and M. Albrecht, *Chem. Comm.*, 2013, **49**, 1145–59.

4 J. Bouffard, B. K. Keitz, R. Tonner, V. Lavallo, G. Guisado-Barrios, G. Frenking, R. H. Grubbs and G. Bertrand, *Organometallics*, 2011, **30**, 2617–2627.

5 W. Wirschun, M. Winkler, K. Lutz and J. C. Jochims, *J. Chem. Soc. Perkin Trans. 1*, 1998, 1755–1762.

6 N. Al-Masoudi, N. A. Hassan, Y. A. Al-Soud, P. Schmidt, A. E. M. Gaafar, M. Weng, S. Marino, A. Schoch, A. Amer and J. C. Jochims, *J. Chem. Soc. Perkin Trans. 1*, 1998, 947–954.

7 R. Huisgen, *Angew. Chem. Int. Ed.* , 1963, **2**, 565–598.

8 R. Huisgen, *Angew. Chem. Int. Ed.* , 1963, **2**, 633–645.

9 V. V. Rostovtsev, L. G. Green, V. V. Fokin and K. B. Sharpless, *Angew. Chem.*, 2002, **114**, 2708–2711.

10 C. W. Tornøe, C. Christensen and M. Meldal, *J. Org. Chem.*, 2002, **67**, 3057–3064.

11 L. Jin, D. R. Tolentino, M. Melaimi and G. Bertrand, *Sci. Adv.*, 2015, **1**, e1500304

12 B. T. Worrell, J. A. Malik and V. V. Fokin, *Science*, 2013, **340**, 457–460.

13 W. Wirschun, *J. Prakt. Chemie.*, 1998, **340**, 300–308.

14 V. D. Bock, H. Hiemstra and J. H. Van Maarseveen, *Eur. J. Org. Chem.*, 2006, 51–68.

15 L. Hettmanczyk, S. Manck, C. Hoyer, S. Hohloch and B. Sarkar, *Chem. Comm.*, 2015, **51**, 10949–10952.

16 J. A. Connor and J. P. Lloyd, *J. Chem. Soc., Dalton Trans.*, 1972, 1470–1476.

Chapter 3

Synthesis of rhodium(I) triazolylidene complexes

3.1 Background

The first accounts of abnormal NHCs (*a*NHCs) were reports of metal complexes prepared with an abnormally bound NHC ligand, based on an imidazolylidene coordinated to the metal at the C5 position (J, Scheme 1.2, see Chapter 1).[1] Albrecht synthesized the first abnormal 1,2,3-triazolylidene complexes, coordinated to but not restricted to palladium(II) (Scheme 3.1, B),[2] since the silver(I) (C), ruthenium(II) (D), rhodium(I) (E) and iridium(I) (F) metal centers were reported concurrently.

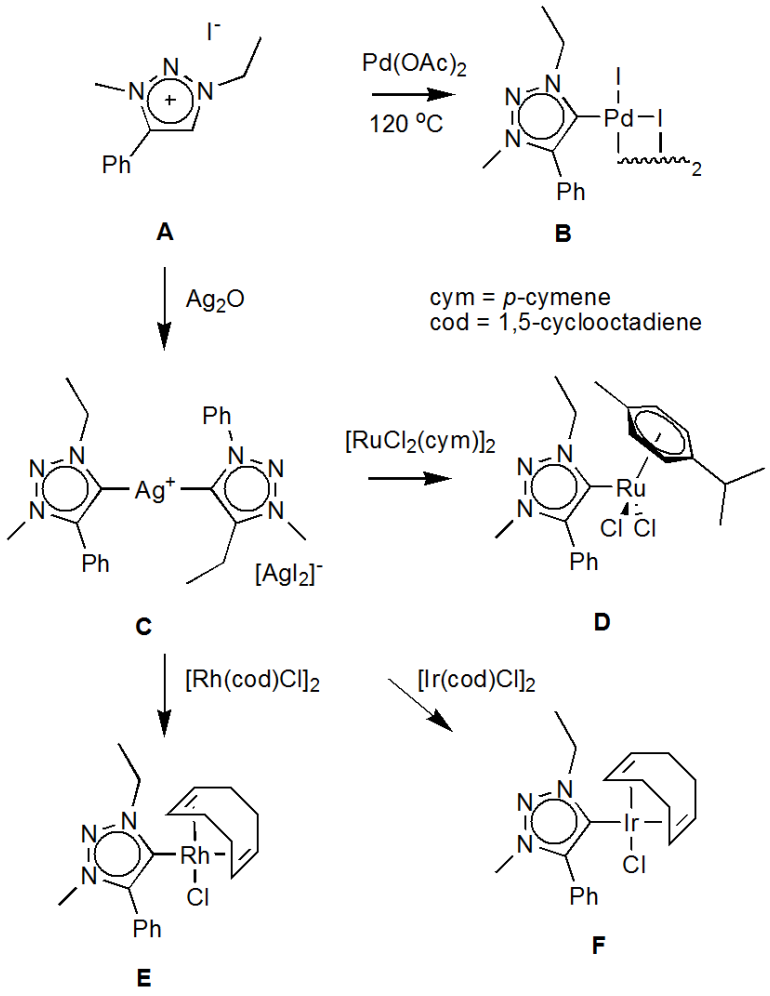

Scheme 3.1. The synthesis of the first reported 1,2,3-triazolylidene complexes.[2]

The syntheses of the *a*NHC complexes **B**–**F** were either achieved by direct metalation of triazolium precursor **A** with palladium(II) acetate (**B**)[3,4] , by means of thermally induced C-H activation, or via transmetalation from the silver(I) carbene intermediate, **C** (**E**–**G**). These indirect synthetic strategies were employed because the free *a*NHCs were deemed too unstable to isolate, with decomposition occurring especially under thermal conditions.[5] The transmetalation route is a highly successful synthetic route provided that the correct metal precursor is used, e.g. $[Rh(cod)Cl]_2$. Such metal precursor complexes with labile halide (X) ligands are especially efficient during transmetalation/carbene transfer from the silver carbene intermediate, as the formation and precipitation of AgX(s) is thermodynamically favored.[6,7] Although this synthetic route is limited since light metals such as iron, manganese and cobalt, are inert towards transmetalation, this route still remains one of the most widely employed routes due to the ease of access and product selectivity obtained.[8]

When the isolation of the first free *a*NHC was published in 2009,[9] as well as the first free triazolylidene (**G**, Scheme 3.2) were achieved in 2010,[10] coordination directly to the free carbene became a viable synthetic route for metal complexes. In both cases, the precursor salt was deprotonated with a strong non-nucleophilic base to generate the free carbene, which can either be isolated or reacted further *in situ* with an appropriate metal precursor (Scheme 3.2) as a versatile alternative to transmetalation approaches.[6]

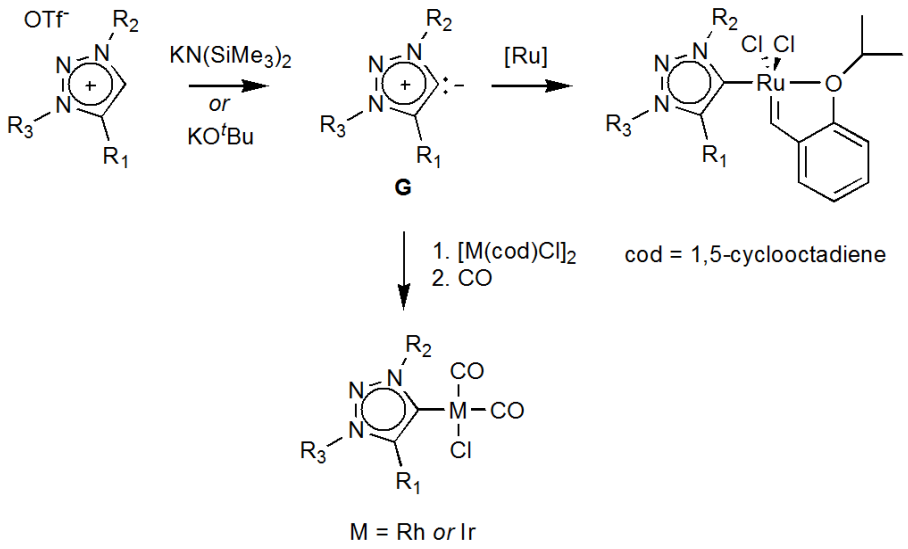

Scheme 3.2. Preparation of triazolylidene metal complexes by coordination of the free carbene, **G**.[6,10,11]

In order for deprotonation to occur at C5 to form the imidazole-5-ylidene (*a*NHC) blocking of the C2 position is essential, since the proton on C2 is the most acidic proton present. For triazol-based *a*NHCs, this blocking step is redundant as the ring-2 position is a N-atom..[2,6,10] Even though this route seems more favourable to use for the synthesis of triazolylidene complexes, especially since the scope for metals have widen *vs.* the transmetalation approach, not all triazolium salts yield the corresponding free carbene once deprotonated.[10] N1- and N3-diarylated triazolium salts, as previously mentioned, are more stable and hence form the free carbene when treated with KO^{t}Bu (pK_a = 22).[6,11] When N3 is alkylated, a stronger base is required (e.g. $KN(SiMe_3)_2$ (pK_a = 26)), but migration of the alkyl group can still occur especially when a weaker base is used along with warmer conditions (Scheme 3.3 (a)). When both N1 and N3 are alkylated, the free carbene does not form and instead undergoes *N*-dealkylation (Scheme 3.3 (b)).[10] Thus, for coordination of the free carbene to be successful, robust carbenes that have longer lifetimes (kinetically stable) are required.[12]

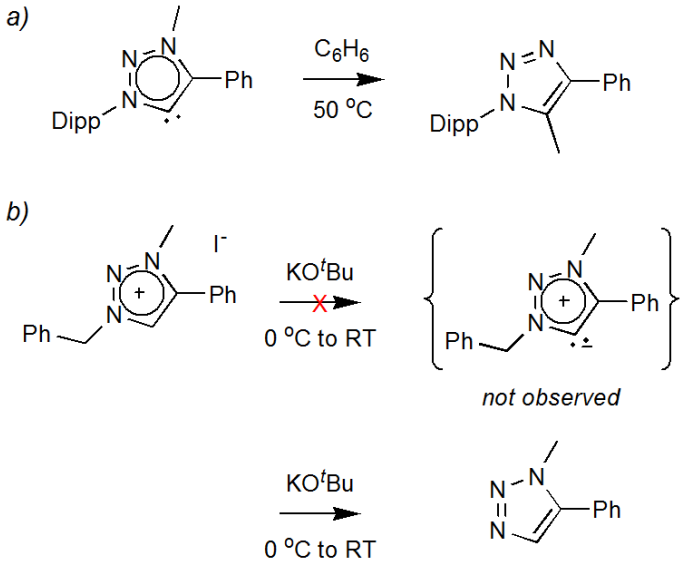

Scheme 3.3. N-dealkylation of (a) N3-alkylated triazolium salts and (b) N1 -and N3-alkylated triazolium salts (b).[6,10]

Base-mediated C-H activation has shown to be a successful metalation technique especially for dialkylated triazolium salts, and was reported by the groups of Sarkar[13] and Bertrand.[12] The synthetic route involves a one-pot metalation containing the triazolium salt, base for deprotonation and the metal precursor, Scheme 3.4. There is little evidence in distinguishing this route from coordination to the free carbene or C-H activation via the possible *in situ* generation of the M(O^{t}Bu) intermediate.[6]

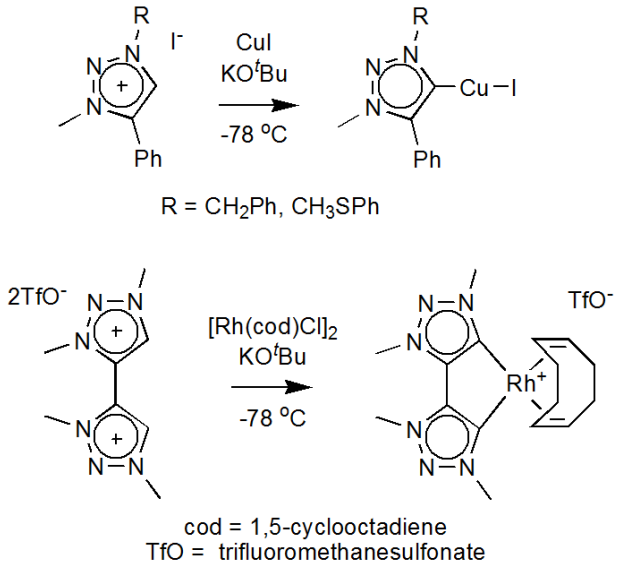

Scheme 3.4. Triazolylidene complexes prepared via base-mediated C-H activation.[12,13]

Rhodium(I) is a π-basic metal, which enables coordination to π-ligands such as 1,5-cyclooctadiene (cod) and CO. In addition, the presence of a donating carbene scaffold (with limited π-accepting ability) should further enhance the back-donation capabilities of the metal.[14,15] In rhodium(I) cod complexes, the rhodium metal bonds to both alkenes of the cod, in a bidentate fashion, forcing *cis*-geometry. The donation of electrons originates from the C=C π-electrons into an empty metal d_σ orbital. Back donation from the metal d_π-orbital into the ligands LUMO (π*) (lowest unoccupied molecular orbital), creates a delocalized 2-electron, 3-centre ($2e^-$,3c) bond between the metal and olefin carbons. Carbonyl ligands are even stronger π-accepting ligands as the empty π^*-orbital (LUMO) is located on the *sp*-hybridized carbon of the carbonyl ligand, and receives electrons via backbonding from the HOMO (highest occupied molecular orbital) of the metal (Md_π). However, the σ-bond between the metal and the carbonyl is formed due to the donation of the carbon lone-pair (*sp*-orbital, HOMO) to the LUMO (Md_σ) of the metal.

Coordination of carbonyl ligands to carbene metal complexes have been used as a strategy to investigate the donor ability of the carbene (L), by examining the stretching frequencies of the C–O bond of the carbonyl through IR (infrared) spectroscopy. The M-C π-bond is formed at a cost to the C=O π-bond. As the

metal donates back into the antibonding (*π**) orbital of the carbonyl, the C-O bond order decreases. Less energy is required to stretch the C-O bond, and a lower stretching frequency will be measured. Thus, lower IR frequencies of the C=O bond is indicative of how strongly the metal is able to back-bond, and therefore how strong L is donating towards the metal-center.[14,15]

Employing an averaged CO frequency to determine the donating ability of ligand L is also known as Tolman's electronic parameter (TEP) and was originally calculated for L coordinated as $[Ni(CO)_3L]$.[16] The use of nickel tricarbonyl complexes for TEP calculations proved to be troublesome due to their toxicity and instability, and other metal complexes such as $[RhCl(CO)_2L]$ (Equation 3.1) and $[IrCl(CO)_2L]$ have replaced the model $[Ni(CO)_3L]$.[17,18] The TEP allows for direct and complete comparison of systems of L, whether L is a NHC or a phosphorus ligand etc., provided that the IR spectroscopy measurements was carried out under constant conditions and either nickel, iridium or rhodium was used.

$$\text{TEP (cm}^{-1}\text{) [Rh to Ni]} = 0.8001\tilde{\nu}_{CO}^{av/Rh}\,(\text{cm}^{-1}) + 420.0\,(\text{cm}^{-1}) \quad \textit{... (3.1)}$$

3.2 Aim

In the preceding chapter, the syntheses of the precursor triazolium salts were discussed. In this chapter, the coordination of the triazolylidene ligands (generated from the precursor salts) will be coordinated to rhodium(I) using either the base-mediated C-H activation or free carbene approach. The complexes will bear the *π*-donating cod co-ligands (rhodium(I) complexes **4**–**6**, Figure 3.1), which are also to be substituted with *π*-accepting carbonyl ligands (rhodium(I) dicarbonyl complexes **7**–**9**, Figure 3.1).

The electronic properties of each carbene is evaluated with the calculation of TEP,[16] derived from the carbonyl stretching vibrations obtained from infrared spectroscopy analysis.

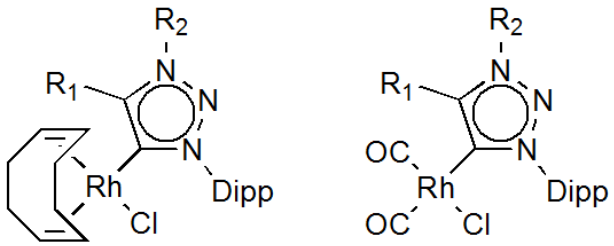

4: R_1 = Fc, R_2 = Dipp **7**: R_1 = Fc, R_2 = Dipp

5: R_1 = Fc, R_2 = Ethyl **8**: R_1 = Fc, R_2 = Ethyl

6: R_1 = Ph, R_2 = Ethyl **9**: R_1 = Ph, R_2 = Ethyl

Dipp = 2,6-diisopropylphenyl

Figure 3.1. The rhodium(I) triazolylidene complexes reported in this chapter.

3.3 Results and discussion

3.3.1 Synthesis and characterization of the N1-, N3-diarylated triazolylidene rhodium(I) complexes, **4** and **7**.

Complex **4** was prepared by the reaction of the *in situ* generated free carbene from triazolium precursor **1** (Scheme 3.5) with the appropriate rhodium(I) precursor $[Rh(cod)Cl]_2$.

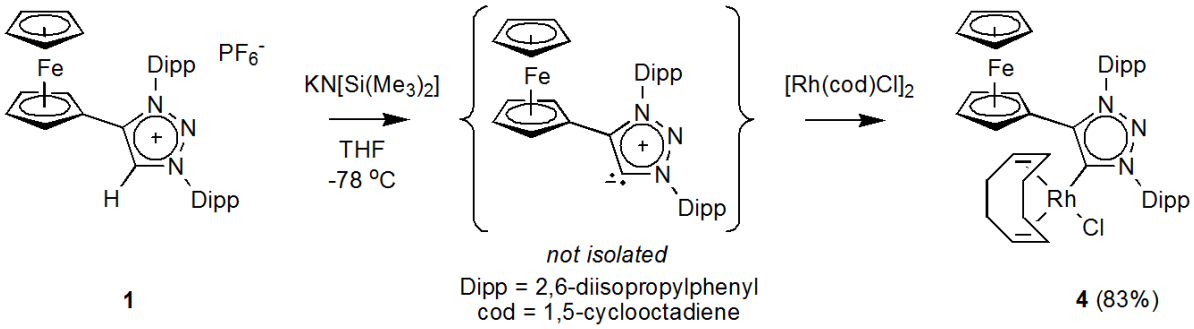

not isolated

Dipp = 2,6-diisopropylphenyl
cod = 1,5-cyclooctadiene

1 **4** (83%)

Scheme 3.5. Metalation of **1**, from the *in-situ* generation of the free carbene, with rhodium(I) to afford complex **4**.

The synthesis involves the deprotonation of the acidic C5-H of the ligand precursor salt[7,9] with a strong non-nucleophilic base, $KN[Si(Me)_3]_2$. The reaction was performed at low temperature (-78 °C), as the decomposition temperature of the free carbene is not known. The orange solution turned dark red, thereby indicating that deprotonation was successful, and the reaction towards the precursor, $[Rh(cod)Cl]_2$, was ready to proceed. The red solution turned brown

overnight as it was permitted to reach room temperature. The solvent was removed under reduced pressure and washed with hexane, to remove the unreacted rhodium(I)-precursor. In previously reported syntheses for neutral triazolylidene metal complexes, the corresponding complexes were extracted with diethyl ether.[19,20] Complex **4**, which is neutral, proved only marginally soluble in diethyl ether and was more efficiently extracted with toluene. The difference in solubility can be attributed to the metal-containing substituent, ferrocene, on the C4 position.

Evidence of the formation of complex **4** was verified by the ^{1}H NMR spectrum (Figure 3.2) with the disappearance of the acidic triazolium proton peak of **1** at 9.06 ppm (Figure 2.3, *see Chapter 2*) and the appearance of the rhodium(I)-carbene signal (doublet) at 171.9 ppm, with a coupling constant of J = 46.6 Hz in the ^{13}C NMR spectrum (Figure 3.3)

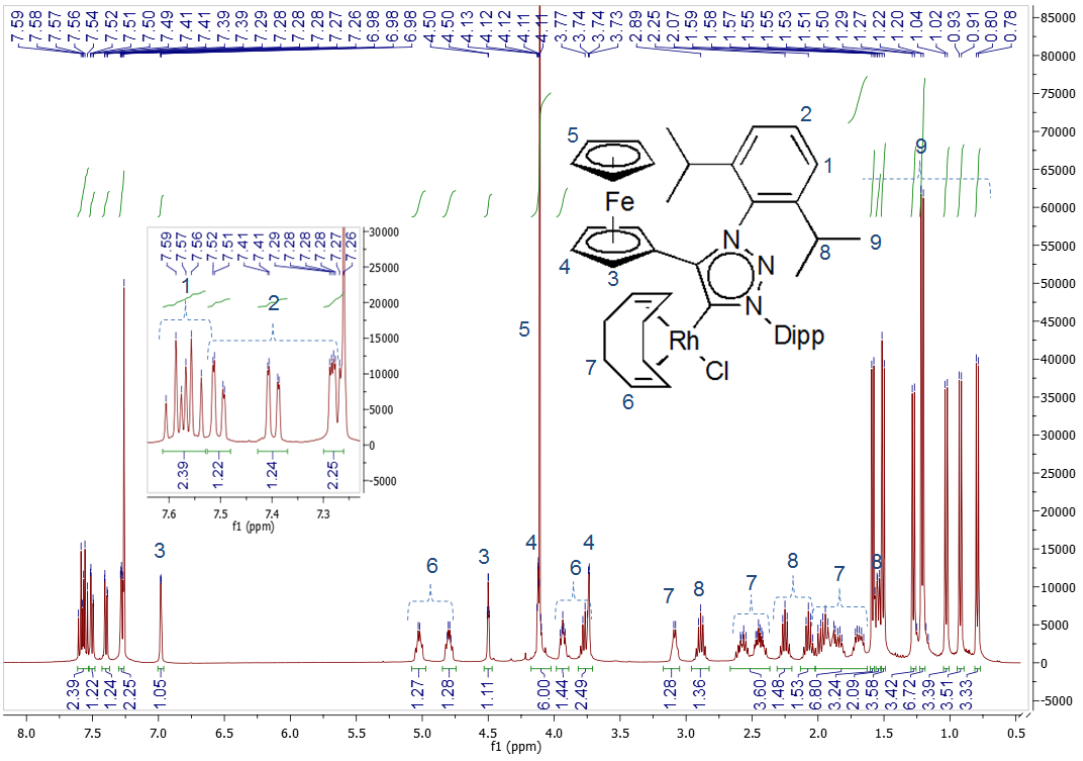

Figure 3.2. The ^{1}H NMR spectrum of complex **4** in solvent $CDCl_3$.

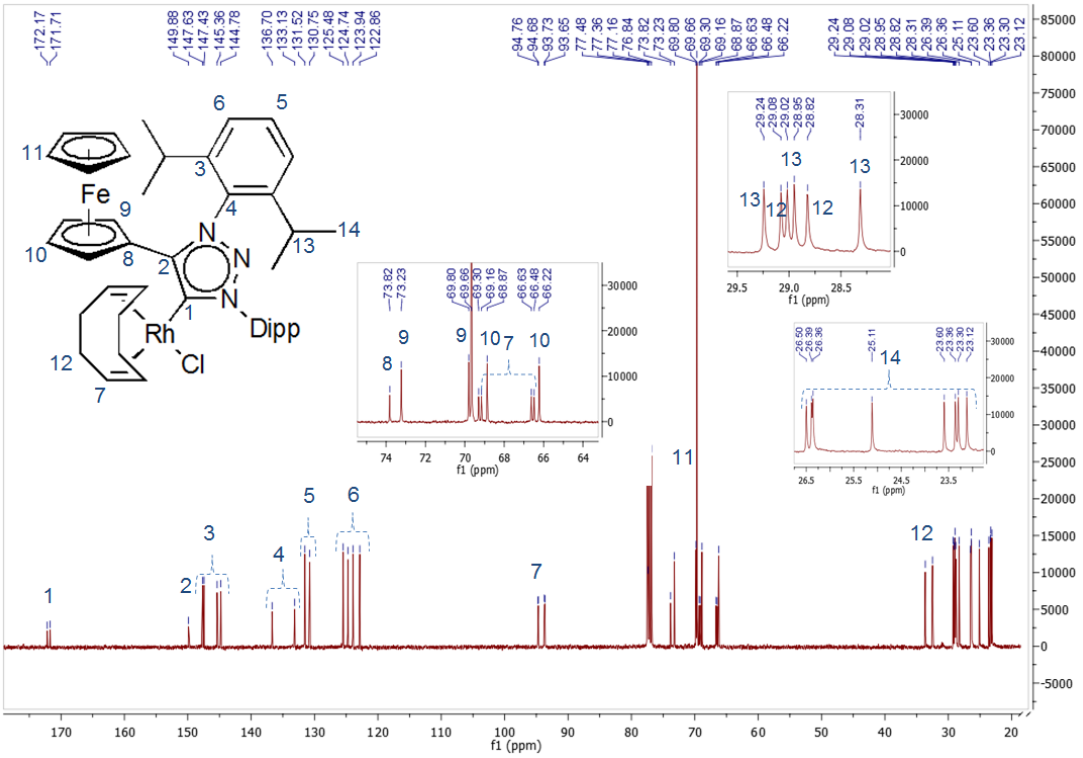

Figure 3.3. The ^{13}C NMR spectrum of complex **4** in solvent $CDCl_3$

The pronounced influence of the asymmetric coordination sphere around the rhodium(I) metal on the chemical environment of the triazolylidene ligand was demonstrated in both the ^{1}H and ^{13}C NMR spectra. Separate resonances for each individual carbon were observed in the ^{13}C NMR spectrum. Similarly, individual proton resonances are observed for each of the substituted cyclopentadienyl ring protons of the ferrocenyl substituent in the ^{1}H NMR spectrum. The far downfield shift of one of the ferrocenyl protons (α-proton H4) at 6.98 ppm was surprising (confirmed by HSQC, Figure 8.12, see Chapter 8), and prompted further investigation into the structural properties of the complex.

Crystals suitable for X-ray diffraction were already observed growing in the NMR test tube, after an overnight ^{13}C NMR experiment. In the molecular structure of **4** (Figure 3.4 (a)), the distance between the ferrocenyl α-proton and the rhodium(I) metal center was found to be only 2.783 Å; much shorter than the average distance found of all the other ferrocenyl protons (5.889 Å). The proximity to the Rh(I) therefore explains the unusual low-field shift of this Fc' proton. Furthermore, the crystal structure of the complex showed that the rhodium(I) complex is square planar with bond angles around the metal center

of 87.22(6)–91.45(7) Å. The carbene bond angle (N3-C1-C2) is 101.40(17)°, which decreased from the 106(19)° (triazolium salt, **1**) as expected[10] and the carbene bond length is 2.059(2) Å. Coordination of the cod ligand is further confirmed by the increased alkene bond length to 1.404(4) Å (C28–C29) and 1.385(4) Å (C32–33) relative to the free alkene bond length (1.337 Å)[14,15] and the triazolium ring bond lengths become intermediate between single (1.370(3) Å, 1.375(3) Å, 1.403(3) Å) and double bonds (1.328(3) Å, 1.335(2) Å); an indication of electron delocalization.[10]

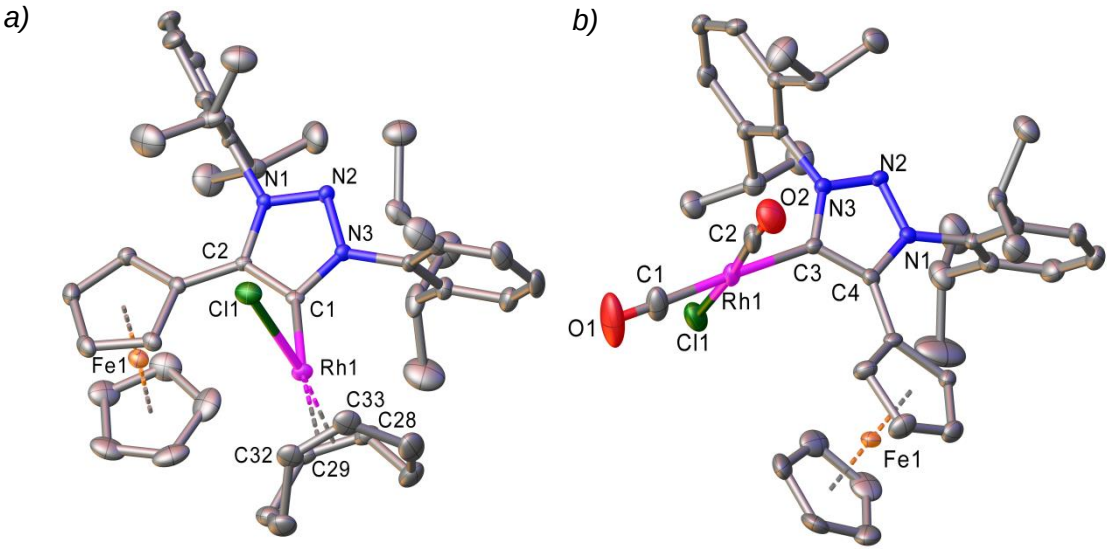

Figure 3.4. Molecular structures of triazolium rhodium(I) complexes, **4** and **7,** showing 50% probability ellipsoids and partial atom-numbering scheme. Selected bond lengths (Å) and angles (°) for **4**: C1–Rh1 2.059(2); N1–N2 1.328(3); N1–C2 1.370(3); N2–N3 1.335(2); N3–C1 1.375(3); C1–C2 1.403(3); N3–C1–C2 101.40(17). C1–Rh1–Cl1 87.22(6). For **7**: Rh1–C3 2.079(4); Rh1–C1 1.896(5); Rh1–C2 1.868(15); N1–N2 1.335(4); N1–C4 1.376(); N2–N3 1.334(4); N3–C3 1.375(5); C3–C4 1.393(5); N3–C3–C4 102.50(3). C3–Rh1–Cl1 90.80(12). Hydrogens are omitted for clarity.

The corresponding carbonyl complex, **7** was obtained by bubbling CO (g) through a solution of **4** in DCM at room temperature for approximately 5 minutes.[21] The cod ligand is easily displaced by two π-accepting carbonyl ligands. Washing with hexane, to rid the reaction mixture of free cod, afforded the bright orange solid (**7)** in quantitative yield (Scheme 3.6).

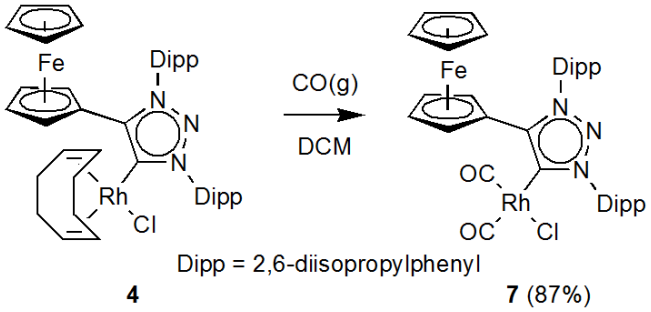

Scheme 3.6. The synthesis of complex **7** from **4**.

Evidence of the formation of complex **7**, i.e. the substitution of the cod by two carbonyl ligands, was found in the disappearance of the cod-ligand signals in both the ^{1}H NMR (Figure 3.5) and ^{13}C NMR (Figure 3.6) spectra, along with the appearance of two carbonyl doublet resonances at 186.1 ppm (J_{RhC} = 54.5 Hz, *trans* to carbene) and 184.5 ppm (J_{RhC} = 74.8 Hz, *trans* to the chlorido) and a new carbene doublet at 165.8 ppm (J_{RhC} = 44.8 Hz), respectively. Again, the steric influence of the triazolylidene substituents resulted in an asymmetric coordination sphere around the Rh(I) center with subsequent loss of symmetry observed in the NMR spectra. The principle difference between the ^{13}C NMR spectra of both complexes, **4** and **7**, is the shift (Δ = 6 ppm) of the carbene signal, with the carbene signal of **4** more downfield than **7**, indicating less efficient shielding of the carbene carbon atom by the cod-substituted Rh-complex. This has been observed with complex **E** (Scheme 3.1) with a shift of approx. 10 ppm.[2]

The Rh-$C_{carbene}$ coupling constant of **7** is only slightly smaller (**7**: J = 44.8 Hz vs. **4**: J = 46.6 Hz) than **4**. The CO-ligand has a stronger *trans* influence than the olefin (cod), which results in a smaller coupling constant for the carbene.[2,22,23] Since the carbene is a stronger σ-donor than the chlorido ligand, the carbene will have a higher *trans* effect on the CO *trans* to the carbene, than what the CO ligand experience from the *trans* chlorido ligand. Therefore, the Rh-$C_{carbonyl}$ coupling constant of the CO-ligand *trans* to the carbene is smaller (J = 54.5 Hz) than the CO-ligand *trans* to the chlorido (J = 74.8 Hz).[14,22]

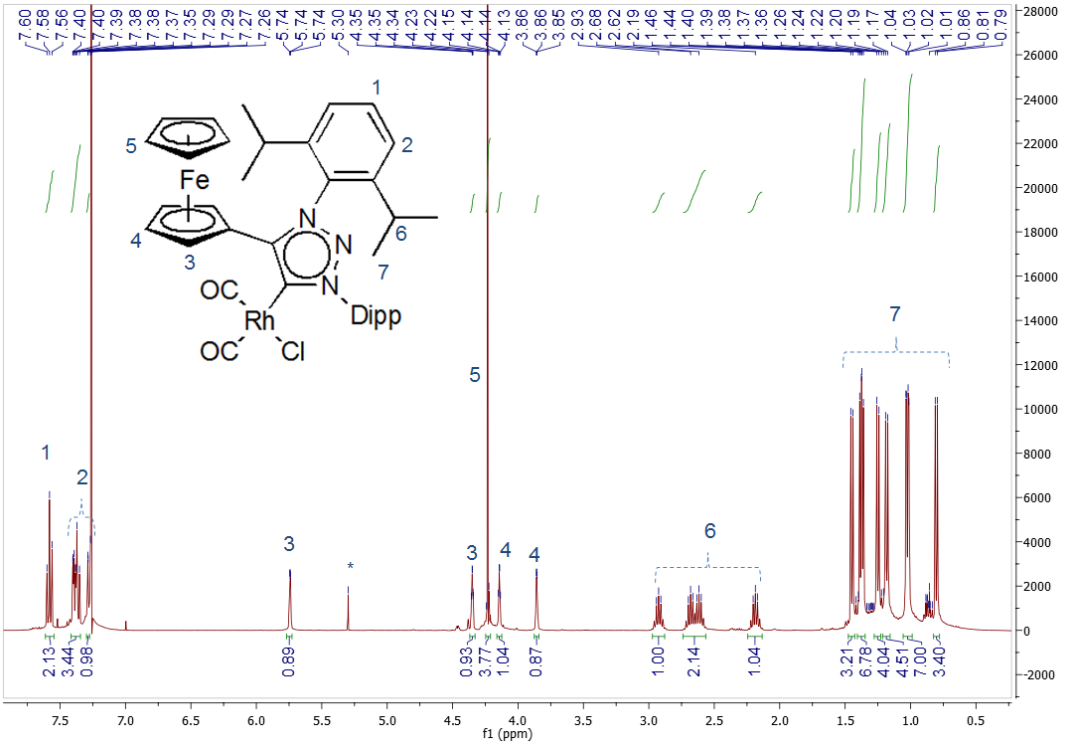

Figure 3.5. The ^{1}H NMR spectrum of complex **7** in solvent $CDCl_3$

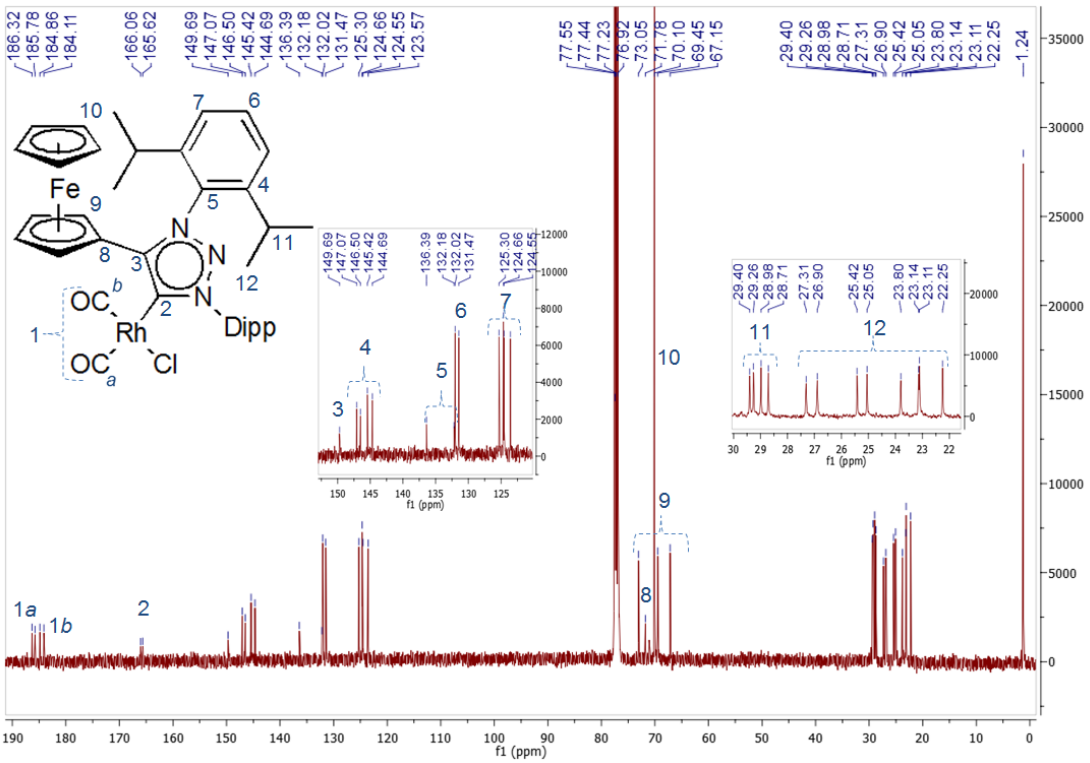

Figure 3.6. The ^{13}C NMR spectrum of complex **7** in solvent $CDCl_3$

The X-ray crystal structure of **7** is shown alongside complex **4** in Figure 3.4 (b), for ease of comparison. Crystals of **7** were grown in the fridge from a saturated DCM solution. The geometry of complex **7** more closely approaches ideal square planar geometry with bond angles closer to 90° (C1-Rh1-Cl1: 90.80(12)°), than for the cod-complex **4** (87.22(6)°). The most significant difference is the effect of the different co-ligands on the carbene bond length. Complex **4** has a shorter Rh1-C1(carbene) bond (2.059(2) Å), than complex **7** (2.079(4) Å) due to the stronger *trans* influence the dicarbonyl ligands provide rather than the cod ligand.

3.3.2 Synthesis and characterization of the N1-alkylated, N3-arylated triazolylidene rhodium(I) complexes, **5**–**6**, **8**–**9**.

Metalation of the precursor triazolium salts, **2** and **3** proceeded via the base-mediated metalation (different than the coordination of the free carbene, *vide supra*), whereby the triazolium salt, the base ($KN[Si(Me)_3]_2$) and the metal precursor, $[Rh(cod)Cl]_2$ were all added together in a purged Schlenk, cooled down to -78 °C and dissolved in THF (Scheme 3.7). After the reaction was stirred overnight, the solution was evaporated under reduced pressure and washed with hexane. Following extraction with toluene, the corresponding rhodium complexes, **5** and **6**, were afforded in reasonable (**5**: 59%) to low yield (**6**: 30%). The yield for complex **4** of 85%, was much higher than what was obtained for **5** and **6**, and may be indicative of the increased stability of the reaction intermediate (free carbene) generated during the preparation of **4**, provided by the additional aryl substituent on N1.

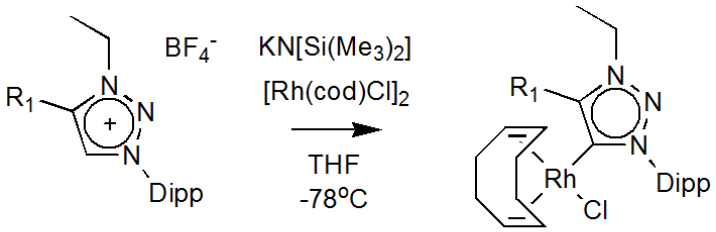

2: R_1 = Fc
3: R_1 = Ph

5: R_1 = Fc (59%)
6: R_1 = Ph (30%)

Dipp = 2,6-diisopropylphenyl
cod = 1,5-cyclooctadiene

Scheme 3.7. The synthesis of the N1-alkyl, N3-aryl rhodium(I)-triazolylidene complexes, **5** and **6**, via base-mediated C-H activation.

For both complexes **5** and **6**, the disappearance of the precursor triazolium acidic proton in the ^{1}H NMR spectra (**2**: 8.67 ppm, Figure 8.4; **3**: 8.66 ppm, Figure 8.7, *see Chapter 8*) and the appearance of the carbene signal in the ^{13}C NMR spectra (**5**: 172.3 ppm (J = 47.1 Hz), Figure 8.15; **6**: 173.2 ppm (J = 47.3 Hz), Figure 8.17) were evidence for the formation of the rhodium(I)-complexes. The carbene signals are in the range of previously reported rhodium(I) triazolylidene complexes.[2,12]

The synthesis of the rhodium-dicarbonyl complexes, **8** and **9** (from **5** and *6*, respectively), follows the synthesis reported for **7** from **4**. (Scheme 3.8).

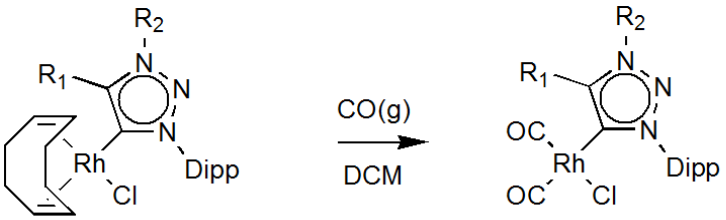

5: R_1 = Fc, R_2 = Ethyl
6: R_1 = Ph, R_2 = Ethyl

8: R_1 = Fc, R_2 = Ethyl (33%)
9: R_1 = Ph, R_2 = Ethyl (22%)

Dipp = 2,6-diisopropylphenyl

Scheme 3.8. The synthesis of the dicarbonyl-rhodium complexes, **8** and **9** from **5** and **6**, respectively.

The carbene resonance of complex **8** was observed at 165.2 ppm (J = 40.0 Hz), and the carbonyls' chemical shifts were at 185.9 ppm (J = 54.1 Hz) and 183.7 ppm (J = 75.2 Hz), for the carbonyl ligands *trans* to the carbene and chlorido,

respectively (Figure 8.21)). For complex **9** (Figure 8.24), the carbene chemical shift was found at 166.2 ppm (J = 40.5 Hz), and the carbonyls resonated at 185.7 ppm (*J* = 54.3 Hz, *trans* to carbene) and 183.4 ppm (*J* = 75.0 Hz, *trans* to chlorido). The carbene and carbonyl signals correspond to the range of previously reported rhodium(I) triazolylidene complexes.[2,12]

3.3.3 Evaluation of donor properties of complex **4**–**9**

Considering the results from the previous chapter, the precursor triazolium salts, **2** and **3**, have very similar electronic properties. Moreover, it was suggested that the substituent on N3 (aryl vs. alkyl) had a more profound effect on the electronics, rather than the substituent on C4 (ferrocenyl vs. phenyl). Evaluation of the donor properties of the carbene in the coordinated complexes should shed some light if the trend concluded in Chapter 2 is to be followed through to the coordinated complexes. A widespread method to evaluate the donor ability of carbenes is to measure the stretching frequencies of the carbonyl ligands via IR spectroscopy.

The dicarbonyl-rhodium complexes, **7**–**9** underwent solution IR spectroscopy measurements in DCM at room temperature and the results are illustrated in Figure 3.7 and tabulated in Table 3.1.

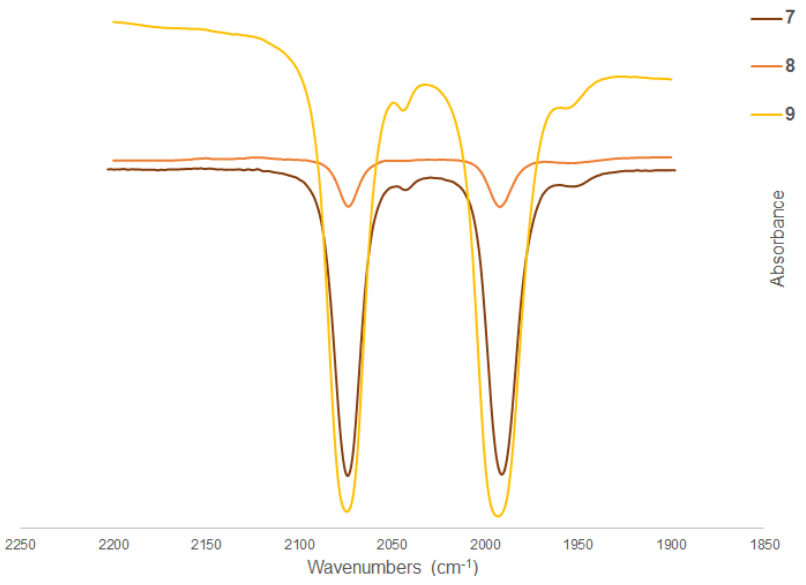

Figure 3.7. Overlaid IR spectra in the carbonyl stretching frequency region for the complexes **7**–**9**.

Table 3.1. The IR results of the carbonyl stretching frequencies of complexes **7**–**9**, and the calculated TEP in cm^{-1}.

Entry	Complex	$\tilde{\nu}$(CO)[a] (cm^{-1})	$\tilde{\nu}$(CO)[b] (cm^{-1})	$\tilde{\nu}(CO)_{av}$ (cm^{-1})	TEP[c] (cm^{-1})
1	**7**	2075	1992	2034	2047
2	**8**	2074	1992	2033	2047
3	**9**	2074	1993	2034	2047

[a] CO ligand *trans* to Cl

[b] CO ligand *trans* to carbene

[c] Calculated using the linear regression model: TEP = 0.8001$\tilde{\nu}_{CO}^{avg/Rh}$ (cm^{-1}) + 420.0 (cm^{-1}).[16]

Each carbonyl ligand in the complex is either *trans* to a carbene or a chlorido ligand, and thus two stretching bands are observed for each complex (Figure 3.7). Table 3.1 shows the IR frequencies for the carbonyl ligand *trans* to the Cl-ligand, the carbonyl ligand *trans* to the carbene, the average of both frequencies and the calculated TEPs.

The high-energy stretching frequency of free CO (2145 cm^{-1}) reflects the high C-O bond order (triple bond), and thus any coordinated CO-ligands will have stretching frequencies lower than 2145 cm^{-1}, usually in the region of 2150 to 1820 cm^{-1}.[14] The chlorido ligand is a σ,π-donor, hence providing no competition for π-backdonation to the carbonyl ligand coordinated in the *trans* position (in fact, enhancing metal-to-carbonyl π-donation to the *trans*-CO). Thus, the carbonyl *trans* to the chlorido will have an increased C-O bond order and therefore have a higher stretching frequency than the carbonyl *trans* to the carbene (σ-donor, negligible π-acceptor).

The previously reported TEPs of triazolylidenes are in the range 2047 – 2033 cm^{-1}.[2,6] Abnormal NHCs have TEPs of 2039[24] and 2033[16] cm^{-1}, normal NHCs are in the range of 2057–2049 cm^{-1} and phosphines have TEPs of 2057–2090 cm^{-1}. [17,18] Recently, in our group, ferrocenyl rhodium(I) Fischer carbene complexes[25] have been synthesized and the TEPs calculated were between 2054–2049 cm^{-1}. Complexes **7**–**9** have TEPs (2047 cm^{-1}) in the higher range of

reported TEP values for triazolylidenes, indicating that these triazolylidenes are not more donating than other reported triazolylidenes, but are at least more donating than normal NHCs, phosphines and ferrocenyl Fischer carbene ligands.

Furthermore, the calculated TEPs for each complex in this study is the same, 2047 cm^{-1}, thus although carbonyl stretching frequencies are a useful method to distinguish between different classes of ligands, it is not a sufficiently sensitive tool to probe subtle electronic effects of substituent variation.[26,27]

Huynh and Yuan recently reported the synthesis of $^{i}Pr_2$-bimy palladium triazolylidenes complexes[6,27] ($^{i}Pr_2$-bimy = 1,3-diisopropylbenzimidazolin-2-ylidene) as complex probes to evaluate the donor ability of varying triazolylidenes. The ^{13}C NMR resonance of the $^{i}Pr_2$-bimy ligand is sensitive to the substituent changes in the triazolylidene in the *trans* position. Hereby, giving rise to the use of the spectroscopic shifts of carbenes in ^{13}C NMR to evaluate the donor properties of the carbenes. The carbene resonances of complexes **4**–**6** follows a trend: **6** (173.2 ppm) > **5** (172.3 ppm) > **4** (171.9 ppm). The more donating carbene belongs to **4** which also had the most acidic triazolium proton in the precursor ligand salt, **1** (9.06 ppm). While the least donating carbene belongs to complex **6** (173.2 ppm), which had the least acidic triazolium proton in the precursor salt, **3** (8.66 ppm).

3.4 Conclusion:

The successful synthesis of the triazolylidene rhodium(I) complexes **4**–**6**, via either the free carbene route (**4**) or base-mediated activation (**5** and **6**) from the corresponding triazolium salts, **1**–**3** were discussed. Following the successful synthesis of the dicarbonyl complexes (**7**–**9**) from the corresponding rhodium-cod complexes (**4**–**6**). In all three cases, whereby the cod-ligand were replaced for the carbonyl ligands, an upfield shift of the carbene resonance were observed. A decrease in the coupling constant (Rh-$C_{carbene}$) were followed along, due to the stronger *trans* influence of the carbonyl ligand on the Rh-$C_{carbene}$ bond.

The measurement of the carbonyl stretching frequencies via IR spectroscopy gave a good representation of what the donating ability of the triazolylidenes of complexes **7**–**9** are relative to other ligand classes, but were not sensitive enough to evaluate the effect of the variation of substituents. The $^{i}Pr_2$-bimy probe of the free carbene would have been a better suited method. However, even though the corresponding $^{i}Pr_2$-bimy complexes were not synthesized, the ^{13}C NMR resonances of the carbenes of complexes **4**–**6** does follow a trend, whereby the most upfield carbene resonance of 171.9 ppm belongs to **4**, which had the most acidic triazolium proton (**1**: 9.06 ppm). The chemical shift of the triazolium precursor acidic proton can be taken as a measure of the inverse basicity of the deprotonated free carbene. Furthermore, the trans influence of the carbonyl is observed, when comparing the carbene coupling constants ($J_{RhCcarbene}$) of complexes **7** (J = 44.8 Hz), **8** (J = 40 Hz) and **9** (J = 40.5 Hz) and suggest how each carbene competes with the *trans* carbonyl for effective σ-donation towards the metal.

3.5 References

1 S. Gründemann, A. Kovacevic, M. Albrecht, J. W. Faller and R. H. Crabtree, *Chem. Comm.*, 2001, **4**, 2274–2275.

2 P. Mathew, A. Neels and M. Albrecht, *J. Am. Chem. Soc.*, 2008, **130**, 13534–13535.

3 W. A. Herrmann, J. Schwarz and M. G. Gardiner, *Organometallics*, 1999, **18**, 4082–4089.

4 M. Heckenroth, E. Kluser, A. Neels and M. Albrecht, *Dalton Trans*, 2008, 6242.

5 H. K. W. Hui and H. Shechter, *Tetrahedron Lett.*, 1982, **23**, 5115–5118.

6 K. F. Donnelly, A. Petronilho and M. Albrecht, *Chem. Comm.*, 2013, **49**, 1145–59.

7 M. Albrecht, *Chem. Comm.*, 2008, 3601–3610.

8 B. Liu, Q. Xia and W. Chen, *Angew. Chem.*, 2009, **121**, 5621–5624.

9 E. Aldeco-Perez, A. J. Rosenthal, B. Donnadieu, P. Parameswaran, G. Frenking and G. Bertrand, *Science*, 2009, **326**, 556–559.

10 G. Guisado-Barrios, J. Bouffard, B. Donnadieu and G. Bertrand, *Angew. Chemie. Int. Ed.*, 2010, **49**, 4759–4762.

11 J. Bouffard, B. K. Keitz, R. Tonner, V. Lavallo, G. Guisado-Barrios, G. Frenking, R. H. Grubbs and G. Bertrand, *Organometallics*, 2011, **30**, 2617–2627.

12 G. Guisado-Barrios, J. Bouffard, B. Donnadieu and G. Bertrand, *Organometallics*, 2011, **30**, 6017–6021.

13 S. Hohloch, C. Y. Su and B. Sarkar, *Eur. J. Inorg. Chem.*, 2011, 3067–3075.

14 R. H. Crabtree, *The Organometallic Chemistry of the Transition Metals*, Wiley-Interscience, 4th edn., 2005.

15 G. O. Spessard and G. L. Miessler, *Organometallic Chemistry*, Oxford University Press Inc., 2nd edn., 2010.

16 T. Dröge and F. Glorius, *Angew. Chemie. Int. Ed.*, 2010, **49**, 6940–6952.

17 A. Chianese, X. Li, M. Janzen, J. Faller and R. Crabtree, *Organometallics*, 2003, **22**, 1663–1667.

18 R. A. Kelly III, H. Clavier, S. Giudice, N. M. Scott, E. D. Stevens, J. Bordner, I. Samardjiev, C. D. Hoff, L. Cavallo and S. P. Nolan, *Organometallics*, 2008, **27**, 202–210.

19 M. J. López-Gómez, D. Martin and G. Bertrand, *Chem. Comm.*, 2013, **49**, 4483–5.

20 D. R. Tolentino, L. Jin, M. Melaimi and G. Bertrand, *Chem. Asian. J.*, 2015, **10**, 2139–2142.

21 M. J. Burk and R. H. Crabtree, *Inorg. Chem*, 1986, **25**, 931–932.

22 A. Poulain, D. Canseco-Gonzalez, R. Hynes-Roche, H. Müller-Bunz, O. Schuster, H. Stoeckli-Evans, A. Neels and M. Albrecht, *Organometallics*, 2011, **30**, 1021–1029.

23 D. Canseco-Gonzalez, A. Petronilho, H. Mueller-Bunz, K. Ohmatsu, T. Ooi and M. Albrecht, *J. Am. Chem. Soc.*, 2013, **135**, 13193–13203.

24 A. R. Chianese, A. Kovacevic, B. M. Zeglis, J. W. Faller and R. H. Crabtree, *Organometallics*, 2004, **23**, 2461–2468.

25 G. K. Ramollo, M. J. López-Gómez, D. C. Liles, L. C. Matsinha, G. S. Smith and D. I. Bezuidenhout, *Organometallics*, 2015, **34**, 5745–5753.

26 H. V. Huynh, Y. Han, R. Jothibasu and J. A. Yang, *Organometallics*, 2009, **28**, 5395–5404.

27 D. Yuan and H. V. Huynh, *Organometallics*, 2012, **31**, 405–412.

Chapter 4

Electrochemistry and Chemical Oxidation

4.1 Background

The inclusion of a redox-active substituent, ferrocene, in the ligand backbone of the mesoionic carbene, allows for the evaluation of the redox switching effect on the metal center. These changes may alter the activity of the catalyst precursor, similarly as reported for the oxidation of the ferrocenyl substituent of a gold(I) carbene complex, which showed enhancement of the activity of the gold pre-catalyst in the hydroamination of alkenes.[1] Moreover, when the same complex was used for the cyclization of alkynes with furans, the neutral complex was proved to be inactive, compared to the promoted activity of the oxidized complex. Likewise, such catalyst activation for the synthesis of oxazoles was also reported by the utilization of a similar strategy.[2]

Cyclic voltammetry (CV) is a straightforward electroanalytical method whereby the formal potential of a half-reaction can be measured, provided that both the oxidized and reduced products are stable during the experimental time.[3] Measurement is taken by applying a start voltage, where no redox reaction occurs (Figure 4.1, E_i) to the working electrode, then linearly changing the potential (forward scan) to a final set potential E_{Al}, then the scan is reversed (reverse scan). The potential at which the electrochemical reaction of the measured substance occurs should fall in between the initial and final potentials, usually due to the width of the range indicated.[4] The potential range depends on the electrode used e.g. glassy carbon, platinum or gold etc., the supporting electrolyte like KNO_3 or $[NBu_4][PF_6]$ etc., and the solvent employed. In the case of the complexes explored in this chapter, the electrode used was glassy carbon, which is more redox innocent in electrochemical reactions[5], since both Pt -and Au electrodes can mediate adsorbed oxide formation and reduction resulting in reduced potential ranges. Both the solvent and the supporting electrolyte are chosen per the compound under investigation; the compound and the supporting electrolyte should be fully soluble, to avoid decreasing the potential window even further.

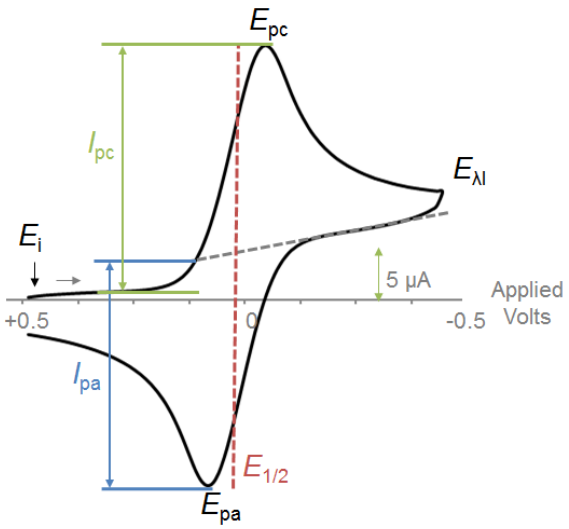

Figure 4.1. A typical cyclic voltammogram indicating the start potential (E_i), stop potential ($E_{\lambda l}$), cathodic potential peak (E_{pc}), anodic potential peak (E_{pa}), cathodic peak current (i_{pc}), anodic peak current (i_{pa}) and the half-wave potential ($E_{1/2}$).[3,4]

The plot obtained from a CV experiment, the cyclic voltammogram, is the current response plotted against the function of the potential applied (Figure 4.1).[3–6] The working electrode remains stationary in an unstirred solution and reduces the starting material near the surface of the electrode. Reduction occurs at the electrode when the electrode is negative enough to reduce the substrate. This is observed in the forward scan, which was negatively scanned (positive to negative). The result is an increase in cathodic current until a peak is reached, E_{pc}, where the concentration of starting material has been depleted, relative to the reduced species at the surface of the electrode. The current continues to decrease afterward since the concentration of the starting material in the solution is depleting due to the conversion to reduced species. The scan direction is changed to positive (reverse scan), whereby the reduced species are oxidized back to the original starting material due to the electrode being sufficiently positive enough to do so. The anodic current is generated with an anodic peak reached (E_{pa}), after which the reduced species continues to be oxidized until no reduced species remain. The cycle ends when the initially applied potential is reached.

In most cases, when the formal reduction potential is calculated, the average of the forward and reverse scan measurements are taken, known as the redox

couple.[4] However, this is not always possible since the redox couple is only possible with reversible and/or quasi-reversible processes when there is a return peak to measure. Electrochemical reactions which are fast enough to maintain the concentrations of the oxidized or reduced forms of the substrate at the electrode surface until the scan is reversed, for the regeneration of starting material, are considered reversible. To regard the reaction as the reversible, the separation of the peak potentials of the forward and reverse reaction shouldn't be separated by more than 58*n* mV, where *n* is the number of electrons being transferred[6] (equation 4.1). Moreover, the peak height of both reactions should be equal (equation 4.2) and proportional to the square root of the scan rate, equation 4.3.

$$E_{pa} - E_{pc} = \Delta E_p = 58n \text{ mV} \qquad \ldots (4.1)$$

$$I_{pc} = I_{pa} = I_p \qquad \ldots (4.2)$$

$$I_p = kv^{1/2} \qquad \ldots (4.3)$$

When ΔE_p increases to more than 58*n* mV, as the scan rate increases, the reaction is said to be quasi-reversible. This is also the case when the two peaks are separated by 58*n* mV, but the peak heights are not equal. However, when the peaks are too far apart from one another, the reaction is irreversible. Reactions where no return peak can be measured, due to the inability of products to be recycled e.g. due to bond breaking etc., are considered chemically irreversible.

4.2 Aim

Following the synthesis of the N1-, N3-diarylated triazolium salt, **1** and the complexation to rhodium(I) to yield complexes **4** and **7**, the electrochemical redox potentials are measured with cyclic voltammetry, and the results are reported in this chapter. Of interest is the redox potential of the Fe^{II}/Fe^{III} redox couple of the ferrocenyl substituent in each compound, to determine suitability of chemical oxidation with appropriate chemical redox agents and to enable selective oxidation i.e. to avoid oxidation of the rhodium(I) metal center as well. Ultimately, the evaluation of the reversibility of the compounds' redox-activity

will determine if the complexes are stable under electrochemical conditions and therefore have the possibility of being isolable to avoid decomposition during catalytic studies.

4.3 Results and discussion

4.3.1. Cyclic voltammetry experiments:

Cyclic voltammetry experiments were carried out on compounds **1**, **4** and **7** (Figure 4.2) to evaluate the electrochemical properties of these compounds.

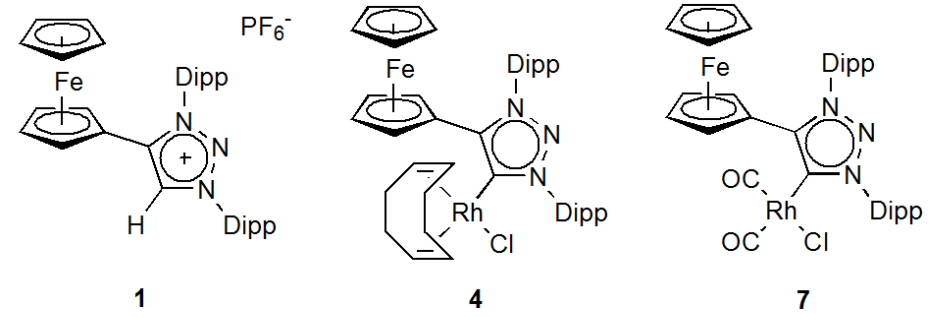

1 **4** **7**

Dipp = 2,6-diisopropylphenyl

Figure 4.2. The compounds, **1**, **4** and **7** investigated by electrochemical methods.

The CV results obtained for **1** is reported in entries 1 and 2, Table 4.1. Two redox processes were distinguishable: the oxidation and reduction of the triazolium ring, and the ferrocenyl substituent, Figure 4.3. The oxidation of the ferrocene substituent took place at 336 mV, and can easily be regarded as reversible since the i_{pc}/i_{pa} is close to unity, but the ΔE_p is larger than 60 mV (entry 2, Table 4.1), meaning that the oxidation of the ferrocenyl moiety in **1** should rather be classified as quasi-reversible.[6] The reduction of the triazolium ring was more reversible than the ferrocenyl substituent with the ΔE_p closer to 60 mV, and the anodic peak current is equal to the cathodic peak current.

Table 4.1. Cyclic voltammetry (CV) results for **1**, **4** and **7**, showing the E_{pa}, E_{pc}, $E_{1/2}$, ΔE_p in mV and the i_{pc}/i_{pa} ratio.

Entry	Redox couple	E_{pa} (mV)	E_{pc} (mV)	$E_{1/2}$ (mV)	ΔE_p (mV)	i_{pc}/i_{pa}
			1			
1	Trz-H(I)/(0)	-2121	-2191	-2156	70	1.11
2	Fc(II)/Fc(III)	336	256	296	80	1.07
			4			
3	Fc(II)/Fc(III)	104	-46.8	28.7	57.4	1.02
4	Rh(I)/(III)	608	458	533	151	0.89
			7			
5	Fc(II)/Fc(III)	145	64.6	105	80.6	0.89
6	Rh(I)/(II)*	568	/	/	/	/
7	Rh(II)/(III)*	960	/	/	/	/

*Overlapping redox-processes: Rh(I)/Rh(II); Rh(II)/Rh(III)

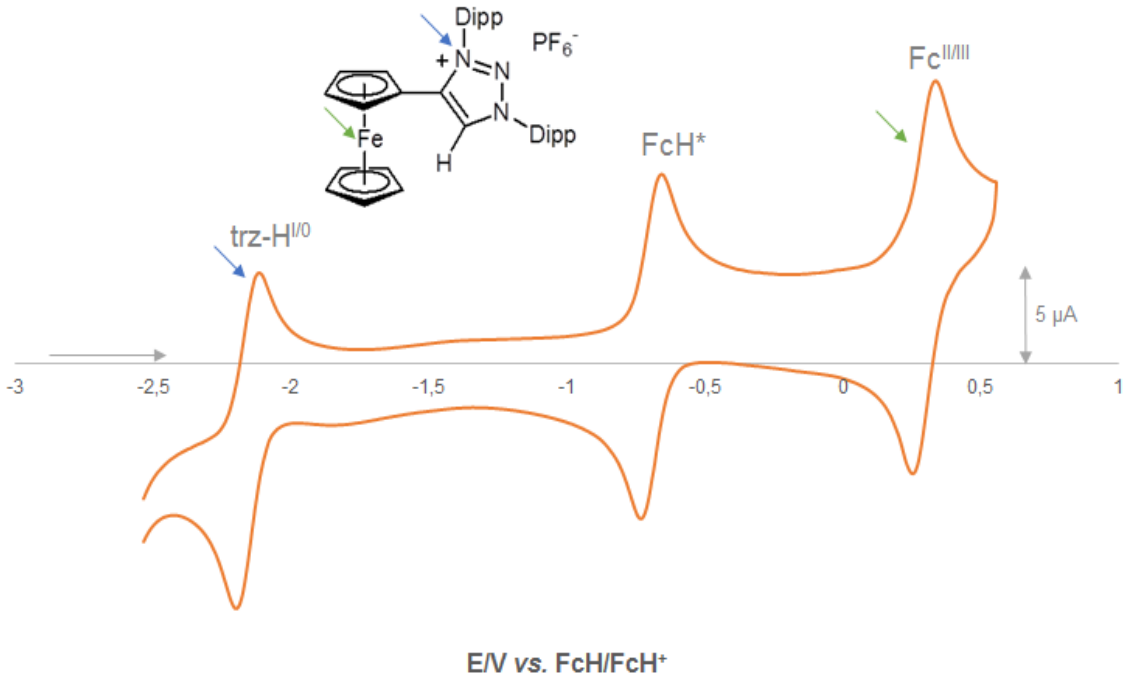

Figure 4.3. The CV obtained from **1** at a glassy carbon electrode at a scan rate of 0.1 V. s^{-1} in CH_2Cl_2, with decamethylferrocene (FcH*) as internal standard.

For the rhodium complexes **4** and **7**, two redox processes were also observed for each complex (Figure 4.4), the Fc(II/III) redox couple and the oxidation of the metal center, rhodium(I) to rhodium(III). The fully reversible ferrocene substituent, in complex **4** (entry 3, Table 4.1), oxidized at a low 104 mV and the oxidation of rhodium(I) to rhodium(III) has a redox potential of 608 mV. The difference in E_p of 150 mV represents a two-electron process (entry 4, Table 4.1), which ideally should be 120 mV. Complex **7** on the other hand, shows no reversible peak for the oxidation of rhodium(I), and two separate oxidation events for the rhodium metal, at 568 mV (Rh(I/II) couple, entry 6, Table 4.1) and 960 mV (Rh(II/III) couple, entry 7, Table 4.1), but no ΔE_p and i_{pc}/i_{pa} could be calculated. Moreover, the ferrocenyl substituent of complex **7** oxidized at 145 mV, showing quasi-reversibility (entry 5), with a ΔE_p of 81 mV and i_{pc}/i_{pa} of 0.9.

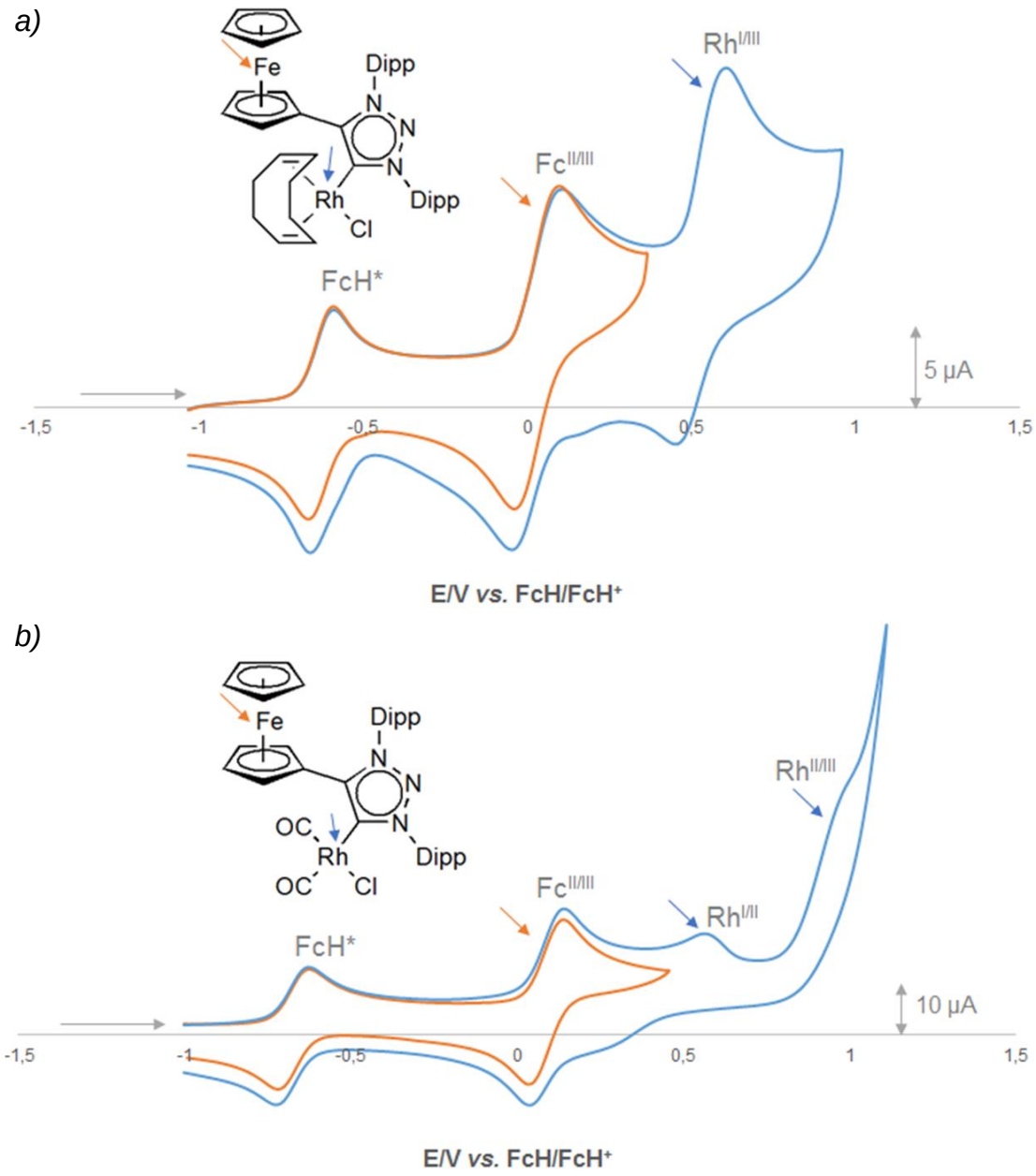

Figure 4.4. The CVs obtained from (a) **5** and (b) **7** at a glassy carbon electrode at a scan rate of 0.1 V. s^{-1} in CH_2Cl_2, with decamethylferrocene (FcH*) as internal standard. In both cases, the individual redox event of the ferrocenyl moiety is overlaid in orange.

The stepwise oxidation of the rhodium metal in complex **7** remains speculative, since linear sweep voltammetry is required to fully estimate the number of electrons being transferred with each oxidation. Also, there exists very few examples in reported literature where this stepwise oxidation is observed,[7] even less so with dicarbonyl ligands.

The oxidation potentials for the ferrocenyl moiety range between 336 mV (**1**), 104 mV (**4**) and 145 mV (**7**). The difference in the oxidation potential of **1**, compared to **4** and **7** is due to the cationic nature of the triazolium salt. The compound is generally electron deficient, and thus any oxidation event will occur at a more positive potential. For **4** and **7**, the difference lies in the electronic nature of the coordinated ligands, i.e. the 1,5-cyclooctadiene (**4**) and the carbonyl ligands (**7**). More positive potential is needed to oxidize the ferrocenyl substituent of **7**, due to the strongly π-accepting CO-ligands present on the rhodium(I). The oxidation potentials of the oxidation events for complexes **4** and **7**, could however not be compared as one 2-electron oxidation (Rh(I/III) couple) was observed for **4**, while two separate 1-electron oxidation events (Rh(I/II) and Rh(II/III) couples) were observed for **7**.

4.3.2 The chemical oxidation of **1**, **4** and **7**.

The cyclic voltammetry experiments provided insight into the electrochemical properties of **1**, **4** and **7**. The chemical oxidation of each of these compounds' ferrocenyl substituent was carried out in the laboratory, and the oxidized compounds were characterized as best as time allowed (decomposition of the oxidized compounds were predominant).

Since the oxidizing potential of the ferrocenyl substituent of **1**, was measured to be 0.34 V, $AgPF_6$ ($E°$= 0.65 V in DCM)[8] was chosen as a suitable oxidizing agent. The oxidation of **1** followed the addition of 1.1 equivalents of $AgPF_6$ to ligand salt **1**, under an argon atmosphere in DCM at -78 °C. The solution turned dark green from orange, and after 10 minutes, the reaction was filtered at room temperature. The solvent was evaporated, affording **1ox** as a dark green solid which were stored in the glovebox (Scheme 4.1).

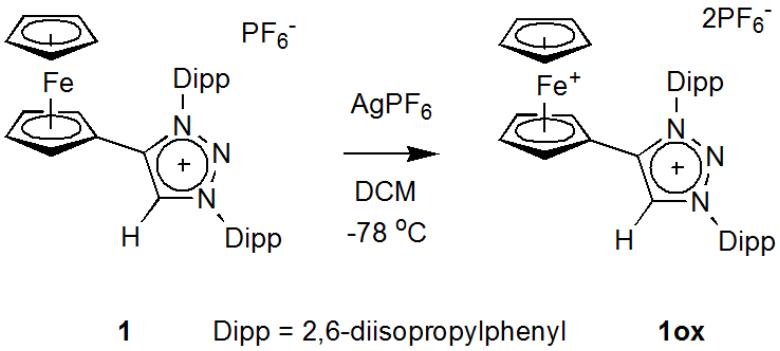

1 Dipp = 2,6-diisopropylphenyl **1ox**

Scheme 4.1. The oxidation **1** with $AgPF_6$ as an oxidizing agent in DCM to afford the N1-, N3-diarylated ferrocenium triazolium salt, **1ox**.

Due to the paramagnetic nature of the ferrocenium ion, complex **1ox** could not be characterized via ^{1}H NMR, ^{13}C NMR or ^{31}P NMR. However, a doublet resonance appeared on the ^{19}F NMR spectrum (Figure 4.5 (a)) at -85.07 ppm (J = 969.09 Hz) in solvent CD_2Cl_2, which was shifted *ca*. 13 ppm upfield of the chemical shift of the doublet for PF_6^- counterion of **1** in solvent CD_2Cl_2 (-72.42 ppm, J = 712.62 Hz, Figure 4.5 (b)). The change in chemical shift of the counterion ion has also been reported by Bezuidenhout and co-workers when they studied the oxidation of ferrocenyl tungsten Fischer carbenes, with the corresponding increase in the coupling constant.[9]

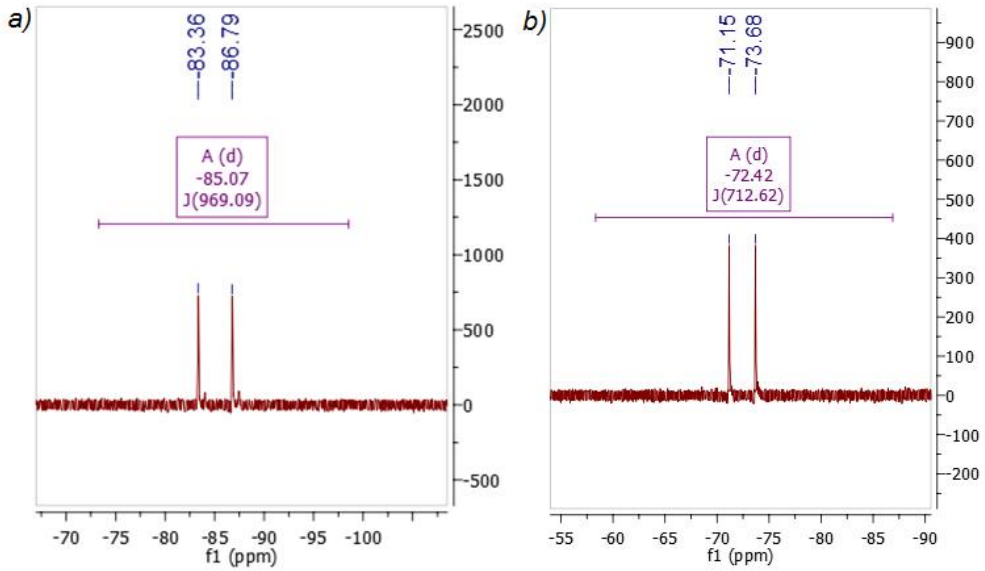

Figure 4.5. The ^{19}F NMR spectra of (a) **1ox** and (b) **1** in solvent CD_2Cl_2.

Crystals of **1ox**, were obtained by slow evaporation of a concentrated solution of **1ox** in DCM, and these crystals were mounted inside the glovebox for single crystal X-ray diffraction analysis. The molecular structures of both **1ox** and **1** are given in Figure 4.6, for assessment of the extent to which the ligand precursor salt is affected by the oxidation of the ferrocenyl moiety. In Figure 4.6 (a), the ferrocenium triazolium salt, **1ox** is shown with two counterions (PF_6^-) and the ferrocenyl Cp-rings (Cp = cyclopentadienyl) are staggered. In Figure 4.6 (b), the neutral triazolium salt is shown, bearing only one counterion (PF_6^-), and eclipsed ferrocenyl Cp rings. There are several slight differences between the bond lengths and angles of **1ox** and **1**. Firstly the triazolium ring bond lengths of **1** are in the range of 1.328–1.383 Å, which are slightly longer than the triazolium ring bond lengths of **1ox** (1.320–1.370 Å). Secondly, the bond angle of the triazolium ring (N1–C2–C1) is smaller (105.70 °) in **1ox**, than in **1** (106.00 °). However, a more significant change is observed when the Fe-Cp bond lengths are evaluated; **1ox** has Fe-Cp bond lengths of 1.708 Å and 1.709 Å, which are considerably longer than the Fe-Cp bond lengths of **1** (1.647 Å and 1.656 Å). These differences imply that the ferrocenyl substituent is the most affected in the oxidation step, as expected.[10]

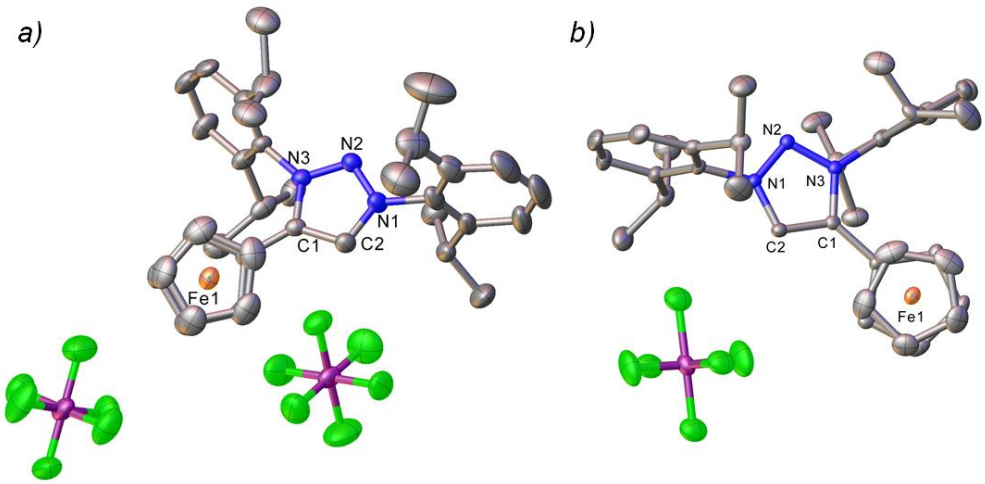

Figure 4.6. The molecular structure of the ferrocenium triazolium salt, **1ox** (a) and the neutral triazolium salt, **1** (b) showing 50% probability ellipsoids and partial atom-numbering scheme. Selected bond lengths (Å) and angles (°) for **1**: N1–N2 1.328(3); N1–C2 1.348(3); N2–N3 1.338(3); N3–C1 1.369(3); C1–C2 1.383(3); N1–C2–C1 106.00(19). For **1ox**: N1–N2 1.320(3); N1–C2 1.348(3); N2–N3 1.321(3); N3–C1 1.370(3); C1–C2 1.364(3); N1–C2–C1 105.70(2). Hydrogens are omitted for clarity.

The chemical oxidation of complex **4**, was carried out with a mild oxidant, acetylferrocenium hexafluorophosphate ([AcFc]PF_6) ($E°$= 0.27 V in DCM).[8] The ferrocenyl substituent of complex **4**, oxidized at 0.104 V, and the rhodium(I) metal at 0.608 V, therefore, Fe(η-C_5H_4COMe)Cp^+]PF_6^- were determined to selectively oxidize the ferrocenyl moiety without oxidizing the rhodium(I) metal as well. The oxidant $AgPF_6$ cannot be used to oxidize the metal, as it could potentially oxidize both iron and rhodium metals. In addition, $AgPF_6$ is a known halide scavenger, and thus the risk of chloride-abstraction is prevalent.

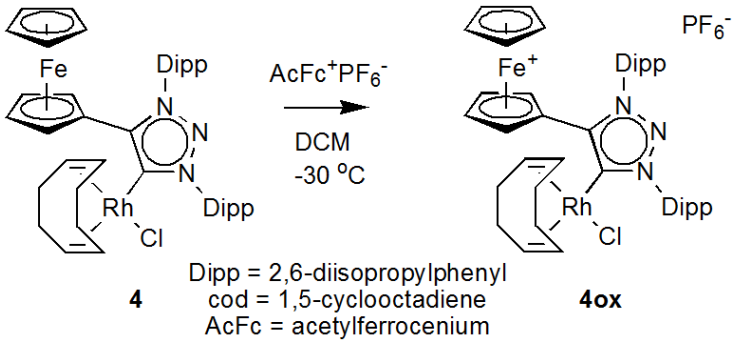

Scheme 4.2. The oxidation of **4** to **4ox**, with the oxidant acetylferrocenium hexafluorophosphate in DCM.

Complex **4**, along with 1.1 equivalents of [AcFc]PF_6were added to a Schlenk, purged with argon gas. The solids were dissolved in DCM at -30 °C, and stirred for half an hour (Scheme 4.2). After this time, the reaction was warmed to room temperature, and filtered. The filtrate was evaporated under reduced pressure and the dark brown solid was washed with ether. The residue, light brown was dried overnight under reduced pressure and stored in the glovebox

Another approach to oxidize complex **4** was attempted, by oxidizing the ligand precursor salt to **1ox**, using $AgPF_6$, followed by deprotonation and metalation with the $[Rh(cod)Cl]_2$ (Scheme 4.3). The synthesis involved the generation of **1ox**, *vide supra,* followed by the addition of **1ox** to an argon purged Schlenk, in the glovebox, with 1.1 eq $KN(SiMe_3)_2$ and 0.6 equivalents of $[Rh(cod)Cl]_2$. The solids were suspended in THF at -78 °C, and stirred for 1 hour at this temperature. After reaching room temperature, instead of isolating complex **4ox**, CO(g) were bubbled through and an infrared spectroscopy analysis were done on the dark brown solid (**7ox**) in DCM (Figure 4.7). In this way, indirectly

characterizing the formation of **4ox** by analysing the corresponding dicarbonyl complex, **7ox**.

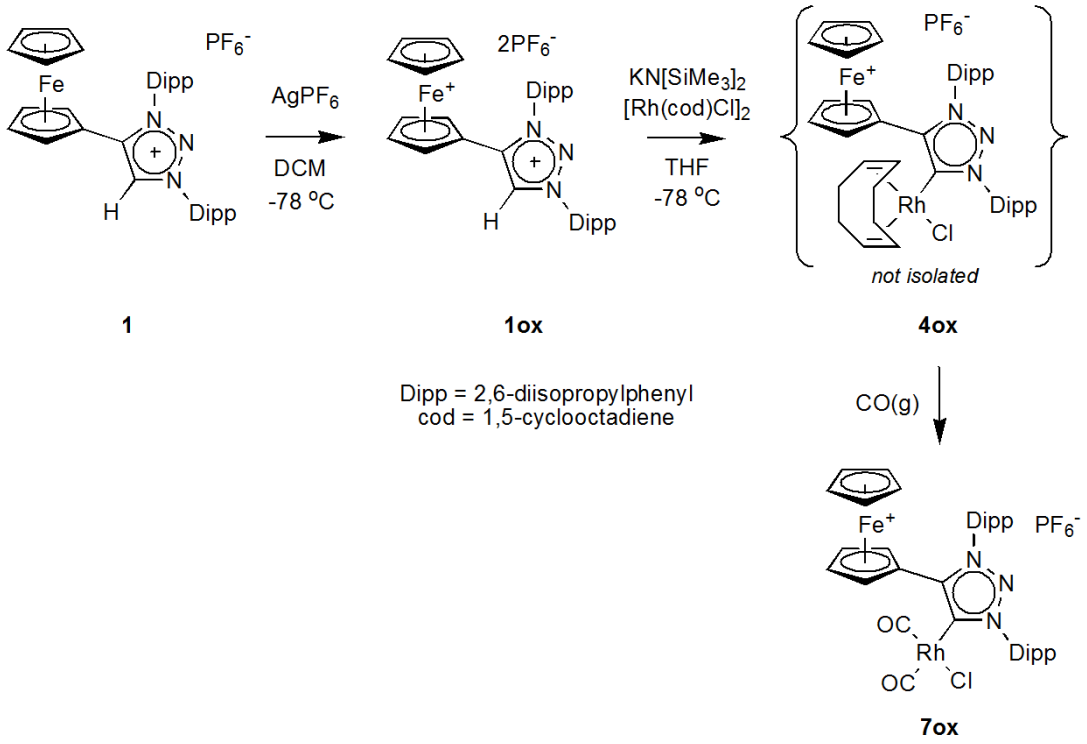

Scheme 4.3. The oxidation of **1**, then subsequent deprotonation and metalation with $[Rh(cod)Cl]_2$ to yield **4ox** (not isolated) and **7ox**.

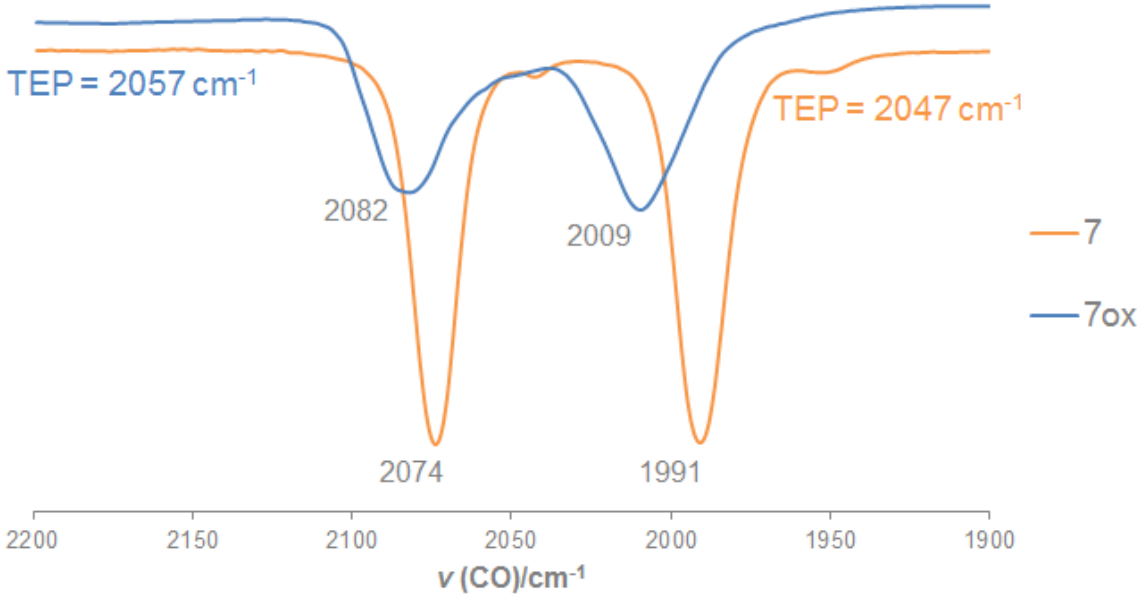

Figure 4.7. The carbonyl stretching frequencies obtained from IR measurements in solvent DCM of the complexes **7** and **7ox**. The calculated TEP values in cm^{-1}, calculated as TEP (cm^{-1}) [Rh to Ni] = 0.8001$\tilde{\nu}_{CO}^{av/Rh}$ (cm^{-1}) + 420.0 (cm^{-1}),[9] are indicated.

The carbonyl stretching frequencies of the neutral ferrocenyl triazolylidene rhodium(I) complex, **7** and the ferrocenium triazolylidene rhodium(I) complex, **7ox** are shown in Figure 4.7. Both complexes displayed two absorption bands, since one carbonyl is *trans* to the carbene and one carbonyl is *trans* to the chlorido ligand. The stretching frequencies for **7** were found to be 2074 cm^{-1} (CO *trans* to Cl) and 1991 cm^{-1} (CO *trans* to carbene), while the stretching frequencies for **7ox** was 2082 cm^{-1} (CO *trans* to Cl) and 2009 cm^{-1} (CO *trans* to carbene).

A significant difference is observed between the carbonyl stretching frequency *trans* to the carbene, where **7ox** has an increased frequency of 18cm^{-1} (2009 cm^{-1} vs. 1991 cm^{-1} for **7ox** and **7** respectively). Thereby signifying an increase in the C-O bond order for **7ox**, and therefore less metal π-backbonding is experienced (decreased donation in the π* CO orbital). Being the carbene *trans* to the carbonyl involved, the decrease in the metal's ability to back bond is influenced by the decrease in the carbene's donation towards the metal, and the average shift in the carbonyl IR frequencies (2033 cm^{-1} (**7**) vs. 2046 cm^{-1} (**7ox**)) corresponds to the change in inductive effect when the ferrocenyl moiety is oxidized to ferrocenium.[9]

Furthermore, the TEPs for each complex was calculated as 2047 cm^{-1} for **7** and 2057 cm^{-1} for **7ox** using the linear regression; TEP (cm^{-1}) [Rh to Ni] = 0.8001$\tilde{\nu}_{CO}^{av/Rh}$ (cm^{-1}) + 420.0 (cm^{-1}).[11] The oxidation of ferrocenyl moiety shifted the TEP of the triazolylidene in the ranges of the traditional NHCs (2057–2049 cm^{-1}) and phosphine ligands (2057-2090 cm^{-1}),[12,13] which again illustrates the functional group versatility NHCs can accommodate, and moreover, the possible electronic modulation that the ferrocene substituent offers.

4.4 Conclusion

The electrochemical properties of the N1-, N3-diarylated ferrocenyl triazolium salt, **1** and triazolylidene rhodium(I) complexes **4** and **7** was elucidated with cyclic voltammetry. Of interest was the ferrocenyl redox event in each of the compounds, and the ferrocenyl substituent oxidized at 336 mV, 104 mV and 145 mV for **1**, **4** and **7** respectively. The cationic triazolium salt, **1** exhibited the

highest oxidation potential for the ferrocenyl moiety (due to the cationic nature of the triazolium ring). On the other hand, the ease of the ferrocene oxidation of the rhodium(I) complex was illustrated as a result of the π-donating diene ligands (1,5-cyclooctadiene) coordinated to the rhodium(I). The oxidation of the metal in **4**, occurs as a quasi-reversible two-electron process, whereby separate irreversible one-electron oxidation of the rhodium(I) metal is observed in **7**.

The electronic influence of the ferrocenium substituent on the compounds **1**, **4** and **7** was evaluated by chemical oxidation experiments, whereby **1ox**, **4ox** and **7ox** were synthesized. Evidence of **1ox**, is the upfield shift (-85.07 ppm (**1ox**) vs. -72.42 ppm (**1**)) in the chemical resonances observed in the ^{19}F spectrum of the PF_6^- counterion, as well as changes in the bond lengths of **1ox** and **1**, especially the lengthening of the Fe-Cp bond lengths in **1ox** compared to **1**. The significant difference in the carbonyl stretching frequencies of **7** and **7ox**, lead to the deduction that the inductive effect on the carbene (and consequently, the rhodium(I)) is altered due to the electron-withdrawing nature of the ferrocenium moiety. The calculated TEP of **7ox** positions the ferrocenium triazolylidene in the donating ranges of normal NHCs and phosphine ligands, thereby demonstrating the redox-switch potential of the ligand.

4.5 References

1 S. Ibáñez, M. Poyatos, L. N. Dawe, D. Gusev and E. Peris, *Organometallics*, 2016, **35**, 2747–2758.

2 L. Hettmanczyk, S. Manck, C. Hoyer, S. Hohloch and B. Sarkar, *Chem. Comm.*, 2015, **51**, 10949–10952.

3 D. H. Evans, K. M. O. Connell, A. Petersen and M. J. Kelly, *J. Chem. Educ.*, 1983, **60**, 290–293.

4 G. a. Mabbott, *J. Chem. Educ.*, 1983, **60**, 697–702.

5 J. J. Van Benschoten, J. Y. Lewis, W. R. Heineman, D. a. Roston and P. T. Kissinger, *J. Chem. Educ.*, 1983, **60**, 772.

6 P. T. Kissinger and W. R. Heineman, *J. Chem. Educ.*, 1983, **60**, 702.

7 R. Winter, D. T. Pierce, W. E. Geiger and T. J. Lynch, *J. Chem. Soc. Chem. Commun.*, 1994, 1949–1950.

8 N. G. Connelly and W. E. Geiger, *Chem. Rev.*, 1996, **96**, 877–910.

9 D. I. Bezuidenhout, I. Fernandez, B. van der Westhuizen, P. J. Swarts and J. C. Swarts, *Organometallics*, 2013, **32**, 7334–7344.

10 L. Hettmanczyk, S. Manck, C. Hoyer, S. Hohloch and B. Sarkar, *Chem. Comm.*, 2015, **51**, 10949–10952.

11 T. Dröge and F. Glorius, *Angew. Chemie. Int. Ed.*, 2010, **49**, 6940–6952.

12 A. Chianese, X. Li, M. Janzen, J. Faller and R. Crabtree, *Organometallics*, 2003, **22**, 1663–1667.

13 R. a. Kelly III, H. Clavier, S. Giudice, N. M. Scott, E. D. Stevens, J. Bordner, I. Samardjiev, C. D. Hoff, L. Cavallo and S. P. Nolan, *Organometallics*, 2008, **27**, 202–210.

Chapter 5

Hydroformylation of 1-octene.

5.1 Background

Hydroformylation is the addition of syngas (a mixture of CO and H_2) to olefins in the presence of a catalyst to produce, depending on the nature of the olefin and the rate of isomerization, linear and branched aldehydes (Figure 5.1) as major products, while undesirable by-products include internal octenes, octanes, and alcohols.[1] This is a widely used process since several hundred metric tons of aldehydes are produced annually and utilized extensively in bulk chemicals and pharmaceuticals globally.

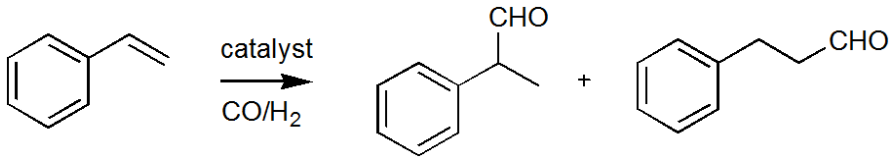

Figure 5.1. Reaction illustrating the hydroformylation process: the conversion of terminal alkenes to aldehydes.

Otto Roelen[1,2] serendipitously discovered the process in 1938 and optimized the process by using a mixture of cobalt, thorium, and magnesium oxide as catalyst precursors, with the conclusion that [$HCo(CO)_3$] is the active specie. Unmodified cobalt catalysts were developed but had to be used under severe reaction conditions (high temperatures and pressures). The addition of phosphine ligands assisted in increasing the activity of the catalysts, thereby allowing milder reaction conditions, but this occurred at a cost to the reaction selectivity with the formation of alcohols. Industry today still employs Co-based catalysts in the hydroformylation of long chain- and branched alkenes at temperatures of 120–190 °C and pressures of 40–300 bar, usually in heterogeneous processes where the molecular reaction mechanism remains not clearly defined.

Phosphine-ligand modified Rh-based catalysts started appearing in the 1970's and displayed activity under milder reaction conditions at moderate temperatures of 85–130 °C and syngas pressures from 18–60 bar. However,

the addition of excess phosphines is required to stabilize the rhodium complex and increase linear selectivity. Although Rh-catalysts show high activity for the process, Rh-phosphine catalysts are susceptible to poisons in the feedstock e.g. oxygen, peroxides, water etc., due to the presence of the air- and moisture-sensitive phosphine ligands, and subsequently degrade over time,[1] whereas cobalt-based catalysts are more robust. Nevertheless, rhodium can be 1000 times more active than cobalt and thus research in modifying Rh-catalysts has expanded to include more than just phosphines as ancillary ligands.

Rh-NHC complexes as a replacement for phosphine complexes have been developed since NHCs have been used as phosphine mimics on various research topics. NHCs offer regioselectivity and stability as suitable criteria in catalyst design. In the 2011 review by Gil and Trzeciak,[3] the electronic and steric effects of phosphines are compared to NHCs. In short; for phosphines that are electron-withdrawing, higher selectivity and activity are shown, as anti-Markovnikov addition is favored leading to linear aldehydes. NHCs are generally more donating than the most donating phosphine ligands but can be altered by the nature of the azole ring and electron-withdrawing substituents. For phosphine-substituted Rh-complexes, the bulkier substituted analogues proved to be more active in the hydroformylation reaction (higher turnover numbers; TON = mol product/mol [Rh]). Thus, designing pre-catalysts based on sterically demanding substituents with an electron-withdrawing NHC backbone should prove a plausible strategy, comparable to the use of phosphines as ancillary ligands in the design of both active and chemo-, regio- and stereoselective hydroformylation catalysts by exploiting the ability of NHCs to be modified to specific constraints (both sterically and electronically).

In 2000, Crudden et al.,[4,5] synthesized two rhodium(I)-NHC complexes, Figure 5.2 (**A**, **B**) and tested these complexes as hydroformylation catalyst precursors for the conversion of various vinylarenes at moderate conditions. Complex **A** proved to be very selective towards branched aldehydes (96%) but only achieved full conversion of the substrate after 19 hrs. Furthermore, **B** showed half the reactivity than **A** with TOFs (TOFs = turn-over frequencies, calculated as TOF = mol aldehydes/mol cat.h^{-1}) of 4 h^{-1} and 7 h^{-1} obtained, respectively.

However, even at low TOFs, the selectivity of complex **B** remained high and thus, to increase the activity of **B**, 2 equivalents of triphenylphosphine was added. The addition provided results comparable to complex **A**. These results proved superior to the results obtained for the Rh-phosphine analogue, $[Rh(CO)(Cl)(PPh_3)_2]$, and the Wilkinson catalyst, $[RhCl(PPh_3)_3]$.[6]

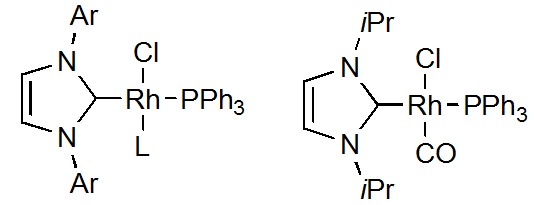

L = PPh3 (**A**)
L = CO (**B**)
Ar = 2,4,6-trimethylbenzene

C

Figure 5.2. Rh(I)-NHC complexes prepared by Crudden et al.[4,5](**A**, **B**), in 2000 and Raubenheimer et al.[7] (**C**), in 2005.

Crudden's work placed NHC's on the platform for application in the hydroformylation of vinylarenes with the very high regioselectivities presented. The hydroformylation for 1-octene was also studied but with limited success. A linear to branched aldehyde ratio (n/*iso*) of 2.1:1 was obtained with quantitative conversion achieved after 16 hrs, with no isomerization observed.

In the hydroformylation reaction of aliphatic alkenes, selectivity will often decrease due to the possibility of hydrogen *β*-elimination leading to the formation of internal olefins (isomerization).[3] Since these internal olefins have the possibility to undergo hydroformylation, these products lead to the formation of branched aldehydes. Crudden's catalysts (**A**, **B**) offer great selectivity in particular to aromatic alkene substrates, however, the addition of phosphines and bases as additives are necessary to assist in raising the activity. Interestingly, similar carbene complexes were studied by Raubenheimer[7] in 2005, using alkyl substituents (**C**, Figure 5.2) in the hydroformylation of 1-hexene. Selectivity was lower (1.7:1) favouring linear formation, but with enhanced activity since the full conversion was reached after only 9 hrs instead of 16 (Table 5.1, entry 1).

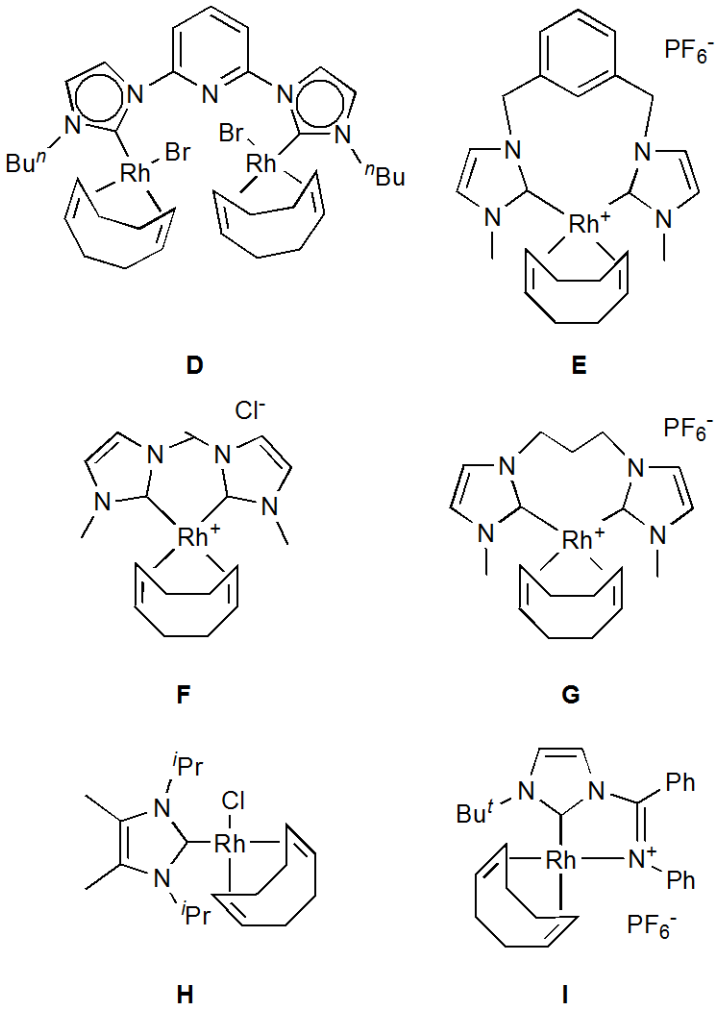

Figure 5.3. Rh(I) NHC complexes prepared for application in the hydroformylation of 1-octene by Peris et al., [8](**D**, **E**) Raubenheimer et al., [7] (**F–H**), and Coleman et al.,[9] (**I**).

The effect of a dinuclear rhodium(I) biscarbene complex on hydroformylation was investigated by Peris et al.,[8] (**D**, Figure 5.3). In the hydroformylation of styrene, **D** showed 100% conversion at 80 °C/80 bar after 24 hrs. The TOF of 29.1 h^{-1} obtained showed a significantly higher activity than that obtained by Crudden with the mononuclear Rh(I) complexes - even without the addition of excess phosphines. In addition, selectivity was maintained as 86% branched aldehydes were obtained, although they achieved 100% conversion with harsher conditions than reported by Crudden. However, 100% conversion at moderate conditions was achieved by increasing the catalyst loading to 0.25 mol %. It is worth noting that as the reaction temperature was increased, the selectivity towards branched aldehydes decreased and the addition of NEt_3 had no effect on activity. Peris also compared the activity of **D** to a cationic chelated

Rh(I)-carbene complex, **E** for hydroformylation, but surprisingly the chelate complex showed no activity even at higher conditions. Substrates other than styrene were also investigated, namely aliphatic alkenes, in particular, 1-octene. Reasonable conversion (70%) was obtained at relatively mild conditions (Table 5.1, entry 2) with equal branched to linear aldehyde ratios.

A number of mono-, bis- and chelated carbene Rh(I) complexes were also analyzed in the hydroformylation of 1-hexene by Raubenheimer[7] (**F**, **G**, Figure 5.3). Of all the bis- and chelated carbene complexes analyzed, of type **F,** entry 3 (Table 5.1), displayed decreased activity when compared to the monocarbenes of type **C**, (entry 1, Table 5.1, Figure 5.2) and **H**, (entry 5, Table 5.1, Figure 5.2). The exception was the activity obtained from **G** (entry 4, Table 5.1) which closely resembled the results of **C** and **H**. Similar success was achieved by complex **I**, reported by Coleman (entry 6).[9]

These results suggest that even though the biscarbene complex (**D**) shows higher activity than Crudden's in the hydroformylation of vinylarenes (**A**, **B**), the performance of bis- and chelate carbene complexes (**D**–**I**) in the hydroformylation of aliphatic alkenes are harder to predict.

Table 5.1. Hydroformylation of aliphatic alkenes with Rh-NHC catalysts.[a]

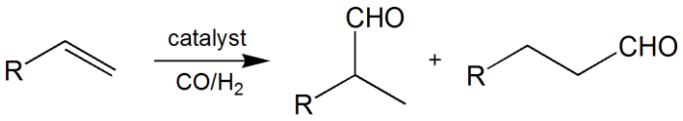

Entry	Catalyst	Substrate	Conversion (%)	TOF(h^{-1})	n/*i*
1[b]	**C**	1-hexene	100	111	1.7
2[c]	**D**	1-octene	70	11.6	1.3
3[d]	**F**	1-hexene	29	-	1.7
4[d]	**G**	1-hexene	100	-	1
5[d]	**H**	1-hexene	100	-	1.1
6[e]	**I**	1-octene	100	-	1.3
7[f]	**J**	1-octene	30	520[g]	0.7
8[f]	**K**	1-octene	20	480[g]	0.7
9[f]	**L**	1-octene	40	1480[g]	1.1
10[f]	**M**	1-octene	40	1340[g]	1.3

[a] Cited throughout the introduction (5.1). [b] 0.1 mol %, 80°C, 40 bar of 1:1 CO/H_2, 9hrs; [c] 0.1 mol %, 80°C, 80 bar of 1:1 CO/H_2, 16hrs; [d] 0.25 mol %, 40°C, 40 bar of 1:1 CO/H_2, 24hrs; [e] 0.1 mol %, 100°C, 20 bar of 33:67 CO/H_2, 24hrs; [f] 0.02mol %, 100°C, 50 bar of 1:1 CO/H_2, 4hrs; [g] derived from the maximum slope at the onset of reaction.

Tetrahydropyrimidine-2-ylidenes as NHC ligands for Rh-complexes were also investigated toward the hydroformylation of 1-octene (Figure 5.4) by Buchmeiser and Nuyken et al.,[10] and were reported to display high TOFs of 480 h^{-1} (**J, K**, entries 7, 8Table 5.1) to 1480 h^{-1} (**L, M**, entries 9, 10, Table 5.1) at 100 °C/50 bar. Unfortunately, as the reaction proceeded, so did isomerization. Time-dependant studies were carried out and after 4 hrs, the n/*iso* ratio decreased from 2.4 initially to 0.8. Substituting the halide ligand, Br for Cl, did not result in a significant difference in activity. However, the variation of R-groups from 2-propyl (**J, K**) to mesityl (Mes) = 2,4,6-trimethylphenyl) (**L, M**), significantly increased activity; even the induction period was halved to 0.5 hour. The induction period observed for all catalysts corresponds well with Wilkinson's halide inhibition[6] due to the slow formation of catalytically active species by hydrogenolysis, which is often sped up by die addition of bases such as NEt_3. Although the catalysts described are highly active initially, the overall TOFs were not reported and > 80% conversion was only achieved after 19 hrs. However, the time-dependent study done by Buchmeiser and Nuyken showed how selectivity is forfeited at high activities and corresponds to the studies reported by both Crudden (**A, B**) and Peris (**D**).

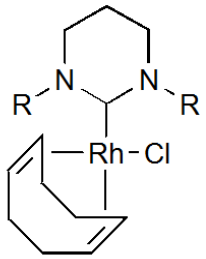

R = 2-propyl; X = Br (**J**) or Cl (**K**)
R = 2, 4, 6-trimethylphenyl;
X = Br (**L**) or Cl (**M**)

Figure 5.4. Buchmeiser and Nyuken's tetrahydropyrimidines synthesized in 2005.[10]

5.2 Aim

For the purpose of this project, hydroformylation studies were carried out using the 1,2,3-triazol-5-ylidene-Rh(I) complexes (**4**–**6**, Figure 5.5) to investigate the effect of the triazole-*N*-substituent (aryl *vs* alkyl), and to consider the effect of the donating ferrocenyl substituent on the activity and selectivity of the catalyst precursors. In addition, both neutral (**N**) and cationic (**O**) bidentate *N*-donor functionalised triazolylidene Rh(I) complexes[11] were included for comparative purposes under similar reaction conditions (since previously reported Rh-NHC complexes were employed as catalyst precursors under varying reaction

conditions). The utilization of the redox-active ferrocenyl substituent as a donating group *vs* the electron-withdrawing effect of the ferrocenium substituent was investigated by the *in situ* generation of complex **4ox** with the addition of an oxidant as an additive during the catalytic reaction.

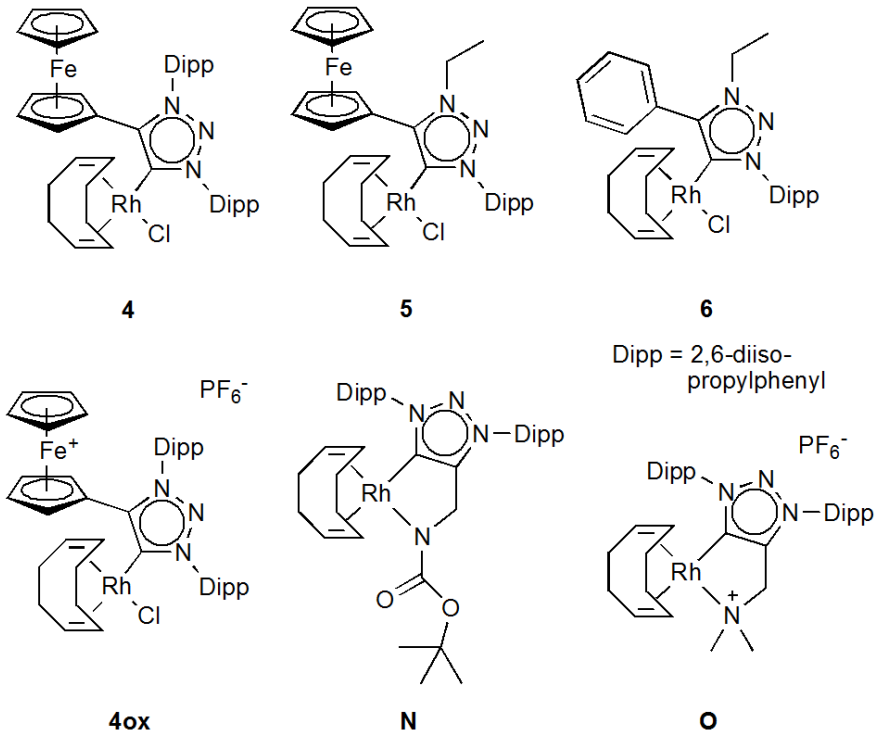

Figure 5.5. Complexes **4**–**6, 4ox** and **N**, **O** evaluated as precursor catalysts for the hydroformylation of 1-octene.

5.3 Results and discussion

Complex **4** was subjected to optimization studies, whereby reaction conditions were changed until near complete conversion of the substrate was obtained. Firstly, the time was varied between 4 to 8 hrs at set conditions of 75 °C/40 bar and with a [Rh]: substrate ratio of 1:2500. (entries 1–3, Table 5.2). Under these circumstances, the syngas pressure was also adjusted to 50 bar (entry 4, Table 5.2). Once the optimized time was set at 8 hrs, the mol ratio was increased to 1:1250 ([Rh]: substrate), and the temperature was varied from 55–75 °C at 40 bar syngas pressure (entry 5–7). Entries 8 and 9 follows variation on syngas pressure at the increased mole ratio of 1:1250 ([Rh]: substrate), with the temperature constant at 75 °C for 8 hrs.

Table 5.2. Optimization results[a] of the hydroformylation of 1-octene with catalyst precursor, **4**.

Entry	Reaction conditions	% con-version	% Alde-hydes	% Iso-octene	% Non-anal	% Branched	TOF[b]	TON[c]	n/*iso*
Variation of time and syngas pressure. Temperature = 75 °C; [Rh]: substrate = 1:2500 (0.04 %)									
1	40 bar/ 4 hrs	70 (6.48)	70 (4.42)	30 (4.42)	70 (0.44)	30 (0.44)	305 (42.40)	1219 (169.62)	2.3 (0.05)
2	40 bar/ 6 hrs	85 (7.19)	67 (9.42)	33 (9.42)	69 (2.32)	31 (2.32)	238 (17.72)	1425 (106.32)	2.20 (0.24)
3	40 bar/ 8 hrs	81 (8.59)	59 (7.91)	41 (7.91)	70 (2.64)	30 (2.64)	148 (21.23)	1187 (169.80)	2.4 (0.29)
4	50 bar/ 8 hrs	86 (15.05)	71 (8.33)	29 (8.33)	6666 (0.71)	34 (0.71)	189 (16.50)	1509 (132.04)	1.9 (0.06)
Variation of temperature. Syngas pressure = 40 bar; time = 8 hr; [Rh]:substrate = 1:1250 (0.08 %)									
5	55 °C	56 (20.33)	82 (16.12)	18 (16.12)	59 (1.28)	41 (1.28)	70 (19.74)	558 (157.96)	1.5 (0.08)
6	75 °C	96 (2.40)	67 (3.39)	33 (3.39)	71 (3.21)	29 (3.21)	100 (7.07)	798 (56.57)	2.4 (0.36)
7	95 °C	99 (0.40)	70 (3.56)	31 (3.56)	62 (1.76)	38 (1.76)	107 (5.17)	857 (41.39)	1.6 (0.12)
Variation of syngas pressure. Temperature = 75°C; time = 8 hr; [Rh]:substrate = 1:1250									
8	30 bar	75 (18.84)	65 (3.09)	35 (3.09)	70 (0.70)	30 (0.70)	76 (15.79)	606 (126.32)	2.3 (0.08)
9	50 bar	86 (7.56)	78 (4.10)	22 (4.10)	64 (2.81)	36 (2.81)	105 (13.61)	838 (108.88)	1.8 (0.21)

[a]Reactions carried out in triplicate, average of three runs given with standard deviation in parentheses.

[b]Turnover frequency, calculated as TOF = mol aldehydes/mol cat.h^{-1}

[c]Turnover number, calculated as TON = mol aldehydes/mol cat.

Complex **4** was active towards the hydroformylation of 1-octene and underwent subsequent reactivity testing under varied reaction conditions for the optimized conversion of 1-octene. No full conversion was achieved under any of the reaction conditions employed (entries 1–9, Table 5.2). At 0.04 mol % catalyst loading, the best conversion was observed after 6 hrs (85%, entry 2, Table 5.2). However, at 8 hrs the regioselectivity was higher, (n/*iso* = 2.4, entry 3, Table

5.2) than at 6 hrs (n/*iso* = 2.2, entry 2, Table 5.2). For this reason, 8 hrs were chosen as the optimum time for the following experiments. To reach higher conversions, the catalyst loading was increased to 0.08 mol %. At 75 °C, 40 bar at 0.04 mol %, only 80 % conversion was reached (entry 3, Table 5.2), where at the same conditions with double the catalyst loading, a conversion of 95 % was obtained (entry 6, Table 5.2). Succeeding experiments (entries 5, 7–9, Table 5.2), describe reactivity testing whereby the catalyst loading was kept at 0.08 mol %. With a rise in temperature (entries 5–7, Table 5.2), the conversion increases to near full conversion of 99 % at 95 °C (entry 7, Table 5.2), at a price to regioselectivity (n/*iso* = 1.6), compared to 75 °C (n/*iso* = 2.4) as the reaction temperature (entry 6, Table 5.2). In addition, internal alkene formation was observed to occur at this high temperature with the observance of 3-octene (not seen at lower reaction temperatures). Thus, even though 99% conversion was achieved at 95 °C, the significant drop in both chemo- and regioselectivity at 95 °C, and significantly lower conversions at lower temperatures, (55 °C, entry 5) confirmed 75 °C as the optimum temperature. Similarly, increased syngas pressure (entry 9, 50 bar, Table 5.2), lead to a decrease in the chemoselectivity, while pressures lower than 30 bar (entry 8, Table 5.2) significantly reduced conversions. This is consistent with the results obtained from the 0.04% mol ratio reactions (entries 3, 4, Table 5.2), and thus 40 bar was set as optimum syngas pressure.

The reactivity of complexes **5**, **6** and **N**, **O** were studied under these optimized conditions i.e. 75 °C/40 bar for 8 hrs at 0.08 mol % catalyst loading (Table 5.3).

Table 5.3. The hydroformylation of 1-octene with catalyst precursors, **4**–**6, N**, **O**.[a,b]

Entry	Catalyst precursor	% conversion	% Aldehydes	% Isooctenes	% Nonanal	% Branched	TOF	TON	n/*iso*
1	**4**	96 (2.40)	67 (3.39)	33 (3.39)	71 (3.21)	29 (3.21)	100 (7.07)	798 (56.57)	2.4 (0.36)
2	**5**[c]	100	80	20	64	36	125	1004	1.8
3	**6**	100 (0.0)	75 (3.33)	25 (3.33)	63 (6.55)	37 (6.55)	117 (5.20)	935 (41.64)	1.8 (0.45)
4	**N**	83 (3.69)	60 (0.67)	40 (0.67)	67 (1.63)	33 (1.63)	78 (3.69)	627 (29.50)	2.0 (0.16)
5	**O**	100 (0.17)	97 (0.72)	2.7 (0.87)	54 (0.46)	46 (0.46)	152 (1.61)	1213 (12.85)	1.2 (0.02)

[a]Reactions carried out in triplicate, average of three runs given with standard deviation in parentheses.

[b]Conditions: 75°C/40 bar for 8 hours at substrate: [Rh] ratio of 1250 (0.08% mol).

[c]Single catalytic run

To exclude the possibility of heterogeneous catalytic activity, a mercury drop test was performed on complex **4**. The activity of the catalyst decreased slightly, indicating some degree of mercury poisoning but a heterogeneous catalytic mode of action can be ruled out.[12] To ensure that the ferrocenyl moiety of complex **4** does not participate in the catalytic transformation of 1-octene, the precursor triazolium salt, **1**, was subjected to reactivity testing, and was shown to be catalytically inactive.

All complexes **4**–**6, N**, **O** proved to be active in the hydroformylation of 1-octene under the constant reaction conditions, namely 75 °C /40 bar for 8 hrs, (entries 1–5, Table 5.3). Among the complexes, complex **O** (Figure 5.5), the cationic *N*-donor functionalized rhodium(I) complex, displayed the highest TOF and a 97% yield in aldehydes, entry 5 (Table 5.3). Furthermore, **O** demonstrated excellent chemoselectivity but poor regioselectivity towards linear and branched aldehydes. On the other side of the spectrum, with the lowest TOF, is complex **N** (Figure 5.5), the neutral *N*-donor functionalized rhodium(I) complex containing both a donating MIC and donating amido-moiety coordinated to the Rh(I) center (entry 4, Table 5.3). However, a significant increase in the regioselectivity of this catalyst precursor was observed. Among the complexes,

the N1-, N3-diarylated ferrocenyl rhodium(I) complex, **4** delivered the highest regioselectivity (n/*iso* = 2.4, entry 1, Table 5.3) with 96% conversion. The N1-alkyl, N3-arylated rhodium(I) complexes, **5** and **6** each had near full conversion of substrate, with similar regioselectivities obtained, and slight differences in chemoselectivity (entries 2 and 3, Table 5.3).

Figure 5.6 illustrates the results expressed in Table 5.3, and the emerging trends that could be determined. From the results portrayed in Figure 5.6 (a), it is shown that the increase in activity is associated by an increase yield in aldehydes and a decrease yield in isomers (increased chemoselectivity). The complexes' carbene ^{13}C NMR chemical shift is also given along the complexes' corresponding IR carbonyl stretching frequencies. As the stretching frequencies increase, so does the activity of the pre-catalyst increase. This is especially prevalent in the difference observed between the activity of the N-donor functionalized complexes, **N** and **O**. As mentioned before, selectivity is often forfeited for activity, and therefore it is expected that since **N** has the lowest activity, by default **N** should have the highest regioselectivity. However, this is not the case when comparing **N** and **4**, where complex **4** showed the highest regioselectivity. In addition, when comparing **5** and **6**, insignificant differences in the activity and chemoselectivity of these catalyst precursors are observed. No observable trends could be identified from the carbene chemical shifts or the carbonyl stretching frequencies. This observation strengthens previously reported notions, that regioselectivity is more influenced by the steric bulk of the complex, rather than the electron density around the metal (*vide supra*).

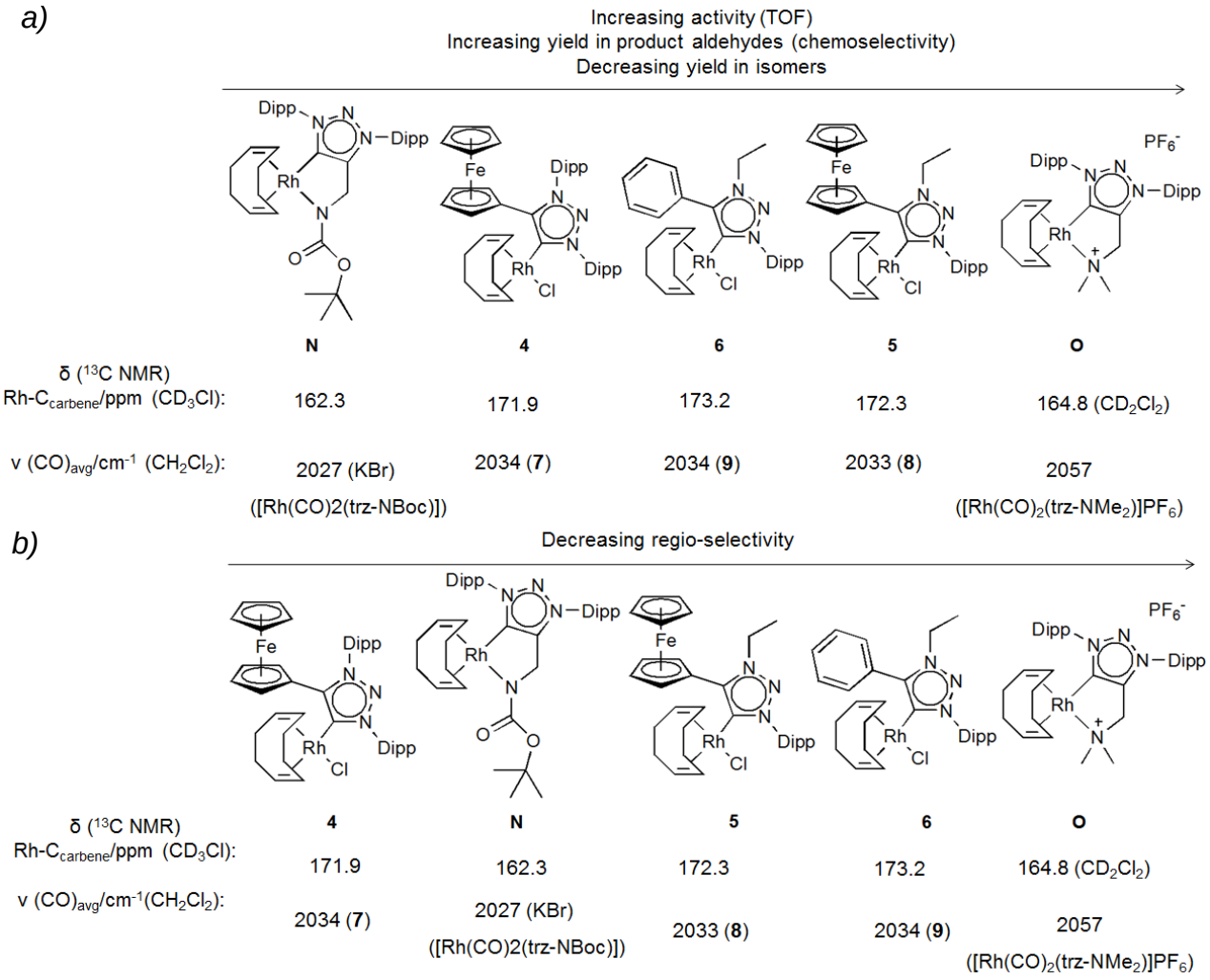

Figure 5.6. Concluding trends observed from the catalytic results (Table 5.3) obtained for complexes **4**–**6**, **N**, **O**. In addition, the ^{13}C NMR carbene chemical shift and the average CO stretching frequencies of the analogous carbonyl complexes are given.

Both steric and electronic factors must be evaluated in discussing the performance of the catalyst precursors. With regards to regioselectivity; the linear to branched selectivity is determined by the olefin insertion-migration step i.e. formation of the metal-alkyl intermediate, which is somewhat influenced by the steric bulk of the ligand, as previously reported for both phosphine and NHC-Rh(I) complexes.[3] Bulkier systems will favor linear addition, as regioselectivity mainly depends on the different rates of β-hydride elimination between linear and branched metal intermediates (Figure 5.7).[13,14]

Almost all linear alkyl intermediates undergo CO insertion to form the respective linear aldehyde whereby β-hydride elimination of branched intermediates are

faster than CO insertion, and hence revert to terminal or internal olefins (Figure 5.7). The result is the slower formation of branched aldehydes from Markonikov additions. Thus, when the catalytic run is complete, all anti-Markonikov (anti-M) additions are likely to be linear aldehydes, but only some Markonikov (M) additions were converted to branched aldehydes, with high amounts of internal isomers left in solution, thereby also decreasing the overall chemoselectivity of the pre-catalyst.

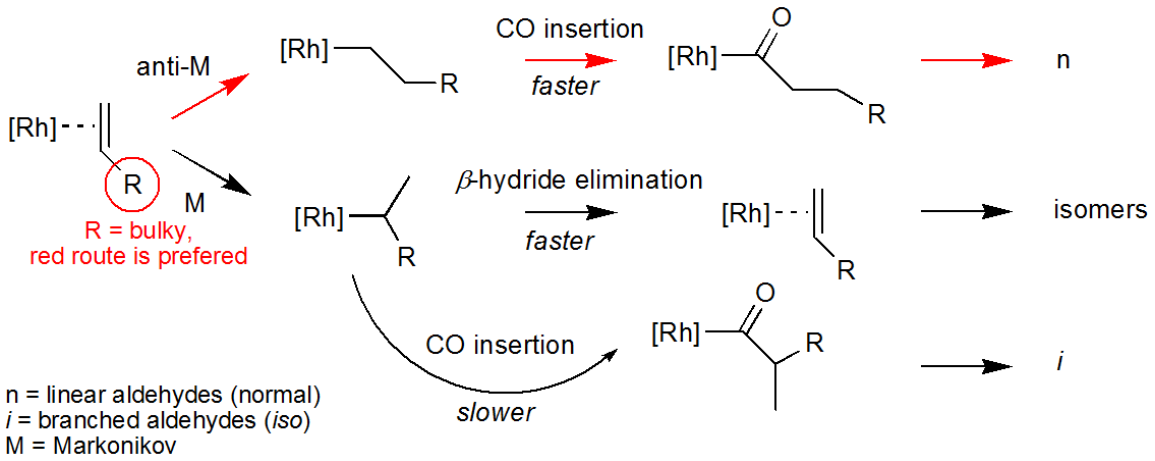

Figure 5.7. The linear to branched selectivity is determined by the olefin insertion-migration step in the hydroformylation of aliphatic alkenes.[13,14]

Results from Table 5.3 and Figure 5.6 (b), show that among the complexes, **4** (n/iso = 2.4, entry 1, Table 5.3) and **N** (n/*iso* = 2.0, entry 4, Table 5.3) had the highest regioselectivities of the series. Both the complexes have fairly bulky R-groups on C4; the bulky ferrocenyl substituent (**4**) and the hemilabile amido-Boc group (**N**) (Boc = *tert*-butoxycarbonyl). This can hinder access to the metal center, thereby favoring anti-M addition for an increase in the yield of linear aldehydes. Consequently, these bulky substituents do provide the possibility of hindering the CO insertion of the branched intermediate if M-addition do occur, so that the branched aldehydes are not formed, but instead the yield of the internal isomers increase (**4**: 33%, entry 1 and **N**: 40%, entry 4). For the other complexes, the regioselectivity decreases from **5** (n/*iso* = 1.8, entry 2, Table 5.3) to **O** (n/*iso* = 1.2, entry 5, Table 5.3) as their yield in isomers decrease as well (**5**: 20%, entry 2 and **O**: 3%, entry 5).

From an electronic perspective: electron donating systems stabilize the metal intermediates in such a way that changing from one transition state to the next require higher energy barriers than for electron withdrawing systems.[15] Thus, for a sterically demanding and electron-donating system, the rate of alkene insertion will be slower, consequently so also CO insertion, hence allowing enough time for isomerization of alkenes to ensue. Overall catalytic activity is influenced by the electronic density around the metal center, and evidence thereof is depicted in Table 5.3 and Figure 5.6(a). The pre-catalyst that demonstrate the highest activity, **O** (TOF = 152 hr^{-1}, entry 5, Table 5.3) was also the only cationic complex and the most electron deficient complex in the series (confirmed by the carbonyl stretching frequencies). As seen in Figure 5.6(a), as the stretching frequencies decrease, the activity of the complexes decreases as well.

The presence of the ferrocenyl substituent was evaluated by comparing the results obtained from **5** and **6**. From previous chapters, it was concluded that the ferrocenyl C4-substituent contributes electronically no differently than the phenyl substituent. The performance of **5** and **6** as pre-catalysts in the hydroformylation of 1-octene closely resemble one another, with insignificant differences.

In view of the fact that the ferrocenyl substituent is redox-active, the possibility of utilizing pre-catalyst rhodium complex **4** as a redox switchable catalyst was investigated by generating complex **4ox** *in situ* with the addition of a suitable oxidant (Table 5.4). As an oxidized ferrocenium moiety is known to be just as electron-withdrawing as a CF_3-substituent,[16] the advantages of both the bulky tri-arylated ligand scaffold of **4** as well as the significantly lesser electron-donating ability of a substituted ferrocenium was planned as a strategy to increase the activity of the catalyst, without a concurrent loss in regioselectivity.

Table 5.4. The hydroformylation of 1-octene with redox-switchable catalyst precursor, **4**[a,b] with the addition of oxidant (**4ox**)[c].

	% conversion	% Aldehydes	% Iso-octenes	% Nonanal	% Branched	TOF	TON	n/*iso*
4	96 (2.40)	67 (3.39)	33 (3.39)	71 (3.21)	29 (3.21)	100 (7.07)	798 (56.57)	2.4 (0.36)
4ox	100 (0.00)	76 (2.35)	24 (2.35)	61 (1.53)	39 (1.53)	119 (3.67)	952 (29.51)	1.6 (0.11)

[a]Reactions carried out in triplicate. an average of three runs given with standard deviation in parentheses.

[b]Conditions: 75°C/40 bar for 8 hours at substrate to [Rh] ratio of 1250 (0.08% mol).

[c]Addition of 1 equivalent (0.08% mol) acetylferrocenium hexafluorophosphate to Rh precursor catalyst **4** to generate **4ox** *in situ*.

The oxidation of **4** to **4ox** resulted in a higher rate of conversion of 1-octene (TOF = 119 hr-1) with nearly 10% increased preference to aldehydes compared to **4**. Furthermore, **4ox** demonstrated an increase in chemoselectivity. Surprisingly, **4** still showed enhanced regioselectivity (n/*iso* = 2.4) compared to **4ox** (n/*iso* = 1.60).

As expected, the catalytic activity of **4ox** increased as anticipated for decreased electron density at the metal (Rh(I)) centre, by use of an electron-withdrawing ferrocenium substituent on the triazolylidene ligand. Surprisingly, the regioselectivity decreased even though the steric bulk of the ligand scaffold was maintained. One possible reason for the decrease in the regioselectivity can be ascribed to the effect the electron deficiency of the metal has on the rate of the reactions; the steric bulk will favour linear aldehydes, but if the branched intermediate forms, the intermediate is less stable than it was with the neutral complex. Consequent faster CO-insertion into the branched [Rh]-alkyl intermediate can result in more branched aldehydes and less internal isomer products.

Furthermore, the reactivity of **4ox** closely resembles that of complexes **5** and **6**, which is unexpected since the electronic properties of the triazolylidene ligand are different to those of **5** and **6** (compare the dicarbonyl analogue of **4ox** ($\nu(CO)_{avg}/cm^{-1}$ for **7ox**: 2046) *vs* the dicarbonyl analogues of **5** and **6** ($\nu(CO)_{avg}/cm^{-1}$ for **8**: 2033; **9**: 2034). Although only the electronic properties of

complex **4** was changed upon chemical oxidation, the reactivity of the resultant complex (**4ox**) bear a resemblance to the reactivity of **5.** Complex **5**, on the other hand, displays electronic properties very similar to those observed for **4**; only a difference on the N1-wingtip substituents (steric effect) results in a significant change in catalytic reactivity. It is therefore not possible to completely distinguish between steric and electronic effects on the outcome of regioselectivity and activity of a pre-catalyst.[1,3]

5.4 Conclusion

Monodentate 1,2,3-triazol-5-ylidene Rh(I) complexes (**4**–**6**) and bidentate *N*-donor functionalised triazol-5-ylidene Rh(I) complexes (**N**,**O**) were evaluated as potential pre-catalysts in the hydroformylation of 1-octene. All complexes showed catalytic activity at the optimized conditions of 40 bar/ 75 °C, for 8 hrs at 0.08 % mol catalyst loading. Comparing these complexes to the literature Rh(I) NHC complexes discussed in the introduction (*vida supra*, 5.1), the complexes **4**–**O** showed trends of similar to higher TOFs (78–152 hr^{-1}) than what was reported (11.6–111 hr^{1}) and higher regioselectivities of n/*iso* = 2.4–1.2 for **4**–**O** (vs. n/*iso* = 1.7–0.7). However, the reaction conditions employed in this study were not identical to the previously reported studies, nor were the structure of the pre-catalysts employed analogous to the literature-reviewed compounds, which precludes a direct comparison of the results with other reported Rh(I)-carbene complexes as hydroformylation catalysts.

Among the complexes **4**–**O** studied, the complex that exhibited the highest activity in the hydroformylation of 1-octene, was complex **O** (TOF = 152 hr^{-1}) and is attributed to the electron deficient nature of the complex (only cationic complex in the series). The similar reactivity of complexes **5** (C4-Fc) and **6** (C4-Ph) leads to the conclusion that there is no significant difference between these complexes, either electronically or sterically (also confirmed by spectroscopic studies). However, complex **4**, bearing the ferrocenyl group like **5**, but with bulky arylated wingtip groups, showed the highest regioselectivity (n/*iso* = 2.4), possibly indicating that the accumulative steric bulk provided by the ferrocenyl moiety and the N1-, N3-dipp groups increased the regioselectivity of complex **4** (although **4**, **5**, and **6** display virtually identical electronic properties).

Higher activity of **4** (TOF = 100 hr^{-1}) was achieved with the addition of an oxidant to generate **4ox** (TOF = 119 hr^{-1}) *in situ*, at a cost to regioselectivity (n/iso 2.4 vs. 1.6). Surprisingly, the reactivity of oxidized complex **4ox** closely resembles that of complex **5** and **6**, although these complexes are electronically different. This observation is further evidence that neither steric hindrance around the catalytic metal centre (Rh(I)), nor electronic influences of the coordinated ligands, can be used as independent predictors for the activity of the pre-catalysts.

5.5 References

1 R. Franke, D. Selent and A. Börner, *Chem. Rev.*, 2012, **112**, 5675–5732.

2 G. D. Frey, *J. Organomet. Chem.*, 2014, **754**, 5–7.

3 W. Gil and A. M. Trzeciak, *Coord. Chem. Rev.*, 2011, **255**, 473–483.

4 J. M. Praetorius and C. M. Crudden, *Dalton Trans.*, 2008, **9226**, 4079–4094.

5 A. C. Chen, L. Ren, A. Decken and C. M. Crudden, *Organometallics*, 2000, **19**, 3459–3461.

6 D. Evans, J. A. Osborn and G. Wilkinson, *J. Chem. Soc. A Inorganic, Phys. Theor.*, 1968, **566**, 3133.

7 A. Neveling, G. R. Julius, S. Cronje, C. Esterhuysen and H. G. Raubenheimer, *Dalton Trans*, 2005, **1**, 181.

8 M. Poyatos, P. Uriz, J. A. Mata, C. Claver, E. Fernandez and E. Peris, *Organometallics*, 2003, **22**, 440–444.

9 S. Dastgir, K. S. Coleman, A. R. Cowley and M. L. H. Green, *Organometallics*, 2006, **25**, 300–306.

10 M. Bortenschlager, M. Mayr, O. Nuyken and M. R. Buchmeiser, *J. Mol. Catal. A Chem.*, 2005, **233**, 67–71.

11 I. Strydom, *Synthesis and application of N-donor functionalised*

triazolylidenes, University of Pretoria, MSc. dissertation., 2016.

12 J. A. Widegren and R. G. Finke, *J. Mol. Catal. A Chem.*, 2003, **198**, 317–341.

13 R. P. J. Bronger, P. C. J. Kamer and P. W. N. M. van Leeuwen, *Organometallics*, 2003, **22**, 5358–5369.

14 C. P. Casey, E. Lin Paulsen, E. W. Beuttenmueller, B. R. Proft, L. M. Petrovich, B. A. Matter and D. R. Powell, *J. Am. Chem. Soc.*, 1997, **119**, 11817–11825.

15 M. Sparta, K. J. Børve and V. R. Jensen, *J. Am. Chem. Soc.*, 2007, **129**, 8487–8499.

16 D. I. Bezuidenhout, I. Fernandez, B. van der Westhuizen, P. J. Swarts and J. C. Swarts, *Organometallics*, 2013, **32**, 7334–7344.

Chapter 6

Gold(I) triazolylidene complexes

6.1 Background

Gold(I) chlorido complexes have recently emerged as a popular target for mediating numerous catalytic transformations, specifically in organic synthetic approaches.[1] Gold(I) chlorido complexes of the type [L(Au)Cl] are activated in the presence of a halide scavenger, such as silver salts (AgOTf, $AgSbF_6$) or potassium salts ($[K(B(C_6F_5)_4)]$) as a mono-ligated cationic catalyst.[2] The ancillary ligand (L) is most often required for strong electronic and steric stabilization of the cationic catalyst – often provided by ligands such as NHCs - even though L can also modulate the reactivity and selectivity of the catalyst.

The group of Crowley[2] was among the first to synthesize triazolylidene gold(I) chlorido complexes (**A**, Scheme 6.1), by using the transmetalation protocol.[3,4] In this methodology, the triazolium salt was reacted with Ag_2O in the presence of NMe_4Cl to generate the Ag-complex *in situ*. Subsequent addition of $Au(SMe_2)Cl$ afforded the gold(I) chlorido complex **A**. Furthermore, complex **A** was evaluated as precursor catalyst in carbene transfer- and cyclisation reactions. In the presence of $AgSbF_6$, successful carbene transfer of ethyl diazoacetate into O-H bonds of primary, secondary and tertiary alcohols transpired.[5]

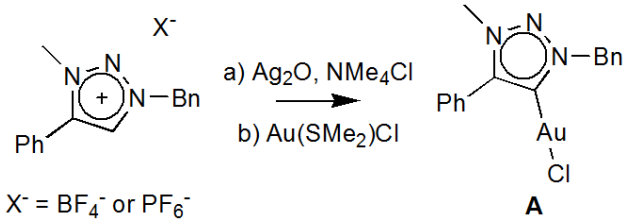

Scheme 6.1. The synthesis of the triazolylidene gold(I) chlorido complex, **A** employing an in situ transmetalation route.[2]

Carbene transfer from silver(I) to gold(I) complexes can yield either neutral monocarbene gold(I) halide or cationic biscarbene gold(I) complexes, depending on the nature of the precursor ligand counterion. However, the

nature of the anion is not the only determining factor for mono- or biscarbene transfer. For instance, Crowley et al.[2] (Scheme 6.1) prepared the gold(I)-halide complex (**A**) from a triazolium salt with a PF_6^- counterion, whereas Lin and Wang[3] synthesized the biscarbene Ag(I) complex (**E**), from an imidazolium salt also bearing a PF_6^- counterion (**C**, Scheme 6.2). In the review written by Garrison,[6] it is stated that non-coordinating anions favour the formation of the biscarbene gold(I) complexes, while the coordinating anions favour gold(I) halide complex formation. Therefore, by either having a salt with a coordinating counterion such as Br^- (**B**), or by adding a coordinating halide donor, such as NMe_4Cl or KCl, the gold(I) halide complexes can selectively be prepared. Furthermore, the biscarbene gold complexes of the type **F** are formed from the transmetalation of the biscarbene silver complexes of the type **E**.

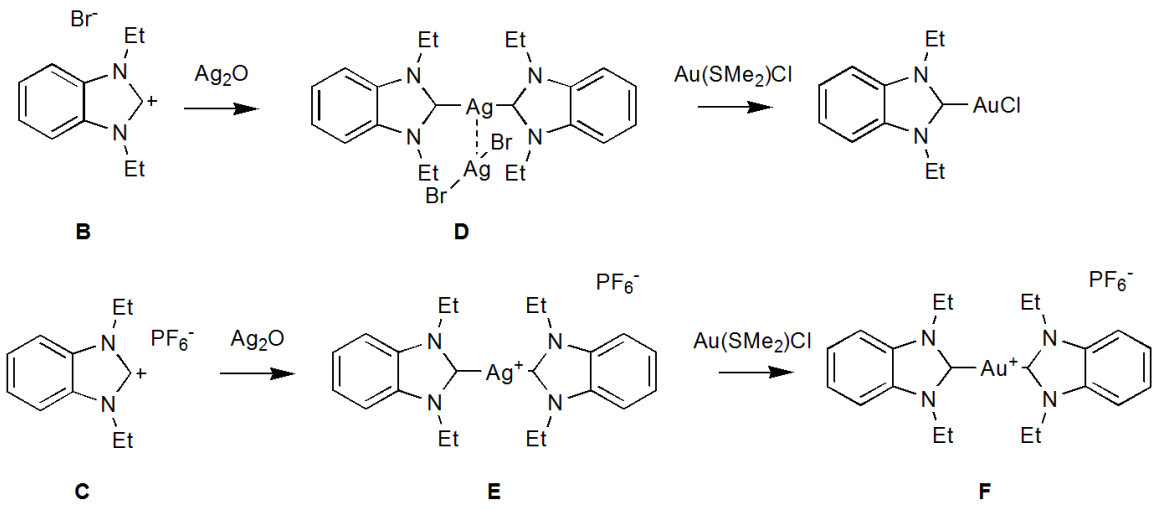

Scheme 6.2. The counterion dependent syntheses of the gold(I)-triazolylidene chlorido complex and the gold(I) bis(triazolylidene) complex via transmetalation.[3]

The deprotonation of the triazolium salts to generate the free carbene with subsequent metalation with Au(tht)Cl (tht = tetrahydrothiophene), to afford gold(I)-chlorido complexes is another synthetic approach.[7] However, this method has shown to be unselective, generating both the monocarbene gold(I) chlorido and the biscarbene gold(I) complexes.[8,9] Successful selective monocarbene complex preparation was achieved with Anti-Bredt N-heterocyclic carbenes (one of the neighbouring N-atoms of the carbene has reduced donating ability by being coordinated in a strained bridgehead position)[10],

whereby 2 equivalents of the free carbene was added to Au(tht)Cl to afford the NHC-Au-Cl complex in 85% yield (Scheme 6.3).

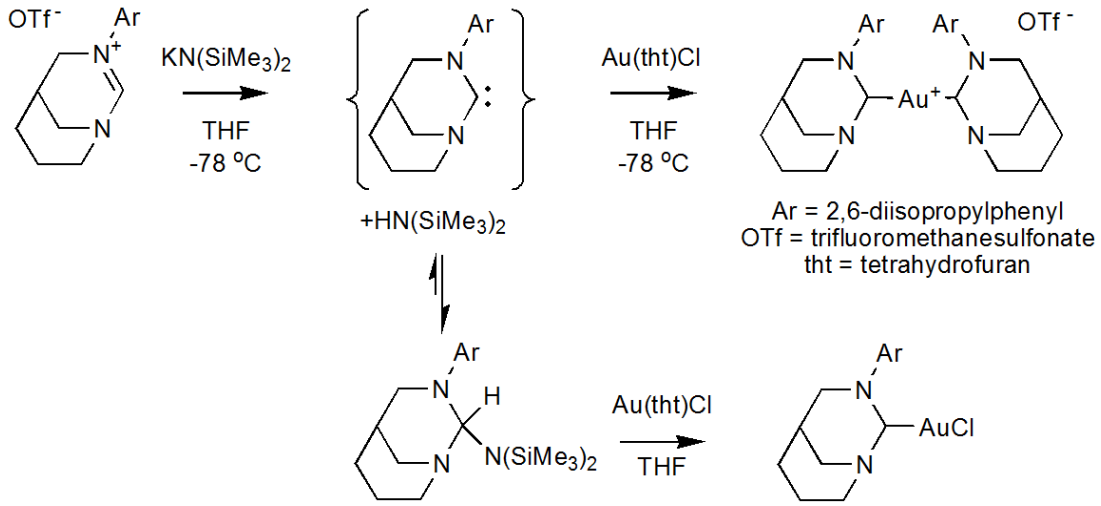

Scheme 6.3. The synthesis of the biscarbene gold(I) complex and the monocarbene gold(I) chlorido complex via the free-carbene route.[8]

The biscarbene gold(I) complex of the type **F** is known to be catalytically inactive,[8,11] and therefore when coordination to the free carbene yields mixtures of both complexes, the yield of the desired complex (gold(I) halide) is compromised. Bertrand and co-workers reported a novel synthetic route for the exclusive synthesis of the gold(I) chlorido complexes (Scheme 6.4).[12] The synthesis involves the coordination of $Au(PPh_3)Ph$ to the free carbene, generating the gold(I) phenyl complex (**I, J**), whereby the triazolylidene readily replaces PPh_3. Following hydrolysis of the phenyl ligand with HCl, complexes **K** and **L** were afforded in high yield.

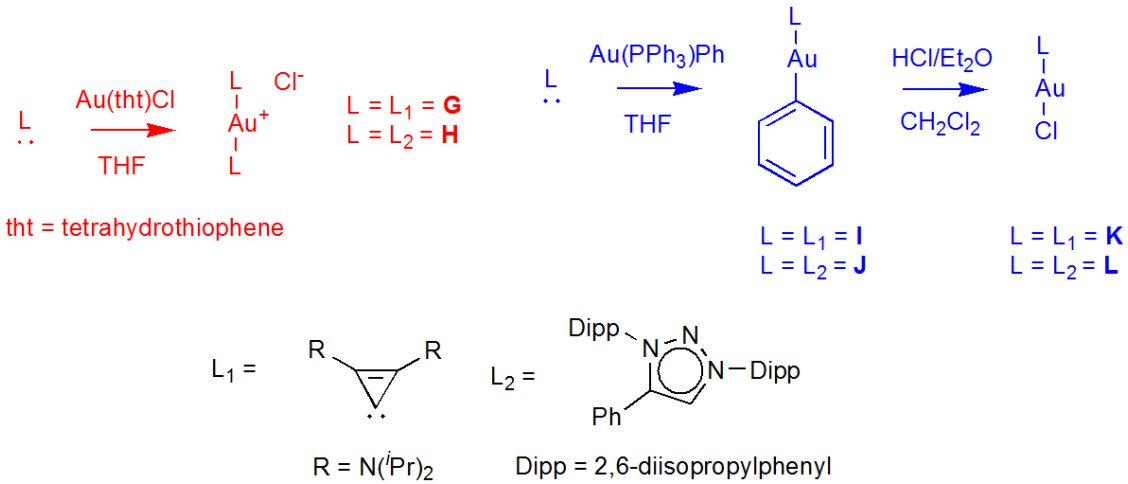

Scheme 6.4. The exclusive synthesis of the gold(I) chlorido complexes, **K** and **L** (blue), from the hydrolysis of the gold(I) phenyl complexes. In addition the synthesis of the biscarbene gold(I) complexes, **G** and **H** (red) are shown.[11]

Complexes **K** and **L** underwent catalytic reactivity testing for the functionalization of hydrazine and terminal alkynes. While complex **K** showed minimal activity, complex **L** managed to fully convert the acetylene. Moreover, both nitrogens in the parent hydrazine were functionalized, which is a first for transition metal catalysis.

The group of Albrecht has applied gold(I) triazolylidenes as pre-catalysts in the synthesis of oxazolines.[13] They have synthesized complexes **M**–**O**, and subsequent reactivity testing provided some insights into the role of the presence of the silver ions used as an additive in the reaction (Scheme 6.5). It was found that the biscarbene gold(I) complex **O**, and the phosphine gold(I) complex **N**, were poor catalyst precursors. Complex **M** only showed improved activity with the addition of the $AgBF_4$ and a base (NEt^iPr_2), with preference for the *trans* isomer formation. However, it was shown that complex **O** could be prepared from **M** with the addition of $AgBF_4$ to two equivalents of complex **M**. Thus, the addition of $AgBF_4$ to complex **M** as additive in the reactivity testing, suggests that the role of the silver(I) goes beyond halide scavenging, and involves the dissociation of the triazolylidene from the gold(I), thereby facilitating the carbene transfer process.

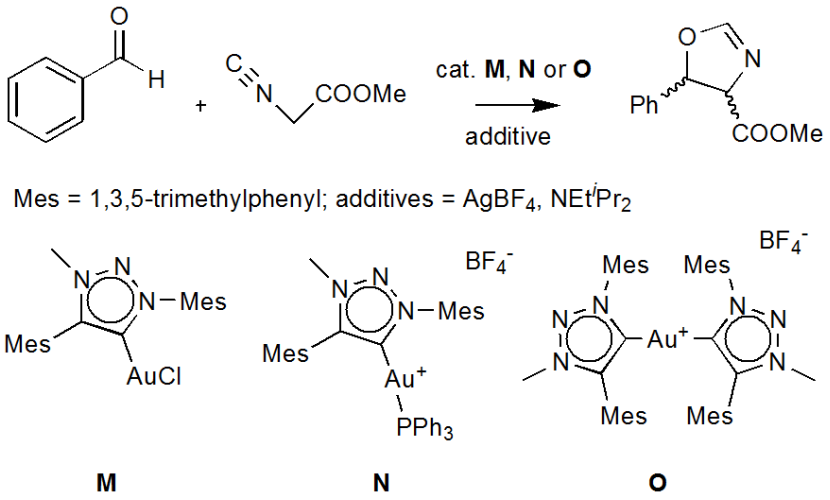

Scheme 6.5. The catalytic conversion of benzaldehyde and methylisocyanoacetate, with the pre-catalysts **M**–**O**.[12]

In addition, Albrecht recently reported on the catalytic application of triazolylidene gold(I) complexes in the silver(I)-free synthesis of oxazolines.[14] The addition of potassium salts as chloride scavengers, instead of silver(I), successfully activated the gold(I) pre-catalyst. However, the addition of silver delivers substantially higher catalytic activity.

The effect of a redox-switchable ferrocene substituent in triazolylidene gold(I) complexes as precursor catalysts were evaluated by Sarkar et al.[14] Complex **P** (Figure 6.1) was assessed as pre-catalyst in the synthesis of oxazolines by internal cyclisation. It was found that the oxidized ferrocenium complex delivered 88% conversion of substrate after 24 hrs, where the neutral complex only gave 12% conversion in the same time; and the significant effect of the oxidized moiety on the catalytic activity of the gold(I) complex could be concluded.

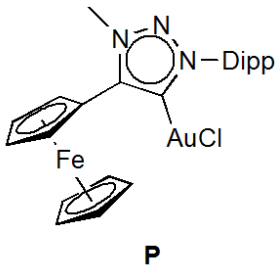

P

Dipp = 2,6-diisopropylphenyl

Figure 6.1. The ferrocenyl triazolylidene gold(I) chlorido complex **P** as pre-catalyst for the synthesis of oxazoles.[14]

6.2 Aim

The synthesis, characterization of complex **10** and preliminary catalytic conversion of oxazolines by **10** was discussed in this section. Four synthetic

routes were employed for the synthesis of complex **10** for the pursuit of high yields in **10**: Initially, the coordination to the free carbene, using an appropriate gold metal precursor, Au(tht)Cl was regarded the route of choice. Secondly the transmetalation protocol was investigated, ultimately allowing for the isolation of the silver(I) biscarbene complex **11**. Lastly, the synthetic route reported by Bertrand and co-workers, via the hydrolysis of the gold(I)-phenyl complex **12**, was also attempted. Furthermore, an unpublished method was investigated for the synthesis of **10**, using $Au(PPh_3)Cl$ as metal precursor, but produced complex **13** instead. The cyclic voltammetry of complexes **10** and **13** are reported.

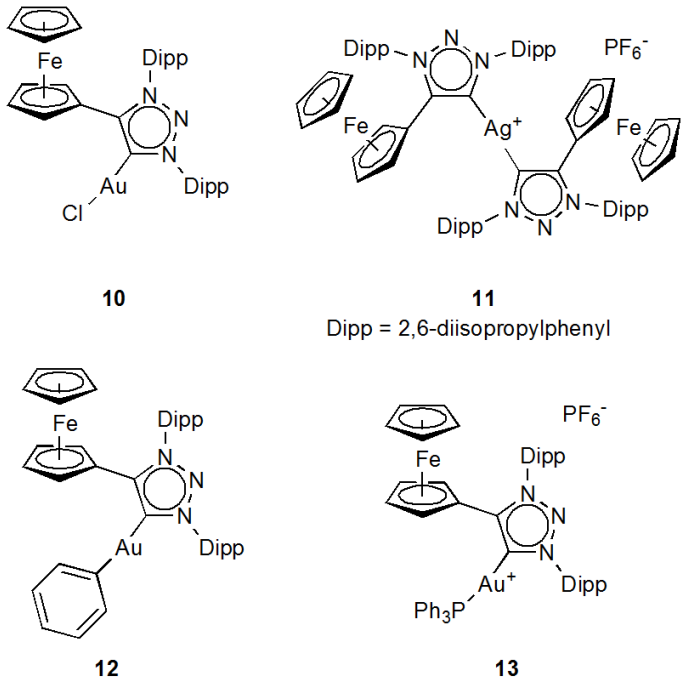

Figure 6.2. The triazolylidene gold(I) complexes (**10**, **12**, **13**) and the bis(triazolylidene) silver(I) complex (**11**) discussed in this chapter.

6.3 Results and discussion

6.3.1 Synthesis of the gold(I) triazolylidene complexes

Previously (Chapter 3), the successful metalation of the N1-, N3-diarylated, ferrocenyl triazolium salt 1 to rhodium(I) via the free carbene route with an appropriate metal precursor, [Rh(cod)Cl]2 (cod=1,5-cyclooctadiene), was discussed. To synthesize the gold(I) triazolylidene complex 10, the same

approach was employed using Au(tht)Cl as metal precursor.8 The metal precursor was added to the in situ generated free carbene, by the addition of base, (KN[SiMe$_3$]$_2$) to the ligand precursor salt **1** at -78 °C (Scheme 6.6).

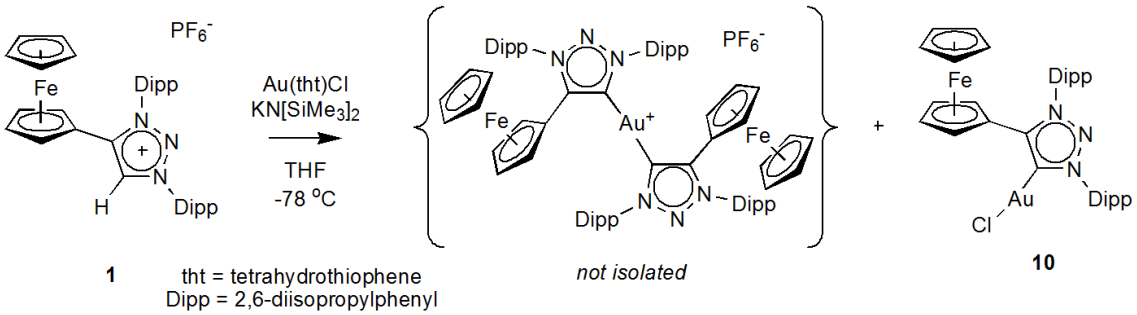

Scheme 6.6. The synthesis of both the bis(triazolylidene) gold(I) complex and the triazolylidene gold(I) chlorido complex, **10** via the free-carbene route.

After 24 hrs, the dark red solution was evaporated under reduced pressure and the residue was washed with hexane. Extraction with toluene yielded a pale-yellow solution which, upon concentration had very low yield. Extraction with DCM resulted in a red-orange solution, which when analyzed by means of NMR spectroscopy (Figure 6.3 and Figure 6.4) was determined to be a solution of two products: the mono-triazolylidene gold(I) complex (**10**) and the bis(triazolylidene) gold(I) complex.

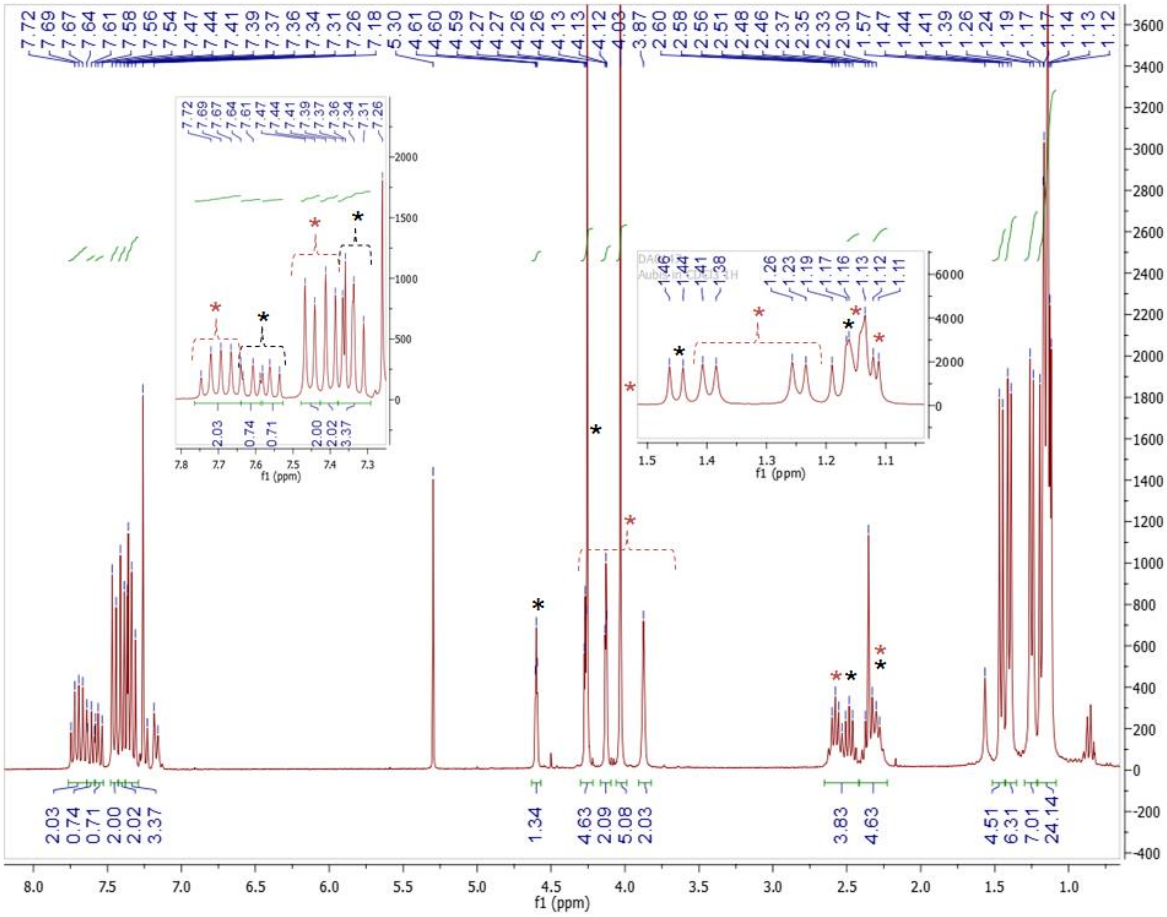

Figure 6.3. The ^{1}H NMR spectrum showing the presence of two gold(I) complexes, where (*) denotes the peaks belonging to the biscarbene gold(I) complex, and (**) complex **10** in solvent $CDCl_3$.

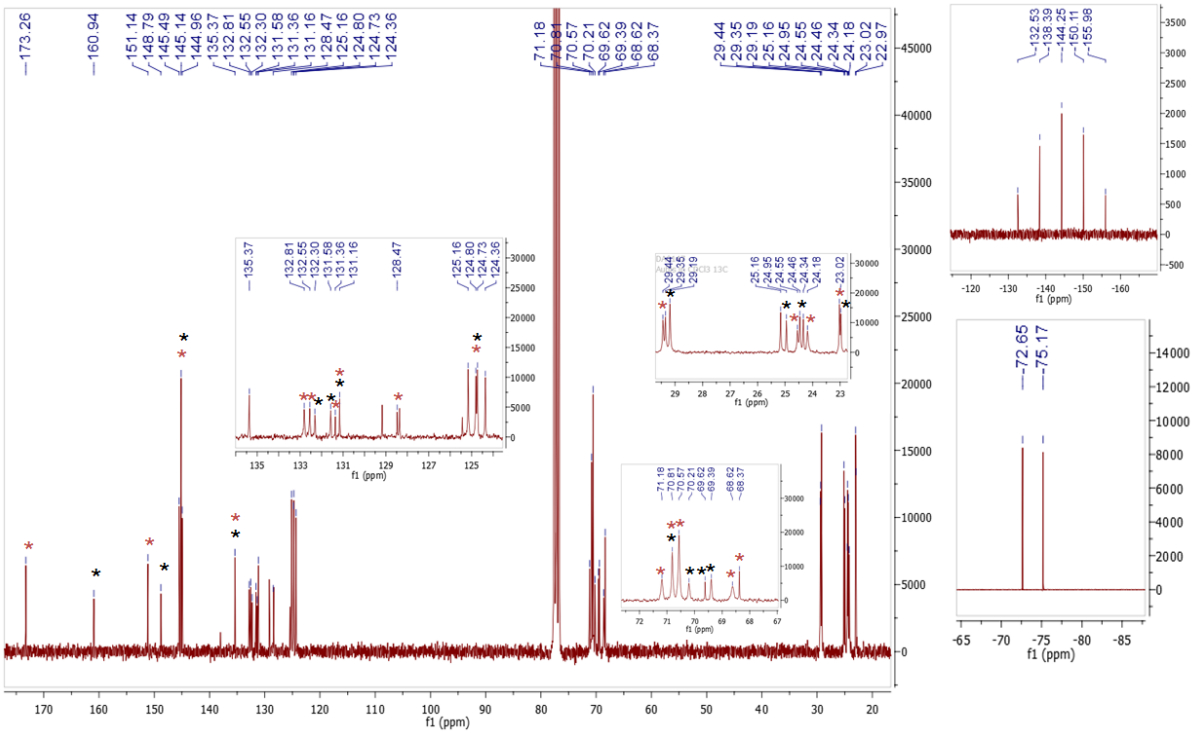

Figure 6.4. The ^{13}C NMR spectrum showing the presence of two gold(I) complexes, where (*) denotes the peaks belonging to the bis-carbene gold(I) complex, and (*) complex **10** in solvent $CDCl_3$. The ^{31}P NMR spectrum is shown top right, and the ^{19}F NMR spectrum bottom right.

In Figure 6.3, two sets of peaks were observed, each for the corresponding complex, where the red asterisk (*) indicate the signals belonging to the biscarbene gold(I) complex, and the black asterisk (*) annotates signals corresponding to the monocarbene gold(I) chlorido complex, **10**. Furthermore, no acidic proton at 9.06 ppm was observed, ruling out the possibility of the second set of peaks observed in Figure 6.3 belonging to the unreacted triazolium precursor salt **1**. Further evidence was the additional carbene peak of 176.3 ppm observed in ^{13}C NMR spectrum (Figure 6.4), where the chemical shift of the carbene for **10** is at 160.9 ppm. Likewise, the ^{31}P NMR and ^{19}F NMR spectra indicates the presence of a counterion, PF_6. The diarylated biscarbene gold(I) complex reported by Bertrand[12] (**F**, Scheme 6.4) displayed a carbene chemical shift of 173.3 ppm and Albrecht reported[13] the N1-alkyl, N3-arylated bis(triazolylidene) gold(I) complex (**M**, Scheme 6.5) with a carbene chemical shift of 175.8 ppm.

Another synthetic approach to obtain **10**, was the transmetalation from the corresponding bis(carbene) silver(I) complex, bearing the halogeno counterions of the type $[AgX_2]^-$ (complex of the type **D**, Scheme 6.2).[2,3,6] The synthesis of the silver complex involves the addition of a silver base, in this case Ag_2O, to the ligand precursor salt **1**. The counterion of the ligand precursor salt, PF_6^-, is regarded as a non-coordinating anion, and thus the addition of KCl is required to serve as an anion donor to facilitate the formation of the counterion, $AgCl_2^-$. Unfortunately, the driving force for this reaction is also the formation of the AgCl salts, discussed in previous chapters, and thus the formation of the easily obtained cationic biscarbene silver(I) complex **11**, with the PF_6^- counterion, occurred with quantitative yield (Scheme 6.7).

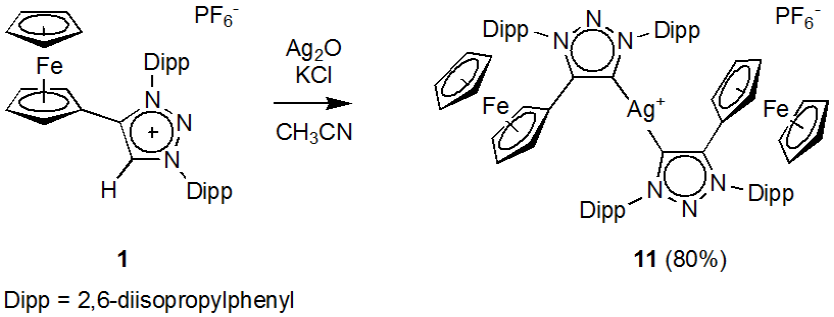

Scheme 6.7. The synthesis of the bis(triazolylidene) Ag(I) complex, **11**.

Raubenheimer[16] reported the synthesis of a biscarbene gold(I) complex following the same route as Crowley et al.[2] (Scheme 6.1), also without the isolation of the silver(I) complex, where Crowley reported the synthesis of complex **A**, the gold(I) chlorido complex. Thus, the outcome from the transmetalation of complex **11** remains unpredictable, and is likely to result in the same mixtures obtained in Scheme 6.6, or the exclusive synthesis of the biscarbene gold(I) complexes.[3,6]

During this time, Bertrand and co-workers published the report[12] on the exclusive obtainment of the mono-triazolylidene gold(I) complexes via the precursor gold(I) triazolylidene phenyl complexes (Scheme 6.8).

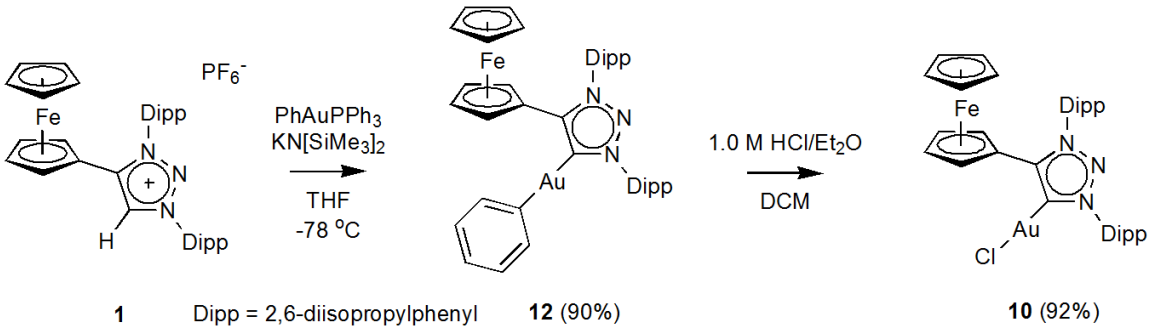

1 Dipp = 2,6-diisopropylphenyl **12** (90%) **10** (92%)

Scheme 6.8. The exclusive formation of **10** from the hydrolysis of **12**, utilizing an adapted synthetic procedure[11]

The synthesis of **12** (Scheme 6.8), the triazolylidene gold(I) phenyl complex involved the addition of base, $KN[SiMe_3]_2$, to the ligand precursor salt **1** to generate the free carbene *in situ*, followed by the addition of the metal precursor, $Ph(PPh_3)Au$. After warming up to room temperature overnight, the solution was evaporated under reduced pressure and complex **12** was extracted with toluene in near quantitative yield as a yellow-orange powder. The chemical shift of the carbene carbon atom in ^{13}C NMR spectrum in solvent $CDCl_3$ presents at 183.1 ppm, which corresponds well to the shift previously reported of 182.5 ppm for complex **J**, Scheme 6.4.

The hydrolysis of **12** with an excess amount of HCl in diethyl ether affords **10** in quantitative yield as a dark yellow powder, Scheme 6.8. The ^1H NMR spectrum (Figure 6.5) shows one set of peaks (vs. Figure 6.3). Since the complex was generated from **12**, the aromatic resonances indicative of the coordinated phenyl ligand are also not present, signifying the complete hydrolysis of **12**. Furthermore, the carbene signal of 160.9 ppm (Figure 6.6) is observed and corresponds to the carbene chemical shift previously observed in Figure 6.3. The reported chemical shift of **L**, Scheme 6.4, resonates at 161.1 ppm.[12] The N1-alkyl, N3-aryl triazolylidenes of type **M**,[13] Scheme 6.4, had a range of carbene signals between 152–165 ppm, which are upfield from their normal NHC analogues (166–195 ppm). The ferrocenyl N1-, N3-arylated triazolylidene **P** (Figure 6.1), exhibited a carbene carbon signal at 161.9 ppm (CD_2Cl_2).[15]

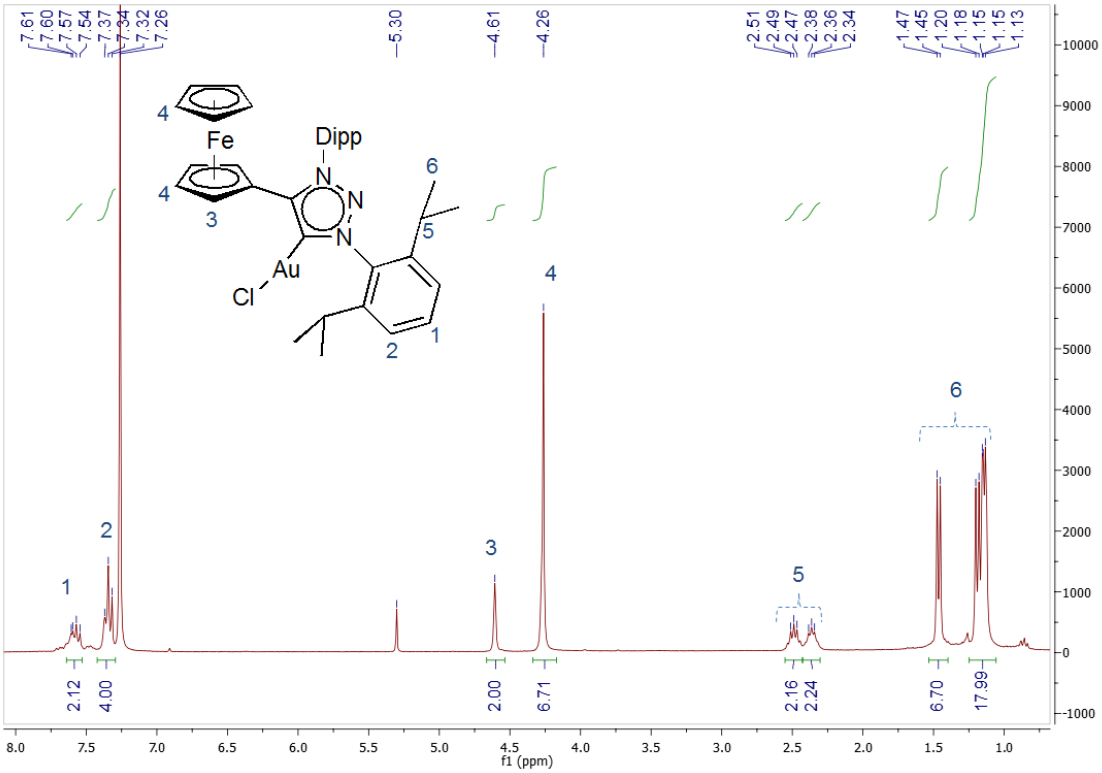

Figure 6.5. The ^{1}H NMR spectrum of **10** in solvent $CDCl_3$.

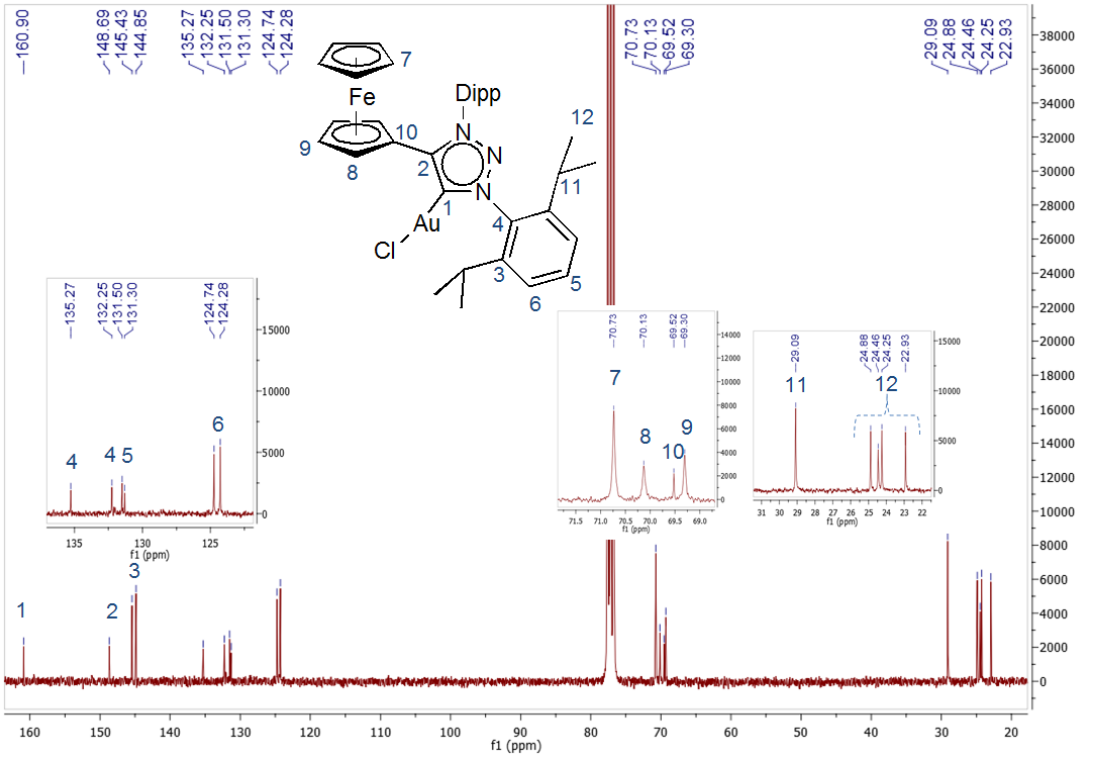

Figure 6.6. The ^{13}C NMR spectrum of **10** in solvent $CDCl_3$.

The $Ph(PPh_3)Au$ metal precursor used to synthesize complex **12**, was synthesized as per published methods.[17] The synthetic pathway is a three-step reaction whereby auric acid is converted to Au(tht)Cl,[18] which is then reacted with PPh_3 to afford $Au(PPh_3)Cl$.[19] Finally, $Au(PPh_3)Cl$ is reacted with the appropriate Grignard reagent to form $PhAuPPh_3$ (Scheme 6.9). Not only does this precursor synthesis require a tedious synthetic method, but it also requires rigorous light exclusion, especially during work-up when column chromatography is required. For this reason, the possibility of $AuPPh_3Cl$ to be used as metal precursor to afford complex **10** was evaluated. In this way, the preparation of **12** can be avoided.

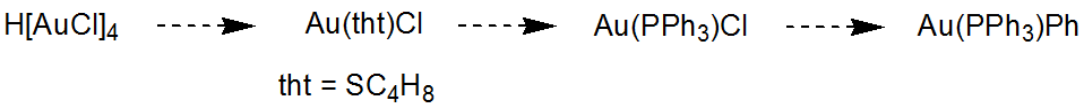

Scheme 6.9. The synthetic route for the formation of $Ph(PPh_3)Au$, to be used as metal precursor for the synthesis of **12**.

The metalation of ligand precursor salt **1** with $Au(PPh_3)Cl$ proceeded via the free carbene route at -78 °C in THF (Scheme 6.10). After an overnight reaction, the solvent was evaporated and washed with hexane. Extraction with solvent DCM, followed by solvent evaporation yielded a bright orange solid. The low-field proton resonance of 9.06 ppm was absent on the ^{1}H NMR spectrum of this compound, and additional resonances in the aromatic region was observed (Figure 6.7). Furthermore, a new doublet appeared at 176.2 ppm with a J = 120.5 Hz in the ^{13}C NMR spectrum, and a singlet at 40.9 ppm in the ^{31}P NMR spectrum (Figure 6.8). This indicates that instead of the ligand coordinating to gold(I) chlorido, coordination to gold(I)-PPh_3 occurred, forming the cationic triazolylidene gold(I) triphenylphosphine complex, **13** (Scheme 6.10).

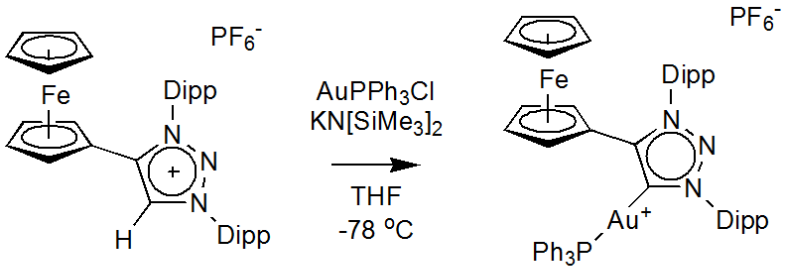

1 Dipp = 2,6-diisopropylphenyl **13** (98%)

Scheme 6.10. The metalation of **1** with $AuPPh_3Cl$ lead to the formation of the cationic gold(I) triphenylphosphine complex, **13**.

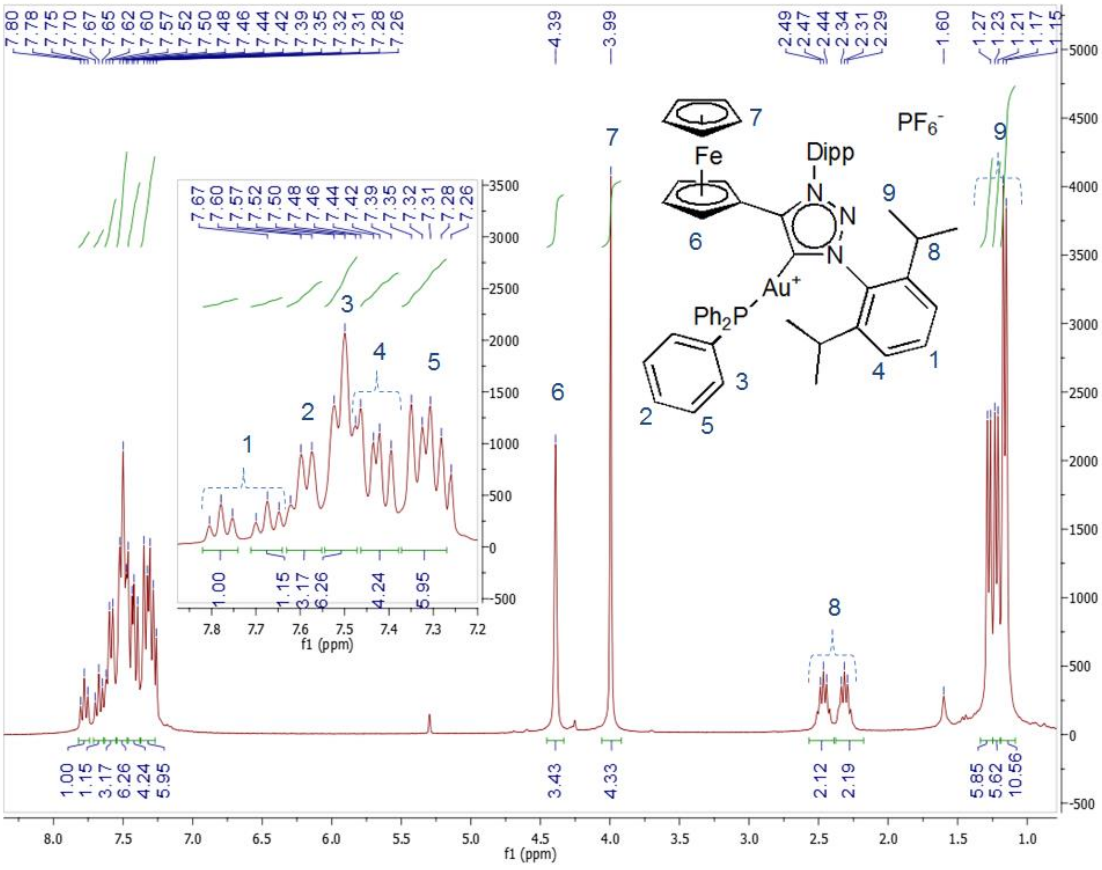

Figure 6.7. The ^1H NMR spectrum of **13** in solvent $CDCl_3$.

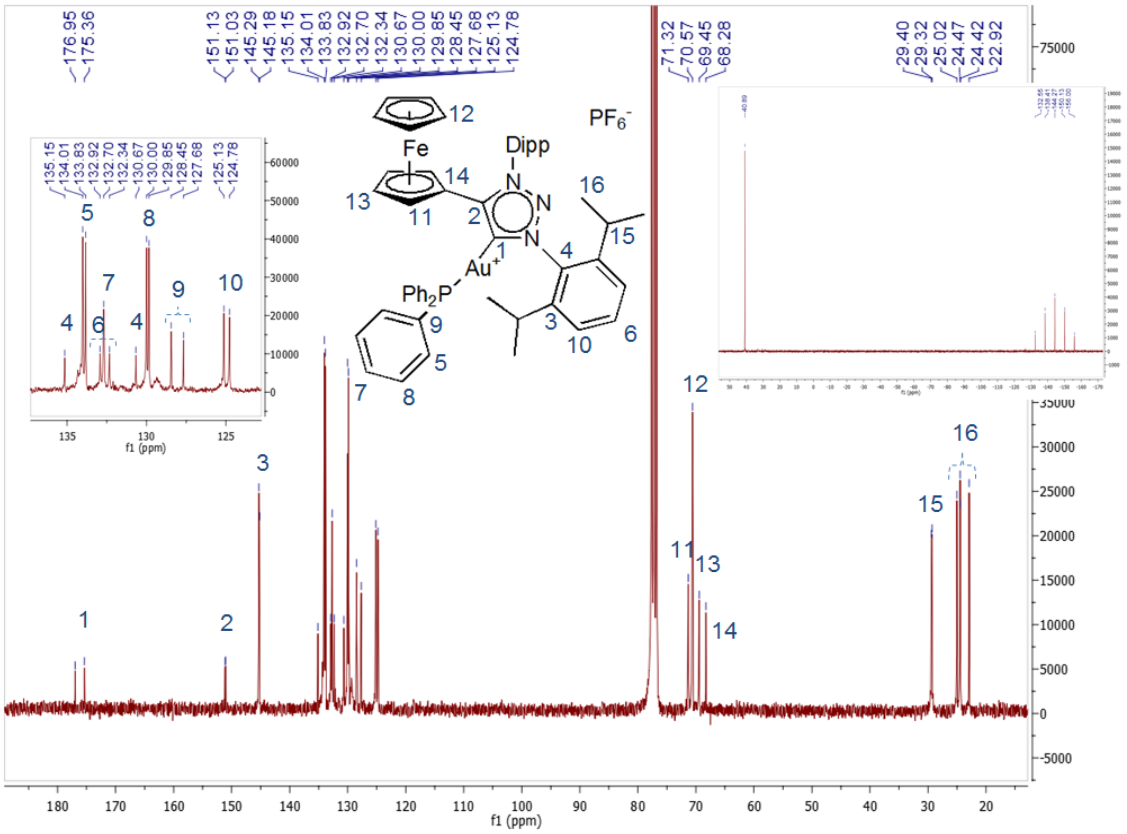

Figure 6.8. The ^{13}C NMR spectrum of **13**, and the ^{31}P NMR spectrum shown top right in solvent $CDCl_3$.

The group of Grützmacher[20] reported a similar synthesis of a normal NHC gold(I) phosphine complex by the addition of KO^{t}Bu to the ligand precursor salt in THF with Au(PPh$_3$)Cl. However, the synthetic method reported also required refluxing after 24 hrs stirring at room temperature, flash chromatography and recrystallization. Nolan reported the synthesis of gold(I) phosphine complexes which involved the protonolysis of [L(Au)(OH)]$^+$, where L = IPr (normal NHC, with aromatic wingtips) with PPh$_3$·HBF$_4$ salts.[21] Contel[22] and Albrecht[13] independently reported the addition PPh$_3$ in the presence of a halide scavenger to NHC(Au)Cl complexes, to substitute the chlorido ligand to afford the cationic [(NHC)AuPPh$_3$]$^+$ complexes. Both routes include the modification of the corresponding gold(I) chlorido complexes. The procedure described above for the synthesis of **13** involved metalation directly to the triazolium salt. Complex **N** (Scheme 6.5) exhibited a carbene chemical shift at δ(^{13}C) 177 ppm (*J* = 122 Hz), and a chemical shift at δ(^{31}P) 40.9 ppm for the coordinated triphenylphosphine P-atom.[13] Nolan reported the carbene carbon chemical shift

of their normal NHC-gold(I) phosphine complex at 188.2 pm with a coupling constant of J = 126 Hz.[11] Both triazolylidene complexes **13** and **N**, had more upfield carbene chemicals shift (triazolylidenes are more donating than normal NHCs)[5] and a smaller coupling constant, which is an indicative of a bigger *trans* influence of the triazolylidene on the triphenylphosphine ligand.[13]

6.3.2 Single crystal X-ray diffraction analysis of complexes **10**, **12** and **13**.

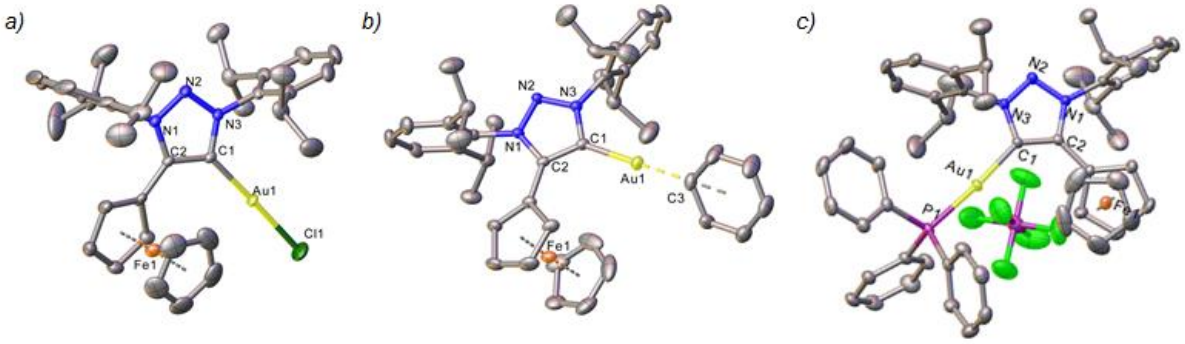

Figure 6.9. Molecular structures of triazolylidene gold(I) complexes (a) **10**, (b) **12** and (c) **13** showing 50% probability ellipsoids and partial atom-numbering scheme. Selected bond lengths (Å) and angles (°) for **10**: N1–N2 1.329(4); N2–N3 1.330(4); N3–C1 1.358(4); C1–C2 1.388(4); N1–C2 1.369(4); Au1–C1 1.981(3); Au1-Cl1 2.2739(10); C1-Au1-Cl1 177.82(10); C2-C1-N3 103.1(3). For **12**: N1–N2 1.331(3); N2–N3 1.336(3); N3–C1 1.367(3); C1–C2 1.395(3); N1–C2 1.364(3); Au1–C1 2.024(2); Au1-C3 2.2040(2); C1-Au1-C3 177.81(9); C2-C1-N3 102.58(17). For **13**: N1–N2 1.328(2); N2–N3 1.332(2); N3–C1 1.363(3); C1–C2 1.388(3); N1–C2 1.375(2); Au1–C1 2.045(19); Au1-P1 2.2834(5); C1-Au1-P1 175.47(6); C2-C1-N3 103.01(16). Hydrogens are omitted for clarity.

Crystals of **10** and **12** (Figure 6.9) were obtained from a solution of $CDCl_3$ (slow evaporation). From the single crystal X-ray diffraction studies of **10**, the carbene bond length was measured as 1.981(3) Å, which is shorter than the reported diarylated triazolylidene gold(I) chloride carbene length of 1.991(6) Å (**L**, Scheme 6.4),[12] and similar to the ferrocenyl N1-alkylated triazolylidene gold(I) complex, reported by Sarkar as 1.982(2) Å (**P**, Figure 6.1).[15] Other triazolylidene bond lengths for N1-alkylated gold(I) chlorido complexes were in the range of 1.980-1.993 Å and the gold(I) chlorido bond lengths of 2.282–2.290 Å were reported.[15,13] For **10**, the gold(I) chlorido bond length is 2.274(10) Å, similar than

the Au(I)–Cl bond length of the diarylated complex reported by Bertrand[12] (**L**, Scheme 6.4) (2.2761(17) Å) and shorter than the N1-alkylated analogues. An increased in Au-Cl bond length, indicates an increased *trans* influence of the triazolylidene ligand, and thus there is a slight decrease in *trans* influence observed for the diarylated triazolylidene as compared to their N1-alkylated analogues.[13] The carbene bond length of complex **12** (2.024(2) Å) is significantly longer, than in complex **10** (1.981 Å), indicating that the phenyl ligand has a pronounced *trans* influence on the triazolylidene ligand compared to the chloride ligand.

Crystals of **13** were grown by preparing a saturated solution of **13** in DCM, layered with toluene (1:1) at ambient temperature (Figure 6.9(c)). The carbene bond length measured via single crystal X-ray diffraction analysis is 2.045(19) Å, with the Au-P bond length of 2.283(5) Å. The N1-alkylated triazolylidene gold(I) complex (**N**, Scheme 6.5)[13] reported had a carbene bond length of 2.028(3) Å and Au-P bond length of 2.2795(7) Å. The “normal” cationic imidazolylidene gold(I) triphenylphosphine reported by Nolan had a carbene bond length of 2.039(5) Å and Au(I)-P bond length of 2.294(15) Å.[21]

The triphenylphosphine ligand displays the strongest *trans* influence on the triazolylidene ligand, compared to the phenyl and chloride ligands and is illuminated by the assessment of the difference in carbene bond lengths (**13** (2.045(19) Å) > **12** (2.024(2) Å) > **10** (1.981(3) Å)). This is to be expected from σ-donating ligands (stronger σ-donors have stronger *trans* influences), which follows in the order (to increasing trans influence):[23]

$$Cl^- < Br^- < CH_3^- < I^- < SCN^- < PR_3$$

6.3.3 Cyclic voltammetry experiments of **10** and **13**.

The redox properties of complexes **10** and **13** were investigated by means of cyclic voltammetry (CV) experiments in DCM. The results are shown in Table 6.1 and Figure 6.10.

Table 6.1. Cyclic voltammetry (CV) results for **10** and **13**, showing the E_{pa}, E_{pc}, $E_{1/2}$, ΔE_p in mV and the i_{pc}/i_{pa} ratio.

Entry	Redox couple	E_{pa} (mV)	E_{pc} (mV)	$E_{1/2}$ (mV)	ΔE_p (mV)	i_{pc}/i_{pa}
			10			
1	Fc(II)/(III)	145	44.4	94.8	100	1.00
			13			
2	Fc(II)/(III)	298	137	217	160	1.83

No redox events associated with the gold metal center was observed. Both complexes only have one redox event on both the CV time-scale and in the solvent window, i.e. the oxidation and reduction of the ferrocenyl substituent. In complex **10**, the ferrocenyl moiety oxidizes at 145 mV (Table 6.1, entry 1), with a much lower oxidizing potential than complex **13**, which only oxidizes at 298 mV (Table 6.1, entry 2). This is due to the electrostatic effect, since complex **13** is a cationic complex, and hence would require larger positive potentials for the loss of an electron from an already positively charged system. The effect of coordination of the triazolylidene ligand to the Lewis acidic gold(I) center, compared to the electron-rich Rh(I) metal, was also reflected in a higher oxidation potential of the Fc-group (145 mV), compared to complex **4** (104 mV, Table 4.1, *vide supra*). However, true comparison between complex **4**, **7** and **10** is hard to achieve, since different metals (Au vs. Rh) and coordination modes (linear vs. square metals) are being compared.

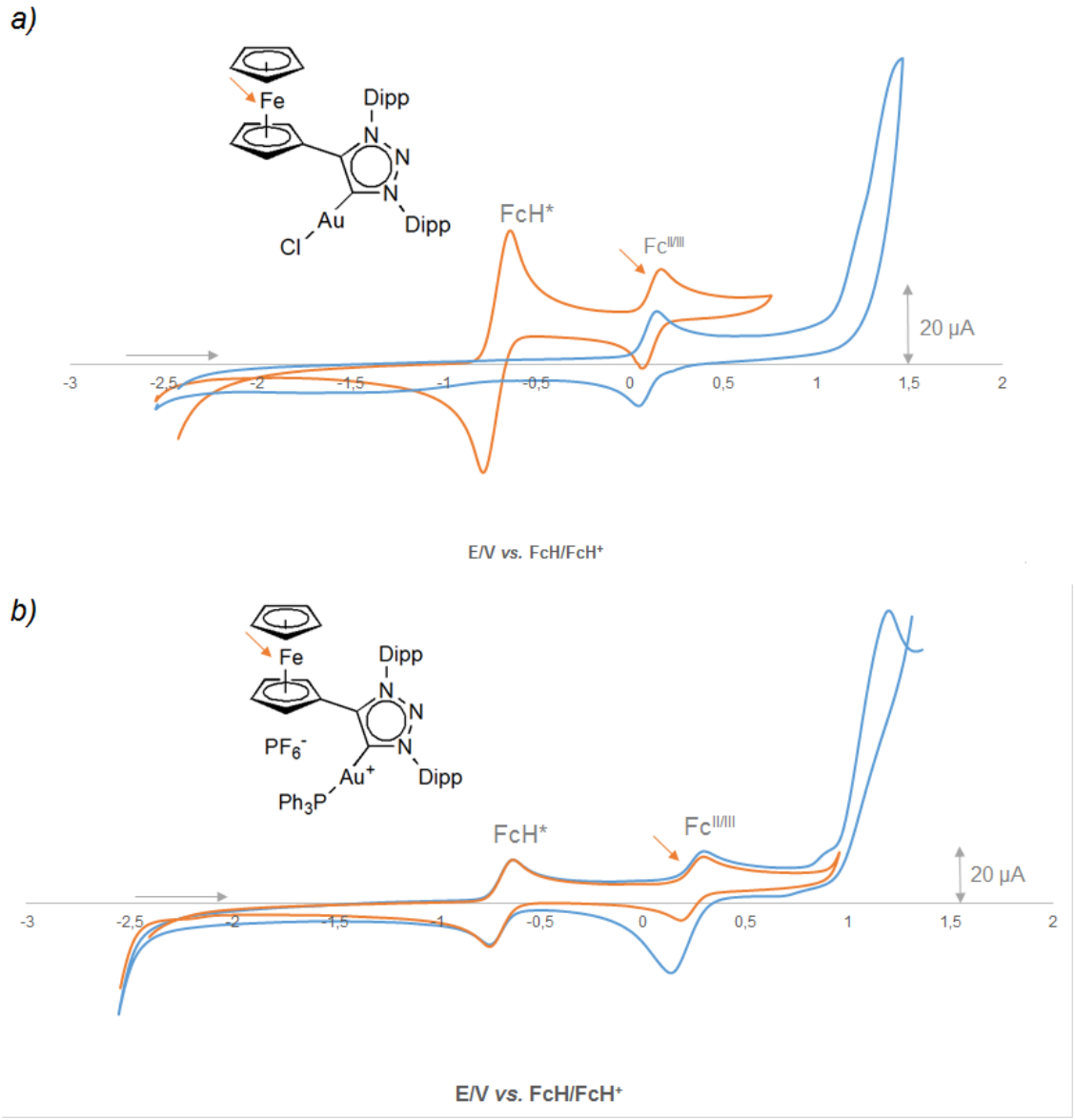

Figure 6.10. The CVs obtained from (a) **10** and (b) **13** at a glassy carbon electrode at a scan rate of 0.1 V. s^{-1} in CH_2Cl_2, with decamethylferrocene (FcH*) as internal standard. In both cases, the individual redox event of the ferrocenyl moiety is overlaid in orange.

What is clear from Table 6.1 and Figure 6.10 is the difference in the reversibility of the ferrocenyl redox event between the two complexes, **10** and **13**. The ferrocenyl oxidation to ferrocenium is considered quasi-reversible for complex **10**, since the i_{pc}/i_{pa} ratio is one (Table 6.1, entry 1), but the ΔE_p, which should be 60 mV, is 100 mV. For complex **13**, this is not the case. The i_{pc}/i_{pa} ratio is close to two (Table 6.1, entry 2) and the ΔE_p is equal to 160 mV. A reverse peak is observed, therefore, although the ferrocene redox event is irreversible on the

experimental time-scale, this can be a direct effect of the cationic nature of complex **13**.[24–27] The dicationic nature of the electrochemically oxidized product of **13** might exhibit slower diffusion resulting in the loss of reversibility, as observed.

6.3.4 The catalytic reactivity testing of complex **10** in the synthesis of oxazolines.

Albrecht reported the catalytic reactivity of the gold(I) triazolylidene complexes (**M**–**O**, Scheme 6.5) in the synthesis of oxazolines, in the presence of a silver salt and a base. He found that the mono-triazolylidene gold(I) chlorido complex **M**, showed the highest activity as a pre-catalyst, and therefore preliminary catalytic reactivity testing was done on complex **10**.

In the case of complex **10**, the addition of the silver salt ($AgPF_6$: $E°$= 0.65 V in DCM),[28] could potentially oxidize the ferrocene substituent, in addition to acting as a halide scavenger. Therefore, the goal of the preliminary catalytic study was to investigate whether the addition of the silver salt will increase the catalytic activity of complex **10** (even if oxidation and/or halide abstraction can occur). The catalysis was followed by ^{1}H NMR spectroscopy, in the presence of an internal standard (1,4-di-*tert*-butylbenzene). Calculations for conversions and the determination of the *cis/trans* ratio were in reference to the internal standard (Figure 6.11).

Table 6.2. Evaluation of complex **10** as pre-catalyst in the synthesis of oxazolines, after 24 hours at 40 °C[a], in DCM.

Entry	Additive	Conversion (%)[b]	*Cis/trans*[b]
1	-	73	1/0.8
2[c]	$AgPF_6$	96	1/1

[a]Conditions: Benzaldehyde (1.5 mmol), Methylisocyanoacetate (1.4 mmol), complex 10 (14 µmol) and 1,4-di-*tert*-butylbenzene as internal standard (0.38 mmol). Addition of $AgPF_6$ (16 µmol).

[b]Determined by ^{1}H-NMR spectroscopy

[c]Presence of a precipitate observed

Table 6.2 shows the results obtained from the reactivity testing of complex **10** in the catalytic synthesis of oxazolines and showed 73% conversion after 24 hours at 40 °C, with no additives (entry 1). The addition of $AgPF_6$, increased the conversion to 96 % (entry 2), while in both cases, the selectivity towards *cis* or *trans* oxazolines were poor. Albrecht reported an increase in activity with the addition of the silver salt (96% vs. 72%), but these results were obtained at room temperature, while the reactions conditions for complex **10** were at 40 °C; at room temperature, complex **10** displayed minimal conversion. Furthermore, Albrecht also reported on the presence of nano-particles (dynamic light scattering), especially when silver(I) was used as additive and described them as potentially catalytically active. Although no light scattering experiments were carried out on the reaction with complex **10** and the silver salt, a precipitate was present.

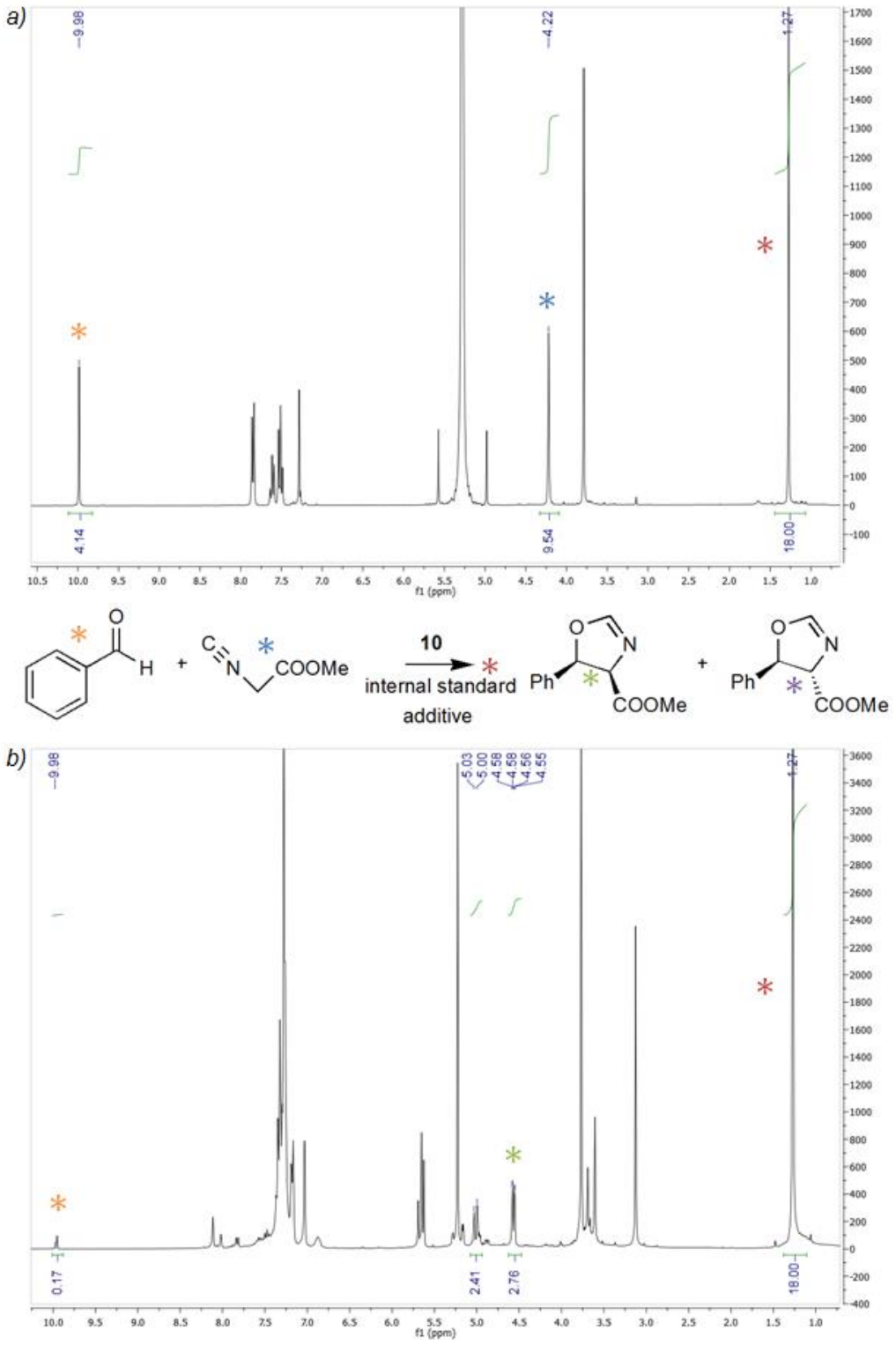

Figure 6.11. The ^{1}H NMR spectra of the catalytic conversion of benzaldehyde and methylisocyanoacetate, in the presence of an internal standard (1,4-ditertbutylbenzene) and pre-catalyst, **10** to cis and trans oxazolines in solvent $CDCl_3$. The reaction at time 0 hr. (a) is shown above with the reaction at time 24 hr. (b) shown below.

6.4 Conclusion

The successful synthesis of **10**, the triazolylidene gold(I) chlorido complex, was achieved by first investigating various synthetic routes, but ultimately hydrolysis of complex **12** (gold(I) phenyl complex) yielded **10** as the exclusive product. In the search to find an alternative method to synthesize **10** with the metal precursor $Au(PPh_3)Cl$, the cationic gold(I) phosphine complex **13** was obtained. Although, only a single report in literature was found on this synthetic route on complexes of type **13**, the reaction time and work-up reported above for the synthesis of **13** is significantly decreased.

The electrochemical properties of complex **10** and **13** were investigated. As expected, the ferrocene/ferrocenium redox couple for **10** occurs at a lower oxidizing potential than **13** (due to the cationic nature of the complex).

The preliminary catalytic reactivity testing of **10** in the synthesis of oxazolines, indicates that the addition of the silver salt does enhance the catalytic activity, although both reactions investigated had lower activity than previously reported complex **M**. Future work on the catalytic testing of **10** is envisaged to investigate the addition of a base, as well as a silver-free oxidant. Moreover, the addition of potassium salts on the catalytic activity will be investigated. Once the optimized reaction conditions are determined, complex **13** will be evaluated as a potential pre-catalyst.

6.5 References

1 N. Marion and S. P. Nolan, *Chem. Soc. Rev.*, 2008, **37**, 1776.

2 K. J. Kilpin, U. S. D. Paul, A.-L. Lee and J. D. Crowley, *Chem. Comm.*, 2011, **47**, 328–330.

3 H. M. J. Wang and I. J. B. Lin, *Organometallics*, 1998, **17**, 972–975.

4 P. Mathew, A. Neels and M. Albrecht, *J. Am. Chem. Soc.*, 2008, **130**, 13534–13535.

5 K. F. Donnelly, A. Petronilho and M. Albrecht, *Chem. Comm.*, 2013, **49**, 1145–59.

6 J. C. Garrison and W. J. Youngs, *Chem. Rev.*, 2005, **105**, 3978–4008.

7 H. G. Raubenheimer and S. Cronje, *Chem. Soc. Rev.*, 2008, **37**, 1998–2011.

8 M. J. López-Gómez, D. Martin and G. Bertrand, *Chem. Comm.*, 2013, **49**, 4483–5.

9 P. de Frémont, N. M. Scott, E. D. Stevens and S. P. Nolan, *Organometallics*, 2005, **24**, 2411–2418.

10 D. Martin, N. Lassauque, B. Donnadieu and G. Bertrand, *Angew. Chem. Int. Ed.*, 2012, **51**, 6172–6175.

11 S. Gaillard, C. S. J. Cazin and S. P. Nolan, *Acc. Chem. Res.*, 2012, **45**, 778–787.

12 D. R. Tolentino, L. Jin, M. Melaimi and G. Bertrand, *Chem. Asian. J.*, 2015, **10**, 2139–2142.

13 D. Canseco-Gonzalez, A. Petronilho, H. Mueller-Bunz, K. Ohmatsu, T. Ooi and M. Albrecht, *J. Am. Chem. Soc.*, 2013, **135**, 13193–13203.

14 R. Pretorius, M. R. Fructos, H. Müller-Bunz, R. A. Gossage, P. J. Pérez and M. Albrecht, *Dalton Trans*, 2016, **45**, 14591–14602.

15 L. Hettmanczyk, S. Manck, C. Hoyer, S. Hohloch and B. Sarkar, *Chem. Comm.*, 2015, **51**, 10949–10952.

16 U. E. I. Horvath, G. Bentivoglio, M. Hummel, H. Schottenberger, K. Wurst, M. J. Nell, C. E. J. van Rensburg, S. Cronje and H. G. Raubenheimer, *New J. Chem.*, 2008, **32**, 533.

17 Y. Shi, S. D. Ramgren and S. A. Blum, *Organometallics*, 2009, **28**, 1275–1277.

18 R. Usón, A. Laguna, M. Laguna, D. A. Briggs, H. H. Murray and J. Fackler John P, *Inorganic Syntheses*, 1989, vol. 26.

19 G. A. Price, A. K. Brisdon, K. R. Flower, R. G. Pritchard and P. Quayle, *Tetrahedron Lett.*, 2014, **55**, 151–154.

20 C. Böhler, D. Stein, N. Donati and H. Grützmacher, *New J. Chem.*, 2002, **26**, 1291–1295.

21 S. Gaillard, P. Nun, A. M. Z. Slawin and S. P. Nolan, *Organometallics*, 2010, **29**, 5402–5408.

22 J. Fernández-Gallardo, B. T. Elie, M. Sanaú and M. Contel, *Chem. Comm.*, 2016, **52**, 3155–3158.

23 P. W. Atkins, T. L. Overton, J. P. Rourke, M. T. Weller and F. A. Armstrong, in *Inorganic Chemistry*, Oxford University Press Inc., Fifth., 2010, p. 514.

24 J. J. Van Benschoten, J. Y. Lewis, W. R. Heineman, D. a. Roston and P. T. Kissinger, *J. Chem. Educ.*, 1983, **60**, 772.

25 D. H. Evans, K. M. O. Connell, A. Petersen and M. J. Kelly, *J. Chem. Educ.*, 1983, **60**, 290–293.

26 P. T. Kissinger and W. R. Heineman, *J. Chem. Educ.*, 1983, **60**, 702.

27 G. a. Mabbott, *J. Chem. Educ.*, 1983, **60**, 697–702.

28 N. G. Connelly and W. E. Geiger, *Chem. Rev.*, 1996, **96**, 877–910.

Chapter 7

Conclusion

From the successful synthesis of the precursor triazolium salts, **1**–**3**, it was already apparent by spectroscopic inspection of the salts, comparing the downfield resonance of the acidic triazolium protons, that the donating ferrocenyl substituent does not influence the electronics of the ring (**2** vs. **3**). Instead, the substituent on the N3-atom (aryl (**1**) vs. alkyl (**2**)) has a more pronounced influence.

Nevertheless, the electronic contribution of the ferrocenyl substituent was further assessed by the synthesis and spectroscopic characterization of the rhodium(I) dicarbonyl complexes (**7**–**9**). However, the IR stretching frequencies of the carbonyls proved an insufficient probe to assess the electronic impact of substituents on the metal center, since the calculated TEPs of each complex were equal. The ^{13}C NMR chemical shift of the carbene carbon atoms of the corresponding rhodium(I) cod complexes (**4**–**6**) did however, show some degree of electronic variation across the range of complexes, whereby the trend (in order of increasing donating strength) of the carbene resonances closely resembled the trend of increasing in acidity, albeit a small variation, observed for the acidic triazolium proton resonance of the precursor salts:

6 (173.2 ppm) > **5** (172.3 ppm) > **4** (171.9 ppm)

3 (H^+: 8.66 ppm) > **2** (H^+: 8.67 ppm) > **1** (H^+: 9.06 ppm)

Complexes **4**–**6** were employed as catalyst precursors in the catalytic reactivity testing in the hydroformylation of 1-octene. Under the optimized reaction conditions of 75 °C/ 40 bar for 8 hrs at 0.08 % mol catalytic loading, TOFs of 99.7–125.2 hr^{-1} were calculated with n/*iso* product aldehyde values of 2.43–1.75. Among the series **4**–**6**, complex **4** showed the highest selectivity (n/*iso* = 2.43), but the lowest activity (TOF = 99.7 hr^{-1}). In an attempt to increase the activity of complex **4**, an oxidant was added as an additive to the catalytic reaction, to generate **4ox**, *in situ*. A slight increase in activity was observed (TOF = 116 hr^{-1}), but at a cost to selectivity (n/*iso* = 1.60). Furthermore, the

reactivity of complex **4ox** closely resembled that of the reactivity of complex **5**, despite having very different electronic properties. This result again affirms that the prediction of a precursor catalyst's ability to perform in hydroformylation reactions does not solely depend on either the electronic or steric properties.

The coordination of the triazolium salt, **1** to gold(I), to obtain the catalytically relevant gold(I) chlorido complex, **10**, were successfully synthesized via the hydrolysis of precursor complex **12**. Complex **10** has shown to be active in the synthesis of oxazoline (73% conversion), with an increase in activity with the addition of $AgPF_6$ (96% conversion), in a preliminary catalytic study. For prospective work, complex **10** will be subjected to further catalytic reactivity testing, whereby the addition of base will be investigated, along with the addition of potassium salts (for a silver-free method). The gold(I)-phosphine complex, **13** was also prepared according to a simplified synthetic route compared to previously described methods, and will also be subjected to reactivity testing.

Cyclic voltammetry experiments on the N1, N3-diarylated ferrocenyl triazolium ligand salt (**1**), the rhodium(I) complexes (**4**, **7**) and the gold(I) complexes (**10**, **13**) were performed. The oxidation potential of the ferrocene substituent of each compound was measured; the ferrocenyl moiety of the cationic ligand salt (**1**) and the cationic gold(I)-phosphine complex (**13**) oxidized at 336 and 298 mV, respectively. Both oxidation potentials are much higher than for the neutral rhodium(I) complexes (**4**: 104 mV; **7**: 145 mV, respectively) and the neutral gold(I) complex (**10**: 145 mV), as expected. The chemically oxidized precursor salt (**1ox**) and complexes **4ox** and **7ox** could not be characterized by NMR spectroscopy due to the paramagnetic nature of the resultant ferrocenium substituent, although FT-IR methods could be used to investigate the electronic effect of the ferrocene-oxidation. The carbonyl stretching bands of the dicarbonyl Rh(I) complex **7ox**, appeared at 7 – 17 cm^{-1} higher frequencies than the neutral precursor **7** (compare 2082, 2009 cm^{-1} for **7ox** to 2075, 1992 cm^{-1} for **7**), which is in accordance with literature precedent for the effect of a ferrocene-substituent oxidation, and not a Rh(I/III) redox event. However, ESR measurements are still required for the unambiguous characterization of the Fe(III)-metal center of the chemically oxidized complexes.

Chapter 8

Experimental Methods

8.1 General Considerations

All synthetic procedures ensued under inert atmosphere (either under nitrogen or argon gas) using standard Schlenk or vacuum line techniques. Air sensitive solids were stored and handled in a PureLab HE glove box. When needed, NMR and XRD samples were prepared in the glove box.

Anhydrous tetrahydrofuran, diethyl ether, toluene and *n*-hexane were distilled over sodium metal under N_2 (g). Dichloromethane and acetonitrile were dried by distillation over CaH_2, under N_2 (g). Ethynylferrocene,[1] 1,3-bis(2,6-diisopropylphenyl)triaz-1-ene (triazene),[2,3] *tert*-butylhypochlorite[4], di-*μ*-chlorido-bis(η^2,η^2-1,5-cyclooctadiene)dirhodium(I),[5] triethyloxonium tetrafluoroborate,[6] chloro(tetrahydrothiophene)gold(I),[7] chloro-(triphenylphosphine)gold(I),[8] and phenyl(triphenylphosphine)gold(I)[9] were synthesized according to previously reported literature methods. All other reagents were commercially available and used without any further purification thereof.

Nuclear magnetic resonance (NMR) spectra were obtained in $CDCl_3$ (δH at 7.26 ppm, δC{H} at 77.16 ppm) and CD_3CN (δH at 1.940 ppm, δC{H} at 118.26 ppm) using Bruker Ultrashield Plus 300 AVANCE 3 operating at 300.13 MHz for ^{1}H, 75.47 MHZ for ^{13}C, 121.49 MHz for ^{31}P and 282.40 MHz for ^{19}F and Bruker Ultrashield 400 AVANCE 3 spectrometers, operating at 400.21 MHz for ^{1}H, 100.64 MHz for ^{13}C, 162.01 MHz for ^{31}P and 376.57 MHz for ^{19}F. The ^{31}P {1H} NMR spectra were referenced to the deuterated lock solvent, which had been referenced to 85% H_3PO_4. The assignment of the NMR spectrum resonances for each complex follows the numbering scheme individually assigned for each compound illustrated below, and is independent from the generally accepted numbering used throughout the dissertation (eg. C4-ferrocenyl substituent, C5-carbene carbon). The spectral coupling patterns are abbreviated as follows: s - singlet; d - double; t - triplet; q - quartet; sept – septet; m – multiplet; br s – broad

signal and the chemical shifts are given in ppm (parts per million). An asterisk (*) denotes solvent contaminant in the NMR spectra.

Single crystal X-ray structure analyses were performed on a Bruker Apex II-CCD detector using Mo-K_α radiation (λ = 0.71073 Å). Crystals were mounted under oil on nylon loops and placed in a cold stream of N_2 at 150 K. Structures were solved using SHELXTL.

Solution infrared spectroscopy analysis was performed on a PerkinElmer Spectrum RXI FT-IR spectrophotometer over the range 4000 to 600 cm^{-1} and were recorded in CH_2Cl_2 using a NaCl cell with a path length of *ca.* 1.0 mm.

Melting points were measured with a Stuart SMP10 melting point apparatus.

Mass spectral analyses were operated on a Waters Synapt G2 HDMS by direct infusion at 5 µL/min for 3 min. Positive electron spray was employed as ionization technique, and measurements were done in acetonitrile over a mass range of 50-2000 Da. Sodium formate (5 mM) was used as calibration.

Microanalysis were carried out with an Elemental Analyser CHNS-O Thermo using acetanilide as standard.

8.2 Details of synthetic procedures and characterization of compounds **1**–**14**.

8.2.1 Synthetic procedures for ligand precursor salts, **1**–**3**.

Synthesis of *1,3-bis(2,6-diisopropylphenyl)-4-ferrocenyl-1H-1,2,3-triazolium hexafluorophosphate(V)* (**1**).

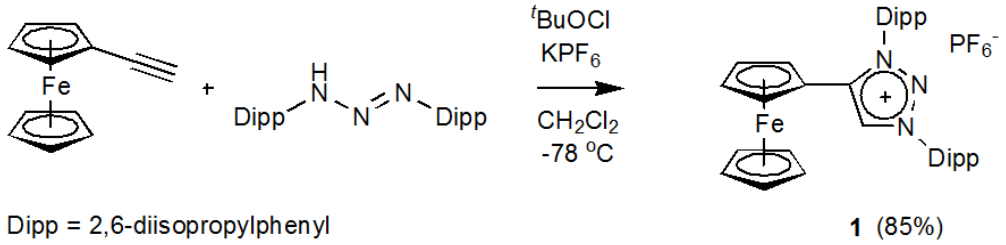

Scheme 8.1. The synthesis of the ligand precursor salt, **1**.

An adapted procedure of the previously reported method for diarylated triazolium salt synthesis was followed.[10] Ethynylferrocene (1.00 g, 4.76 mmol),

2 equivalents of triazene (3.48 g, 9.52 mmol) and excess KPF_6 (2.00 g, 10.8 mmol) were added to a purged Schlenk vessel and dissolved in anhydrous dichloromethane (DCM). The solution was cooled to -78 °C and 2 equivalents of *tert*-butylhypochlorite (1.08 mL, 9.52 mmol) were added dropwise. The solution was kept cold for at least 5 hours and then left to warm up to room temperature overnight. After filtration, the filtrate was concentrated under reduced pressure and the solid was triturated with hexane and diethyl ether, affording **1** as an orange powder. Yield: 2.9 g (85%). Mp: 215–220 °C (decomp). ^{1}H NMR (300 MHz, CD3CN) δ 9.06 (s, 1H, trz-**H, H-1**), 7.77 (t, *J* = 7.9 Hz, 2H, dipp-**H**, **H-2**), 7.56 (dd, *J* = 7.7, 6.0 Hz, 4H, dipp-**H**, **H-3**), 4.56 (m, 2H, Fc-**H**, **H-4**), 4.35 (m, 2H, Fc-**H**, **H-5**), 4.25 (s, 5H, Fc-**H**, **H-6**), 2.42 (dd, *J* = 13.6, 6.8 Hz, 2H, dipp(iso)-C**H**, **H-7**), 2.34 (dd, *J* = 13.1, 6.4 Hz, 2H,dipp(iso)-C**H**, **H-7**), 1.36 (d, *J* = 6.8 Hz, 6H, dipp(iso)-C**H**$_3$, **H-8**), 1.23 (d, *J* = 6.8 Hz, 6H, dipp(iso)-C**H**$_3$, **H-8**), 1.18 (d, *J* = 6.9 Hz, 6H, dipp(iso)-C**H**3, **H-8**), 1.15 (d, *J* = 6.9 Hz, 6H, dipp(iso)-C**H**3, **H-8**). ^{13}C {^{1}H} NMR (75 MHz, CD_3CN) δ 149.0 (Trz-**C**$_q$, **C-1**), 146.5 (dipp-**C**$_q$, **C-2**), 146.2 (dipp-C$_q$, **C-2**), 134.6 (dipp-C$_q$, **C-3**), 134.4 (dipp-C$_q$, **C-3**), 131.5 (Trz-**C**H, **C-4**), 131.3 (dipp-**C**H, **C-5**), 130.4 (dipp-CH, **C-5**), 126.5 (dipp-**C**H, **C-6**), 126.1 (dipp-**C**H, **C-6**), 73.2 (Fc-**C**H, **C-7**), 71.8 (Fc-**C**H, **C-8**), 70.4 (Fc-**C**H, **C-9**), 64.6 (Fc-C$_q$, **C-10**), 30.2 (dipp(iso)-**C**H, **C-11**), 25.2 (dipp(iso)-**C**H$_3$, **C-12**), 24.5 (dipp(iso)-**C**H$_3$, **C-12**), 24.1 (dipp(iso)-**C**H$_3$, **C-12**), 22.8 (dipp(iso)-**C**H$_3$, **C-12**). ^{31}P {^{1}H} NMR (121 MHz, CD_3CN) δ -144.61 (sept, *J* = 706.3 Hz, **P**F_6). ^{19}F {^{1}H} NMR (282 MHz, CD_3CN) δ -72.95 (d, *J* = 706.3 Hz, P**F**$_6$). Anal. Calcd for $C_{36}H_{44}N_3FePF_6$: C 56.55, H 5.80, N 5.50. Found: C 56.19, H 5.51, N 5.50. ESI-HRMS (15 V, positive mode, m/z): calcd for [M]+: 574.2884. Found: 574.2893.

Synthesis of triazoles as percursors to the triazolium salts, **2** and **3**.

The 2,6-diisopropylphenyl-4-Ar-1H-1,2,3-triazoles of the type **A** (Scheme 8.2), where Ar = ferrocenyl[11] or phenyl[12], were synthesized according to an adapted method published by Moses and co-workers.[13]

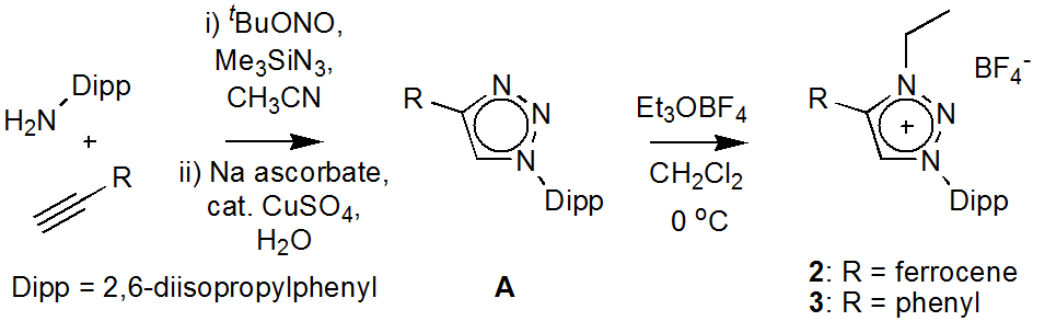

Scheme 8.2. The synthesis of the ligand precursor salts, **2** and **3**.

To acetonitrile (10 mL), diisopropylaniline (1.00 g, 5.64 mmol) was added and cooled to 0 °C. To this, *tert*-butyl nitrite (0.87 g, 8.46 mmol) and trimethylsilyl azide (0.78 g, 6.77 mmol) were added in the dark. The reaction was stirred for 1 hour at room temperature, after which the solution was concentrated. The blue/green oil was purified with flash chromatography (ether) to afford a colourless/pale yellow oil. To this, a solution of alkyne (ethynylferrocene or phenylacetylene, respectively) (5 mmol) in tetrahydrofuran (THF) was added at room temperature, followed by the addition of a solution of $CuSO_4.5H_2O$ (0.25 g, 1.00 mmol) and Na-ascorbate (0.4 g, 2.02 mmol) in water (10 mL). The reaction was left to stir overnight. After evaporation of the organic solvent, a solution of 1:1 DCM: NH_4OH (aq) was added, and stirring was continued overnight. The product was extracted with DCM, dried over $MgSO_4$ and washed with pentane, to afford the known compounds 2,6-diisopropylphenyl-4-ferrocenyl-1H-1,2,3-triazole as an orange solid (1.01 g, 49 % yield)[7] and 2,6-diisopropylphenyl-4-phenyl-1H-1,2,3-triazole as a yellow solid (0.70 g, 46 % yield),[8] respectively.

General procedure for the synthesis of 1-ethyl-3-(2,6-diisopropylphenyl)-4-Ar-1*H*-1,2,3-triazolium tetrafluoroborate(III) (Ar = Fc , **2**; Ar = Ph, **3**).[14,15]

To a solution of the appropriate triazole derivative **A** (2.4 mmol) in DCM, a solution of 3 equivalents of triethyloxonium tetrafluouroborate (7.2 mmol, 1.4 g), in DCM were added at -30 °C and left to reach room temperature overnight. After evaporation of the solvent, the solid was dissolved in minimum ethyl acetate (2 mL) after which diethyl ether (20 mL) were added and stirred for 1

hour. The white precipitate was filtered and dried to yield the corresponding triazolium salt.

Synthesis of *1-ethyl-3-(2,6-diisopropylphenyl)-4-ferrocenyl-1H-1,2,3-triazolium tetrafluoroborate(III)* (**2**) Yield: 1.3 mg (99 %) m.p. 194–198 °C (decomp). ^{1}H NMR (300 MHz, CD_3CN) δ 8.67 (s, 1H, trz-**H**, **H-1**), 7.72 (t, *J* = 7.8 Hz, 1H, dipp-**H**, **H-2**), 7.51 (d, *J* = 7.8 Hz, 2H, dipp-**H**, **H-3**), 4.90 (m, 2H, Fc-**H**, **H-4**), 4.70 (m, *J* = 7.2 Hz, 4H, $CH_3C\mathbf{H}_2$ (2H), **H-5** and Fc-**H** (2H), **H-6**), 4.30 (s, 5H, Fc-**H, H-7**), 2.30 (m, 2H, dipp(iso)-C**H**, **H-8**), 1.65 (t, *J* = 7.2 Hz, 3H, $CH_2C\mathbf{H}_3$, **H-9**), 1.22 (dd, *J* = 20.4, 6.8 Hz, 12H, dipp(iso)-C$\mathbf{H}_3$, **H-10**). ^{13}C {^{1}H} NMR (75 MHz, CD_3CN) δ 146.5 (dipp-$\mathbf{C}_q$, **C-1**), 145.5 (dipp-$\mathbf{C}_q$, **C-2**), 133.9 (trz-**C**H, **C-3**), 131.9 (trz-**C**H, **C-4**), 131.1 (dipp-**C**H, **C-5**), 125.8 (dipp-**C**H, **C-6**), 72.6 (Fc-**C**H, **C-7**), 71.5 (Fc-**C**H, **C-8**), 70.6 (Fc-**C**H, **C-9**), 66.2 (Fc-C_q, **C-10**), 49.3 (-$CH_3\mathbf{C}H_2$, **C-11**), 29.5 (dipp-(iso)-**C**H, **C-12**), 24.4 (dipp-(iso)-**C**H_3, **C-13**), 23.9 (dipp-(iso)-**C**H_3, **C-13**), 13.8 (-$CH_2\mathbf{C}H_3$, **C-14**). ^{19}F NMR (282 MHz, CD_3CN) δ -151.69 (d, *J* = 15.0 Hz, B$\mathbf{F}_4$). Anal. Calcd for $C_{26}H_{32}N_3FeBF_4$: C 58.41, H 6.03, N 7.86. Found: C 58.41, H 5.745, N 7.56. ESI-HRMS (15 V, positive mode, m/z): calcd for [M]+: 442.1945. Found: 442.1904

Synthesis of *1-ethyl-3-(2,6-diisopropylphenyl)-4-phenyl-1H-1,2,3-triazolium tetrafluoroborate(III)* (**3**) Yield: 1.0 g, 99%. m.p. 94–98 °C. ^{1}H NMR (300 MHz, CD_3CN) δ 8.66 (s, 1H, trz-**H**, **H-1**), 7.75 (m, 5H, Ph-C**H**, **H-3** + m, 1H, dipp-C**H, H-2** at 7.72), 7.52 (d, *J* = 7.8 Hz, 2H, dipp-C**H**, **H-4**), 4.68 (q, *J* = 7.2 Hz, 2H, -C$\mathbf{H}_2CH_3$, **H-5**), 2.40 (m, 2H, dipp-(iso)-C**H**, **H-6**), 1.62 (t, *J* = 7.2 Hz, 3H, -$CH_2C\mathbf{H}_3$, **H-7**), 1.21 (dd, *J* = 15.0, 6.8 Hz, 12H, dipp-(iso)-C$\mathbf{H}_3$, **H-8**). ^{13}C {^{1}H} NMR (75 MHz, CD_3CN) δ 146.6 (dipp-$\mathbf{C}_q$, **C-1**), 144.7 (dipp-$\mathbf{C}_q$, **C-2**), 133.9 (dipp-**C**H, **C-3**), 132.9 (Ph-**C**H, **C-4**), 132.0 (Ph-C**H**, **C-4**) 131.9 (trz-$\mathbf{C}_q$, **C-5**) 130.8 (trz-**C**H, **C-6**), 130.5 (Ph-**C**H, **C-4**), 125.8 (dipp-**C**H, **C-7**), 123.1 (Ph-$\mathbf{C}_q$, **C-8**), 49.3 (-$\mathbf{C}H_2CH_3$, **C-9**), 29.4 (dipp-(iso)-**C**H, **C-10**), 24.7 (dipp-(iso)-**C**H_3, **C-11**), 23.7 (dipp-(iso)-**C**H_3, **C-11**), 13.9 (-$CH_2\mathbf{C}H_3$, **C-12**). ^{19}F NMR (282 MHz, CD_3CN) δ -151.82 (d, *J* = 15.0 Hz). Anal. Calcd for $C_{22}H_{28}N_3BF_4$: C 60.40 H 6.45 N 9.60. Found: C 60.61 H 6.20 N 9.46. ESI-HRMS (15 V, positive mode, m/z): calcd for [M]+: 334.2283. Found: 334.2247.

8.2.2 Synthetic procedures for 1,2,3-triazol-5-ylidene rhodium(I) complexes, **4**–**9**.

Synthesis of *1,3-bis(2,6-diisopropylphenyl)-4-ferrocenyl-1,2,3-triazol-5-ylidene chlorido-η^4-1,5-cyclooctadienerhodium(I)* (**4**).

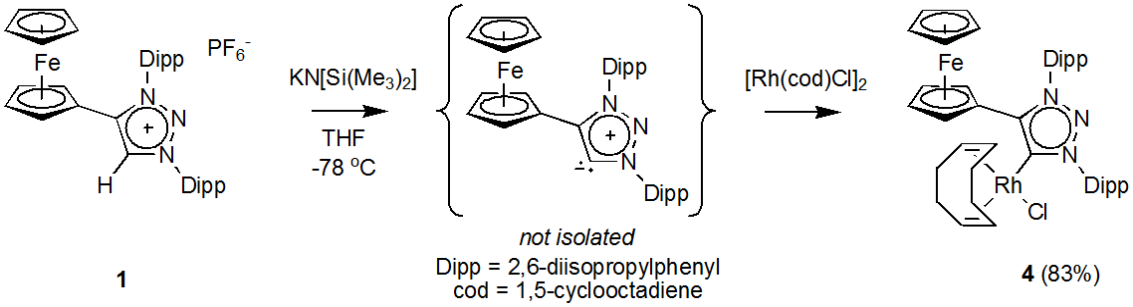

Scheme 8.3. Synthesis of rhodium triazolylidene complex, **4**.

To a purged Schlenk were added triazolium salt **1** (0.5 g, 0.69 mmol) and one equivalent of $KN(SiMe_3)_2$ (0.15 g, 0.76 mmol), and the solid reactants were dissolved in THF. The solution was cooled to -78 °C and stirred for 10 minutes. At -78 °C, the solution was added to 0.5 equivalents of $[Rh(cod)Cl]_2$ (0.17 g, 0.35 mmol) dissolved in THF. The reaction was left to stir overnight and warm up to room temperature. The solvent was evaporated under reduced pressure, followed by extraction with anhydrous toluene and washing with hexane to afford the complex as an orange powder. Yield: 0.47 g (83 %). M.p. 240–250 °C (decomp). ^{1}H NMR (400 MHz, $CDCl_3$) δ 7.57 (dt, *J* = 12.0, 7.8 Hz, 2H, dipp-C**H**, **H-1**), 7.50 (dd, *J* = 7.8, 1.3 Hz, 1H, dipp-C**H**, **H-2**), 7.40 (dd, *J* = 7.8, 1.2 Hz, 1H. dipp-C**H**, **H-2**), 7.28 (dd, *J* = 1.3, 2.8 Hz, 2H, dipp-C**H**, **H-2**), 6.98 (m, 1H, Fc-**H**, **H-3**), 5.02 (m, 1H, cod-C**H**, **H-6**), 4.80 (m, 1H, cod-C**H**, **H-6**), 4.50 (m, 1H, Fc-**H**, **H-3**), 4.11 (m, 6H, Fc-**H**, **H-4** + **H-5**), 3.93 (m, 1H, cod-C**H**, **H-6**), 3.82 – 3.71 (m, 2H, Fc-**H**, **H-4** and cod-C**H, H-6**), 3.09 (m, 1H, cod-C$\mathbf{H}_2$, **H-7**), 2.89 (m, 1H, dipp(iso)-C**H**, **H-8**), 2.56 (m, 1H, cod-C$\mathbf{H}_2$, **H-8**), 2.44 (m, 1H, cod-C$\mathbf{H}_2$, **H-7**), 2.25 (m, 1H, dipp(iso)-C**H**, **H-8**), 2.06 (m, 1H, dipp(iso)-C**H**, **H-8**), 1.92 (m, 4H, cod-C$\mathbf{H}_2$, **H-7**), 1.68 (m, 2H, cod-C$\mathbf{H}_2$, **H-7**), 1.58 (t, *J* = 6.6 Hz, 3H, dipp(iso)-C$\mathbf{H}_3$, **H-9**), 1.55 (m, 2H, dipp(iso)-C**H**, **H-9**), 1.51 (d, *J* = 6.8 Hz, 3H, dipp(iso)-C$\mathbf{H}_3$, **H-9**), 1.28 (d, *J* = 6.8 Hz, 3H, dipp(iso)-C$\mathbf{H}_3$, **H-9**), 1.21(d, J = 6.8 Hz, 6H, dipp(iso)-C$\mathbf{H}_3$, **H-9**), 1.03 (d, *J* = 6.9 Hz, 3H, dipp(iso)-C$\mathbf{H}_3$, **H-9**), 0.92 (d, *J* = 6.8 Hz, 3H, dipp(iso)-C$\mathbf{H}_3$, **H-9**), 0.79 (d, *J* = 6.6 Hz, 3H, dipp(iso)-C$\mathbf{H}_3$,

H-9). ^{13}C {^{1}H} NMR (101 MHz, $CDCl_3$) δ 171.9 (d, J_{RhC} = 46.6 Hz, $C_{carbene}$, **C-1**), 149.9 (trz-C_q, **C-2**), 147.6 (dipp-C_q, **C-3**), 147.4 (dipp-C_q, **C-3**), 145.4 (dipp-C_q, **C-3**), 144.8 (dipp-C_q, **C-3**), 136.0 (dipp-C_q, **C-4**), 133.1 (dipp-C_q, **C-4**), 131.5 (dipp-CH, **C-5**), 130.8 (dipp-CH, **C-5**), 125.5 (dipp-CH, **C-6**), 124.7 (dipp-CH, **C-6**), 123.9 (dipp-CH, **C-6**), 122.9 (dipp-CH, **C-6**), 94.7 (d, *J* = 7.7 Hz, cod-CH, **C-7**), 93.7 (d, *J* = 7.7 Hz, cod-CH, **C-7**), 73.8 (Fc-C_q, **C-8**), 73.2 (Fc-CH, **C-9**), 69.8 (Fc-CH, **C-9**), 69.7 (Fc-CH, **C-11**), 69.2 (d, *J* = 14.5 Hz, cod-CH, **C-7**), 68.9 (Fc-CH, **C-10**), 66.6 (d, *J* = 14.3 Hz, cod-CH, **C-7**), 66.2 (Fc-CH, **C-10**), 33.6 (cod-CH_2, **C-12**), 32.5 (cod-CH_2, **C-12**), 29.2 (dipp(iso)-CH, **C-13**), 29.1 (cod-CH_2, **C-12**), 29.0 (dipp(iso)-CH, **C-13**), 28.9 (dipp(iso)-CH, **C-13**), 28.8 (cod-CH_2, **C-12**), 28.3 (dipp(iso)-CH, **C-13**), 26.5 (dipp(iso)-CH_3, **C-14**), 26.4 (dipp(iso)-CH_3, **C-14**), 26.4 (dipp(iso)-CH_3, **C-14**), 25.6 (dipp(iso)-CH_3, **C-14**), 25.1 (dipp(iso)-CH_3, **C-14**), 25.0 (dipp(iso)-CH_3, **C-14**), 24.2 (dipp(iso)-CH_3, **C-14**), 23.6 (dipp(iso)-CH_3, **C-14**), 23.4 (dipp(iso)-CH_3, **C-14**), 23.3 (dipp(iso)-CH_3, **C-14**), 23.1 (dipp(iso)-CH_3, **C-14**). Anal. Calcd for $C_{44}H_{55}N_3FeRhCl$ (with 0.3 eq H_2O): C 62.38 H 6.54 N 4.96. Found: C 62.68 H 6.67 N 4.71. ESI-HRMS (15 V, positive mode, m/z): calcd for [M–Cl]+ : 784.2800. Found: 784.2834.

General procedure for the synthesis of *1-ethyl-3-(2,6-diisopropylphenyl)-4-Ar-1,2,3-triazol-5-ylidene chlorido-η⁴-1,5-cyclooctadiene-rhodium(I) (Ar = Fc,* ***5****; Ar = Ph,* ***6****).*

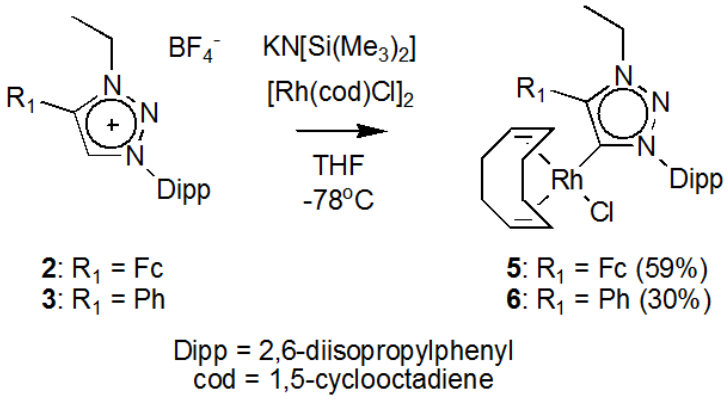

Scheme 8.4. Synthesis of rhodium triazolylidene complexes, **5** and **6**.

0.75 mmol of the appropriate triazolium salt **2** or **3** was weighed off, along with one equivalents of $KN(SiMe_3)_2$ (0.16 g, 0.83 mmol) and 0.5 equivalents of $[Rh(cod)Cl]_2$ (0.18 g, 0.38 mmol) in a Schlenk tube purged with argon gas. The

solid mixture was cooled down to -78 °C, and a cooled solution of THF (*ca.* 10 mL) was added. The reaction was left to stir overnight while warming up to room temperature. The solvent was evaporated under reduced pressure. Following extraction with anhydrous toluene and washing with hexane, complex **5** was afforded as an orange powder, and complex **6** as a yellow powder.

Synthesis of *1-ethyl-3-(2,6-diisopropylphenyl)-4-ferrocenyl-1,2,3-triazol-5-ylidene chlorido-η⁴-1,5-cyclooctadienerhodium(I)* (**5**). Yield: 0.31 g (59 %). M.p. 155–158 °C. ^{1}H NMR (300 MHz, CDCl3) δ 7.55 (t, *J* = 7.7 Hz, 1H, dipp-C**H**, **H-1**), 7.46 (d, *J* = 7.6 Hz, 1H, dipp-C**H**, **H-2**), 7.26 (d, *J* = 7.4 Hz, 1H, dipp-C**H**, **H-2**), 5.85 (m, 1H, Fc-C**H**, **H-3**), 5.77 (m, 1H, Fc-C**H**, **H-3**), 4.92 (dd, *J* = 13.7, 7.2 Hz, 1H, -C**H**$_2$CH$_3$, **H-4**), 4.80 (br, 2H, cod-C**H**, **H-5**), 4.69 (dd, *J* = 13.7, 7.2 Hz, 1H, -C**H**$_2$CH$_3$, **H-4**), 4.54 (m, 2H, Fc-C**H**, **H-6**), 4.24 (m, 5H, Fc-C**H**, **H-7**), 3.62 (m, 1H, dipp(iso)-C**H**, **H-8**), 3.40 (m, 1H, cod-C**H**, **H-5**), 2.80 (m, 1H, cod-C**H**, **H-5**), 2.46 (m, 2H, dipp(iso)-C**H**, **H-8**), 2.17 (m, 2H, cod-C**H**$_2$, **H-9**), 1.98 - 1.61 (m, 6H, cod-C**H**$_2$, **H-9**), 1.71 (t, *J* = 7.3 Hz, 3H, -CH$_2$C**H**$_3$, **H-10**), 1.51 (d, *J* = 6.2 Hz, 3H, dipp(iso)-C**H**$_3$, **H-11**), 1.42 (m, 3H, cod-C**H**$_2$, **H-9**), 1.16 (d, *J* = 6.8 Hz, 6H, dipp(iso)-C**H**$_3$, **H-11**), 1.00 (d, *J* = 6.9 Hz, 3H, dipp(iso)-C**H**$_3$, **H-11**). ^{13}C {^{1}H} NMR (75 MHz, CDCl$_3$) δ 172.3 (d, J_{RhC} = 47.1 Hz, **C**$_{carbene}$, **C-1**), 147.3 (dipp-**C**$_q$, **C-2**), 145.3 (dipp-**C**$_q$, **C-2**), 143.9 (trz-**C**$_q$, **C-3**), 136.7 (dipp-**C**$_q$, **C-4**), 130.7 (dipp-**C**H, **C-5**), 124.6 (dipp-**C**H, **C-6**), 122.9 (dipp-**C**H, **C-6**), 96.2 (d, *J* = 7.2 Hz, cod-**C**H, **C-7**), 93.8 (d, *J* = 7.81, cod-**C**H, **C-7**), 72.5 (Fc-**C**$_q$, **C-8**), 70.9 (Fc-**C**H, **C-9**), 69.9 (Fc-**C**H, **C-9**), 69.6 (Fc-**C**H, **C-10**), 66.8 (cod-**C**H, **C-7**), 66.6 (cod-**C**H, **C-7**), 46.1 (-**C**H$_2$CH$_3$, **C-11**), 34.4 (dipp(iso)-**C**H, **C-12**), 31.2 (cod-**C**H$_2$, **C-13**), 29.9 (cod-**C**H$_2$, **C-13**), 29.2 (cod-**C**H$_2$, **C-13**), 28.8 (dipp(iso)-**C**H, **C-12**), 27.9 (cod-**C**H$_2$, **C-13**), 26.7 (dipp(iso)-**C**H$_3$, **C-14**), 25.9 (dipp(iso)-**C**H$_3$, **C-14**), 23.3 (dipp(iso)-**C**H$_3$, **C-14**), 22.4 (dipp(iso)-**C**H$_3$, **C-14**), 14.9 (-CH$_2$**C**H$_3$, **C-15**). ESI-HRMS (15 V, positive mode, m/z): calcd for [M–Cl]+: 652.1861. Found: 652.1918.

Synthesis of *1-ethyl-3-(2,6-diisopropylphenyl)-4-phenyl-1,2,3-triazol-5-ylidene chlorido-η⁴-1,5-cyclooctadienerhodium(I)* (**6**). Yield: 0.07 g (30 %). M.p. 145 °C (decomp.). ^{1}H NMR (300 MHz, CDCl3) δ 8.09 (d, *J* = 7.4 Hz, 1H, dipp-C**H**, **H-1**), 7.56 (dt, *J* = 12.6, 6.5 Hz, 5H, ph-C**H**, **H-2**), 7.44 (m, 1H, dipp-C**H**, **H-3**), 4.66

(m, 2H, cod-C**H**, **H-4**), 4.40 (m, 2H, -C**H**$_2$CH$_3$, **H-5**), 3.45 (m, 1H, dipp(iso)-C**H**, **H-6**), 3.23 (m, 1H, dipp(iso)-C**H**, **H-6**), 2.90 (m, 1H, cod-C**H**, **H-4**), 2.00 (m, 4H, cod-C**H**, **H-4** + cod-C**H**$_2$, **H-7**), 1.63 (m, 8H, cod-C**H**$_2$, **H-7**), 1.50 (m, 3H,-CH$_2$C**H**$_3$, **H-8**), 1.19–1.04 (m, 12H, dipp(iso)-C**H**$_3$, **H-9**). ^{13}C {^{1}H} NMR (75 MHz, CDCl$_3$) δ 173.2 (d, J_{RhC} = 47.3 Hz, **C**$_{carbene}$, **C-1**), 145.8 (trz-**C**$_q$, **C-2**), 144.9 (dipp-**C**$_q$, **C-3**), 136.3 (dipp-**C**$_q$, **C-4**), 130.9 (ph-**C**H, **C-6**), 130.7 (dipp-**C**$_q$, **C-5**), 129.6 (ph-**C**H, **C-6**), 128.9 (ph-**C**H, **C-6**), 128.5 (dipp-**C**H, **C-7**), 124.9 (ph-**C**$_q$, **C-8**), 95.5 (cod-**C**H, **C-9**), 70.8 (cod-**C**H, **C-9**), 45.6 (-**C**H$_2$CH$_3$, **C-10**), 33.4 (cod-**C**H$_2$, **C-11**), 32.2 (cod-**C**H$_2$, **C-11**), 31.1 (dipp(iso)-**C**H, **C-12**), 29.0 (cod-**C**H$_2$, **C-11** + dipp-**C**H$_3$, **C-13**), 28.3 (cod-**C**H$_2$, **C-11**), 26.6 (dipp-**C**H$_3$, **C-13**), 24.8 (dipp-**C**H$_3$, **C-13**), 23.7 (dipp-**C**H$_3$, **C-13**), 14.9 (-CH$_2$**C**H$_3$, **C-14**). ESI-HRMS (15 V, positive mode, m/z): calcd for [M–Cl]+: 544.2199. Found: 544.2197.

General procedure for the synthesis of *1,3-bis(2,6-diisopropylphenyl)-4-ferrocenyl-1,2,3-triazol-5-ylidene chloridodicarbonyl-rhodium(I),* **7** and 1-ethyl-3- (2,6-diisopropylphenyl)-4-Ar-1,2,3-triazol-5-ylidene *chloridodicarbonyl rhodium(I)* (Ar = Fc, **8**; Ar = Ph, **9**).

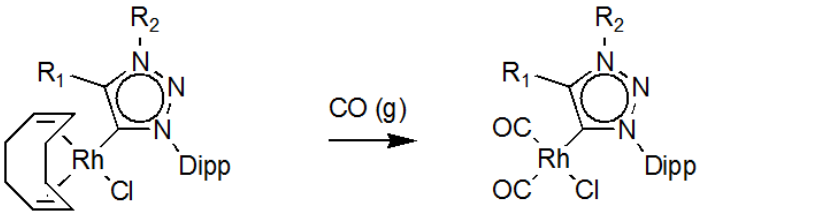

4: R_1 = Fc, R_2 = Dipp
5: R_1 = Fc, R_2 = Ethyl
6: R_1 = Ph, R_2 = Ethyl

7: R_1 = Fc, R_2 = Dipp (87%)
8: R_1 = Fc, R_2 = Ethyl (33%)
9: R_1 = Ph, R_2 = Ethyl (22%)

Dipp = 2,6-diisopropylphenyl

Scheme 8.5. Synthesis of rhodium triazolylidene complexes, **7**–**9**.

The appropriate 1,2,3-triazol-5-ylidene chloro-η^4-1,5-cyclooctadiene complex (**4**: 0.61 mmol; **5**: 0.15 mmol; **6**: 0.08 mmol) was dissolved in DCM and gaseous CO was passed through the solution for 10–20 minutes. The solvent was evaporated and the residue was washed with hexane. The solid was dried overnight, affording **7** and **8** as orange powders and **9** as a light-yellow powder.

1,3-bis(2,6-diisopropylphenyl)-4-ferrocenyl-1,2,3-triazol-5-ylidene chloridodicarbonylrhodium(I), **7**. Yield: 0.41 g (87%). M.p. 199 °C (decomp.) ^{1}H NMR

(400 MHz, $CDCl_3$) δ 7.58 (t, *J* = 7.8 Hz, 2H, dipp-C**H**, **H-1**), 7.40 (m, 3H, dipp-C**H**, **H-2**), 7. 29 (m, 1H, dipp-C**H**, **H-2**), 5.74 (m, 1H, Fc-**H**, **H-3**), 4.35 (m, 1H, Fc-**H**, **H-3**), 4.23 (m, 4H, Fc-**H**, **H-5**), 4.14 (m, 1H, Fc-**H**, **H-4**), 3.86 (m, 1H, Fc-C**H**, **H-4**), 2.93 (dt, *J* = 13.4, 6.7 Hz 1H, dipp(iso)-C**H**, **H-6**), 2.65 (dtd, *J* = 20.2, 13.6, 6.8 Hz, 2H, dipp(iso)-C**H**, **H-6**), 2.19 (dt, *J* = 13.6, 6.8 Hz, 1H, dipp(iso)-C**H**, **H-6**), 1.45 (d, *J* = 6.7 Hz, 3H, dipp(iso)-C**H**$_3$, **H-7**), 1.37 (dd, *J* = 6.7, 4.8 Hz, 6H, dipp(iso)-C**H**$_3$, **H-7**), 1.25 (d, *J* = 6.8 Hz, 3H, dipp(iso)-C**H**$_3$, **H-7**), 1.19 (t, *J* = 6.2 Hz, 3H, dipp(iso)-C**H**$_3$, **H-7**), 1.02 (dd, *J* = 6.9, 2.5 Hz, 6H, dipp(iso)-C**H**$_3$, **H-7**), 0.80 (d, *J* = 6.7 Hz, 3H dipp(iso)-C**H**$_3$, **H-7**). ^{13}C {^1H} NMR (101 MHz, $CDCl_3$) δ 186.1 (d, J_{RhC} = 54.5, Rh-**C**O (*trans* to carbene), **C-1a**), 184.5 (d, J_{RhC} = 74.9, Rh-**C**O (*trans* to chlorido), **C-1b**), 165.8 (d, J_{RhC} = 44.8, **C**$_{carbene}$**, C-2**), 149.7 (trz-**C**$_q$**, C-3**), 147.1 (dipp-**C**$_q$**, C-4**), 146.5 (dipp-**C**$_q$**, C-4**), 145.4 (dipp-**C**$_q$**, C-4**), 144.7 (dipp-**C**$_q$**, C-4**), 136.4 (dipp-**C**$_q$**, C-5**), 132.2 (dipp-**C**$_q$**, C-5**), 132.0 (dipp-**C**H**, C-6**), 131.5 (dipp-**C**H**, C-6**), 125.3 (dipp-**C**H**, C-7**), 124.7 (dipp-**C**H**, C-7**), 124.6 (dipp-**C**H**, C-7**), 123.6 (dipp-**C**H**, C-7**), 73.1 (Fc-**C**H**, C-9**), 71.8 (Fc-**C**$_q$**, C-8**), 70.1 (Fc-**C**H**, C-10**), 69.5 (Fc-**C**H**, C-9**), 67.2 (Fc-**C**H**, C-9**), 29.4 (dipp(iso)-**C**H**, C-11**), 29.3 (dipp(iso)-**C**H**, C-11**), 28.9 (dipp(iso)-**C**H**, C-11**), 28.7 (dipp(iso)-**C**H**, C-11**), 27.3 (dipp(iso)-**C**H$_3$**, C-12**), 26.9 (dipp(iso)-**C**H$_3$**, C-12**), 25.4 (dipp(iso)-**C**H$_3$**, C-12**), 25.1 (dipp(iso)-**C**H$_3$**, C-12**), 23.8 (dipp(iso)-**C**H$_3$**, C-12**), 23.1(4) (dipp(iso)-**C**H$_3$**, C-12**), 23.1(1) (dipp(iso)-**C**H$_3$**, C-12**), 22.3 (dipp(iso)-**C**H$_3$**, C-12**). Anal. Calcd for $C_{38}H_{43}N_3O_2FeRhCl$ (with 1.6eq H_2O): C 57.28 H 5.44 N 5.27. Found: C 57.15 H 5.52 N 4.88. ESI-HRMS (15 V, positive mode, m/z): calcd for [M–CO–Cl]+ : 704.1810. Found: 704.1766. IR (ν_{CO}, CH_2Cl_2): 2075 cm^{-1}, 1992 cm^{-1}.

1-ethyl-3- (2,6-diisopropylphenyl)-4-ferrocenyl-1,2,3-triazol-5-ylidene chlorido-dicarbonylrhodium(I), ***8***. Yield: 0.03 g (33%). ^1H NMR (400 MHz, $CDCl_3$) δ 7.55 (t, *J* = 7.7 Hz, 1H, dipp-C**H**, **H-1**), 7.34 (m, 2H, dipp-C**H**, **H-2**), 5.46 (m, 1H, Fc-**H**, **H-3**), 5.30 (m, 1H, Fc-**H**, **H-3**), 4.78 (m, 2H, -C**H**$_2$CH$_3$, **H-4**), 4.50 (m, 2H, Fc-**H**, **H-5**), 4.27 (m, 5H, Fc-C**H**, **H-6**), 2.85 (m, 1H, dipp(iso)-C**H**, **H-7**), 2.28 (m, 1H, dipp(iso)-CH, **H-7**), 1.72 (t, J = 7.2 Hz, 3H, -CH$_2$C**H**$_3$, **H-8**), 1.33 (d, *J* = 6.5 Hz, 6H, dipp(iso)-C**H**$_3$, **H-9**), 1.21–1.06 (m, 6H, dipp(iso)-C**H**$_3$, **H-9**). ^{13}C {^1H} NMR (101 MHz, $CDCl_3$) δ 185.9 (d, J_{RhC} = 54.1, Rh-**C**O (*trans* to carbene), **C-1a**), 183.7 (d, J_{RhC} = 75.2, Rh-**C**O (*trans* to chlorido), **C-1b**), 165.2 (d, J_{RhC} =

40.0, $\mathbf{C}_{carbene}$, **C-2**), 145.6 (dipp-$\mathbf{C}_q$, **C-3**), 145.4 (trz-$\mathbf{C}_q$, **C-4**), 136.4 (dipp-$\mathbf{C}_q$, **C-5**), 131.3 (dipp-**C**H, **C-6**), 124.5 (dipp-**C**H, **C-7**), 123.5 (dipp-**C**H, **C-7**), 72.2 (Fc-**C**H, **C-8**), 71.3 (Fc-$\mathbf{C}_q$, **C-9**), 71.1 (Fc-**C**H, **C-10**), 70.9 (Fc-**C**H, **C-10**), 70.2 (Fc-**C**H, **C-11**), 69.9 (Fc-**C**H, **C-12**), 46.4 (-$\mathbf{C}H_2CH_3$, **C-13**), 29.0 (dipp(iso)-**C**H, **C-14**), 26.5 (dipp(iso)-$\mathbf{C}H_3$, **C-15**), 26.1 (dipp(iso)-$\mathbf{C}H_3$, **C-15**), 24.8 (dipp(iso)-$\mathbf{C}H_3$, **C-15**), 23.9 (dipp(iso)-$\mathbf{C}H_3$, **C-15**), 22.8 (dipp(iso)-$\mathbf{C}H_3$, **C-15**), 21.9 (dipp(iso)-$\mathbf{C}H_3$, **C-15**), 14.9 (-$CH_2\mathbf{C}H_3$, **C-16**). (ESI-HRMS (15 V, positive mode, m/z): calcd for [M–COCl]+ : 572.0871. Found: 572.0882. IR (ν_{CO}, CH_2Cl_2): 2075 cm^{-1}, 1992 cm^{-1}.

1-ethyl-3- (2,6-diisopropylphenyl)-4-phenyl-1,2,3-triazol-5-ylidene chlorido-dicarbonylrhodium(I), ***9***. Yield: 0.01 g (22%). ^{1}H NMR (400 MHz, $CDCl_3$) δ 7.82 (m, 1H, dipp-C**H**, **H-1**), 7.64 (m, 1H, ph-C**H**, **H-2**), 7.54 (m, 4H, ph-C**H**, **H-3**), 7.50 (d, *J* = 7.5, 2H, dipp-C**H**, **H-4**), 4.48 (dd, *J* = 13.6, 6.6 Hz, 2H, -C$\mathbf{H}_2CH_3$, **H-5**), 2.56 (m, 2H, dipp(iso)-C**H**, **H-6**), 1.54 (t, *J* = 6.9, 3H, -$CH_2C\mathbf{H}_3$, **H-7**), 1.35 (d, *J* = 6.1 Hz, 6H, dipp(iso)-C$\mathbf{H}_3$, **H-8**), 1.10 (d, *J* = 6.30 Hz, 6H, dipp(iso)-C$\mathbf{H}_3$, **H-8**). ^{13}C {^{1}H} NMR (101 MHz, $CDCl_3$) δ 185.7 (d, J_{RhC} = 54.3, Rh-**C**O (*trans* to carbene), **C-1a**), 183.4 (d, J_{RhC} = 75.0, Rh-**C**O (*trans* to chlorido), **C-1b**), 166.2 (d, J_{RhC} = 40.5, $\mathbf{C}_{carbene}$, **C-2**), 146.3 (trz-$\mathbf{C}_q$, **C-3**), 145.8 (dipp-$\mathbf{C}_q$, **C-4**), 135.9 (dipp-$\mathbf{C}_q$, **C-5**), 131.3 (dipp-**C**H, **C-6**), 130.9, 130.3, 130.0, 128.9 (all ph-**C**H, **C-7**), 127.3 (ph-$\mathbf{C}_q$, **C-8**), 124.0 (dipp-**C**H, **C-9**), 46.0 (-C$\mathbf{H}_2CH_3$, **C-10**), 31.0 (dipp(iso)-**C**H, **C-11**), 29.1 (dipp(iso)-**C**H, **C-11**), 26.7 (dipp(iso)-$\mathbf{C}H_3$, **C-12**), 26.2 (dipp(iso)-$\mathbf{C}H_3$, **C-12**), 24.8 (dipp(iso)-$\mathbf{C}H_3$, **C-12**), 23.8 (dipp(iso)-$\mathbf{C}H_3$, **C-12**), 22.6 (dipp(iso)-$\mathbf{C}H_3$, **C-12**), 14.9 (-$CH_2\mathbf{C}H_3$, **C-13**). ESI-HRMS (15 V, positive mode, m/z): calcd for [M–COCl+ACN]+: 505.1475. Found: 505.1546. IR (ν_{CO}, CH_2Cl_2): 2074 cm^{-1}, 1993 cm^{-1}.

8.2.3 Synthetic procedure for the 1,2,3-triazol-5-ylidene gold(I) complexes, **10**, **12**–**13**.

Synthesis of *1,3-bis(2,6-diisopropylphenyl)-4-ferrocenyl-1,2,3-triazol-5-ylidene gold(I) phenyl,* ***12****.*

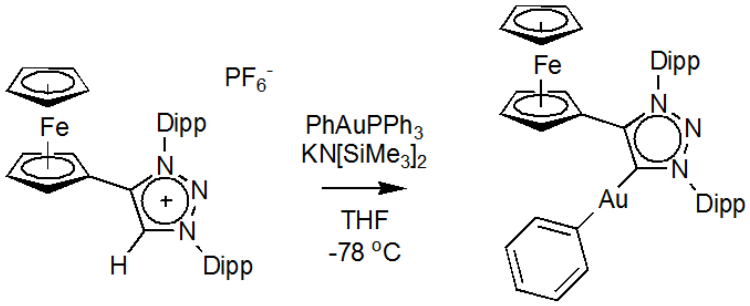

1 Dipp = 2,6-diisopropylphenyl **12** (90%)

Scheme 8.6. The synthesis of the gold(I) phenyl complex, ***12*** *from* ***1****.*

From a previously published method:[16] a solution of $PhAuPPh_3$ (0.41 g, 0.76 mmol) in THF at -30 °C was added dropwise to a solution of **1** (0.5 g, 0.69 mmol) and $KN[SiMe_3]_2$ (0.14 g, 0.76 mmol) in THF at -78 °C. The reaction was left to stir overnight, while reaching room temperature. After the solvent was evaporated, the residue was washed with hexane and the product was extracted with toluene, as a yellow solid in quantitative yield. Yield: 0.53 g (90%). ^{1}H NMR (400 MHz, $CDCl_3$) δ 7.59 (t, *J* = 7.8 Hz, 1H, dipp-C**H, H-1**), 7.53 (m, 1H, dipp-C**H, H-1**), 7.48 (dd, *J* = 7.6, 1.3 Hz, 2H, dipp-C**H**, **H-2**), 7.34 (dd, *J* = 11.9, 7.9 Hz, 4H. phenyl-C**H, H-3**), 7.18 (t, *J* = 7.5 Hz, 2H, dipp-C**H, H-2**), 6.98 (dd, *J* = 10.3, 4.4 Hz, 1H, phenyl-C**H, H-4**), 4.73 (m, 2H, Fc-C**H**, **H-5**), 4.29 (m, 5H, Fc-C**H**, **H-6**), 4.23 (m, 2H, Fc-C**H**, **H-7**), 2.61 (dt, *J* = 13.7, 6.9 Hz, 2H, dipp(iso)-C**H, H-8**), 2.44 (dt, *J* = 13.6, 6.8 Hz, 2H, dipp(iso)-C**H, H-8**), 1.52 (d, *J* = 6.8 Hz, 6H, dipp(iso)-C**H$_3$, H-9**), 1.21 (d, *J* = 6.9 Hz, 6H, dipp(iso)-C**H$_3$, H-9**), 1.16 (d, J = 6.8, 12H, dipp(iso)-C**H$_3$, H-9**). ^{13}C {^{1}H} NMR (75 MHz, $CDCl_3$) δ 183.1 (**C**$_{carbene}$, **C-1**), 172.7 (Au-Ph**C**$_q$, **C-2**), 149.5 (trz-**C**$_q$, **C-3**), 145.7 (dipp-**C**$_q$, **C-4**), 145.0 (dipp-**C**$_q$, **C-4**), 140.9 (phenyl-**C**H, **C-5**), 136.0 (phenyl-**C**H, **C-6**), 131.9 (dipp-**C**$_q$, **C-7**), 131.0 (dipp-**C**$_q$, **C-7**), 127.1 (phenyl-**C**H, **C-8**), 124.7 (dipp-**C**H, **C-9**), 124.4 (dipp-**C**H, **C-10**), 124.1 (dipp-**C**H, **C-9**), 71.1 (Fc-**C**H, **C-11**), 70.8 (Fc-**C**H, **C-12**), 69.9 (Fc-**C**$_q$, **C-13**), 68.5 (Fc-**C**H, **C-14**), 29.2 (dipp(iso)-**C**H, **C-15**), 25.0 (dipp(iso)-**C**H$_3$, **C-16**), 24.6 (dipp(iso)-**C**H$_3$, **C-16**), 24.3 (dipp(iso)-**C**H$_3$, **C-16**), 23.0 (dipp(iso)-**C**H$_3$, **C-16**). ESI-HRMS (15 V, positive mode, m/z): calcd for [M+ACN]+: 811.2732. Found: 811.2764.

Synthesis of *1,3-bis(2,6-diisopropylphenyl)-4-ferrocenyl-1,2,3-triazol-5-ylidene gold(I) chloride,* ***10.***

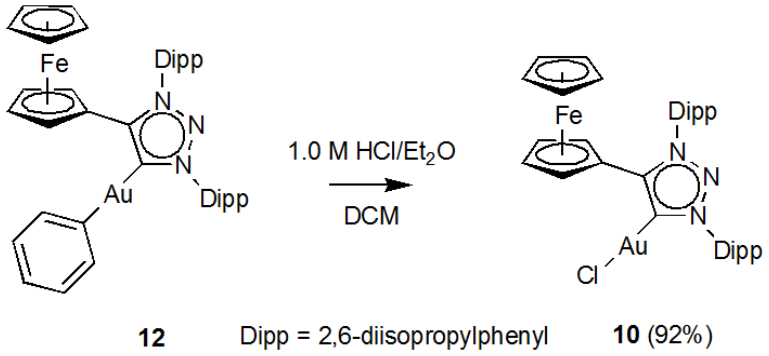

12 Dipp = 2,6-diisopropylphenyl **10** (92%)

*Scheme 8.7. Synthesis of the triazolylidene gold(I) chlorido complex, **10** from the hydrolysis of **12**.*

Complex **12** (0.52 g, 0.62 mmol) was suspended in DCM and an excess of 1.0 M HCl in diethyl ether (3.8 mL) was added and stirred for one hour. The solvent was evaporated affording **13** as a yellow brown solid in near-quantitative yield. Yield: 0.45 g (92%). M.p. 145–149 °C. ^{1}H NMR (400 MHz, $CDCl_3$) δ 7.57 (m, 2H, dipp-C**H, H-1**), 7.34 (t, J = 7.8, 4H, dipp-C**H, H-2**), 4.61 (br s, 2H, Fc-C**H**, **H-3**), 4.26 (br s, 7H, Fc-C**H**, **H-4**), 2.49 (dt, *J* = 13.4, 6.7 Hz, 2H, dipp(iso)-C**H, H-5**), 2.37 (dd, *J* = 12.1, 5.8 Hz, 2H, dipp(iso)-C**H, H-5**), 1.46 (d, *J* = 6.8 Hz, 6H, dipp(iso)-C**H$_3$, H-6**), 1.16 (m, 18H, dipp(iso)-C**H$_3$, H-6**). ^{13}C {^{1}H} NMR (75 MHz, $CDCl_3$) δ 160.9 (**C**$_{carbene}$, **C-1**), 148.7 (trz-**C**$_q$, **C-2**), 145.4 (dipp-**C**$_q$, **C-3**), 144.9 (dipp-**C**$_q$, **C-3**), 135.3 (dipp-**C**$_q$, **C-4**), 132.3 (dipp-**C**$_q$, **C-4**), 131.5 (dipp-**C**H, **C-5**), 131.3 (dipp-**C**H, **C-5**), 124.7 (dipp-**C**H, **C-6**), 124.3 (dipp-**C**H, **C-6**), 70.7 (Fc-**C**H, **C-7**), 70.1 (Fc-**C**H, **C-8**), 69.5 (Fc-**C**$_q$, **C-10**), 69.3 (Fc-**C**H, **C-9**), 29.0 (dipp(iso)-**C**H, **C-11**), 24.9 (dipp(iso)-**C**H_3, **C-12**), 24.5 (dipp(iso)-**C**H_3, **C-12**), 24.2 (dipp(iso)-**C**H_3, **C-12**), 22.9 (dipp(iso)-**C**H_3, **C-12**). Anal. Calcd for $C_{36}H_{43}N_3FeAuCl$ (1 eq H_2O): C 52.48, H 5.26, N 5.10. Found: C 52.73, H 4.92, N 4.70. ESI-HRMS (15 V, positive mode, m/z): calcd for [M]+: 1253.4663. Found: 1253.4719.

Synthesis of *1,3-bis(2,6-diisopropylphenyl)-4-ferrocenyl-1,2,3-triazol-5-ylidene gold(I) triphenylphosphine, **13.***

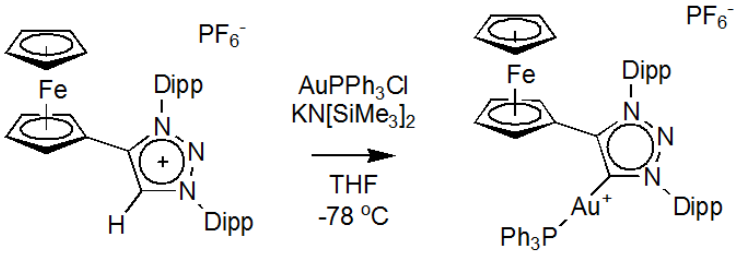

1 Dipp = 2,6-diisopropylphenyl **13** (98%)

Scheme 8.8. The synthesis of the cationic triazolylidene gold(I) triphenylphosphine complex, **13** from **1**.

A solution of $AuPPh_3Cl$ (0.08 g, 0.15 mmol) in THF was added to a solution of **1** (0.1 g, 0.14mmol) and $KN[SiMe_3]_2$ (0.03 g, 0.15 mmol) in THF at -78 °C, and reaction proceeded overnight while warming to room temperature. The solvent was evaporated and the residue was washed with toluene, followed by extraction by DCM affording **13**, as an orange solid in near-quantitative yield. Yield: 0.16 g (98%). M.p. 249–256 °C (decomp.). ^{1}H NMR (400 MHz, $CDCl_3$) δ 7.78 (t, *J* = 7.8, 1H, dipp-C**H, H-1**), 7.67 (t, *J* = 7.8, 1H, dipp-C**H, H-1**), 7.60 (m, 3H, ph-C**H**, **H-2**), 7.50 (t, *J* = 7.2, 6H, ph-C**H**, **H-3**), 7.43 (dd, *J* = 12.5, 8.3 Hz, 4H, dipp-C**H**, **H-4**), 7.32 (dd, *J* = 12.9, 7.4 Hz, 6H, ph-C**H**, **H-5**), 4.39 (br s, 4H, Fc-C**H**, **H-6**), 3.99 (br s, 5H, Fc-C**H**, **H-7**), 2.47 (dt, *J* = 13.4, 6.7 Hz, 2H, dipp(iso)-C**H, H-8**), 2.30 (dd, *J* = 13.5, 6.7 Hz, 2H, dipp(iso)-C**H, H-8**), 1.28 (d, *J* = 6.8 Hz, 6H, dipp(iso)-C**H$_3$, H-9**), 1.22 (d, *J* = 6.8 Hz, 6H, dipp(iso)-C**H$_3$, H-9**), 1.16 (d, *J* = 6.8 Hz, 12H, dipp(iso)-C**H$_3$, H-9**). ^{13}C {^{1}H} NMR (75 MHz, $CDCl_3$) δ 176.2 (d, J_{CP} = 120.5 Hz, **C**$_{carbene}$, **C-1**), 151.1 (d, J = 7.8 Hz, trz-**C**$_q$, **C-2**), 145.3 (dipp-**C**$_q$, **C-3**), 145.2 (dipp-**C**$_q$, **C-3**), 135.2 (dipp-**C**$_q$, **C-4**), 133.9 (d, *J* = 13.6 Hz, ph-**C**H, **C-5**), 132.9 (dipp-**C**$_q$, **C-6**), 132.7 (ph-**C**H, **C-7**), 132.3 (dipp-**C**H, **C-6**), 130.7 (dipp-**C**$_q$, **C-4**), 129.9 (d, *J* = 11.5, ph-**C**H, **C-8**), 128.0 (d, *J* = 58.3, ph-**C**$_q$, **C-9**), 125.1 (dipp-**C**H, **C-10**), 124.8 (dipp-**C**H, **C-10**), 71.3 (Fc-**C**H, **C-11**), 70.6 (Fc-**C**H, **C-12**), 69.5 (Fc-**C**H, **C-13**), 68.3 (Fc-**C**$_q$, **C-14**), 29.4 (dipp(iso)-**C**H, **C-15**), 24.3 (dipp(iso)-**C**H_3, **C-15**), 25.0 (dipp(iso)-**C**H_3, **C-16**), 24.5 (dipp(iso)-**C**H_3, **C-16**), 24.4 (dipp(iso)-**C**H_3, **C-16**), 22.9 (dipp(iso)-**C**H_3, **C-16**). ^{31}P {^{1}H} NMR (121 MHz, $CDCl_3$) δ 40.9 (s, Ph_3-**P**-Au), -144.27 (dt, *J* = 712.3 Hz, 1424.5 Hz, **P**F_6). ^{19}F {^{1}H} NMR (282 MHz, $CDCl_3$) δ -73.85 (d, *J* = 712.2 Hz, P**F**$_6$). Anal. Calcd for $C_{54}H_{58}N_3FeAuP_2F_6$ (6.5eq H_2O): C 50.05, H 4.51, N

3.24. Found: C 50.47, H 4.21, N 2.84. ESI-HRMS (15 V, positive mode, m/z): calcd for [M]+: 1032.3383. Found: 1032.3416.

8.2.4 Synthetic procedure for the bis-1,2,3-triazol-5-ylidene silver(I) complex, **11**.

Synthesis of bis-(*1,3-bis(2,6-diisopropylphenyl)-4-ferrocenyl-1,2,3-triazol-5-ylidene silver(I) hexafluorophosphate,* ***11****.*

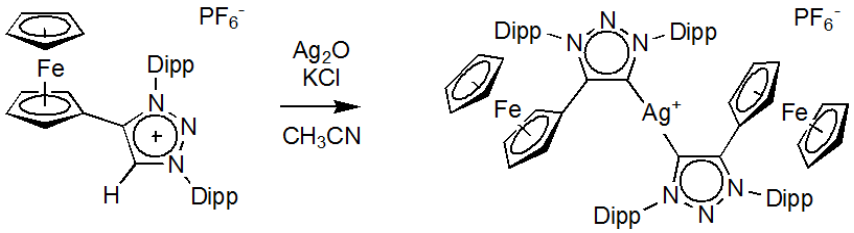

Dipp = 2,6-diisopropylphenyl

Scheme 8.9. The synthesis of the silver(I) bis-triazolylidene complex, **11.**

Triazolium salt, **1** (0.2 g, 0.28 mmol), Ag_2O (0.26 g, 1.11 mmol) and KCl (0.12 g, 1.67 mmol) was added to a purged foil-covered Schlenk, and cooled down to 0 °C. Cooled degassed CH_3CN was added, and the reaction was left to stir for 30 minutes, after which it was permitted to stir overnight at room temperature. After evaporation of solvent, the residue was washed with toluene, and the product was extracted with DCM, affording **11** as a light orange powder. Yield: 0.3 g (80%). M.p. 252–258 °C (decomp.). ^{1}H NMR (400 MHz, $CDCl_3$) δ 7.74 (t, *J* = 7.8 Hz, 1H, dipp-C**H, H-1**), 7.67 (t, *J* = 7.8, 1H, dipp-C**H, H-1**), 7.47 (d, *J* = 7.9 Hz, 2H. dipp-C**H, H-2**), 7.41 (d, *J* = 7.9 Hz, 2H, dipp-C**H, H-2**), 4.17 (m, 2H, Fc-C**H**, **H-3**), 4.04 (s, 4H, Fc-C**H**, **H-4**), 3.83 (m, 2H, Fc-C**H**, **H-5**), 2.54 (dt, *J* = 13.7, 6.7 Hz, 2H, dipp(iso)-C**H, H-6**), 2.29 (dt, *J* = 14.1, 7.0 Hz, 2H, dipp(iso)-C**H, H-6**), 1.34 (d, *J* = 6.8 Hz, 6H, dipp(iso)-C**H$_3$, H-7**), 1.26 (d, *J* = 6.9 Hz, 6H, dipp(iso)-C**H$_3$, H-7**), 1.16 (d, *J* = 6.7 Hz, 4.1 Hz, 12H, dipp(iso)-C**H$_3$, H-7**). ^{13}C NMR (75 MHz, $CDCl_3$) δ 167.3 (dd, J_{AgC} = 181.2, 13.1 Hz **C**$_{carbene}$, **C-1**), 151.6 (trz-**C**$_q$, **C-2**), 151.5 (trz-**C**$_q$, **C-2**), 145.2 (dipp-**C**$_q$, **C-3**), 145.0 (dipp-**C**$_q$, **C-3**), 136.0 (dipp-**C**$_q$, **C-4**), 132.7 (dipp-**C**$_q$, **C-4**), 132.32 (dipp-**C**H, **C-5**), 131.0 (dipp-**C**H, **C-5**), 125.0 (dipp-**C**H, **C-6**), 124.8 (dipp-**C**H, **C-6**), 71.1 (Fc-**C**H, **C-7**), 70.5 (Fc-**C**H, **C-8**), 69.5 (Fc-**C**$_q$, **C-9**), 68.6 (Fc-**C**H, **C-10**), 29.4 (dipp(iso)-**C**H, **C-11**), 29.23 (dipp(iso)-**C**H, **C-11**), 25.1 (dipp(iso)-**C**H_3, **C-12**), 24.6 (dipp(iso)-

CH$_3$, **C-12**), 24.3 (dipp(iso)-**C**H$_3$, **C-12**), 23.0 (dipp(iso)-**C**H$_3$, **C-12**). ^{31}P {^{1}H} NMR (121 MHz, CDCl$_3$) δ -144.26 (dt, *J* = 712.3 Hz, 1424.3 Hz, **P**F$_6$). ^{19}F {^{1}H} NMR (282 MHz, CDCl$_3$) δ -73.93 (d, *J* = 712.2 Hz, P**F**$_6$). Anal. Calcd for C$_{72}$H$_{86}$N$_6$Fe$_2$AgPF$_6$ (3 eq (CH$_3$)$_2$CO): C 61.80, H 6.66, N 5.34. Found: C 62.22, H 6.50, N 5.13. ESI-HRMS (15 V, positive mode, m/z): calcd for [M]+: 1253.4663. Found: 1253.4719.

8.3 The NMR spectra and atom-numbering schemes of complexes **1**–**14**.

8.3.1 NMR spectra of ligand precursor salts, **1-3**.

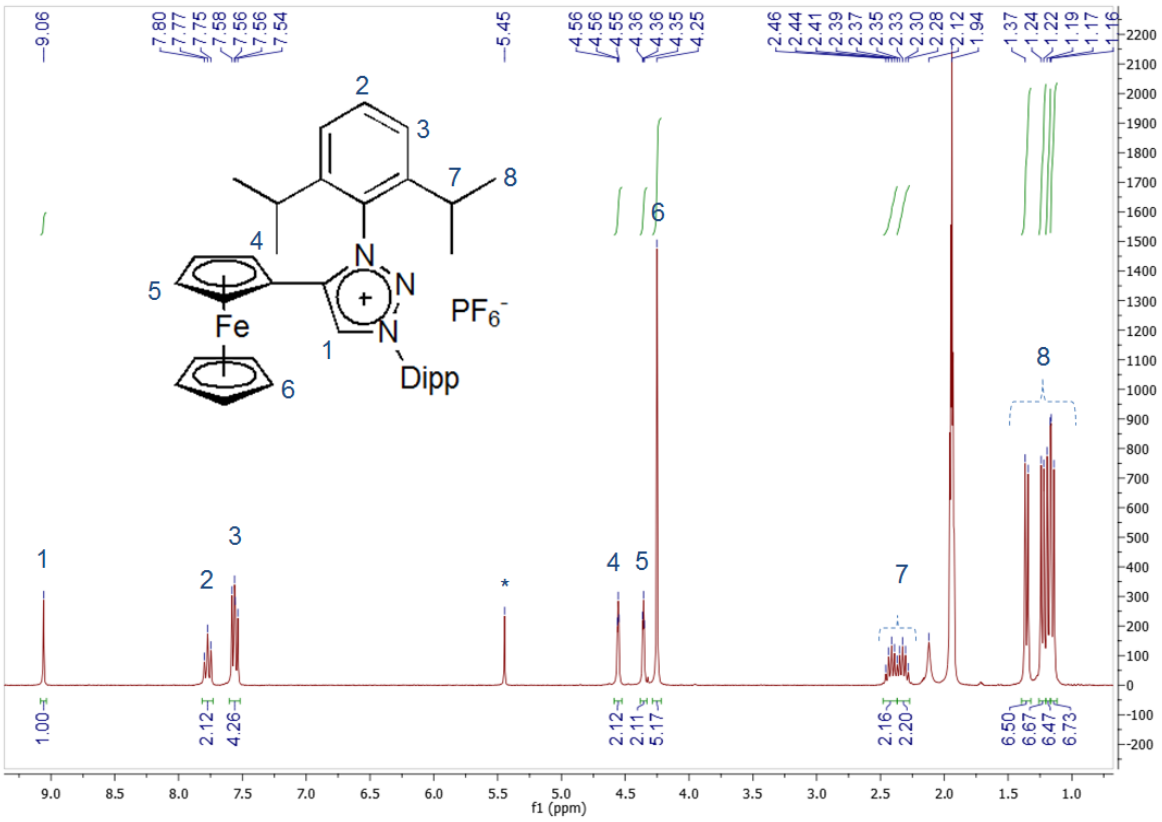

Figure 8.1. The ^{1}H NMR spectrum of ligand precursor salt, **1** in solvent CD$_3$CN.

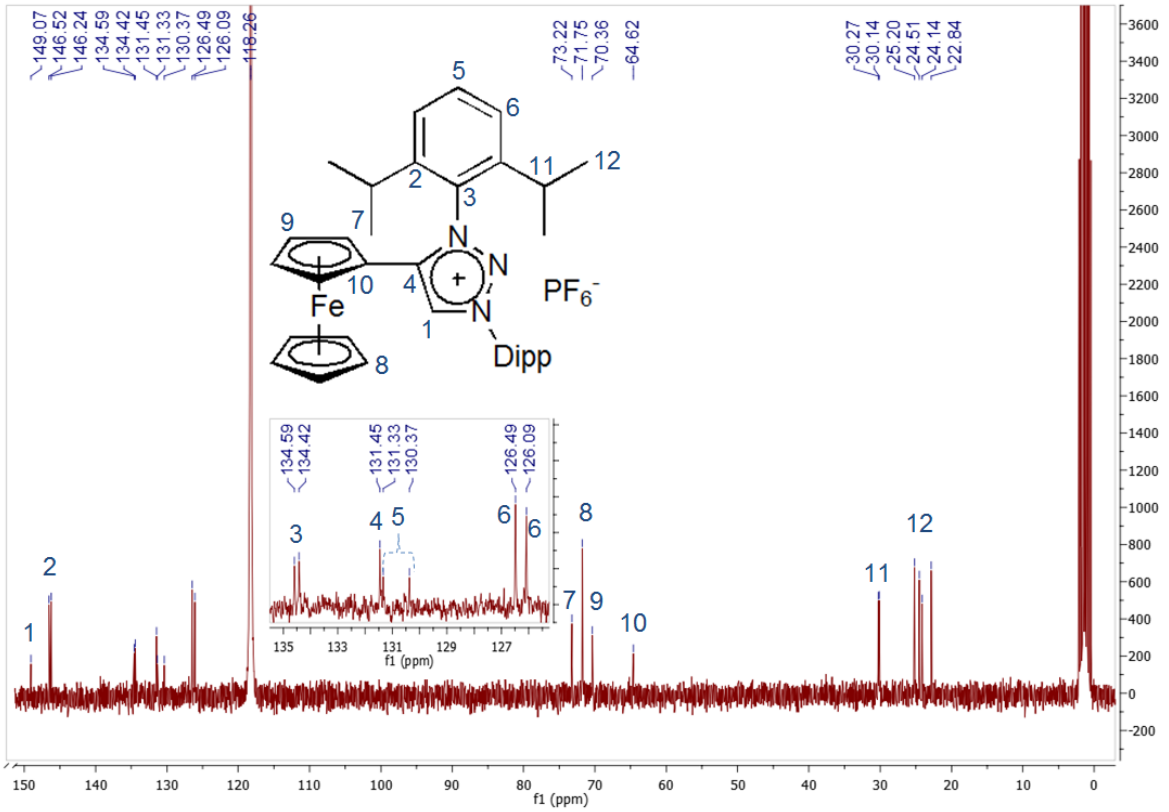

Figure 8.2. The ^{13}C NMR of ligand precursor salt, **1** in solvent CD_3CN.

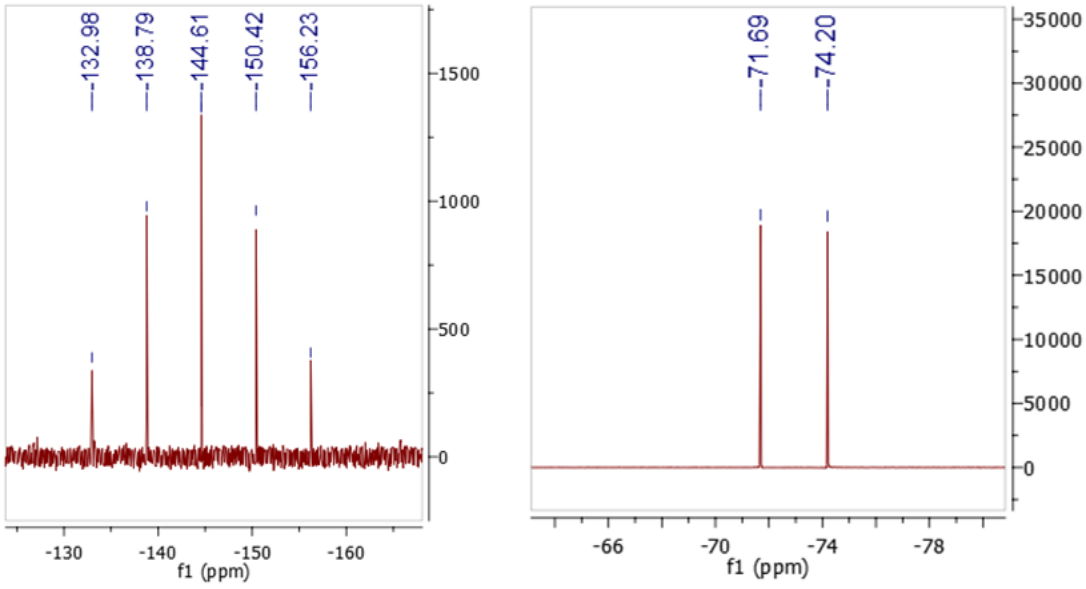

Figure 8.3. The (a) ^{31}P NMR and the (b) ^{19}F NMR spectra of the ligand precursor salt, **1** in solvent CD_3CN.

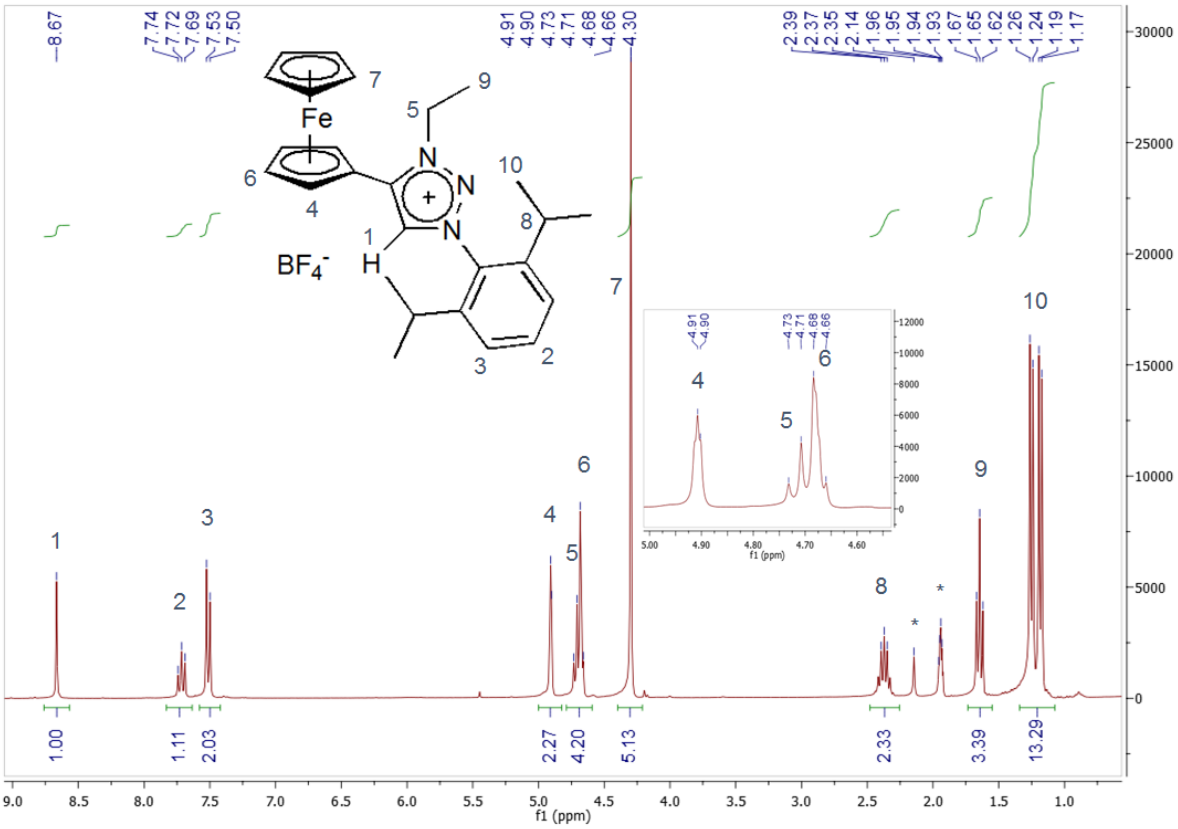

Figure 8.4. The ^{1}H NMR spectrum of the ligand precursor salt, **2** in solvent CD_3CN.

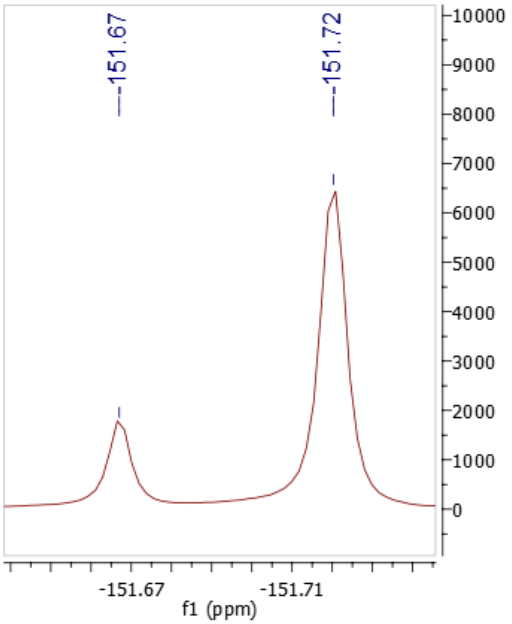

Figure 8.5. The ^{19}F NMR spectrum of the ligand precursor salt, **2** in solvent CD_3CN.

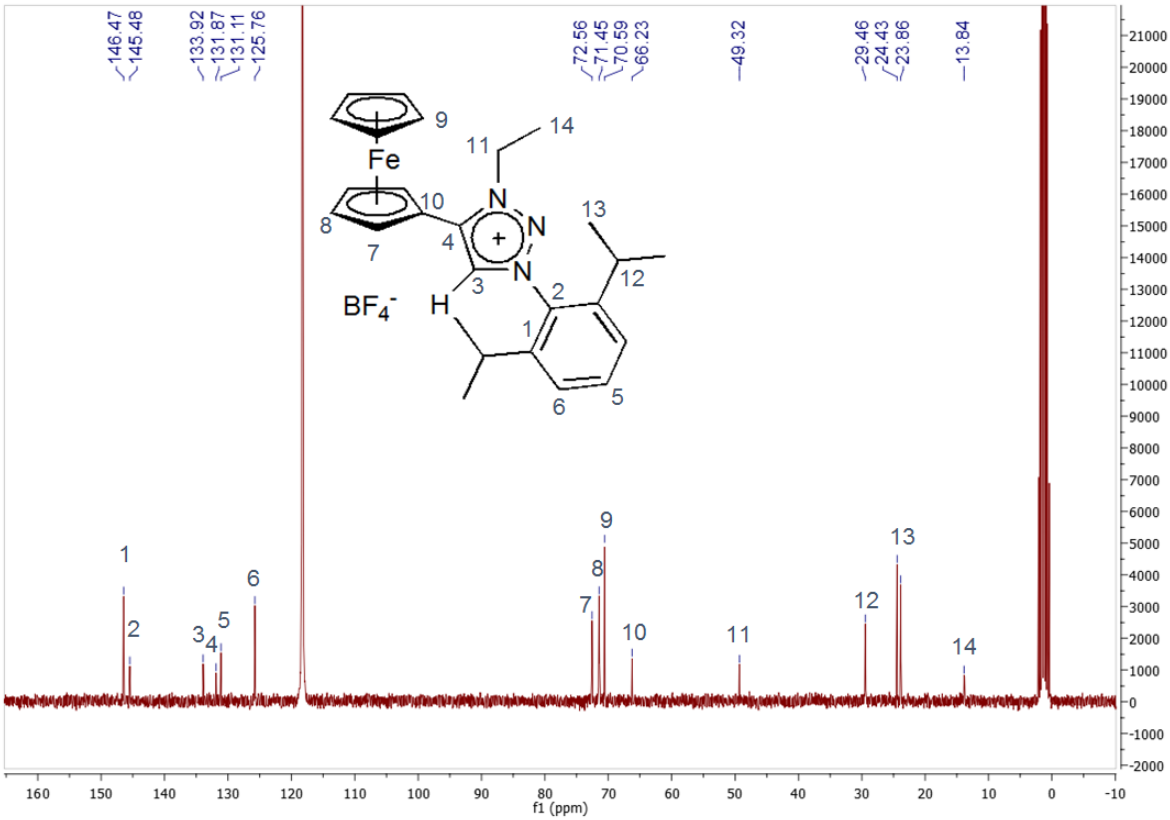

Figure 8.6. The ^{13}C NMR spectrum for the ligand precursor salt, **2** in solvent CD_3CN.

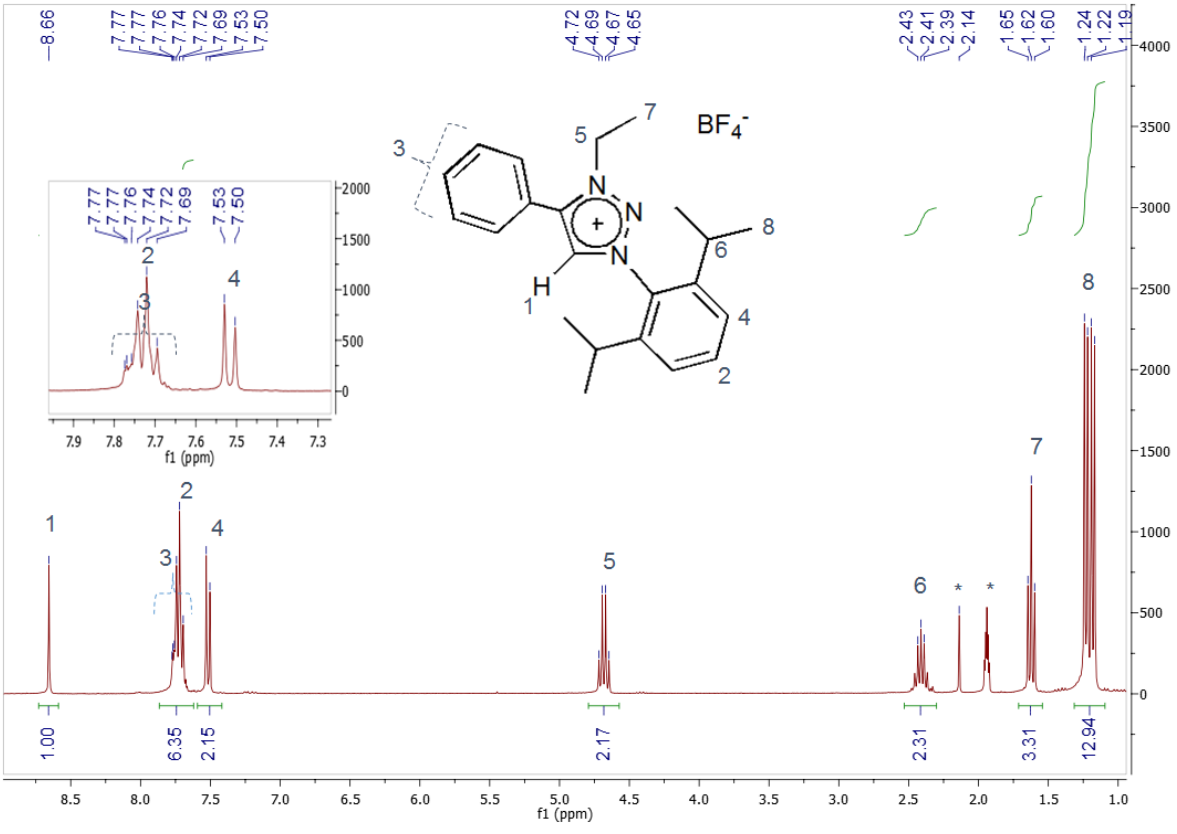

Figure 8.7. The ^{1}H NMR spectrum of the ligand precursor salt, **3** in solvent CD_3CN.

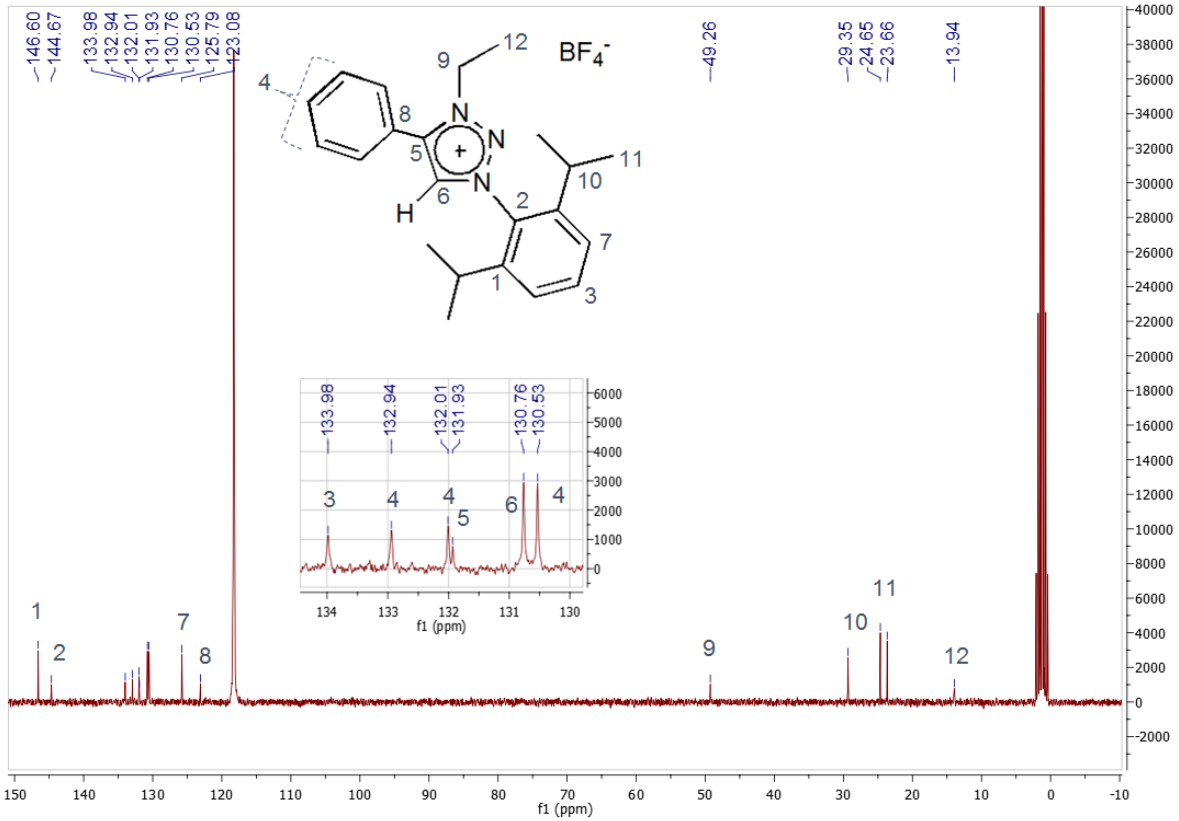

Figure 8.8. The ^{13}C NMR spectrum of the ligand precursor salt, **3** in solvent CD_3CN.

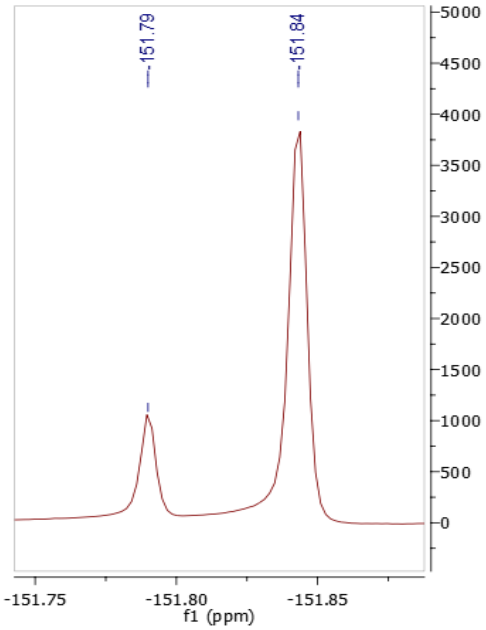

Figure 8.9. The ^{19}F NMR spectrum of the ligand precursor salt, **3** in solvent CD_3CN.

8.3.2 NMR spectra of triazolylidene rhodium(I) complexes, **4-9**.

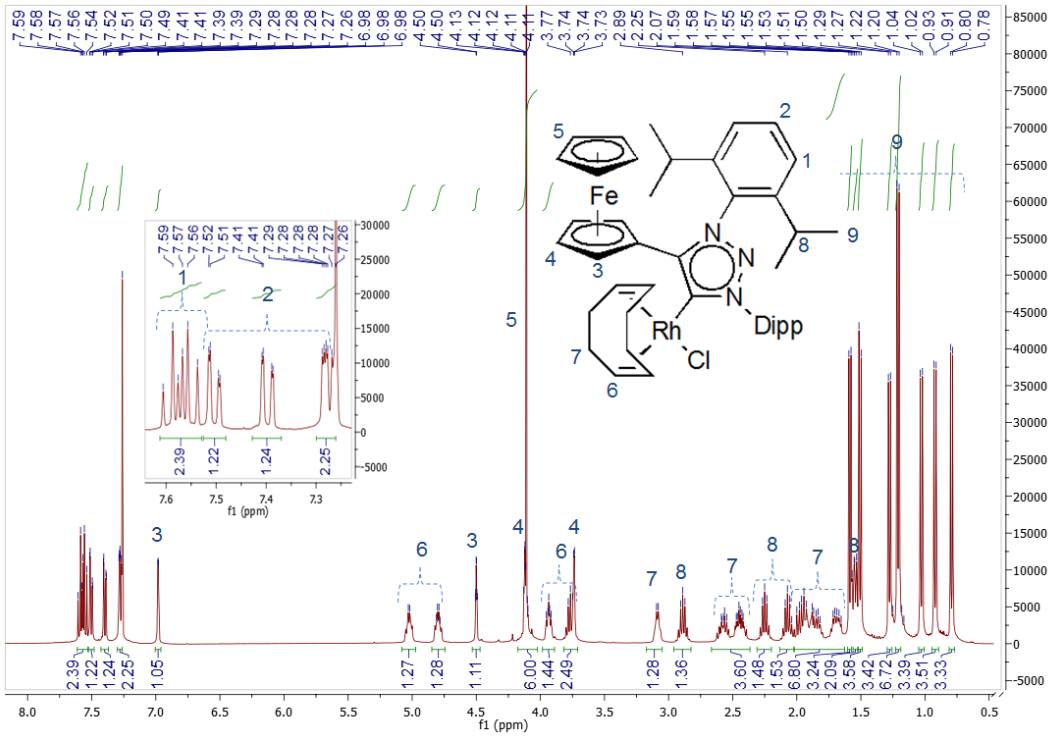

Figure 8.10. The ^{1}H NMR spectrum of the triazolylidene rhodium(I) complex, **4** in solvent $CDCl_3$.

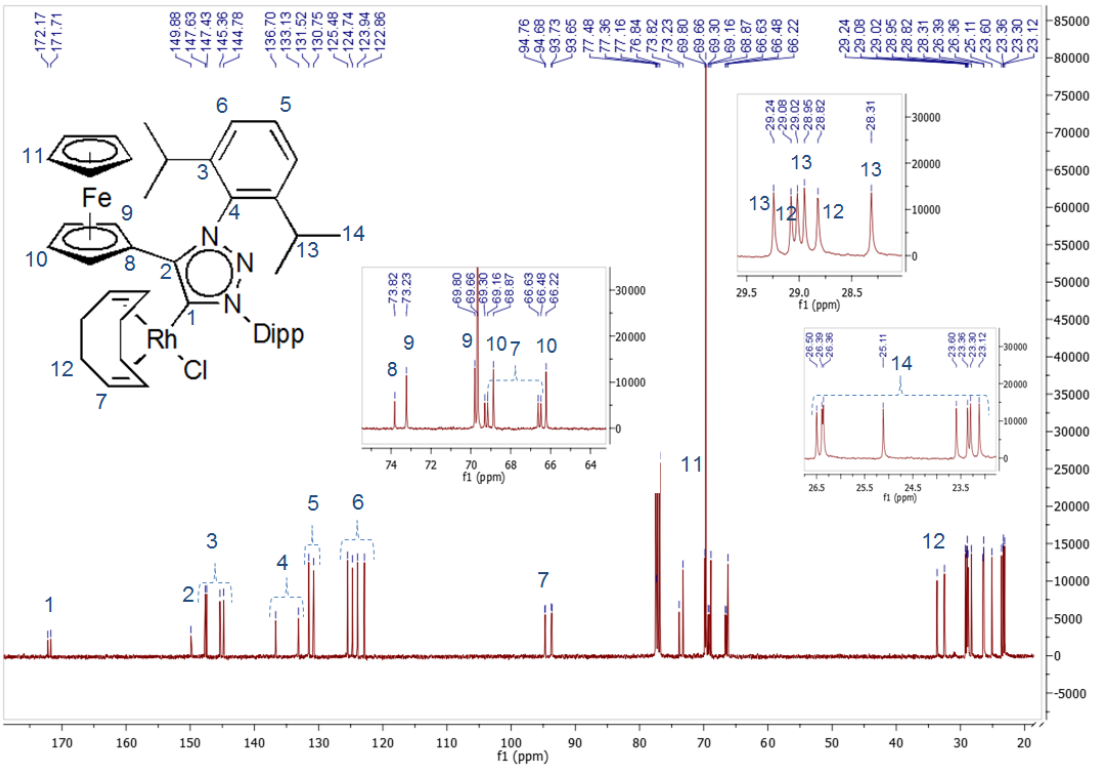

Figure 8.11. The ^{13}C NMR spectrum of the triazolylidene rhodium(I) complex, **4** in solvent $CDCl_3$.

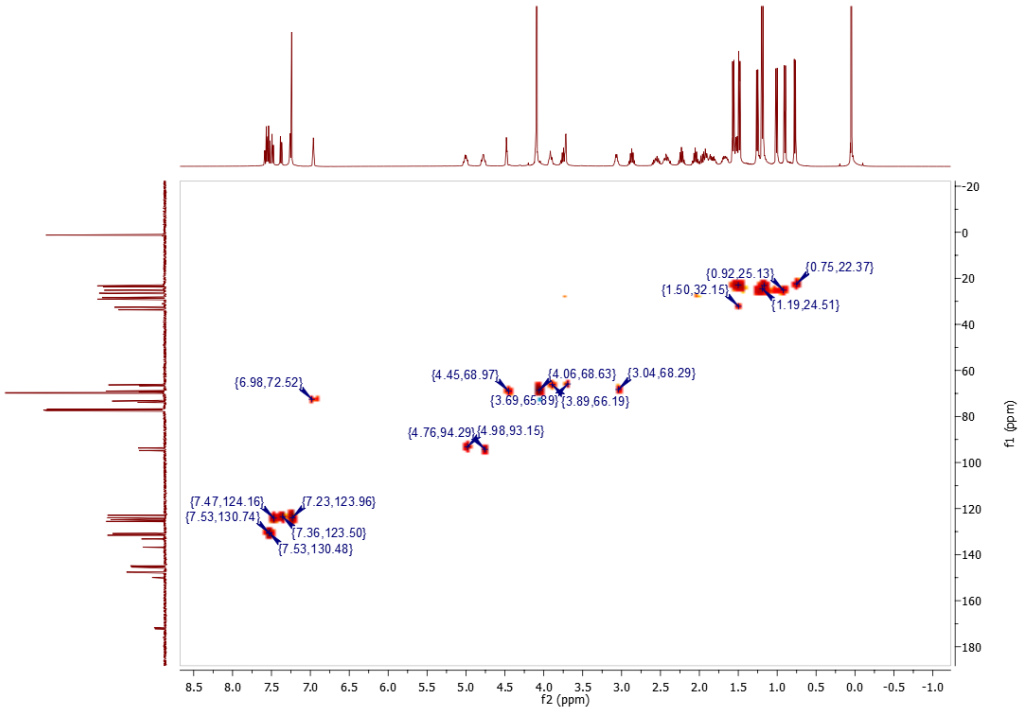

Figure 8.12. The HSQC (2D-NMR) spectrum of the triazolylidene rhodium(I) complex, **4** in solvent $CDCl_3$.

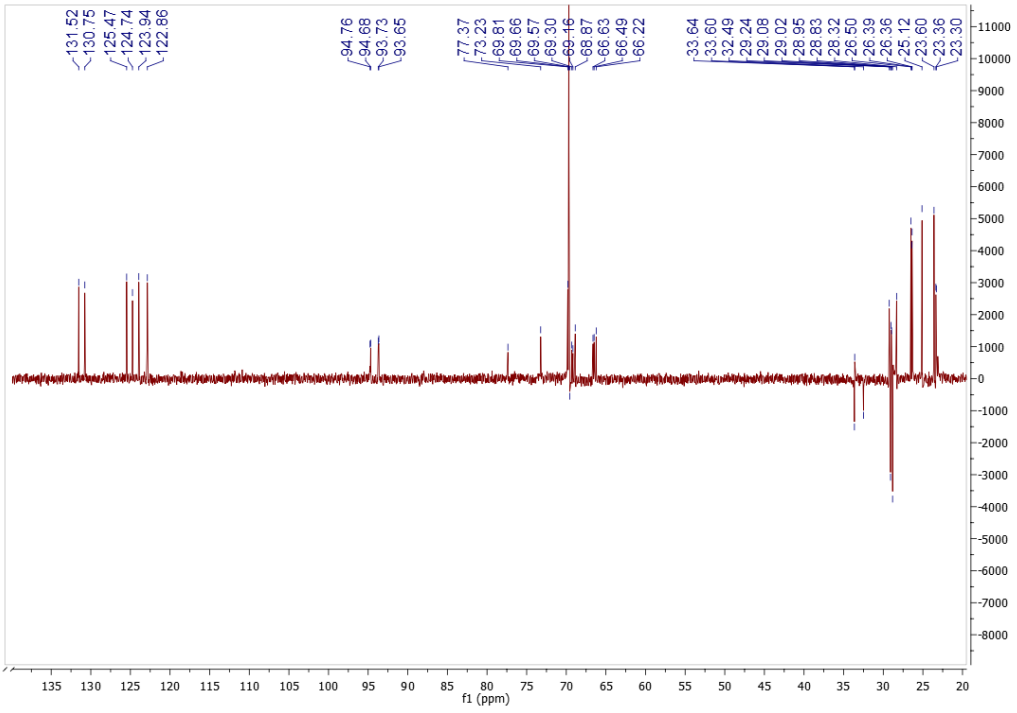

Figure 8.13. The ^{13}C DEPT135 NMR spectrum of the triazolylidene rhodium(I) complex, **4** in solvent $CDCl_3$.

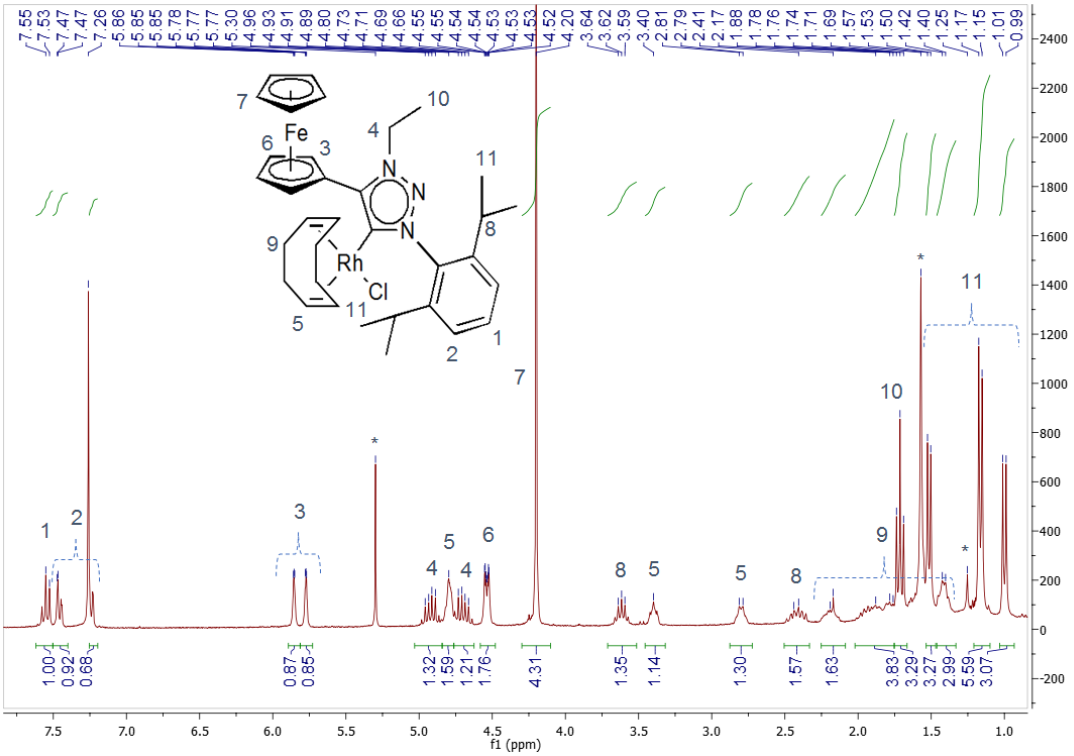

Figure 8.14. The ^{1}H NMR spectrum of the triazolylidene rhodium(I) complex, **5** in solvent $CDCl_3$

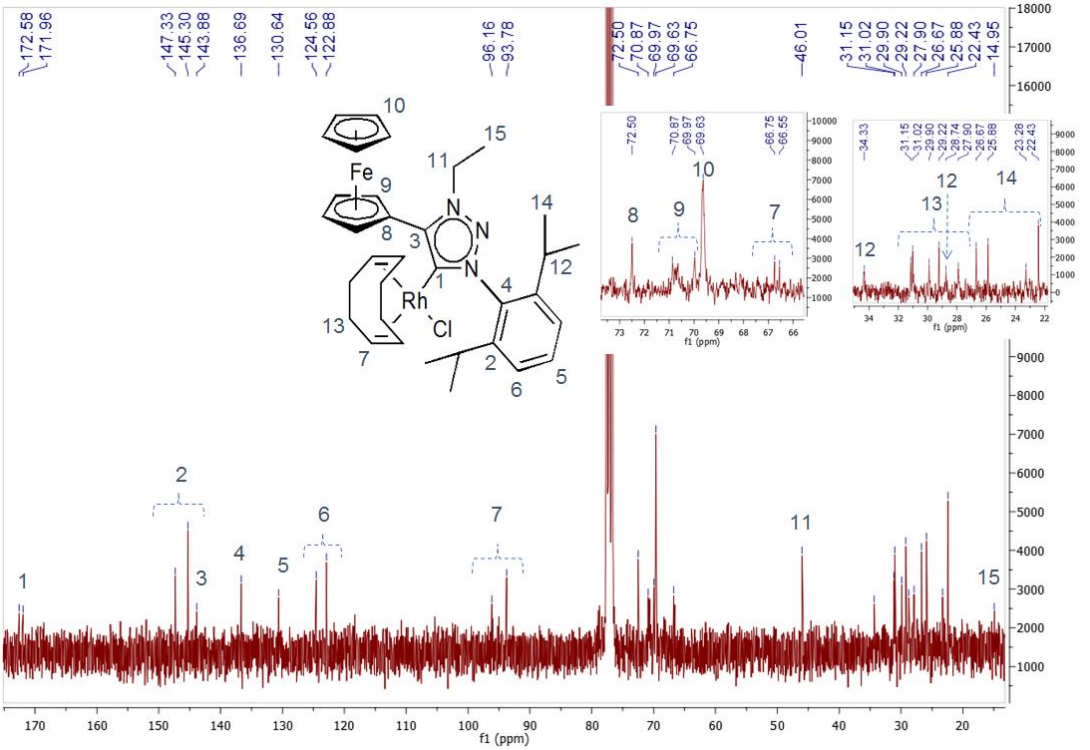

*Figure 8.15. The ^{13}C NMR spectrum of the triazolylidene rhodium(I) complex, **5** in solvent $CDCl_3$*

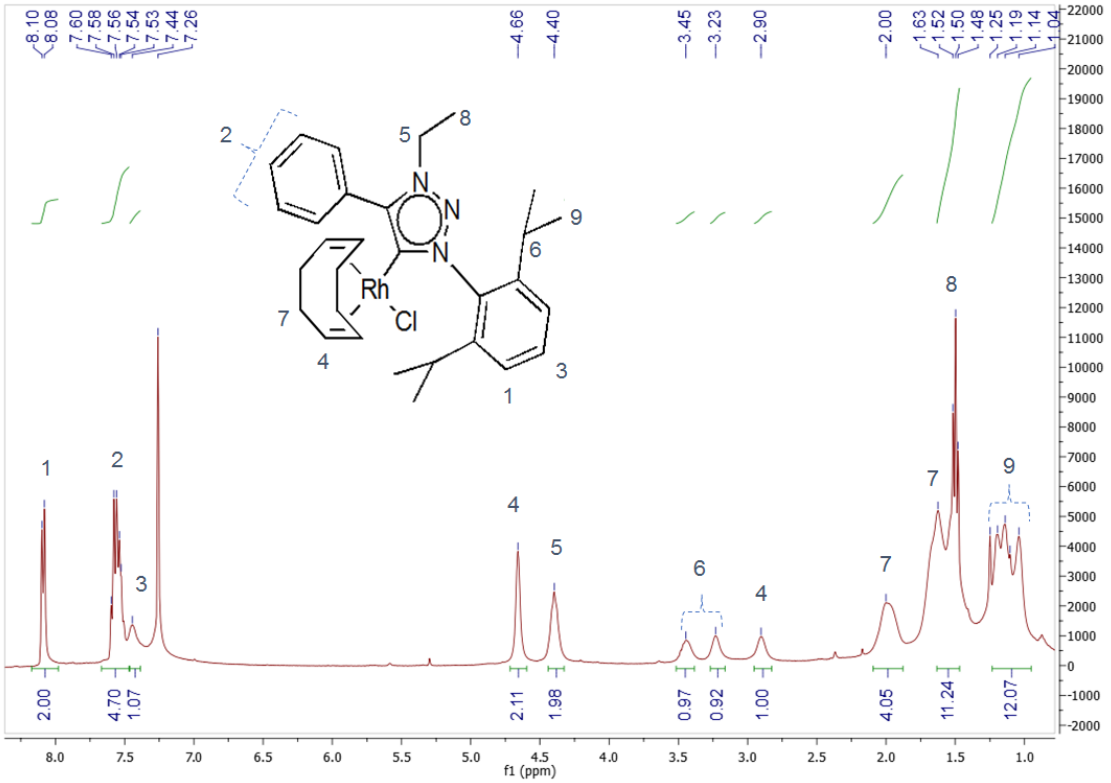

Figure 8.16. The ^{1}H NMR spectrum of the triazolylidene rhodium(I) complex, **6** in solvent $CDCl_3$

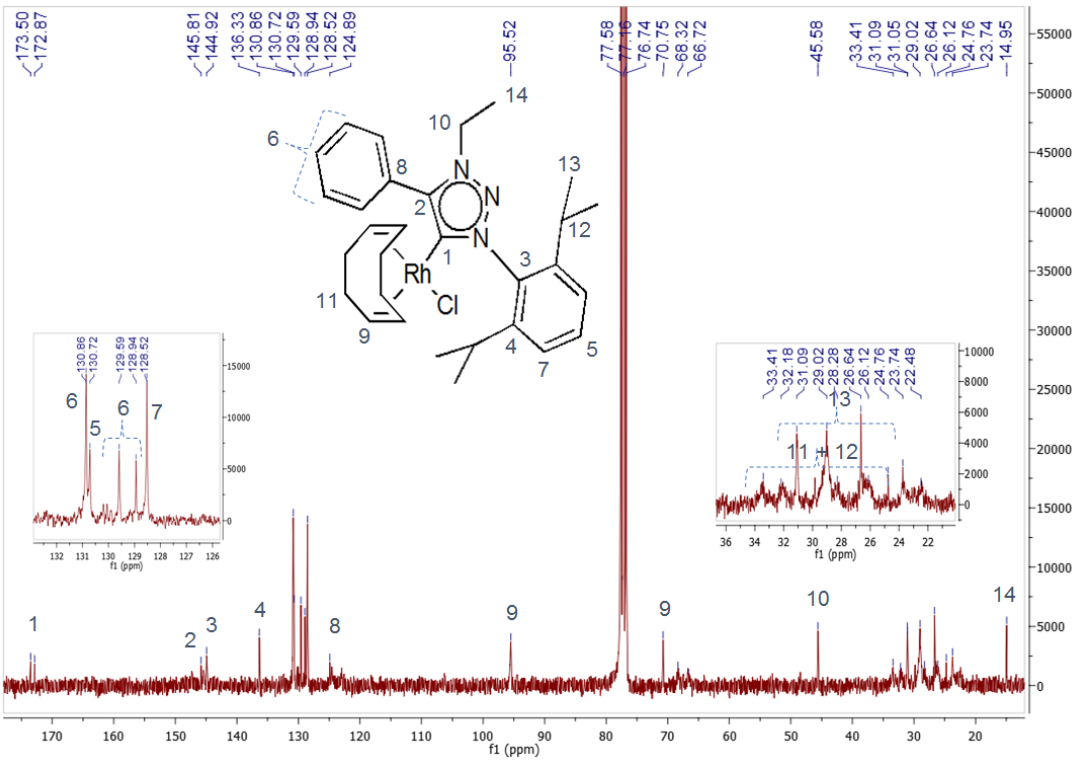

Figure 8.17. The ^{13}C NMR spectrum of the triazolylidene rhodium(I) complex, **6** in solvent $CDCl_3$

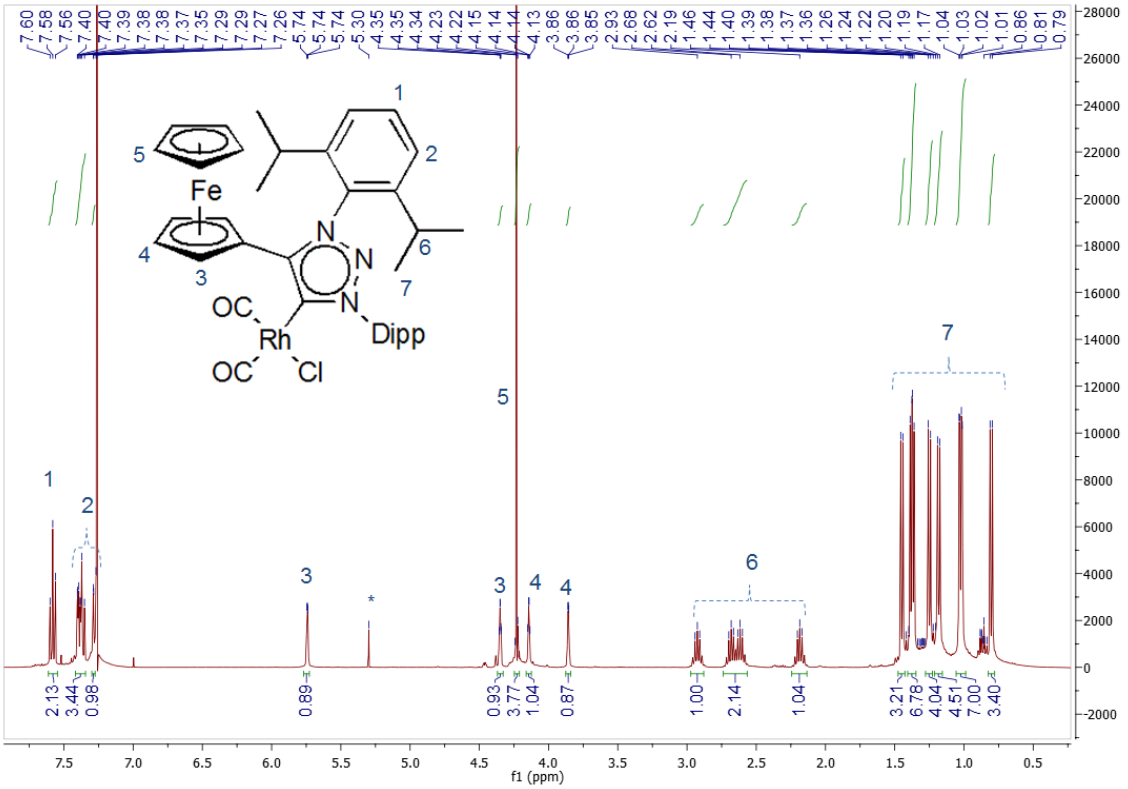

Figure 8.18. The ^{1}H NMR spectrum of the triazolylidene rhodium(I) complex, **7** in solvent $CDCl_3$

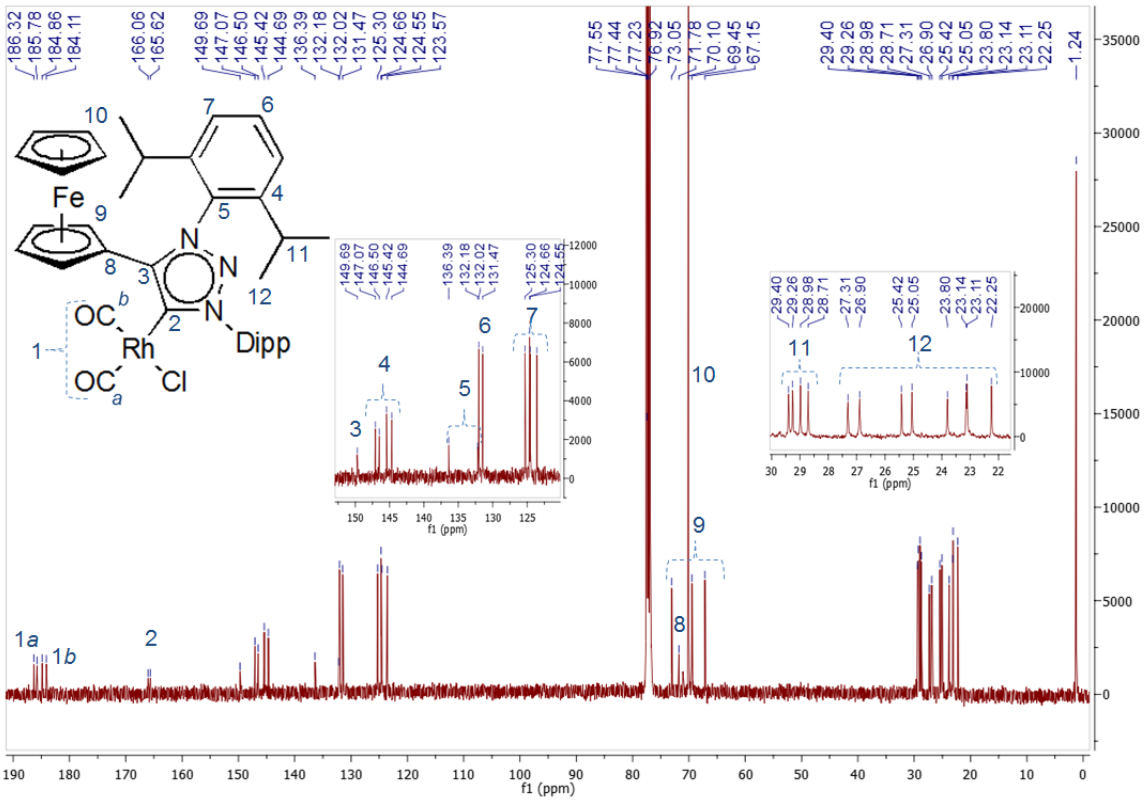

Figure 8.19. The ^{13}C NMR spectrum of the triazolylidene rhodium(I) complex, **7** in solvent $CDCl_3$

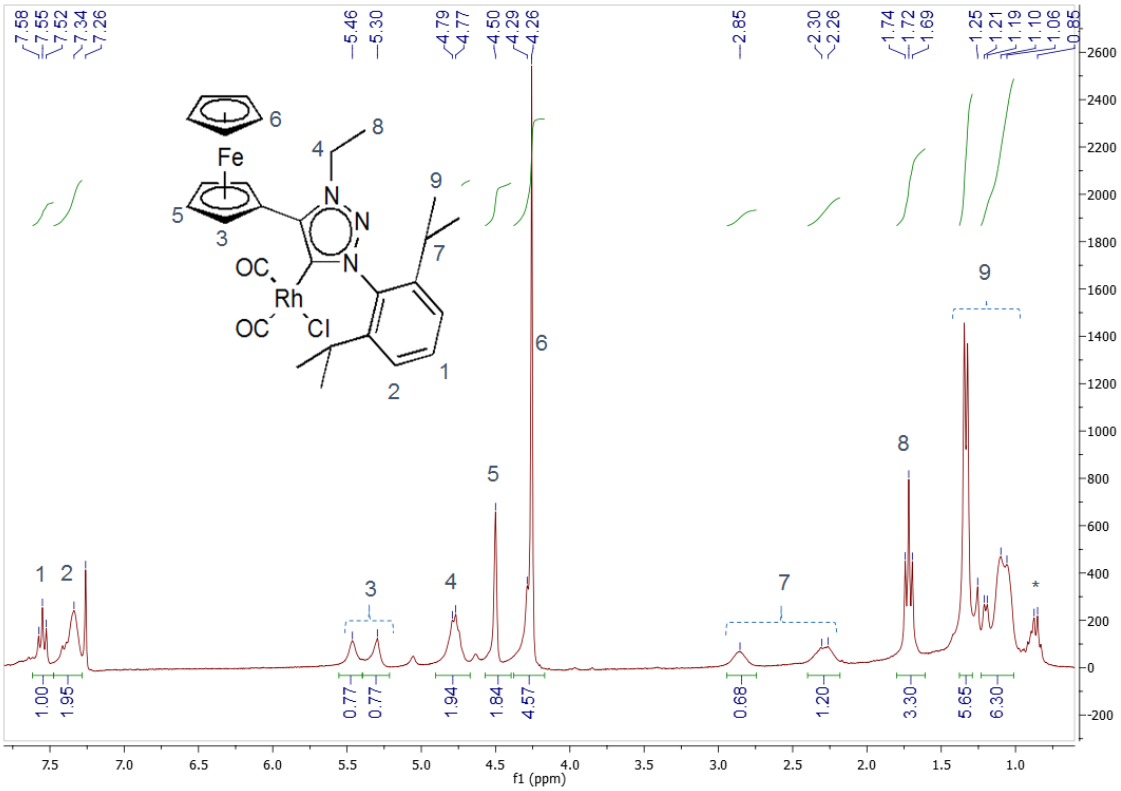

Figure 8.20. The ^{1}H NMR spectrum of the triazolylidene rhodium(I) complex, **8** in solvent $CDCl_3$

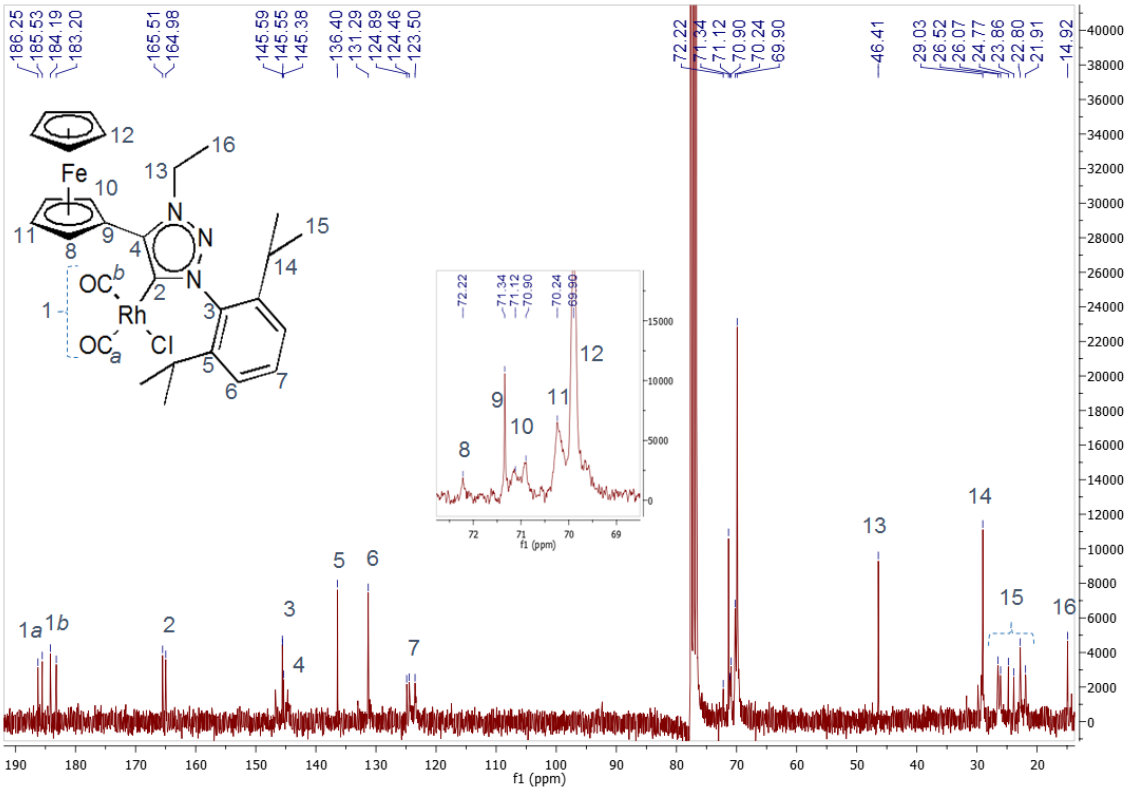

Figure 8.21. The ^{13}C NMR spectrum of the triazolylidene rhodium(I) complex, **8** in solvent $CDCl_3$

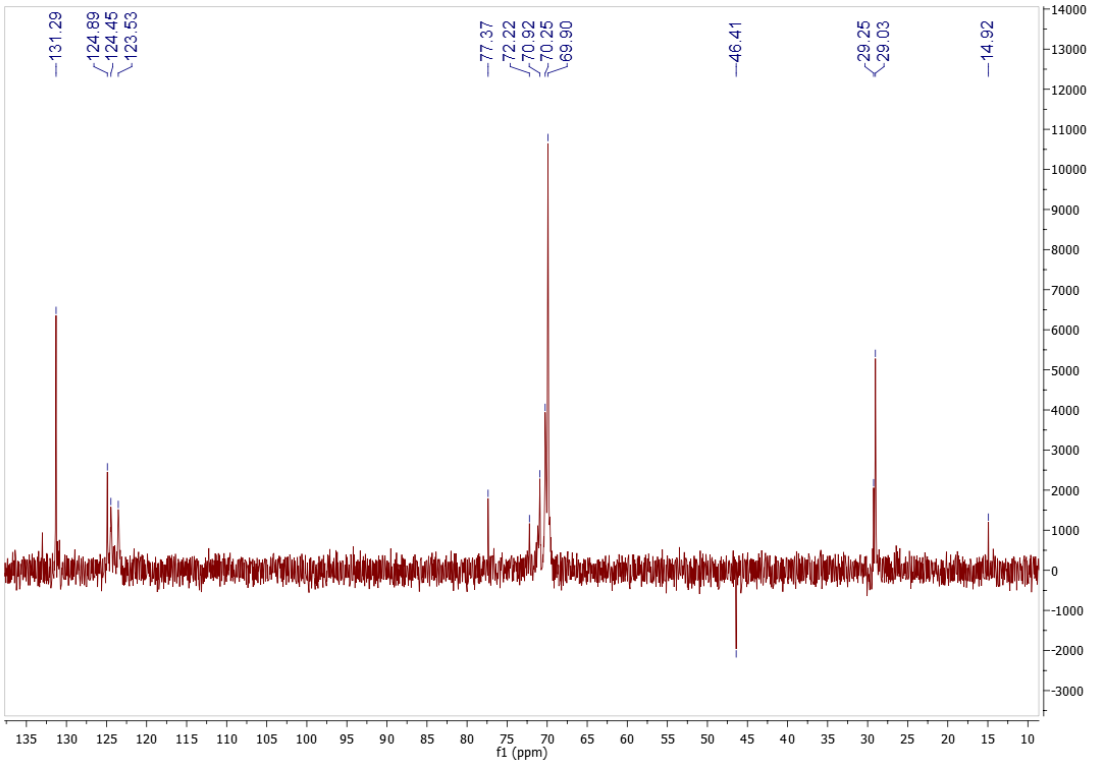

Figure 8.22. The ^{13}C DEPT135 NMR spectrum of the triazolylidene rhodium(I) complex, **8** in solvent $CDCl_3$

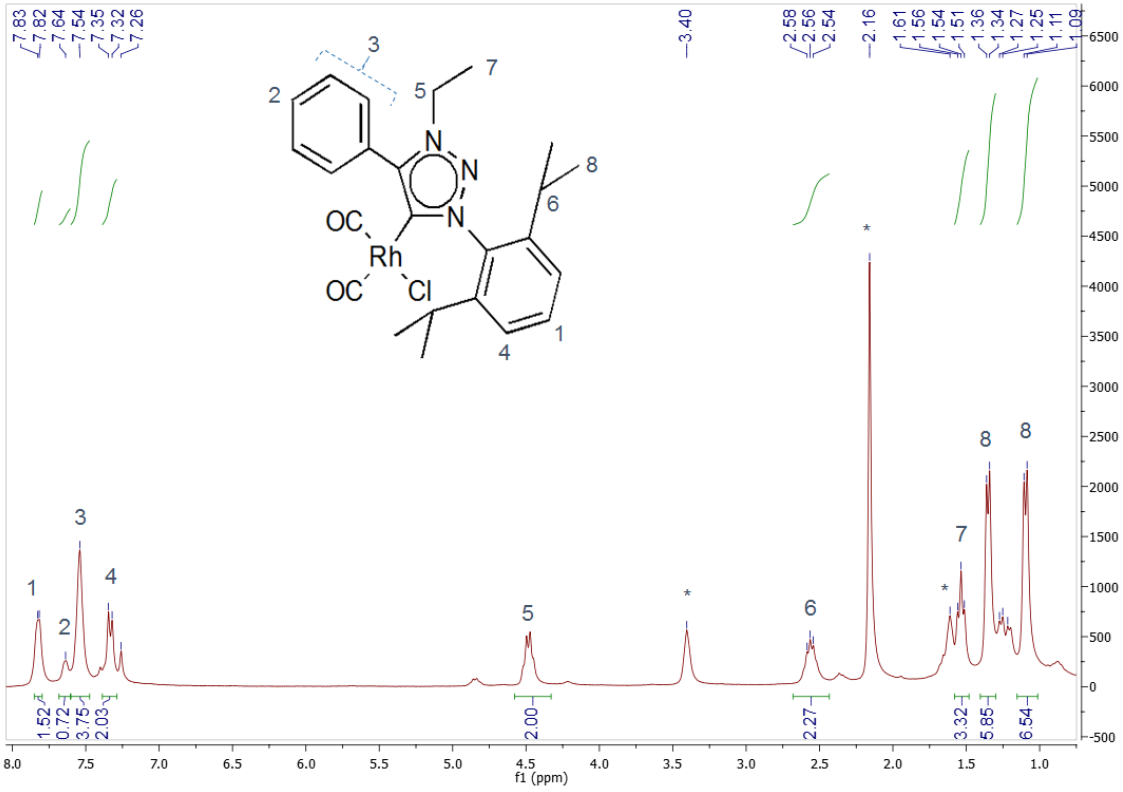

Figure 8.23. The ^{1}H NMR spectrum of the triazolylidene rhodium(I) complex, **9** in solvent $CDCl_3$

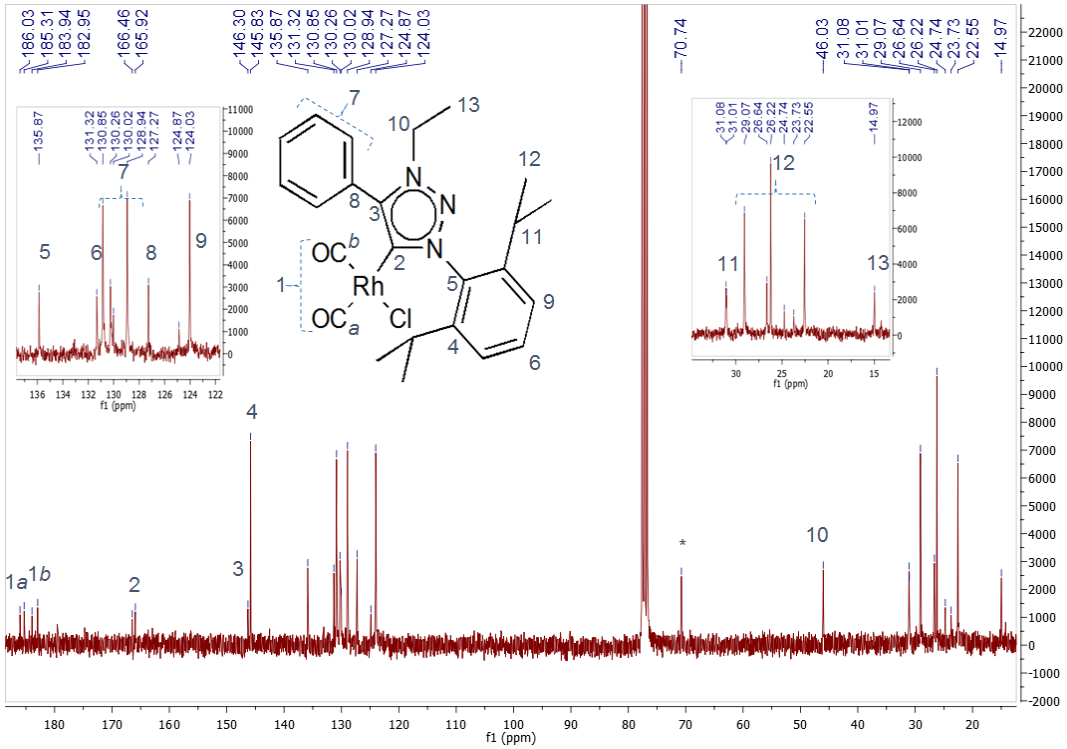

Figure 8.24. The ^{13}C NMR spectrum of the triazolylidene rhodium(I) complex, **9** in solvent $CDCl_3$.

8.3.3 The NMR spectra for the triazolylidene silver and gold(I) complexes, **10–13**.

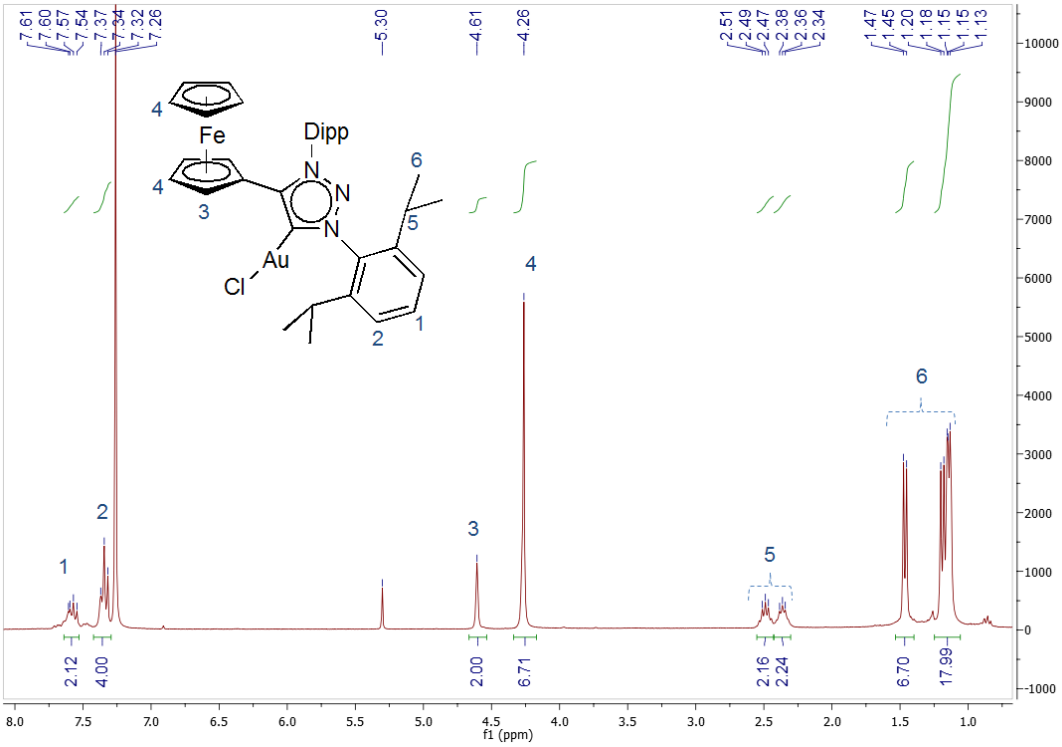

Figure 8.25. The ^{1}H NMR spectrum of the triazolylidene gold(I) complex, **10** in solvent $CDCl_3$.

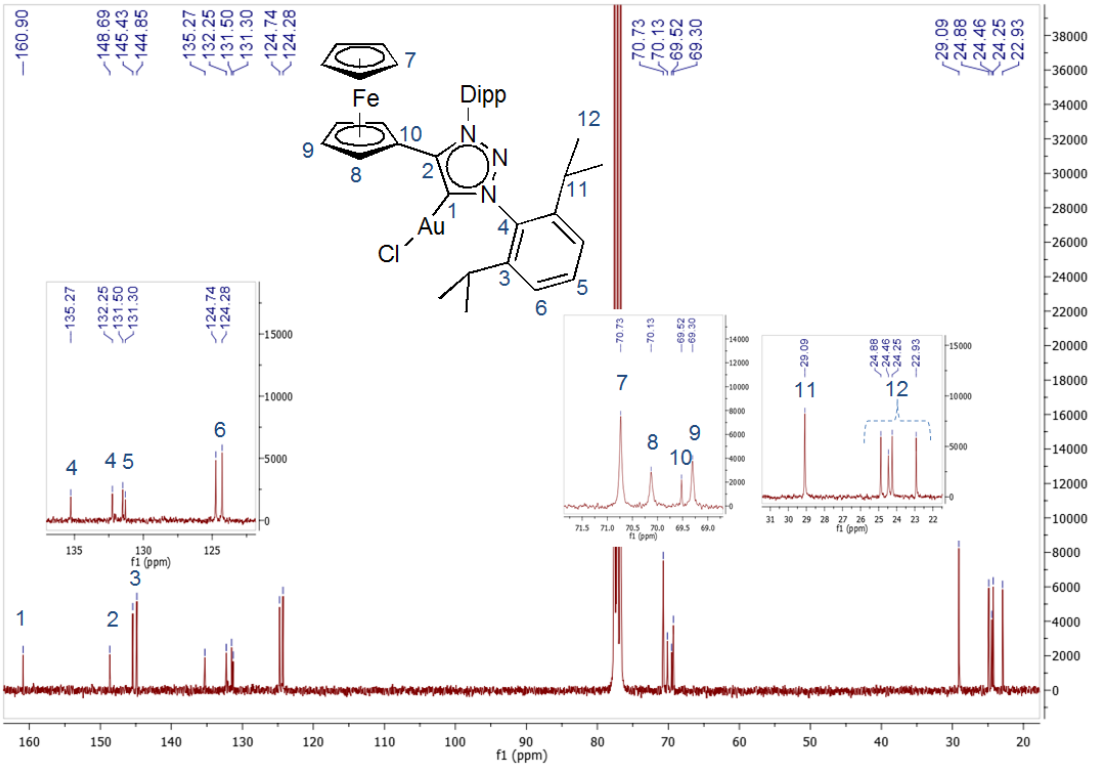

Figure 8.26. The ^{13}C NMR spectrum of the triazolylidene gold(I) complex, **10** in solvent $CDCl_3$.

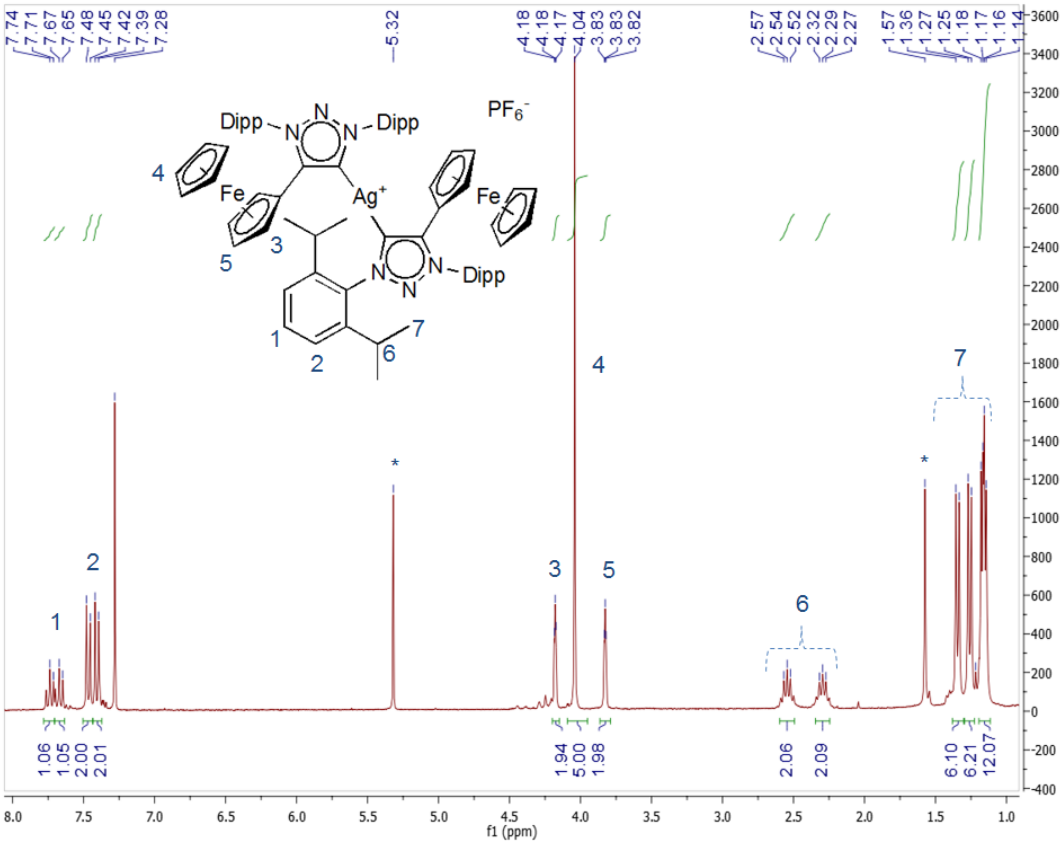

Figure 8.27. The ^{1}H NMR spectrum of the cationic bis(triazolylidene) silver(I) complex, **11** in solvent $CDCl_3$.

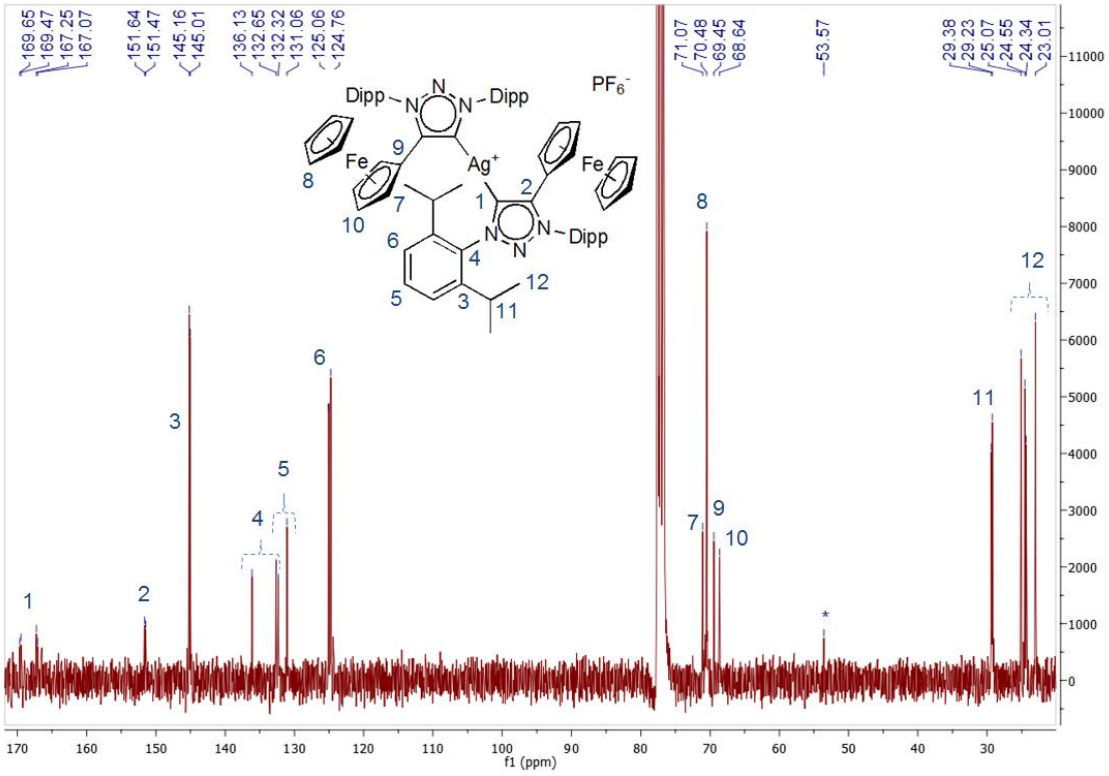

Figure 8.28. The ^{13}C NMR spectrum of the cationic bis(triazolylidene) silver(I) complex, **11** in solvent $CDCl_3$.

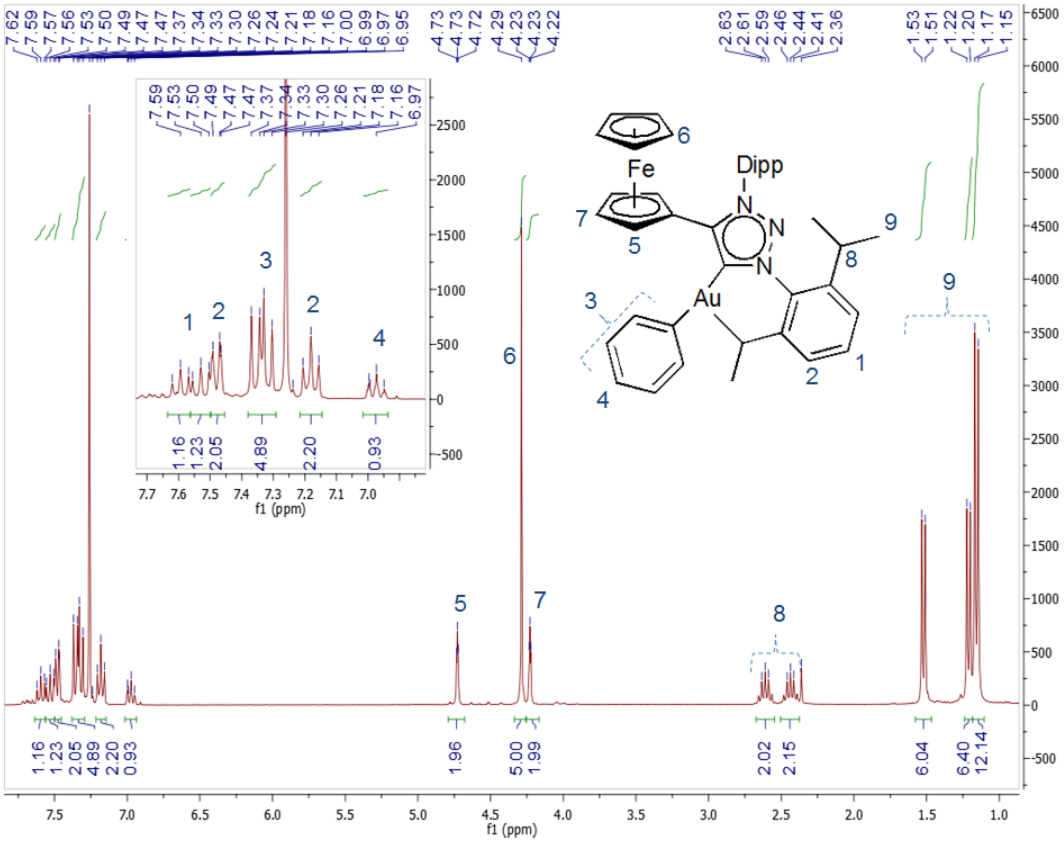

Figure 8.29. The ^{1}H NMR spectrum of the triazolylidene gold(I) complex, **12** in solvent $CDCl_3$.

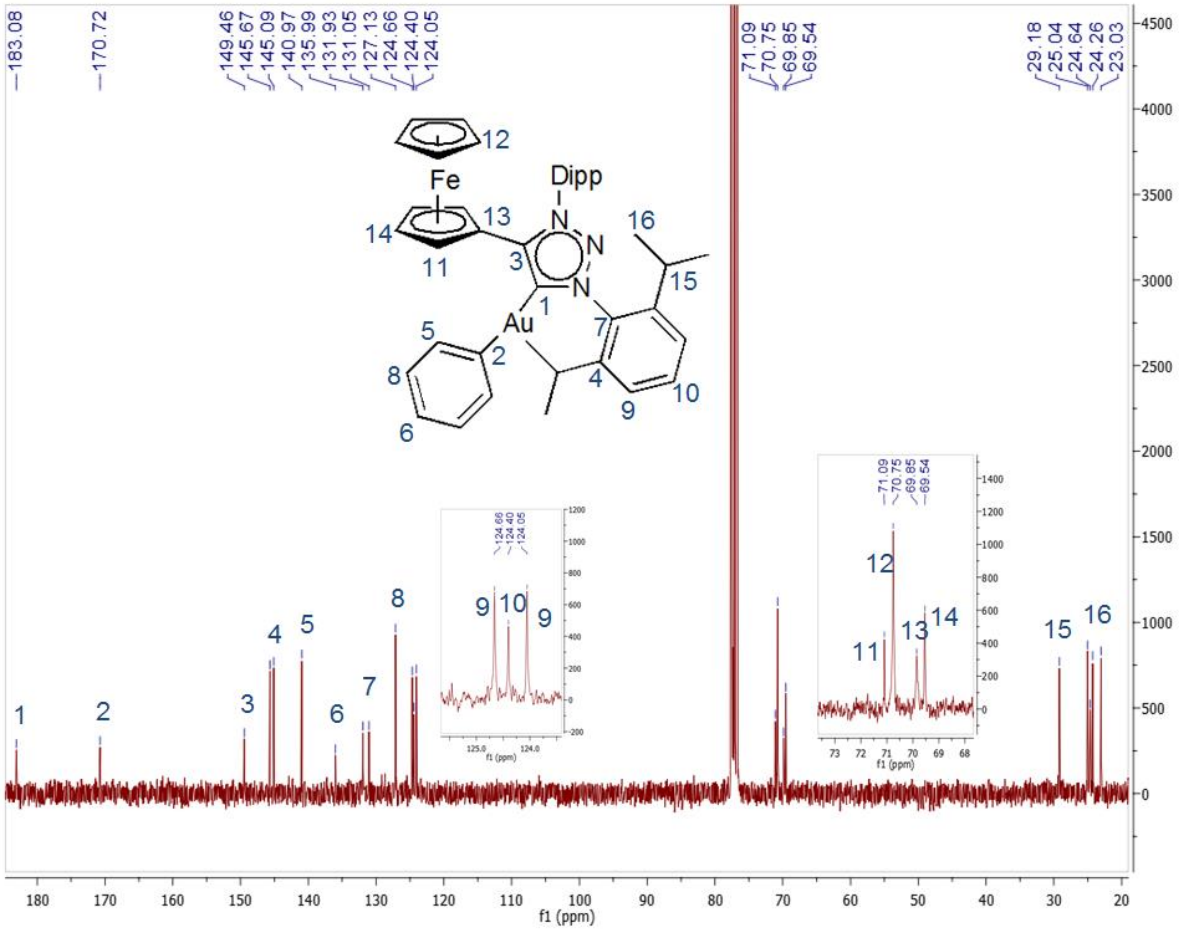

Figure 8.30. The ^{13}C NMR spectrum of the triazolylidene gold(I) complex, **12** in solvent $CDCl_3$.

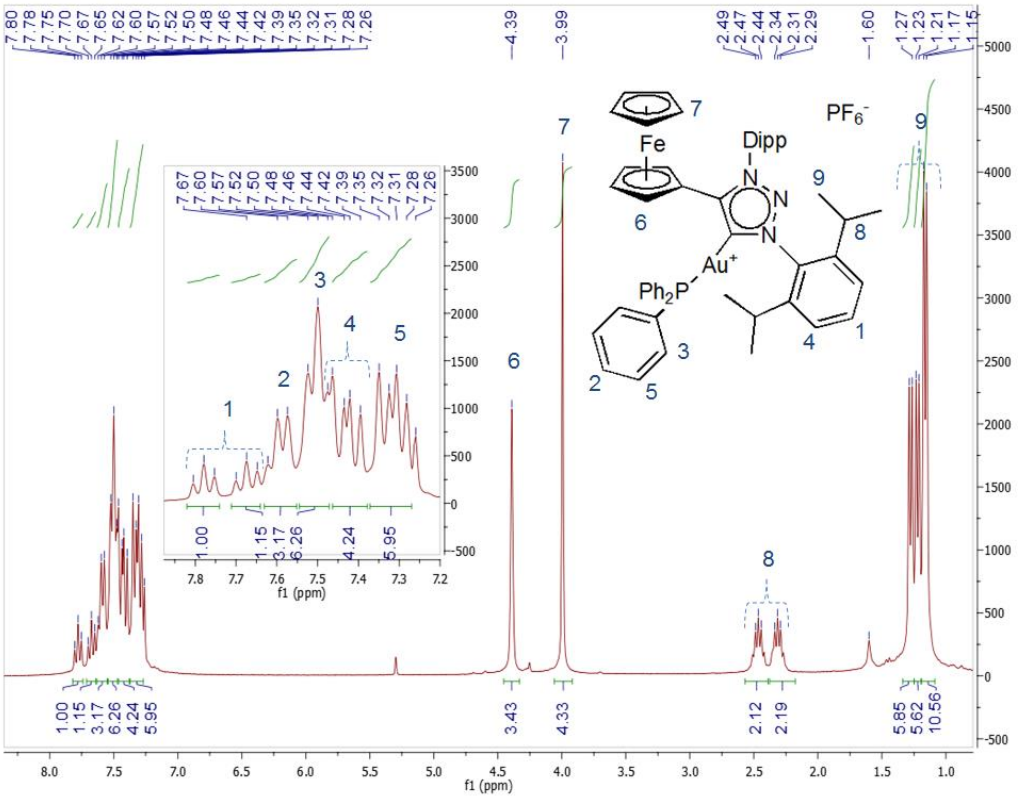

Figure 8.31. The ^{1}H NMR spectrum of the cationic triazolylidene gold(I) complex, **13** in solvent $CDCl_3$.

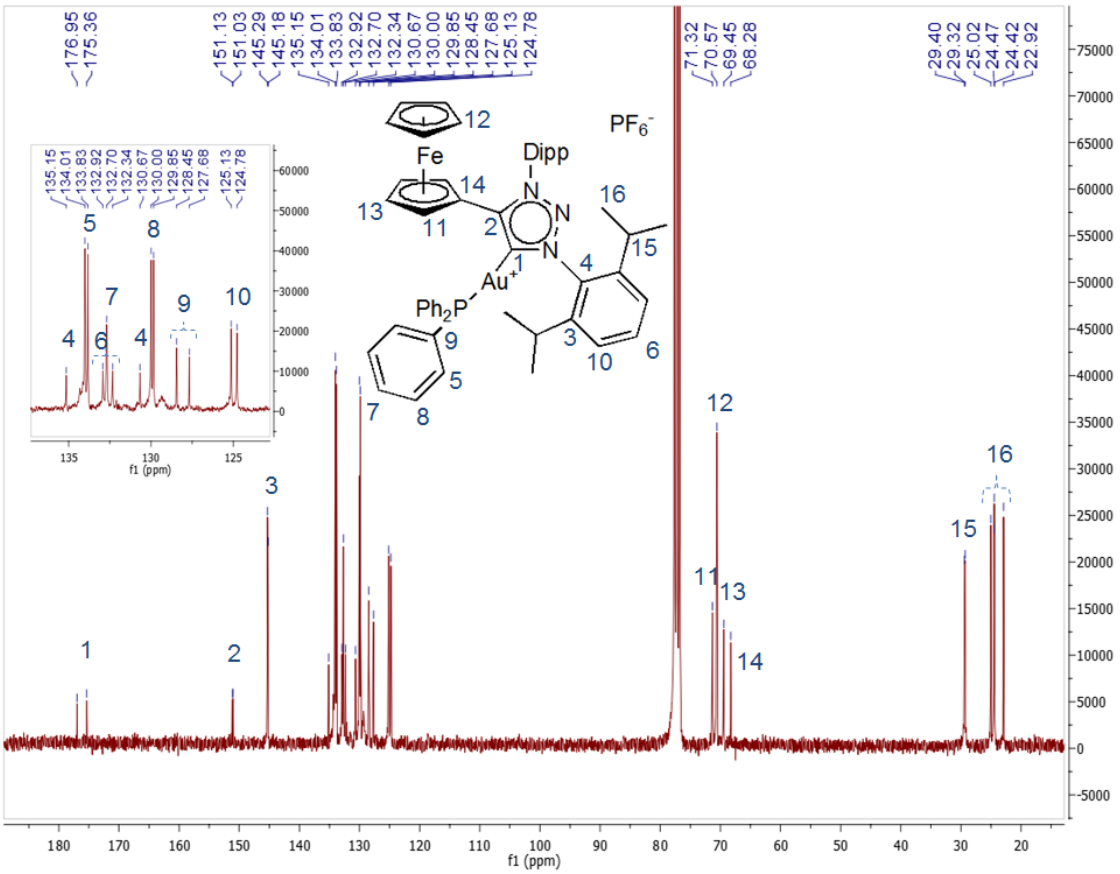

Figure 8.32. The ^{13}C NMR spectrum of the cationic triazolylidene gold(I) complex, **13** in solvent $CDCl_3$.

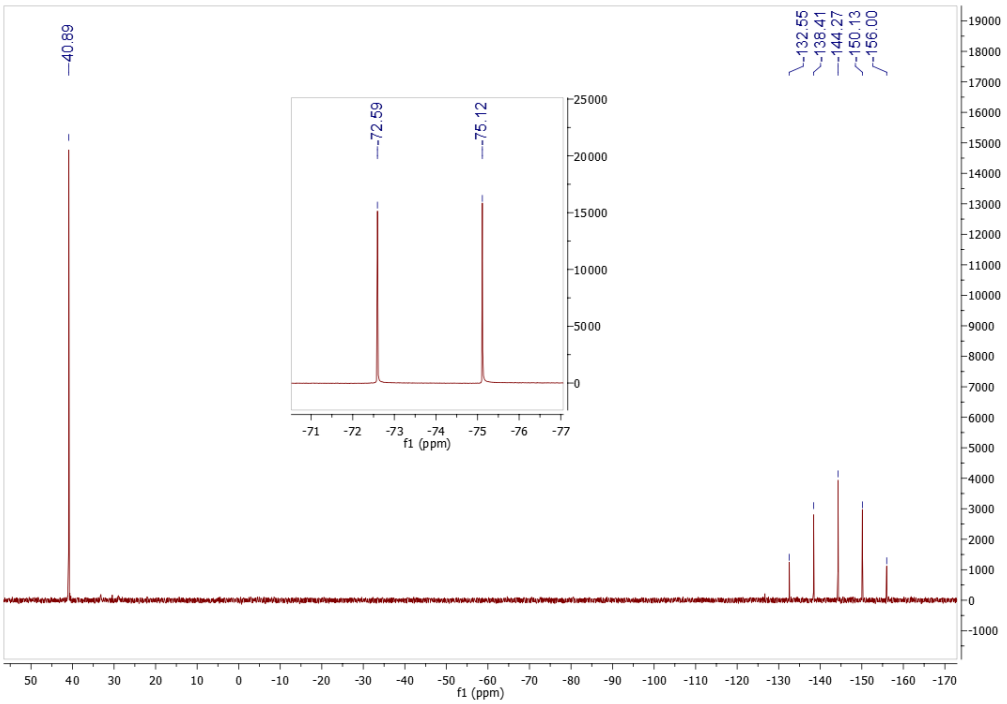

*Figure 8.33. The ^{31}P NMR and the ^{19}F NMR (inside block) spectra of cationic triazolylidene gold(I) complex, **13** in solvent $CDCl_3$.*

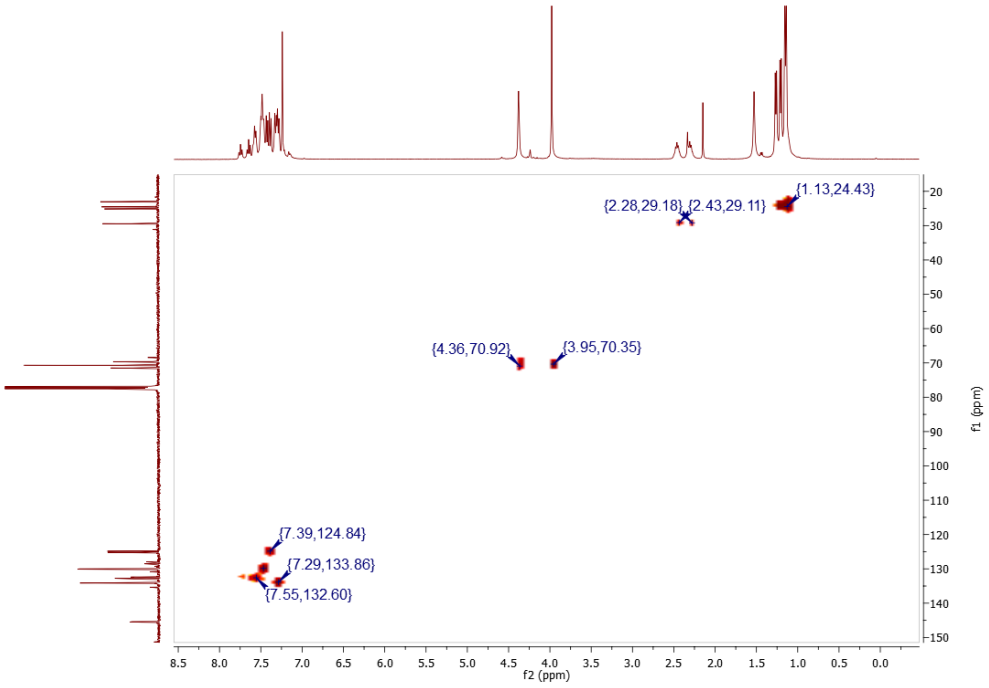

Figure 8.34. The HSQC (2D NMR) spectrum of the cationic triazolylidene gold(I) complex, **13** in solvent $CDCl_3$.

8.4 Experimental details of electrochemistry and chemical oxidation procedures.

8.4.1 Cyclic voltammetry experiments

Electrochemical studies were carried out using a three-electrode cell. The reference electrode was a non-aqueous Ag/Ag^{+} electrode, separated by the test solution by a frit with fine porosity. Glassy carbon disc (3.0 mm diameter) was the working electrode and the counter electrode was a platinum wire. Measurement were done on a Metrohm μAutolab type III potentiostat, using NOVA 2.0 electrochemistry software at scan rates of 100 $mV.s^{-1}$.

To a deoxygenated solution of 0.1 M $[N^{n}Bu_4][PF_6]$ (supporting electrolyte) in HPLC grade CH_2Cl_2, the test compound (1.0 mM) and the internal standard, $[Fe(\eta\text{-}C_5(CH_3)_5)_2]$ was added. Under these conditions, the redox couple for $[Fe(\eta\text{-}C_5H_5)_2]^{0/+1}$ is -0.54 V.

All reagents for cyclic voltammetry studies and chemical oxidation studies were commercially available except acetylferrocenium hexafluorophosphate, [17] which was synthesized according to published methods.

8.4.2 Chemical oxidation of **1**, **4** and **7**.

Synthesis of *1,3-bis(2,6-diisopropylphenyl)-4-ferrocenium-1H-1,2,3-triazolium hexaflourophosphate* (**1ox**)

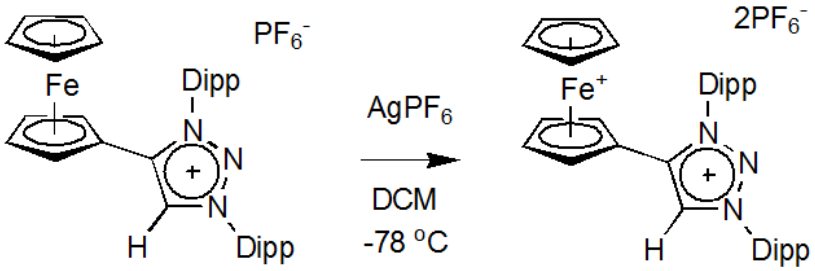

1 Dipp = 2,6-diisopropylphenyl **1ox**

Scheme 8.10. The oxidation of **1**, to yield the ferrocenium compound, **1ox**.

To a solution of **1** (0.1 g, 0.14 mmol) in deoxygenated DCM, 1.1 equivalent of $AgPF_6$ (0.04 g, 0.15 mmol) was added at -78 °C, in the absence of light. The solution underwent a colour change of orange to green, and was stirred at room

temperature for an hour. The reaction mixture was filtered and the solvent evaporated, and the resultant solid stored in the glovebox. ^{19}F $\{^{1}H\}$ NMR (282 MHz, CD_2Cl_2) δ -85.07 (d, *J* = 969.09 Hz, P**F**$_6$).

Synthesis of *1,3-bis(2,6-diisopropylphenyl)-4-ferrocenium-1,2,3-triazolylidene chlorido(η^4-1,5-cyclooctadiene)rhodium(I) hexaflourophosphate* (**4ox**)

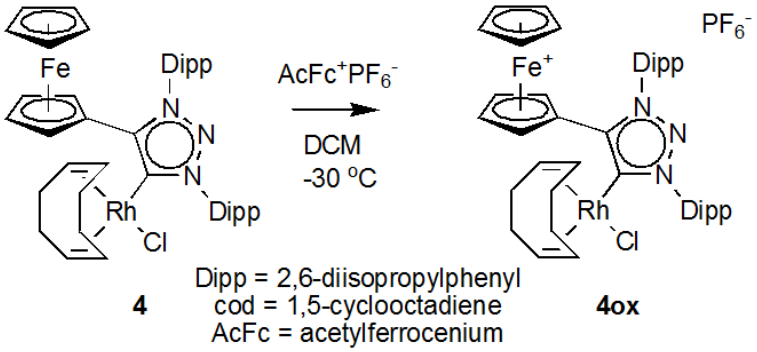

Scheme 8.11. The oxidation of **4** to **4ox** with acetylferrocenium hexafluorophosphate as oxidant.

To a cold solution (*ca*. -30 °C) of **4** (0.1 g, 0.12 mmol) in DCM, acetyl ferrocenium hexafluorophosphate (0.05 g, 0.13 mmol) was added and stirred for 30 minutes. After this time, the solvent was evaporated and the residue was washed with ether. The product was extracted with DCM affording **4ox** as light brown powder.

Synthesis of *1,3-bis(2,6-diisopropylphenyl)-4-ferrocenium-1,2,3-triazolylidene chlorido(dicarbonyl) rhodium(I) hexafluorophosphate* (**7ox**)

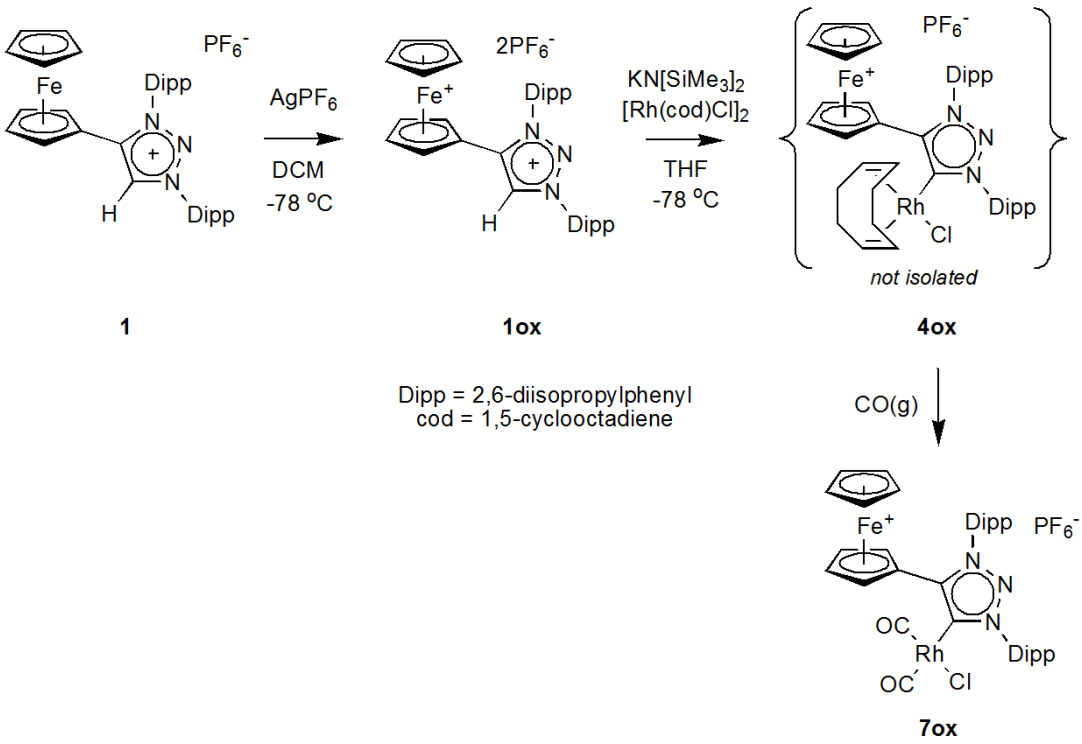

*Scheme 8.12. The synthesis of **7ox**, from metalation on the oxidized ligand precursor salt, **1**.*

To a solution of **1** (0.1 g, 0.14 mmol) in deoxygenated DCM, $AgPF_6$ (0.04 g, 0.15 mmol) was added at -78 °C and stirred for 10 minutes. The solution was filtered and added (as solution) to a solution of $[RhcodCl]_2$ (0.03 g, 0.07 mmol) and $KN[SiMe_3]_2$ (0.03 g, 0.15 mmol) in THF at -78 °C, and stirred for one hour. Carbon monoxide gas then was bubbled through the solution for 5 minutes. The solution (green-brown) was taken speedily for infrared spectroscopy to obtain the carbonyl vibration frequencies of **7ox**. IR (ν(CO), CH_2Cl_2, 2082 cm^{-1}, 2009 cm^{-1})

8.5 General procedure followed for the reactivity testing for the hydroformylation of 1-octene of complexes **4**–**6**, **N**, **O**.

All hydroformylation reactions were conducted in triplicate in a 90 mL stainless steel pipe reactor, to which the catalyst precursor (**4**–**6**, **N**, **O**) (5.74 x 10^{-3} mmol), substrate 1-octene (0.805 g, 7.175 mmol) and *n*-decane (0.204 g, 1.435 mmol) as internal standard were added and dissolved in solvent toluene (5 mL). The airtight reactor was purged with nitrogen gas (three times) then purged with

syngas (1:1, CO/H_2) (twice), after which it was pressurized with syngas to the desired pressure and heated to the required temperature. When reaction time was reached, the reactor was depressurized and cooled to room temperature. The samples were analysed by gas chromatography and the products were confirmed against authentic iso-octene and aldehyde standards. Optimization of reaction conditions was done for catalyst precursor **4**, by varying of the syngas pressure (30–50 bar), temperatures (55–75 °C) and reaction times (4–8 hrs). The reactivity of the oxidized compound, **4ox** was evaluated by the addition of an oxidant, acetyl ferrocenium hexafluorophosphate as an additive to **4.**

8.6 General procedure for the catalytic synthesis of oxazolines.[18]

In a round bottom flask, connected to a condenser, benzaldehyde (0.15 mL, 1.5 mmol), methylisocyanoacetate (0.13 mL, 1.4 mmol), complex **10** (11.3 mg, 14 µmol) and 1,4-*tert*-butylbenzene (0.71 mg, 0.38 mmol) were dissolved in 4 mL DCM, and heated to 40 °C. In some experiments, the additives, triethylamine (0.023 mL, 0.17 mmol) and $AgPF_6$ (4.04 mg, 16 µmol) were added at room temperature, and then heated to 40 °C. Samples were taken at indicated times, by removing 0.1 mL of the reaction mixture via syringe, followed by dilution with $CDCl_3$ (0.4 mL) for analysis by ^{1}H-NMR spectroscopy.

8.7 Crystallographic details of compounds, **1**–**5**, **7**, **10**–**13** and **1ox**.

8.7.1 The crystal structure data of precursor salts, **1**–**3**.

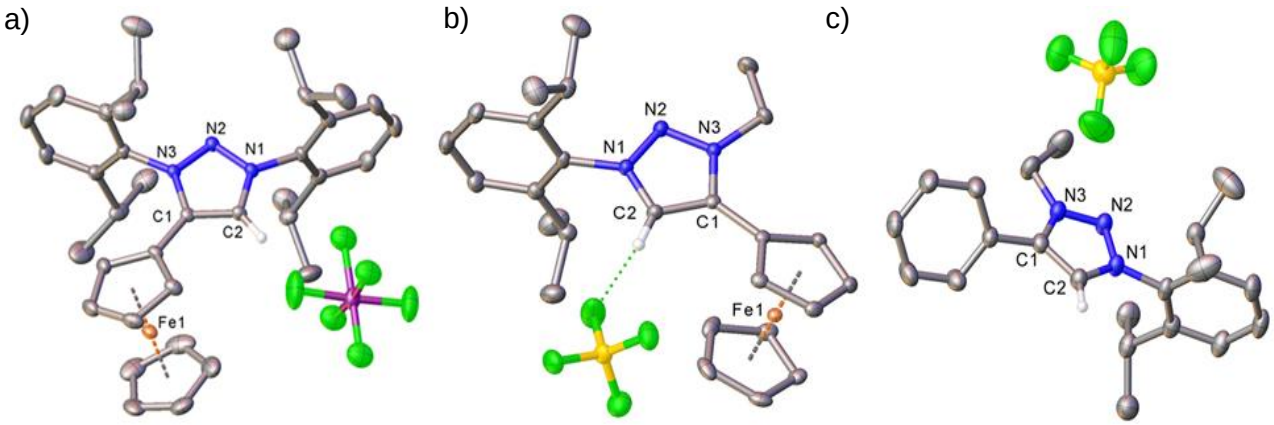

Figure 8.35. Molecular structures of triazolium precursor salts, (a) **1**, (b) **2** and (c) **3**, showing 50% probability ellipsoids and partial atom-numbering scheme.

Crystal data of **1**:

$C_{37.5}H_{47}Cl_3F_6FeN_3P$ (M = 846.95 g/mol): monoclinic, space group C2/c, a = 22.8718(17) Å, b = 14.9273(10) Å, c = 24.0533(19) Å, α = 90°, β = 102.541(4) °, γ = 90°, V = 8016.2(10) Å^3, Z = 8, T = 150 K, D_{calc} = 1.404 g/cm^3, μ(MoKα) = 0.675 mm^{-1}, 137039 reflections measured (4.456° ≤ 2Θ ≤ 54.324°), 8877 unique [R_{int} = 0.0681, R_{sigma} = 0.0240] which were used in all calculations. The final R_1 was 0.0638 (I > 2σ(I)) and wR_2 was 0.1240 (all data).

Crystal data of **2**:

$C_{26}H_{32}BF_4FeN_3$ (M = 529.20 g/mol): monoclinic, space group C2/c, a = 29.3111(19) Å, b = 9.0993(6) Å, c = 18.6543(12) Å, α = 90°, β = 90.198(3) °, γ = 90°, V = 4975.3(6) Å^3, Z = 8, T = 150 K, D_{calc} = 1.413 g/cm^3, μ(MoKα) = 0.656 mm^{-1}, 86054 reflections measured (4.368° ≤ 2Θ ≤ 52.91°), 5134 unique [R_{int} = 0.0323, R_{sigma} = 0.0133] which were used in all calculations. The final R_1 was 0.0293 (I > 2σ(I)) and wR_2 was 0.0705 (all data).

Crystal data of **3**:

$C_{22}H_{28}BF_4N_3$ (M = 421.28 g/mol): monoclinic, space group $CP2_1/c$, a = 8.2036(7) Å, b = 12.5525(11) Å, c = 21.5301(17) Å, α = 90°, β = 92.659(4) °, γ = 90°, V = 2214.7(3) Å^3, Z = 4, T = 150 K, D_{calc} = 1.263 g/cm^3, μ(CuKα) = 0.822 mm^{-1}, 75653 reflections measured (4.368° ≤ 2Θ ≤ 52.91°), 4529 unique [R_{int} = 0.0596, R_{sigma} = 0.0255] which were used in all calculations. The final R_1 was 0.0607 (I > 2σ(I)) and wR_2 was 0.1544 (all data).

8.7.2 The crystal structure data of the triazolylidene rhodium(I) complexes, **4**, **5** and **7**.

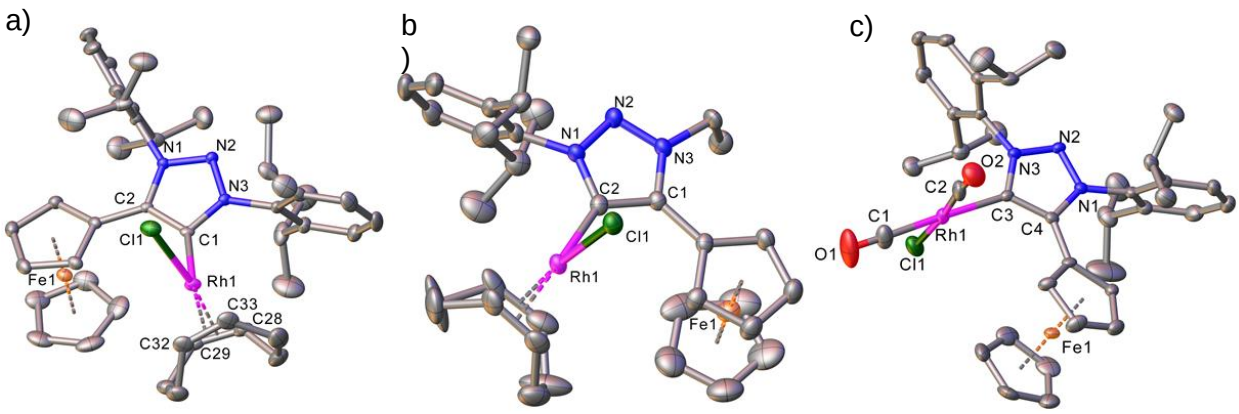

Figure 8.36. Molecular structures of triazolylidene rhodium(I) complexes (a) **4**, (b) **5** and (c) **7**, showing 50% probability ellipsoids and partial atom-numbering scheme.

Crystal data of **4**:

$C_{44}H_{54}ClFeN_3Rh$ (M = 819.11 g/mol): monoclinic, space group P121/n 1, a = 12.1296(6) Å, b = 18.2052(10) Å, c = 17.6479(10) Å, α = 90°, β = 93.435(2) °, γ = 90°, V = 3890.0(4) Å^3, Z = 4, T = 150 K, D_{calc} = 1.400 g/cm^3, μ(MoKα) = 0.900 mm^{-1}, 199624 reflections measured (2.24° ≤ 2Θ ≤ 30.60°), 11951 unique [R_{int} = 0.0991, R_{sigma} = 0.0486] which were used in all calculations. The final R_1 was 0.0767 (I > 2σ(I)) and wR_2 was 0.0816 (all data).

Crystal data of **5**:

$C_{35}H_{44}Cl_4FeN_3Rh$ (M = 808.30 g/mol): monoclinic, space group C2/c, a = 23.530(8) Å, b = 12.3540(16) Å, c = 15.6199(19) Å, α = 100.010(4)°, β = 105.064(4) °, γ = 115.626(4)°, V = 7069.0(4) Å^3, Z = 8, T = 150 K, D_{calc} = 1.519 g/cm^3, μ(MoKα) = 1.209 mm^{-1}, 104552 reflections measured (4.642° ≤ 2Θ ≤

53.092°), 7307 unique [R_{int} = 0.0596, R_{sigma} = 0.0254] which were used in all calculations. The final R_1 was 0.0479 (I > 2σ(I)) and wR_2 was 0.1073 (all data).

Crystal data of **7**:

$C_{38}H_{43}ClFeN_3O_2Rh$ (M = 767.96 g/mol): triclinic, space group P-1, a = 11.3010(15) Å, b = 15.700(5) Å, c = 20.188(7) Å, α = 100.010(4)°, β = 105.064(94) °, γ = 115.626(4)°, V = 1793.1(4) Å^3, Z = 2, T = 150 K, D_{calc} = 1.422 g/cm^3, μ(MoKα) = 0.975 mm^{-1}, 64511 reflections measured (4.794° ≤ 2Θ ≤ 56.25°), 8529 unique [R_{int} = 0.0980, R_{sigma} = 0.0560] which were used in all calculations. The final R_1 was 0.0863 (I > 2σ(I)) and wR_2 was 0.1688 (all data).

8.7.3 The crystal structure data of triazolylidene gold(I) complexes and silver complex, **10–13**.

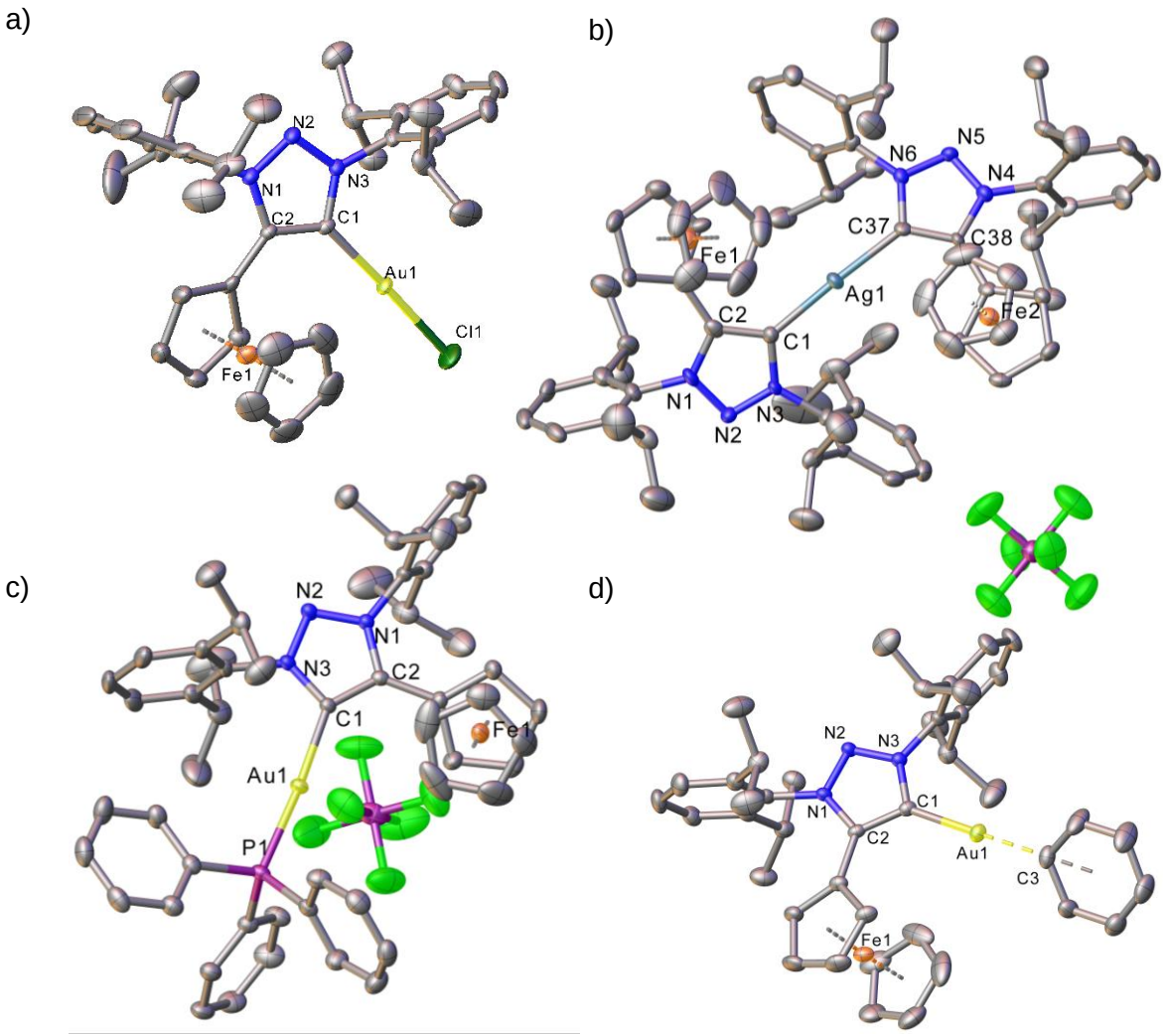

Figure 8.37. Molecular structures of triazolylidene gold(I) and silver(I) complexes (a) **10**, (b) **11**, (c) **13** and (d) **12**, showing 50% probability ellipsoids and partial atom-numbering scheme.

Crystal data of **10**:

$C_{36}H_{43}AuClFeN_3$ (M = 806.00 g/mol): triclinic, space group P-1, *a* = 12.4522(10) Å, *b* = 12.5760(9) Å, *c* = 13.8786(8) Å, *α* = 116.729(2)°, *β* = 95.812(2) °, *γ* = 106.593(2)°, *V* = 1792.1(2) Å^3, *Z* = 2, T = 150 K, D_{calc} = 1.494 g/cm^3, μ(MoKα) = 4.594 mm^{-1}, 75451 reflections measured (2.36° ≤ 2Θ ≤ 28.28°), 8886 unique [R_{int} = 0.0848, R_{sigma} = 0.003] which were used in all calculations. The final R_1 was 0.0501 (I > 2σ(I)) and wR_2 was 0.0665 (all data).

Crystal data of **11**:

$C_{73}H_{88}AgCl_2F_6Fe_2N_6P$ (M = 1484.93 g/mol): triclinic, space group P-1, *a* = 10.6327(7) Å, *b* = 15.5693(9) Å, *c* = 22.4919(14) Å, *α* = 84.938(3) °, *β* = 82.405(3) °, *γ* = 73.491(3) °, *V* = 3533.5(4) Å^3, *Z* = 2, T = 150 K, D_{calc} = 1.396 g/cm^3, μ(MoKα) = 0.839 mm^{-1}, 12534 reflections measured (2.22° ≤ 2Θ ≤ 25.81°), 12534 unique [R_{int} = 0.0559] which were used in all calculations. The final R_1 was 0.01002 (I > 2σ(I)) and wR_2 was 0.1342 (all data).

Crystal data of **12**:

$C_{42}H_{48}AuFeN_3$ (M = 847.65 g/mol): monoclinic, space group $P2_1/n$, *a* = 10.7939(19) Å, *b* = 22.047(4) Å, *c* = 15.733(3) Å, *α* = 90 °, *β* = 90.785(7) °, *γ* = 90 °, *V* = 3743.8(12) Å^3, *Z* = 4, T = 150 K, D_{calc} = 1.504 g/cm^3, μ(MoKα) = 4.334 mm^{-1}, 136890 reflections measured (4.548° ≤ 2Θ ≤ 54.496°), 8341 unique [R_{int} = 0.0490, R_{sigma} = 0.0183] which were used in all calculations. The final R_1 was 0.0254 (I > 2σ(I)) and wR_2 was 0.0503 (all data).

Crystal data of **13**:

$C55H59AuCl_3F_6FeN_3P_2$ (M = 1298.16 g/mol): monoclinic, space group $P2_1/c$, *a* = 17.8411(8) Å, *b* = 11.8539(6) Å, *c* = 26.3035(13) Å, *α* = 90 °, *β* = 97.359(2) °, *γ* = 90 °, *V* = 5517.0(5) Å^3, *Z* = 4, T = 150 K, D_{calc} = 1.563 g/cm^3, μ(MoKα) = 3.182 mm^{-1}, 221967 reflections measured (4.524° ≤ 2Θ ≤ 57.852°), 14373 unique [R_{int} = 0.0522, R_{sigma} = 0.0222] which were used in all calculations. The final R_1 was 0.0338 (I > 2σ(I)) and wR_2 was 0.0523 (all data).

8.7.4 The crystal structure data of the ferrocenium triazolium salt, **1ox**.

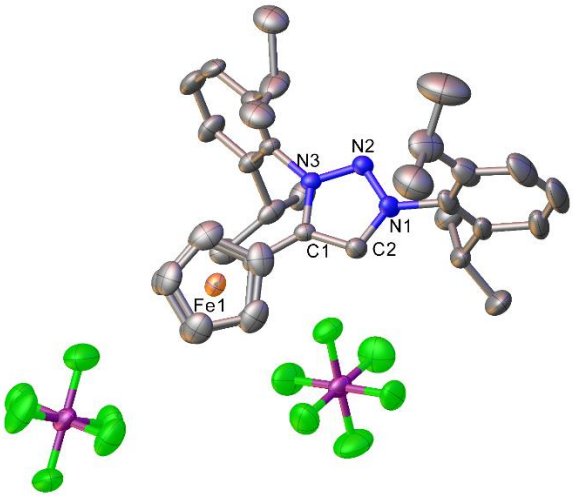

Figure 8.38. Molecular structures of the ferrocenium triazolium salt, **1ox**, showing 50% probability ellipsoids and partial atom-numbering scheme.

Crystal data of **1ox**:

$C_{36.73}H_{45.45}Cl_{1.45}FeF_{12}N_3P_2$ (M = 926.10 g/mol): triclinic, space group P-1, a = 12.3556(9) Å, b = 13.0788(10) Å, c = 16.2759(12) Å, α = 113.596(2)°, β = 90.660(2) °, γ = 115.747(2)°, V = 2115.5(3) Å^3, Z = 2, T = 150 K, D_{calc} = 1.454 g/cm^3, μ(MoKα) = 0.607 mm^{-1}, 82093 reflections measured (5.184° ≤ 2Θ ≤ 53.616°), 9054 unique [R_{int} = 0.0409, R_{sigma} = 0.0267] which were used in all calculations. The final R_1 was 0.0717 (I > 2σ(I)) and wR_2 was 0.1562 (all data).

8.8 References

1 G. Doisneau, G. Balavoine and T. Fillebeen-Khan, *J. Organomet. Chem.*, 1992, **425**, 113–117.

2 N. Nimitsiriwat, V. C. Gibson, E. L. Marshall, P. Takolpuckdee, A. K. Tomov, A. J. P. White, D. J. Williams, M. R. J. Elsegood and S. H. Dale, *Inorg. Chem.*, 2007, **46**, 9988–9997.

3 A. G. M. Barrett, M. R. Crimmin, M. S. Hill, P. B. Hitchcock, G. Kociok-Köhn and P. A. Procopiou, *Inorg. Chem.*, 2008, **47**, 7366–7376.

4 C. Mintz, M. J. Walling, *Org. Synth.*, 1969, **49**, 9.

5 G. Giordano and R. H. Crabtree, *Inorganic Syntheses: Reagents for Transition Metal Complex and Organometallic Syntheses*, J. Wiley & Sons, Hoboken :, Volume 28., 1991.

6 H. Meerwein, *Org. Synth.*, 1966, **46**, 113.

7 R. Uson, A. Laguna and M. Laguna, *Inorganic Syntheses*, John Wiley and Sons, New York, Volume 26., 1989.

8 G. A. Price, A. K. Brisdon, K. R. Flower, R. G. Pritchard and P. Quayle, *Tetrahedron Lett.*, 2014, **55**, 151–154.

9 Y. Shi, S. D. Ramgren and S. A. Blum, *Organometallics*, 2009, **28**, 1275–1277.

10 J. Bouffard, B. K. Keitz, R. Tonner, V. Lavallo, G. Guisado-Barrios, G. Frenking, R. H. Grubbs and G. Bertrand, *Organometallics*, 2011, **30**, 2617–2627.

11 L. Hettmanczyk, S. Manck, C. Hoyer, S. Hohloch and B. Sarkar, *Chem. Comm.*, 2015, **51**, 10949–10952.

12 G. Guisado-Barrios, J. Bouffard, B. Donnadieu and G. Bertrand, *Angew. Chemie. Int. Ed.*, 2010, **49**, 4759–4762.

13 K. Barral, A. D. Moorhouse and J. E. Moses, *Org. Lett.*, 2007, **9**, 1809–1811.

14 G. Guisado-Barrios, J. Bouffard, B. Donnadieu and G. Bertrand, *Organometallics*, 2011, **30**, 6017–6021.

15 T. Romero, R. a. Orenes, A. Tárraga and P. Molina, *Organometallics*, 2013, **32**, 5740–5753.

16 D. R. Tolentino, L. Jin, M. Melaimi and G. Bertrand, *Chem. Asian. J.*, 2015, **10**, 2139–2142.

17 M. R. Cerón, F.-F. Li and L. Echegoyen, *Chem. Eur. J.*, 2013, **19**, 7410–7415.

18 D. Canseco-Gonzalez, A. Petronilho, H. Mueller-Bunz, K. Ohmatsu, T. Ooi and M. Albrecht, *J. Am. Chem. Soc.*, 2013, **135**, 13193–13203.